Max-Planck-Institut für Metallforschung
Stuttgart

Thermodynamic optimization of the PbO-ZrO_2-TiO_2 (PZT) system and its application to the processing of composites of PZT ceramics and copper

Marija Čančarević

Dissertation
an der
Universität Stuttgart

Bericht Nr. 198
März 2007

Thermodynamic optimization of the PbO-ZrO_2-TiO_2 (PZT) system and its application to the processing of composites of PZT ceramics and copper

Dissertation

Von der Fakultät Chemie der Universität Stuttgart
Zur Erlangung der Würde eines
Doktors der Naturwissentschaften (Dr. rer. nat)
Genehmigte Abhandlung

Vorgelegt von
Marija Čančarević
Aus Belgrad

Hauptberichter:	Prof. Dr. rer. nat. Fritz Aldinger
Mitberichter:	Prof. Dr. rer. nat. Dr. hc. Mult. Günter Petzow
Prüfungsvorsitzender:	Prof. Dr. Ir. E. J. Mittemeijer

Tag der mündlichen Prüfung: 23.03.2007.

Max-Planck Institut für Metallforschung und Institut für Nichtmetallische Anorganische Materialien der Universität Stuttgart, Stuttgart
Pulvermetallurgische Laboratorium
2007

Dedicated to my parents

Acknowledgments

It is a pleasure for me to express my thanks to Prof. Dr. Fritz Aldinger for providing me the possibility to carry out my thesis work in his department.

I am very thankful to Dr. M. Zinkevich for the supervision of my work and his thorough reading of my thesis.

I would like to thank Prof. Dr. G. Petzow for his support and accepting to be the “Mitberichter” for my thesis. I am also grateful to Prof. E.J. Mittemeijer for his interest in my work and accepting to examine my thesis.

Many thanks to Dr. O. Fabrichnaya who gave me many important hints that deepened my understanding of thermodynamic modelling as well as to my colleges D. Djurovic and N. Solak for stimulating discussions about my experimental work.

I would like to thank Mr. R. Mager for the careful preparation of my experimental set-up and further experimental support.

Finally, I express my thanks to my family, especially my parents for their support, and my husband who kept me holding on by continuous encouragement and to my son who gave me warm smile in each difficult moment.

Contents

ZUSAMMENFASSUNG UND AUSBLICK

Die festen Lösungen auf der Basis von PZT ($PbZr_xTi_{1-x}O_3$) sind aufgrund ihrer piezoelektrischen, ferroelektrischen und pyroelektrischen Eigenschaften von großem Interesse für die Technik. Es können zwar umfangreiche Informationen über PZT in der Literatur gefunden werden, diese sind jedoch im Wesentlichen auf die physikalischen Materialeigenschaften sowie die Charakterisierung von piezoelektrischen Bauteilen beschränkt. Ungeachtet ihrer großen Bedeutung sowohl für die Präparation und das Sintern der Keramiken als auch für die Optimierung deren Eigenschaften, finden sich nur wenige Angaben über Phasendiagramme und thermodynamische Daten des PZT-Systems in der Literatur. Kenntnisse der Konstitution des Systems Cu-Pb-Zr-Ti-O sind darüber hinaus für eine zuverlässige Abschätzung der Reaktivität zwischen Kupfer, Kupferoxiden und PZT notwendig.

Das Ziel dieser Arbeit bestand darin, einen selbstkonsistenten thermodynamischen Datensatz für das System Cu-Pb-Zr-Ti-O mit Hilfe der CALPHAD-Methode zu entwickeln, um die technologisch relevanten Phasen- und Potentialdiagramme für eine Werkstoffkombination Cu/PZT zu berechnen.

Die thermodynamischen Eigenschaften der festen Phasen wurden mit dem allgemeinen Untergittermodell bzw. dem substitutionellen Lösungsmodel beschrieben. Für die Schmelze wurde das Assoziatmodell herangezogen. Dabei wurden die Wechselwirkungen über Redlich-Kister-Reihen berücksichtigt. Im Vergleich zum thermodynamischen Modell für ionische Schmelzen ist das Assoziatmodell besser geeignet, um die Gleichgewichte mit einer flüssigen Phase im System Cu-Pb-Zr-Ti-O zu berechnen. Beide Modelle führen jedoch bei den binären Systemen (Zr-O, Ti-O, Cu-O, Pb-O) zum gleichen Ergebnis. Die ternären Systeme Cu-Pb-O, Cu-Ti-O und Cu-Zr-O wurden zum ersten Mal thermodynamisch beschrieben. Die binären Systeme Cu-Pb, Cu-Ti, Cu-Zr, Cu-O, Zr-O und Pb-O (leicht modifiziert) wurden der Literatur entnommen. Das binäre System Ti-O wurde im Rahmen dieser Arbeit optimiert.

Das ternäre System Cu-Pb-O zeichnet sich durch eine ausgedehnte Mischungslücke von eigenartiger Form aus, und ist mit den Mischungslücken in den binären Subsystemen verbunden. Die thermodynamischen Eigenschaften der ternären stöchiometrischen Verbindung Cu_2PbO_2 wurden in dieser Arbeit experimentell bestimmt. Für das System Cu-Ti-O wurden drei ternäre Phasen (Cu_3Ti_3O, Cu_2Ti_4O und Cu_3TiO_4) mittels der Phasendiagramm-Information vereinfacht beschrieben. Beim System Cu-Zr-O sind keine ternären Verbindungen stabil, was auch experimentell nachgewiesen wurde.

Die quasi-binären Randsysteme des quasi-ternären Systems PbO-ZrO_2-TiO_2, d.h., PbO-ZrO_2, PbO-TiO_2 und TiO_2-ZrO_2 wurden in dieser Arbeit neu optimiert. Aufgrund der begrenzten Menge an Literaturdaten wurden $PbTiO_3$ (tetragonal und kubisch) und $PbZrO_3$ (kubisch) als stöchiometrische Verbindungen innerhalb der Systeme PbO-ZrO_2 und PbO-TiO_2 betrachtet. Die tetragonale und orthorhombische feste Lösung auf der Basis von PbO, sowie die feste Lösung mit Perowskit-Struktur (PZT, $PbZr_{1-x}Ti_xO_3$), wurden mit dem substitutionellen Lösungsmodell beschrieben.

Die berechneten Phasendiagramme des Systems Cu-Pb-Zr-Ti-O (isobar-isotherme Schnitte und chemisches Potential-Diagramme) wurden experimentell überprüft, wobei die Zusammensetzungen und Temperaturen gemäß der Rechnung gewählt wurden. Experimente bzgl. den Subsystemen Cu_2O-CuO-PbO-ZrO_2 und Cu_2O-CuO-PbO-ZrO_2 wurden unter Umgebungsbedingungen durchgeführt. Die Temperaturen von invarianten Reaktionen wurden mit Hilfe thermischer Analyse bestimmt. Zur Untersuchung der Reaktivität zwischen metallischem Kupfer und $PbZrO_3$, $PbTiO_3$ oder PZT, wurden die Proben unter vermindertem Sauerstoffpartialdruck in Gegenwart von Puffern (Ni/NiO, Cu/CuO) bei jeweils 1073 und 1173 K geglüht. Die Charakterisierung der erhaltenen Proben erfolgte mittels Röntgendiffraktometrie, Differenz-Thermoanalyse, Elektronenmikroskopie und Elektronenstrahl-Mikroanalyse.

Der gewonnene thermodynamische Datensatz ist für extrapolierende Berechnungen im sauerstoffreichen Teil des Systems Cu-Pb-Zr-Ti-O, d.h., in den Subsystemen PbO-ZrO_2-TiO_2, Cu_2O-CuO-PbO-ZrO_2, Cu_2O-CuO-PbO-ZrO_2 und Cu_2O-CuO-TiO_2-

ZrO_2 geeignet. Ferner kann er für eine Vorhersage der Reaktivität zwischen Cu und PZT-Keramik eingesetzt werden, jedoch nicht für Berechnungen in dem Metallsystem Cu-Pb-Zr-Ti.

Für die berechneten Phasendiagramme im System Cu-Pb-Zr-Ti-O wurde eine sehr gute Übereinstimmung gefunden. Es wurde gezeigt, dass Kupfer und PZT (sowie $PbZrO_3$ und $PbTiO_3$) unterhalb von 1273 K unter vermindertem Sauerstoffpartialdruck keine Reaktivität aufweisen.

Für eine technologische Entwicklung sollen noch weitere Untersuchungsmethoden, wie z.B., Messungen der dielektrischen Konstante und Polarisierbarkeit verwendet werden. Insbesondere die genaue Kenntnis der Kinetik der PbO-Verdampfung aus der PZT-Keramik ist eine wichitge Grundvoraussetzung für die Optimierung des Herstellungssprozesses.

ABSTRACT

$PbZr_xTi_{1-x}O_3$ (PZT) or modified PZT solid solutions are of great interest for technological applications, which result from their piezoelectric, ferroelectric and pyroelectric properties. Although extensive experimental studies of the PZT system have been carried out in the past little attention was paid to phase equilibria and thermodynamics of the system Pb-Zr-Ti-O, which are important for the optimization of manufacturing and sintering conditions of the PZT ceramics as well as for tailoring their physical properties. In view of using copper for conductor lines in hybrid systems the compatibility between Cu and PZT become of special interest which requires an understanding also the multicomponent Cu-Pb-Zr-Ti-O system.

The aim of this thesis was to obtain a consistent set of thermodynamic data for the Cu-Pb-Zr-Ti-O system, by means of the CALPHAD method, and then to calculate phase equlibria and chemical potential diagrams, which are relevant to the processing of actuators based on PZT ceramics and copper.

The thermodynamic properties were described using the compound energy formalism (CEF) as well as the substitutional solution model for various solid phases and the associate model for the liquid phase, while the Redlich-Kister series were used to account for the interactions between species. Associate solution model adopted for the description of the liquid phase in the multicomponent Cu-Pb-Zr-Ti-O system was found to be superior for calculating the relevant phase equilibria in comparison with the two-sublattice ionic model, although both models can be successfully applied to the binary systems (Zr-O, Ti-O, Cu-O, Pb-O). The ternary Cu-Pb-O, Cu-Ti-O and Cu-Zr-O systems were assessed for the first time. The binary Cu-O and Pb-O systems were taken from literature with some modifications of the Pb-O system in the liquid phase region, while the binary Ti-O system was completely reassessed in the present work. The ternary Cu-Pb-O system shows a large liquid miscibility gap of peculiar shape, which connects to the miscibility gaps in each of the binary sub-systems. The ternary compound Cu_2PbO_2 was modelled as a stoichiometric compound. Its thermodynamic properties were estimated by

experiments. In the modelling of the ternary Cu-Ti-O system the three ternary compounds, Cu_3Ti_3O, Cu_2Ti_4O and Cu_3TiO_4 were taken as stoichiometric compounds. In the Cu-Zr-O system the literature data show no existence of ternary compounds and it was experimentally proved in this work. The quasibinary PbO-ZrO_2, PbO-TiO_2 and ZrO_2-TiO_2 systems, the edges of the quasiternary PbO-ZrO_2-TiO_2 (PZT) system, were reassessed on the basis of most recent literature data. Thermodynamic properties of the end-members, ZrO_2 and PbO have been taken from the literature, while those of TiO_2 were evaluated in the present work. Due to limited experimental information, $PbTiO_3$ (tetragonal and cubic forms) and $PbZrO_3$ (cubic form) were considered as stoichiometric compounds in the PbO-TiO_2 and PbO-ZrO_2 systems, while the tetragonal and orthorhombic PbO solid solutions were described by a substitutional model. The perovskite solid solution series, $PbZr_xTi_{1-x}O_3$ was modelled as high temperature cubic form using the substitutional model. Calculated phase diagrams, *i.e.*, predicted phase relations in the multicomponent Cu-Pb-Zr-Ti-O system (isobaric-isothermal sections and chemical potential diagrams) were checked experimentally. Experimental points were chosen based on CALPHAD approach and all compositions were prepared by solid state reaction. For the verification of the phase relations and invariant reactions in the oxide rich part (Cu_2O-CuO-PbO-TiO_2 and Cu_2O-CuO-PbO-ZrO_2 isotherms) experiments were done in air. The investigation of the reactivity between Cu and $PbTiO_3$, $PbZrO_3$ or PZT in the solid state was performed at the carefully controlled partial pressure of oxygen using different kinds of buffers (Ni/NiO, Cu/Cu_2O) at 1073 and 1173 K. Microstructural characterization of the samples was done by X-ray, DTA, SEM and EDX analysis.

The database evaluated in this thesis is reliable for extrapolating calculations in the oxygen-rich part of the multicomponent Cu-Pb-Zr-Ti-O system, *i.e.*, in the PbO-ZrO_2-TiO_2, Cu_2O-CuO-PbO-ZrO_2, Cu_2O-CuO-PbO-TiO_2 and Cu_2O-CuO-ZrO_2-TiO_2 sub-systems. In addition, it can be used for prediction of reactions between metals and oxides, *i.e*. between Cu and PZT ceramics (Cu-PbO-ZrO_2-TiO_2 system), for which purpose it was mainly developed, but not for calculations in the Cu-Pb-Zr-Ti system and corresponding subsystems.

The phase diagrams of the multicomponent Cu-Pb-Zr-Ti-O system calculated in this thesis were found to be well consistent with the experimentally obtained results, which clearly show the chemical stability of copper and PZT ceramic at temperatures below 1273 K in reducing atmosphere. The reactivity between copper and $PbTiO_3$, $PbZrO_3$ or $PbZr_xTi_{1-x}O_3$ (x=0.44, 0.5) was not observed using the characterization methods applied in this work. Detailed investigation of the feasibility of using copper in piezoelectric actuators based on PZT solid solutions requires the application of additional characterization methods such as measurements of electrical and polarization properties. In addition, detailed investigation of the kinetics of PbO evaporation seems to be of fundamental importance in optimization of the processing conditions (temperature and time) for PZT-based ceramics.

1. INTRODUCTION

1.1. Piezoelectricity and piezoelectric actuators

Piezoelectricity is a phenomenon which is present in all crystals having a polar axis and in those crystals where a polar axis is generated when they are subjected to mechanical stress. This effect, *i.e.*, creation of an electric charge by applied stress, is named *direct* effect and the charge is proportional to the force. On the other hand, the *converse* effect, by which the same materials show a variation of their dimensions on application of an electric field, is also present [1971Jaf, 1986Dur] (For instance, the deformation is about 0.1 % of the original dimension in lead zirconate titanate, PZT). For both effects the proportionality constant is piezoelectric constant *d* which is numerically identical for both, direct (D = *d*T, D is the dielectric displacement and T is the stress) and converse (S = *d*E, S is the strain and E is the applied field) effects. In addition, the piezoelectric constant may differ for different axis in crystals, and for this reason it is usually expressed in the tensor form. Some natural crystals, *e.g.* quartz, tourmaline and Rochelle salt, can be considered as normal piezoelectric materials, and are used as transducers in both directions, *i.e.*, electrical energy ↔ mechanical energy. Many others materials exhibit the piezoelectric effect, including quartz analogous crystals like berlinite ($AlPO_4$) and gallium orthophosphate ($GaPO_4$), ceramics with perovskite or tungsten-bronze structure ($BaTiO_3$, $SrTiO_3$, $Pb(ZrTi)O_3$, $KNbO_3$, $LiTaO_3$, $BiFeO_3$, Na_xWO_3, $Ba_2NaNb_5O_5$, Pb_2KNbO_{15}).

Pyroelectricity is the ability of certain materials to generate an electrical potential when they are heated or cooled. As a result of this change in temperature, positive and negative charges move to opposite ends through migration (*i.e.*, material becomes polarized) and hence, an electric potential is established. Pyroelectric charge develops on the opposite faces of asymmetric crystals. The direction of the charge propagation is usually constant, but in same materials it can be changed by a nearby electric field. These materials are said to exhibit ferroelectricity, *i.e.*, the ferroelectric effect is an electrical phenomenon whereby certain ionic crystals may exhibit a spontaneous dipole moment, which can be reversed by the application of an electric field. All pyroelectric materials

are also piezoelectric, while all ferroelectrics are at the same time pyroelectrics and piezoelectrics.

Of the thirty-two crystal classes, twenty-one are non-centrosymmetric (not having a centre of symmetry), and of these, twenty exhibit direct piezoelectricity (the 21st is the cubic class 432). Ten of these are polar (*i.e.*, spontaneously polarize), having a dipole in their unit cell, and exhibit pyroelectricity. In a piezoelectric crystal, the positive and negative electric charges are separated, but symmetrically distributed, so that the whole crystal is electrically neutral. Each of these sites forms an electric dipole and dipoles near each other tend to be aligned in regions called Weiss domains. The domains are usually randomly oriented, but can be aligned during *poling*, a process by which a strong electric field is applied across the material, usually at elevated temperature.

Commercially used piezoceramics is primarily lead zirconate titanate (PZT). Being piezoelectric, it develops a voltage difference across two of its faces when compressed (used for sensor applications), or physically changes shape with an applied external electric field (used for actuators). It is also ferroelectric, which means it has a spontaneous polarization which can be reversed in a presence of one electric field. Barium titanate (BT), strontium titanate (ST), quartz, and others are also used. The first piezoelectric ceramics, BT, was widely used in the past. Since about 1957 it has been replaced in most applications by the lead zirconate titanate compositions ($PbZr_xTi_{1-x}O_3$ or PZT) which offer much higher operating temperature, stronger piezoelectric effects, and much larger variety of characteristics. This allows chemical modifications without loss of piezoelectricity and a large variety of compositional modifiers are used in comparison with lead-free piezoelectric ceramics.

The adaptability and lightweight properties of PZT ceramics make them highly desirable materials for use in actuation. Actuators are devices which control a displacement, a force and a velocity of a mechanical load, converting electric, fluidic or other input power to mechanical output power. Piezoelectric ceramic actuators possess

two key features. They are capable of an ultramicroscopic displacement control and a high rate of electromechanical energy conversion.

1.1.1 Working principle

Typical piezoelectric actuators include multilayer stacked (linear), bimorph-type (bending), and rainbow-type assemblages. When a large force and low displacement level are required, multilayer actuators can be used; when large displacement is required, bimorphs are usually employed (low frequency application). Such an actuator consists of two thin slabs of PZT laminated together with two outer electrodes and a common electrode as shown in Fig.1. The two slabs are polarized in opposite directions using the inner electrode. On bending, both parts have a piezoelectric effect pointing in the same direction, so that between the outer electrodes a double voltage appears. A high voltage is necessary to produce for the application such as ignition element for spark plugs (fuel injection pumps).

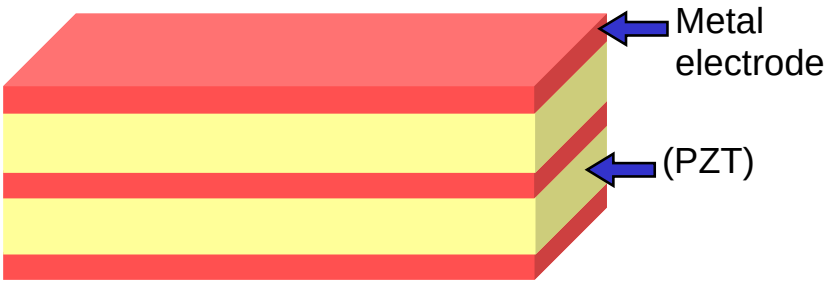

Fig. 1.1 The schematic of the actuator with two slabs of PZT laminated together with two outer electrodes and a common electrode.

Typically, metal electrodes are made of the Ag/Pd alloys, which are co-sintered with ceramics. However, palladium reacts with lead in the ceramics at high temperatures (> 1473 K) that causes defects in the devices. Therefore, to stabilize the electrodes, it is necessary to lower the sintering temperature [1990Zhi, 1992Gui, 1993Moo]. Furthermore, Pd is very expensive. Thus, today the research focus is shifted to base-metal

electrodes such as Cu and Ni, which require low sintering temperatures in reducing atmospheres.

1.1.2. Synthesis and properties of PZT ceramics

In general, the dielectric and piezoelectric properties of PZT are strongly affected by density, compositional homogeneity and microstructure. Although, the large number of works has been published on the preparation of PZT ceramics with enhanced electrical properties, they are not always achieved. In a standard ceramic method PbO excess is commonly used as an aid to enhance the sintering process by means of a transient liquid. However, there is no agreement about the role of PbO during the densification process. In fact, it is difficult to control the activity of PbO in the $PbTiO_3$-$PbZrO_3$ system in view of its volatile nature. Generally, PZT ceramic with good properties is sintered in closed staggers containing some additional PbO or other lead compounds (buffer) to form a lead saturated atmosphere. Depending of the powder state of the buffer and closeness of the system the transfer of PbO from buffer towards PZT or the reverse occurs. It is evident that factors, such as buffer amount and sintering time will play an important role in obtaining a PZT ceramic saturated with PbO but without PbO excess. In such a situation, the preparation of PZT ceramics with reproducible density and microstructure is a big challenge for conventional ceramic processing. The actuators applications require the sintering of metal and ceramics together, therefore the low-temperature sintering is an important technique for suppressing the compositional fluctuation and improving the piezoelectric properties, reliability and reproducibility of PZT ceramics. For this purpose, nonconventional synthesis methods by using the oxide precursors as raw materials and by controlling rigorously the particle size and morphology of the co-precipitated hydroxides as well as the pre-calcinations treatment can be used to obtain highly sinterable powder. The compacts of such powder can be sintered to nearly theoretical density in an air environment without using PbO excess.

1.2 Aim of the study

Although extensive experimental studies of the PZT system have been carried out in the past attention was paid mainly to physical properties, kinetics and device characterization, while a little to phase equilibria and thermodynamics, which are important for the optimization of manufacturing and sintering conditions of the PZT ceramics as well as for tailoring their physical properties.

In addition, investigation of phase equilibria in the multicomponent Cu-Pb-Zr-Ti-O system plays an important role for the understanding and prediction of the reactivity between copper and copper oxides with PZT ceramics, what is important for technologies where copper is in contact with lead-containing piezoelectric materials such as actuators applications.

Due to the complexity of the Cu-Pb-Zr-Ti-O system, and due to many variables influencing the phase stability, an extremely large amount of experimental data would be necessary to understand phase equilibria. The objective of this study is to obtain a consistent thermodynamic database of the Cu-Pb-Zr-Ti-O system by means of the CALPHAD method, i.e., by analytically representing the Gibbs energy of each phase. The systems of the lower order have to be described first; the final system is reached by adding the elements one by one. The predicted phase relations in the multicomponent Cu_2O-CuO-PbO-TiO_2, Cu_2O-CuO-PbO-ZrO_2 and Cu-PbO-ZrO_2-TiO_2 subsystems should be verified by key experiments, but the amount of experimental efforts involved is insignificant comparing to the traditional approach using exclusively experimental determinations. These experiments should also give insight on the stability and reactivity of copper oxides or copper with PZT ceramics. Therefore, the obtained database can be used as a guideline for the processing of PZT ceramic with copper.

2. FUNDAMENTALS

2.1. Experimental determination of phase diagrams and thermodynamic quantities

The conventional experimental methods for the determination of phase diagrams can be divided in two groups:

- Isothermal techniques in combination with sampling/equilibration method: metallography - light microscopy, scanning electron microscopy (SEM), transmission electron microscopy (TEM), as well as X-ray diffraction (XRD) and electron probe micro analysis (EPMA).
- Non-isothermal techniques: differential scanning calorimetry (DSC), differential thermal analysis (DTA), chemical potential method.

The commonly used methods for experimental determination of thermodynamic quantities are:

- Calorimetric methods (isothermal, adiabatic and heat-flow)
- Gas phase equilibria techniques (static method for measurement of vapour pressure, Knudsen effusion and Langmuir free-evaporation method)
- Electromotive force measurement (EMF).

The adiabatic and heat-flow calorimetry are best suited for the direct measurement of heat capacity and enthalpies of transformation. The heat capacity and entropy are thermodynamic properties expressed in the absolute values. The entropy at 298 K can be evaluated from the low temperature heat capacity data by assuming that its value is zero at 0 K (third law of thermodynamics). However, the thermodynamics is not concerted with the absolute value of the energy, or the enthalpy of a system; only the changes with respect to some reference state (*i.e.* relative values) are recorded. The relative values have physical meaning and can be determined experimentally. The standard enthalpy of formation at 298 K (ΔH_{298}), the enthalpy increment (H_T-H_{298}), and the enthalpy of mixing (ΔH_{mix}) can be measured by different methods of calorimetry, while EMF method is suited to obtained Gibbs energy of formation.

2.2. Phase diagram calculations

Phase diagrams are foundation of the basic material research in such fields as solidification, crystal growth, solid state reaction, phase transformation, etc. Phase diagram also serves as a road map for materials design and process optimization since it is the starting point in the manipulation of processing variables to achieve the desired microstructures. Until the last decade of the 20th century, phase diagrams were determined primarily by meticulous and costly experimentation. While this approach has been both feasible and necessary for determination phase equilibria of binaries and those of ternaries over limited compositional regions, it is nearly impossible to obtain phase diagrams of ternary and higher order systems over wide regions of composition and temperatures. One of the real challenges in this field has been and still is to use another approach to obtain the phase diagrams. Although significant progress has been made in the attempt to calculate energies at 0 K and then phase diagram by *ab-initio* methods, this approach is unlikely to be successful from the technological viewpoint in the foreseeable future. Alternatively, one can obtain the parameters of thermodynamic model for the Gibbs energies of the constituent phases in the lower order system, binaries and ternaries, in terms of known thermodynamic and phase equilibrium data. These Gibbs energy values enable us to calculate reliable multicomponent phase diagrams via an extrapolation method in many instances. Experimental work is then only required for confirmation purposes and not for the determination of the whole diagram.

2.2.1. The CALPHAD method

The CALPHAD (CALculation of PHAse Diagrams) approach [2001Kau, 2001Spe] is a method to assess thermodynamic parameters using the diverse type of experimental information: phase diagrams, calorimetry, vapor pressure data, electrochemical measurements, *etc*. The optimal values of the unknown parameters providing the best match between calculated quantities and their experimental counterparts are usually obtained by the weighted non-linear last squares minimization or fitting procedure

(thermodynamic optimization). The selection of the model for a phase must be based on its physical and chemical properties of such as crystallographic structure, type of bonding, ordering, and defect structure. The CALPHAD method is implemented in several commercial software packages based on the different mathematical methods and computer languages (Thermo-Calc, Pandat, MTDATA, FactSage…). In the present thesis, all computations were done using Thermo-Calc software package [2002And] (www.thermocalc.com). Thermo-Calc is general and flexible software for the thermodynamic properties and phase diagram calculations based on the minimization of Gibbs energy of the system. Thermo-Calc is for example the only software that allows explicit condition of individual phase compositions or configuration whereas most software can handle condition on the overall composition only. Thermo-Calc software consists of several basis modules, *i.e.*, TDB for database retrieval and management, TAB for thermodynamic property tabulation of phases and reactions, POLY3 for calculations of individual equilibria and phase diagrams, PARROT for parameter optimizations, *etc*.

Fig. 1.2 shows the way to calculate phase diagrams of multicomponent systems. Firstly, thermodynamic description of the constituent lower-order systems, normally, binaries and ternaries, are obtained based on experimental and “first-principles” total energy information and phase equilibrium data. The term “thermodynamic description” means that the set of thermodynamic models with parameters for phases in a system are obtained so that not only thermodynamic properties of the phases but also phase diagrams of the system can be calculated. However, once descriptions for the lower-order systems are known, it is possible in many cases to obtain thermodynamic description of the higher-order systems by using an extrapolation method so that phase diagrams of multicomponent system can be calculated. It is obvious that the calculated multicomponent phase diagrams must be verified by key experiments, but the amount of experimental efforts involved is insignificant comparing to the traditional approach using exclusively experimental determinations, since the number of phase fields to be examined increases tremendously with increasing number of components. For the rare case when quaternary phases do exist in the system, optimization of model parameters for the quaternary phases in question is necessary.

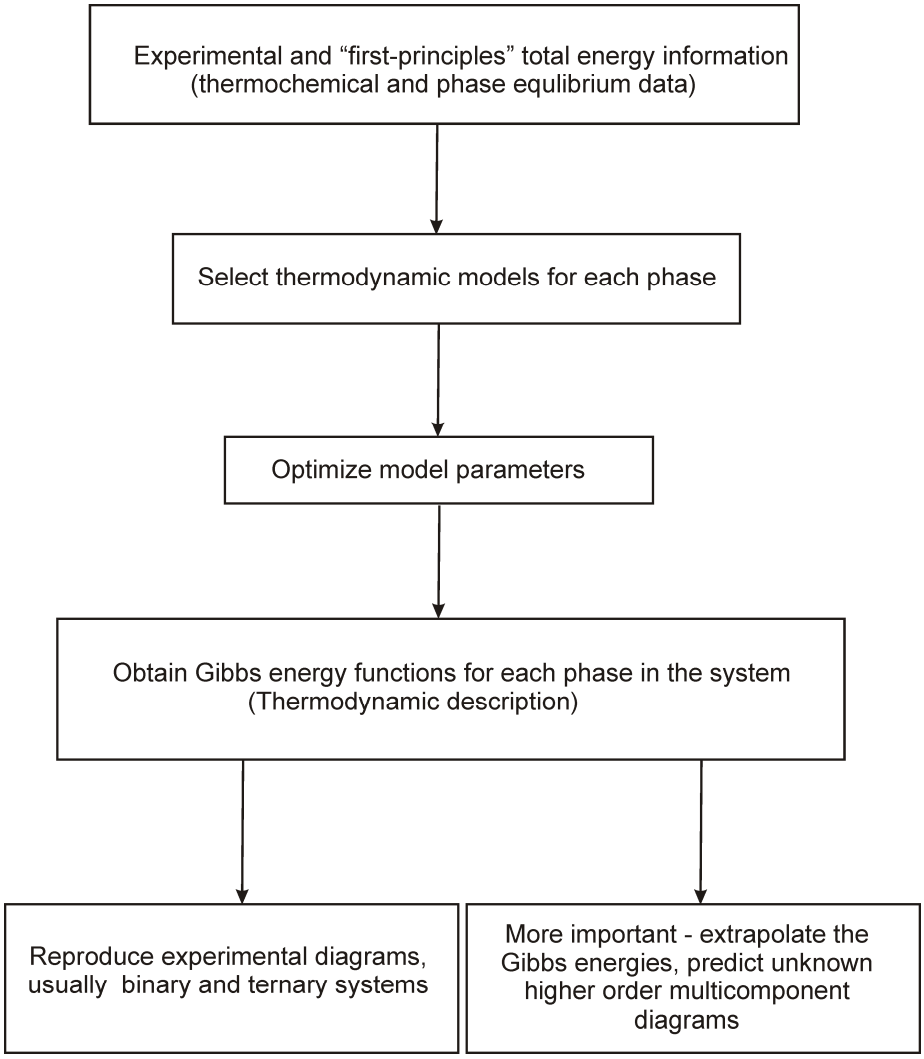

Fig. 1.2. Obtaining thermodynamic description of a multicomponent system by means of the CALPHAD method.

One of critical factor in the CALPHAD approach is selection of input data (experimental and theoretical data). All available data should be carefully evaluated so that the selected data are reasonable and consistent. The second factor is selection of model for phases. Appropriate thermodynamic model has to be adopted to describe the energetic behaviours of phases. Reasonably, only the model based on the structural and physical realities can truly reproduce the thermodynamic behaviour of different phases and the Gibbs energy of the phases can be analytically described.

2.2.2. Analytical description of the Gibbs energy

2.2.2.1. Pure elements and Stoichiometric phases

The Gibbs energy functions of all phases are referred to the enthalpy of pure elements in their stable state at 298.15 K and 1 bar pressure (stable element reference H^{SER}). It is supposed that enthalpy of stable structure of any element at 298.15 K and 1bar is equal to zero, and this assumption is set to be the reference state of elements. Then, the Gibbs energy functions of the pure elements, stoichiometric phases and end-members of solutions are given by

$$^{\circ}G(T) = G(T) - H^{SER} = a + bT + cT\ln(T) + dT^2 + eT^3 + f/T + \sum_n g_n T^n , \qquad (2.1)$$

where a to f and g_n are coefficients, which are evaluated based on experimental data (entropy, enthalpy and heat capacity) and n stands for a set of integers, typically taking the values of 2, 3 and -1. The Eq. 2.1 is given with respect to temperature and it is valid only in a certain temperature range. From Eq. 2.1, further the thermodynamic properties can be expressed

$$S = -b - c - c\ln(T) - \sum n g_n T^{n-1} , \qquad (2.2)$$

$$H = a - cT - \sum (n-1) g_n T^n , \qquad (2.3)$$

$$C_p = -c - \sum n(n-1) g_n T^{n-1} , \qquad (2.4)$$

where the S, H and C_p are temperature dependent functions of entropy, enthalpy and heat capacity, respectively. In this work, the Gibbs energies of pure elements are taken from the SGTE (Scientific Group Thermodata Europe) unary database [2001SGTE]. Descriptions of the stoichiometric binary phases, except for Ti_3O_2 and α-TiO, are adopted from the assessments of the corresponding binary systems [2003Hal, 1998Ris, 1999Wal, 2006Wan, 1986Hay, 1996Kum, 1994Zen]. Thermodynamic properties of the stoichiometric ternary phases Cu_2PbO_2, Cu_3TiO_4, Cu_2Ti_4O, Cu_3Ti_3O, $PbZrO_3$, α$PbTiO_3$, β$PbTiO_3$, α$ZrTiO_4$, and $ZrTi_2O_6$ are evaluated in the present work (Appendix, Table 1).

2.2.2.2. Substitutional solutions

Ideal substitutional solution is characterised by a random distribution of components with an interchange energy equal to zero. Its Gibbs energy is given as

$$G^{\alpha} = \sum_i x_i {}^{o}G_i^{\alpha} + \sum_i RT(x_i \ln x_i), \tag{2.5}$$

where the first term represents the Gibbs energy of mechanical mixture of components and the second one accounts for the entropy of mixing. For ideal solution there is no heat evolved upon mixing and there is no change of volume, while the activity of a component is equal to its atomic fraction (Raoult's law).

There are few, if any, ideal solutions. Generally, solutions show deviation from Raoult's law. This deviation for every component is expressed by its activity coefficient, γ. Activities less than the atomic fractions ($\gamma < 1$ or negative deviation from Raoult's law) are associated with stronger attractive forces between A and B atoms than between similar atoms. This type of behaviour is indicative of formation of intermediate phases between A and B. If the attractive forces between A and B atoms are weaker than those between similar atoms ($\gamma > 1$ or positive deviation from Raoult's law), there is a tendency for phase separation. For the non-ideal substitutional solution of components A and B, Gibbs energy is described by

$$G^{\alpha} = x_A {}^{o}G_A^{\alpha} + x_B {}^{o}G_B^{\alpha} + RT(x_A \ln x_A + x_B \ln x_B) + {}^{E}G^{\alpha} \tag{2.6}$$

If the excess energy of solution arises from the interaction between nearest neighbours only, it is called regular solution. The Gibbs energy of mixing is than

$${}^{E}G^{\alpha} = x_A x_B L, \tag{2.7}$$

where L is a temperature-dependent interaction parameter. The cases $L > 0$ and $L < 0$ correspond to the positive and negative deviation from the Raoult's low, respectively.

However, it has been realised for a long time that the assumption of composition-independed interactions was too crude. This led to the development of sub-regular solution model, where interaction energies are considered to change linearly with composition [1970Kau], or more complex composition dependencies. In general, the excess Gibbs energy in the binary system can be expressed by the Redlich-Kister polynomial [1948Red]:

$$^{E}G^{\alpha} = x_i x_j \sum_{v=0}^{n} {}^{v}L^{\alpha}_{i,j}(x_i - x_j)^v, \tag{2.8}$$

where i and j are indexes which correspond to the species A, B or C. The binary interaction parameters are usually described as linear functions of temperature, $^{v}L^{\alpha}_{i,j} = a_v + b_v \cdot T$. In practice, the value for v does not usually rise above 2.

In the ternary and higher-order systems, the excess Gibbs energy is expressed by the Redlich-Kister-Muggianu description [1975Mug]:

$$\begin{aligned} {}^{E}G^{\alpha} &= \sum_i \sum_j x_i x_j \sum_{v=0} {}^{v}L^{\alpha}_{i,j}(x_i - x_j)^v \\ &+ x_i x_j x_k (b_i {}^{1}L + b_j {}^{2}L + b_k {}^{3}L), \end{aligned} \tag{2.9}$$

where x_i , x_j and x_k are the fractions of constituent *i*, *j* and *k*, respectively, and

$$\begin{aligned} b_i &= x_i + (1 - x_i - x_j - x_k)/3 \\ b_j &= x_j + (1 - x_i - x_j - x_k)/3 \\ b_k &= x_k + (1 - x_i - x_j - x_k)/3 \end{aligned} \tag{2.10}$$

^{1}L , ^{2}L and ^{3}L are functions of temperature and pressure only. In the ternary system b and x are identical, but in extrapolations to quaternary and higher-order systems the sum of b is always unity which is not true for the sum of x .

In general the substitutional solution model can be adopted for the description of the solid and liquid phases. The Gibbs energy of solid phases is well described by Eqs. 2.6 - 2.10. However, in systems showing liquid immiscibility as well as thermodynamically stable compounds the use of the simple substitutional model has not been always successful. In such cases the model needs a large number of coefficients to mimic sharp changes in the enthalpy around the critical composition, and binary systems thus modelled tend to badly predict phase equlibria in the multicomponent systems. Many more advanced models have therefore been proposed to account for the thermodynamic behaviour of ionic liquids (associate solution models, sublattice models, modified quasichemical model, cell model, etc.).

Associate solution model [1974Pre, 1979Sha, 1982Som, 1984Lel, 1985Bjo, 1990Som] is widely used for the description of thermodynamic properties of liquids. There are differences between the authors in the way, how the excess terms are handled, but all consider that some type of complexes or associates are formed in the liquid from the reaction between the components of the system. The thermodynamic properties of the liquid then depend predominantly on the Gibbs energy of formation of these complexes, or associates, rather than on interaction between components of the system. The thermodynamic mixing functions of liquids with compound formation tendency show, in most cases, a strong deviation from the regular solution behavior, which is caused by the existence of chemical short-range ordering (CSRO). This gives rise to proper enthalpy of mixing diagrams which are characterized by sharp changes at critical composition where the associates exist and also by markedly non-ideal mixing entropies. The short range ordered volume parts are summarily described as associates with well defined compositions, while the remaining atoms are regarded to be randomly distributed. The associates are in steady dynamic equilibrium with the non-associated atoms, as governed by the mass action law.

The model is based on the hypothesis that a complex C is formed in the liquid phase by A and B:

$$p\mathrm{A} + q\mathrm{B} \rightarrow \mathrm{A}_p\mathrm{B}_q \,, \qquad (2.11)$$

where A_pB_q corresponds to the C complex. p and q are stoichiometric coefficients. The Gibbs energy can be described by

$$G^{liq} = x_A{}^oG_A^{liq} + x_B \cdot {}^oG_B^{liq} + x_C \cdot {}^oG_C^{liq} + RT(x_A \ln x_A + x_B \ln x_B + x_C \ln x_C) + {}^EG_{ass}^{liq}, \qquad (2.12)$$

where x_A, x_B, and x_C are the mole fractions of the species A, B and C in the liquid**.** The excess term, ${}^EG_{ass}^{liq}$ is described by the same expressions as in the ordinary substitutional model (Eqs. (2.8) – (2.10)).

2.2.2.3. The compound energy formalism (CEF)

The compound energy formalism was introduced in order to describe the Gibbs energy of solution phases with sublattices. The idea of sublattices originates from the thermodynamic treatment of lattice defects introduced by Wagner and Schottky [1930Wag]. The concept of the sublattice model for liquids was outlined first by Temkin [1945Tem] and developed by Hillert and Staffansson [1970Hil] for two-sublattice substances and by Sundman and Agren [1981Sun] for several sublattices. The method has been developed to treat different solutions using a large variety of thermodynamic models [2001Hil]. The models have a physical meaning based on crystallographic information, *i.e.* the modelling of sublattices is connected to the true crystallographic structure. An adequate description of the properties of solution phases can be obtained using any lattice defects or interstitials in the sublattices. It gives possibilities to describe the true nature of different solution phases with substitutional and interstitial species, charged species, ordering behaviour, etc.

Generally, the model for a phase can be expressed by the formula $(A,B,..)_k(D,E,..)_l(\ldots)$, where A and B are constituents on the first sublattice, D and E on the second one, etc. The k, l… are the stoichiometric coefficients and one mole of formula units thus contains ($k + l +\ldots$) moles of atoms. The general notation for the stoichiometric

coefficient is n^s where the superscript s defines the sublattice. The Gibbs energy is given by

$$G = \sum \prod y_j^s {}^oG_{end} + RT \sum_s \sum_j n^s y_j^s \ln(y_j^s) + {}^EG \,, \tag{2.13}$$

where j represents any type of species, *i.e.* atoms, molecules, ions or vacancies. y_j^s is the site fraction of constituent j in the sublattice s and ${}^oG_{end}$ is the Gibbs energy of one mole of formula units of the compound representing the end-member, e.g. A_kD_l. The second term represents the ideal entropy of mixing. The excess Gibbs energy is described within the generalized regular solution expression

$${}^EG = \prod y_j^s \sum y_B^t L_{A,B:D:G.....} + \prod y_j^s \sum \sum y_B^t y_D^u L_{A,B:D,E:G.....} + \quad . \tag{2.14}$$

The commas in the subscripts separate constituents within a sublattice and the colons separate constituents in different sublattice. One summation covers the interaction in one sublattice while each of the other sublattices is only occupied by the single constituent (first term of Eq. 2.15). Double summation covers the simultaneous interaction of species occurred in two sublattices while the other sublattices are only occupied by the single constituent (second term of Eq. 2.15). The parameters can depend on composition and usually are expressed by Redlich-Kister polynomials. The second therm is often called ‘reciprocal parameter’.

For ***the ionic melts,*** the constituents are artificially divided into sublattices occupied by cations or anions only. Occupation of constituents on sublattice varies with the composition to maintain electroneutrality. The two-sublattice model for liquid solutions was developed by Hillert et al. [1985Hil1] and could be presented as $(C_i^{+i})_P(A_j^{-j}, Va^{-Q}, B_j^0)_Q$. The stioichiometric factors P and Q are calculated from the relations

$$P = \sum(-jY_{A_j}) + QY_{Va} \quad \text{and} \quad Q = \sum(+iY_{C_i}) \;, \tag{2.15}$$

where $-j$ and $+i$ are the electric charges of ions and Y is the mole fraction of the species in the sublattice. The inclusion of charged vacancies and neutral molecules gives a continuous description from metallic to ionic and further to polymeric liquids.

2.2.3. The chemical potential diagrams

In the past years, there has been a growing interest in making sophisticated chemical thermodynamic analysis on practical problems in the fields of metallurgy, high-temperature and materials science. These analyses have been made by the complicated chemical equlibria calculations, phase diagram calculations and by the construction of the chemical potential diagrams. If the systems consist of dissimilar materials, *i.e.*, metals and non-metals, it is of great importance to know about the phase relations among metals and oxides as it is the case for composites of copper and PZT ceramics. In order to visualize complicated phase equlibria, it is useful to construct diagrams, where both axes are chemical potentials [1989Yok, 1999Yok, 2005Yok].

The chemical potentials are the key in understanding materials behaviour in various chemical environments. Since practical materials consist of many components the construction of chemical potential diagrams for the multicomponent systems becomes crucial. The chemical potential diagrams can be presented as three-dimensional diagrams, although not all phase relations are visible there, or as sections at selected values of the chemical potential of selected chemical species (Figs. 7.8 - 7.17, Chapter 7.2). One important point in understanding the chemical potential diagrams is that a phase is represented by an area and therefore within the area, chemical potentials can change depending on the thermodynamic conditions such as the oxygen potential, *etc*.

The chemical potential diagrams show the location of stability areas of phases and its relation to chemical reactions. When two stability areas are adjusted in the generalized chemical potential diagram it primarily means that two phases are in equilibrium, *i.e*. two-phase boundaries are represented as lines. Those between stoichiometric compounds are given as straight lines, while effects of forming solutions appear as bend lines. The

triple junctions indicate that three phases can coexist as an equilibrium state. If some intervention occurs between two phases, *i.e.*, A and B phases are intervened by C phase, it can be said that A and B are unstable against the formation of a C phase.

3. EXPERIMENTAL PROCEDURES AND THERMODYNAMIC MODELING

3.1. Experimental procedures

3.1.1. Sample preparations

All investigated compositions were prepared by solid-state reactions. The starting materials for processing were powders of Cu, Cu_2O and CuO from Sigma Aldrich GmbH, Steinheim, Germany and PbO, TiO_2, ZrO_2, $PbTiO_3$, $PbZrO_3$, Ni and NiO from Alfa Aesar GmbH & Co, Karlsruhe, Germany with a purity of > 99.9 %. The homogenization of powder mixtures was done in a planetary ball mill with ethanol for 4 h; thereafter they were isostatically pressed into cylindrical pellets of ~ 400 mg in weight.

The buffers (Ni/NiO and Cu/Cu_2O) were prepared from equimolar powder mixtures of metals and oxides and homogenization in the same manner as the sample mixtures. A specially constructed quartz tube, which perfectly fitted the furnace tube, was used as a buffer holder. It was filled with the buffer mixtures (~70 g per run) using “cotton-wool” like alumina as medium to obtain a developed reactive buffer surface and good contact between the buffer and the carrier gas (argon 5N type) (Fig. 3.1).

The following sample mixtures and heat treatments were used:

a) The compound Cu_2PbO_2 was synthesized from a stoichiometric mixture of Cu_2O and PbO. The pellets were annealed at 910 ± 5 K for 260 h in a sealed quartz ampoule filled with argon (5N type).

b) Powder mixtures of CuO (or Cu_2O) + ZrO_2 in the molar ratios 1:3, 1:1 and 3:1 were prepared for the investigation of the existence of ternary compounds in Cu-Zr-O system. DTA of samples was performed in argon (Cu_2O + ZrO_2) and oxygen atmosphere (CuO + ZrO_2) up to 1430 and 1370 K, respectively, as it is described in Section 3.1.2.

c) The PZT solid solution was prepared from an equimolar mixture of TiO_2, ZrO_2 and PbO while the PbO was used in excess. The pellets were heated at 1373 K for 6 h. The residual PbO was dissolved in the acetic acid and decanted. The PZT precipitate was washed by distilled water, filtered and dried at 333 K.

d) For the investigations of the phase relations in CuO_x-PbO-TiO_2 and CuO_x-PbO-ZrO_2 systems, *i.e*. of the reactivity between the copper oxides and PZT ceramics, powders of PbO + TiO_2 (or ZrO_2) + CuO in the molar ratios 1: 0.4 : 0.6 and 0.4 : 1 : 0.6 were mixed and compacted into pellets. The pellets were heated in air at 1043 K (1: 0.4 : 0.6 mixtures) and 1173 K (0.4 : 1 : 0.6 mixtures) for 100 h and than air quenched. In addition, DTA of samples was performed in air up to 1300 K as it is described in Section 3.1.2.

e) The reactivity between copper and PZT ceramics was studied using equimolar powder mixtures of Cu + $PbTiO_3$, Cu + $PbZrO_3$, Cu + PbO + $PbTiO_3$, Cu + PbO + $PbZrO_3$ and Cu + $PbZr_{.5}Ti_{.5}O_3$. The samples were heated (heating rate 5 $K \cdot min^{-1}$) at 1073 and 1173 K for 50 h in a controlled atmosphere obtained by means of the Ni/NiO and Cu/Cu_2O buffers. The buffers and samples were loaded in the same furnace and heated in a constant argon flow of 0.8 l/h (Fig. 3.1). The samples containing $PbZrO_3$ and PbO were studied using only the Cu/Cu_2O buffer. For this purpose the buffer was held at a temperature 50 K lower than that of the samples to be investigated.

3.1.2. Characterisation methods

Scanning electron microscopy (SEM, from Zeiss DSM 982, 20kV, 10nA, equipped with an energy disperse X-ray microanalyser, EDX, from Oxford-Instrument ISIS 300, standard error ± 0.3 wt.%, calibration with CoK_α line) and X-ray diffraction (XRD, from Siemens D-5000 with the filtered CuK_α radiation, λ=0.15406 nm, 2θ range 10-80°, 2θ step of 0.016°) were used for sample characterization. The XRD analysis of the buffer mixtures were performed before and after each experimental run. Full-profile Rietveld refinement of XRD patterns was carried out using TOPAS software to determine the

weight fraction of the ternary Cu_2PbO_2 compound, as well as of the residual Cu_2O and PbO phases. The specimens for SEM were mechanically ground and polished. The composition of the observed phases was determined by EDX. The enthalpy of formation of the ternary Cu_2PbO_2 compound was determined by a differential scanning calorimeter (HT-DSC; SETARAM S.A., Caliure, France) calibrated with Li_2SO_4 standard. The heat flow was measured from 373 to 1073 K (heating and cooling rate 5 $K \cdot min^{-1}$) in helium atmosphere. The weight of the powdered specimens was in the range of 600-800 mg. Differential thermal analyses (DTA, STA 409 C, NETZSCH, Selb, Germany) of the sample mixtures in argon, oxygen or air (see Section 3.1.1.) were preformed with a heating and cooling rate of 5 $K \cdot min^{-1}$ and samples ~ 300 mg in weight.

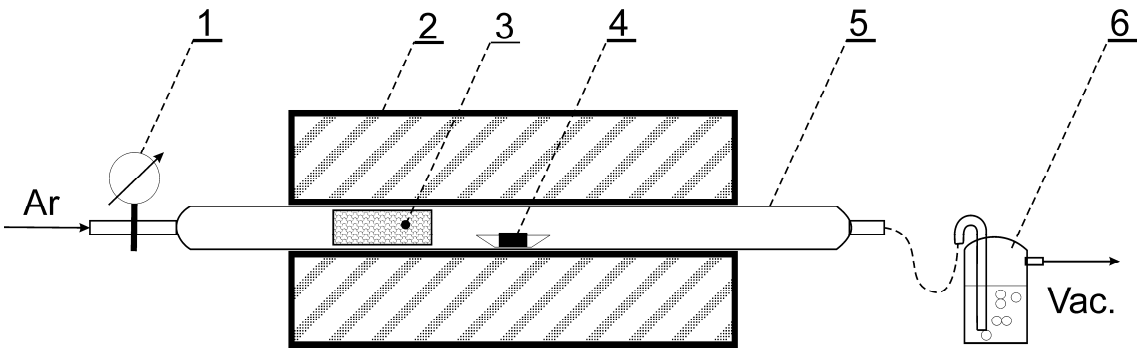

Fig. 3.1. Scheme of the apparatus for the investigation of samples under reducing atmosphere: 1) flow-meter, 2) furnace, 3) buffer tube) 4) sample, 5) furnace tube and 6) gas washer.

3.2. Description of phases in the Cu-Pb-Zr-Ti-O system

3.2.1. The gas phase

The gas phase is described as an ideal mixture containing the species Cu, CuO, O, O_2, O_3, Pb, Pb_2, PbO, Pb_2O_2, Pb_3O_3, Pb_4O_4, Pb_5O_5, Pb_6O_6, Zr, Zr_2, ZrO_2, ZrO, Ti, TiO and TiO_2. The Gibbs energy of the gas phase is given as

$$G^{\text{gas}} = \sum_i x_i \, {}^{\circ}G_i^{\text{gas}} + RT \sum_i x_i \, \ln x_i + RT \ln(P / P_0) \, , \tag{3.1}$$

where x_i is the mole fraction of the specie i in the gas phase, ${}^{\circ}G_i^{\text{gas}}$ the standard Gibbs energy of the gaseous specie i [1997SGTE, 1998Ris], R the gas constant, and P_0 the standard pressure of 1 bar.

3.2.2. The liquid phase

The liquid in the Cu-Pb-Zr-Ti-O system was described by both the two-sublattice ionic liquid model (Cu^{+1}, Cu^{+2}, Pb^{+2}, Zr^{+4}, Ti^{+2}, Ti^{+3}, Ti^{+4})$_p$ (O^{-2},Va)$_q$ (Eqs. 2.13 - 2.15) or by the associate solution model (Cu, Cu_2O, O, Ti, TiO, $TiO_{1.5}$, TiO_2, Pb, PbO, Zr, ZrO_2) (Eqs. 2.11 - 2.12).

3.2.3. The *fcc*, *bcc* and *hcp* solid solutions

All three, *fcc*, *bcc* and *hcp* solid solutions are considered to dissolve oxygen interstitially. The oxygen solubility in all three phases is represented by a two-sublattice model based on the compound energy formalism with one sublattice occupied by metal atoms, Cu, Pb, Ti, and Zr and the other one occupied by oxygen and vacancies, *i.e.*, (Cu, Pb, Ti, Zr)$_1$(O,Va)$_u$. The stoichiometry u of the oxygen sublattice is based on the number of occupied interstitial sites per metal atom. In the case of the *fcc* phase u is equal to 1, while the complete occupation of interstitial sites corresponds to the MO oxide with the NaCl type structure. In the *hcp* phase the oxygen atoms are located in the octahedral sites, i.e. αTi, αZr [1977Mcl] and there is one octahedral site per metal atom. However, it is quite improbable that two neighbouring interstitial sites along the hexagonal *c*-axis are occupied simultaneously. Therefore, the stoichiometry of u = ½ is more realistic to describe the maximum oxygen solubility in the *hcp* phase. Although the location of oxygen atoms in the *bcc* phase is not clearly defined, it is likely that they also occupy octahedral sites. Structurally, there are three interstitial octahedral sites per metal atom, but obviously not all of them are available to oxygen atoms. It would be physically

sensible to assume every oxygen atom to block all the nearest interstitial sites and therefore, the stoichiometry *u* is chosen to be 1. In addition, in the most recent assessments of the Zr-O [2006Wan] and Ce-O [2006Zin] systems the same model for *bcc* was chosen. The molar Gibbs energy of these solid solutions is given by

$$\begin{aligned} G^{\varphi} &= y_{Ti}y_{Va}{}^{o}G^{\varphi}_{Ti:Va} + y_{Ti}y_{O}{}^{o}G^{\varphi}_{Ti:O} + y_{Zr}y_{Va}{}^{o}G^{\varphi}_{Zr:Va} + y_{Zr}y_{O}{}^{o}G^{\varphi}_{Zr:O} + y_{Cu}y_{Va}{}^{o}G^{\varphi}_{Cu:Va} \\ &+ y_{Cu}y_{O}{}^{o}G^{\varphi}_{Cu:O} + y_{Pb}y_{Va}{}^{o}G^{\varphi}_{Pb:Va} + y_{Pb}y_{O}{}^{o}G^{\varphi}_{Pb:O} + RT(y_{Ti}\ln y_{Ti} + y_{Zr}\ln y_{Zr} \\ &+ y_{Cu}\ln y_{Cu} + y_{Pb}\ln y_{Pb}) + uRT(y_{Va}\ln y_{Va} + y_{O}\ln y_{O}) + {}^{E}G^{\varphi}, \end{aligned} \tag{3.2}$$

where $^{\circ}G^{\varphi}_{Ti:Va}, {}^{o}G^{\varphi}_{Zr:Va}, {}^{o}G^{\varphi}_{Cu:Va}, {}^{o}G^{\varphi}_{Pb:Va}$ and $^{\circ}G^{\varphi}_{Ti:O}, {}^{o}G^{\varphi}_{Zr:O}, {}^{o}G^{\varphi}_{Cu:O}, {}^{o}G^{\varphi}_{Pb:O}$ are the expressions for the Gibbs energy of the pure *fcc*, *bcc*- or *hcp* metals, and the hypothetical compounds TiO, ZrO, CuO and PbO with *fcc* or *bcc* structure and Ti_2O, Zr_2O, Cu_2O and Pb_2O with *hcp* arrangements of metal atoms. ${}^{E}G^{\varphi}$ is the excess Gibbs energy which can be formulated by the expression (2.14).

The hypothetical end-members, *i.e.*, *bcc*-Cu, *hcp*-Cu, *bcc*-Pb, *hcp*-Pb, *fcc*-Ti and *fcc*-Zr are taken into consideration in the present work. They are unstable with respect to the structures stable at room temperature and 1 bar pressure. Their Gibbs energies, $^{\circ}G^{fcc}_{Ti:Va}, {}^{o}G^{fcc}_{Zr:Va}, {}^{o}G^{bcc}_{Cu:Va}, {}^{o}G^{hcp}_{Cu:Va}, {}^{o}G^{bcc}_{Pb:Va}, {}^{o}G^{hcp}_{Pb:Va}$ as well as $^{\circ}G^{fcc}_{Ti:O}$ are taken from the SGTE unary database [2001SGTE] and Ref. [1997Lee], respectively, while ${}^{o}G^{fcc}_{Zr:O}, {}^{o}G^{bcc}_{Cu:O}, {}^{o}G^{hcp}_{Cu:O}, {}^{o}G^{bcc}_{Pb:O}$ and $G^{hcp}_{Pb:O}$ are estimated in this work to ensure the instability of these hypothetical respective solid solutions.

3.2.4. The PbO solid solutions (αPbO, βPbO)

The Gibbs energy of the solid solutions of PbO with TiO_2 and ZrO_2 is described by the substitutional solution model. It is expressed by Eq. 2.11 - 2.12.

3.2.5. The $\beta Zr_xTi_{1-x}O_4$ solid solution

The $\beta Zr_xTi_{1-x}O_4$ compound shows a homogeneity range in the quasibinary ZrO_2-TiO_2 section towards both the titania and zirconia solid solution. Consequently, in the present work it is treated as a non-stoichiometric phase. According to the crystal structure [1986Bor], there is only one crystallographic position for the metal atoms, which is shared by Ti and Zr. This phase is modelled using the substitutional solution model (TiO_2, ZrO_2). Its Gibbs energy is represented by Eqs. 2.11-2.12.

3.2.6. The ZrO_2 solid solutions

Similarly to $\beta Zr_xTi_{1-x}O_4$, the substitutional solution model (ZrO_2,TiO_2) is adopted for the description of the solubility of titania in αZrO_2 and βZrO_2 in the TiO_2-ZrO_2 subsystem (Table 1, Appendix). αZrO_2 and βZrO_2 solid solutions exhibit a significant solubility of titania, but they do not show an oxygen non-stoichiometry in the binary Zr-O system. At the same time, the two-sublattice model $(Zr^{+2}, Zr^{+4}, Ti^{+4})_1(O^{-2}, Va)_2$ is used for the modeling of both, oxygen non-stoichiometry and solubility of titania in γZrO_2 (Table 1, Appendix). The description of oxygen non-stoichiometry in γZrO_2 is taken from the literature [2006Wan], while the solubility of titania is modelled in the present work. In the quasibinary TiO_2-ZrO_2 system the model becomes $(Zr^{+4}, Ti^{+4})_1(O^{-2})_2$, which is equivalent to ZrO_2 and TiO_2. The Gibbs energy of αZrO_2 and βZrO_2 is represented by Eqs. 2.11 - 2.12, while the Eqs. 2.13 - 2.14 are valid for γZrO_2.

3.2.7. The $\beta PbZr_xTi_{1-x}O_3$ solid solution

The cubic high-temperature modification of $PbZr_xTi_{1-x}O_3$ solid solution is described using a substitutional model for $PbTiO_3$ and $PbZrO_3$. Similarly as in $\beta Zr_xTi_{1-x}O_4$, titania and zirconia solid solutions, in the $PbZr_xTi_{1-x}O_3$ solid solution one crystallographic position is shared by Ti and Zr [1978Gla]. The Gibbs energy of the end-members is expressed by Eq. 2.1 and that of the solid solutions is given by Eqs. 2.11-2.12.

3.2.8. The TiO_x phase

In the present work, $(Ti^{2+},Ti^{3+},Va)_1(Ti,Va)_1(O^{2-})_1$ model is adopted for the description of the non-stoichiometric TiO_x solid solution directly from the previous assessment of the Ti-O system [1994Lee, 1997Lee]. Although the non-stoichiometric TiO_x exhibits four structural modifications [1987Mur] all these phases were described by a single thermodynamic model, based on the rock-salt structure of the high-temperature γ-TiO modification. The deviations from the stoichiometric composition toward both the Ti- and O-rich side can be successfully described by the introduction of neutral Ti atoms in the interstitial sites and by the introduction of Ti^{3+} ions and vacancies in the cation sublattice, as described in details in Refs. [1994Lee, 1997Lee]. The molar Gibbs energy is defined as

$$\begin{aligned} G^{TiO_x} &= y_{Ti^{2+}} y_{Ti}\, {}^oG_{Ti^{2+}:Ti:O^{2-}} + y_{Ti^{3+}} y_{Ti}\, {}^oG_{Ti^{3+}:Ti:O^{2-}} + y'_{Va} y_{Ti}\, {}^oG_{Va:Ti:O^{2-}} \\ &+ y_{Ti^{2+}} y''_{Va}\, {}^oG_{Ti^{2+}:Va:O^{2-}} + y_{Ti^{3+}} y''_{Va}\, {}^oG_{Ti^{3+}:Va:O^{2-}} + y'_{Va} y''_{Va}\, {}^oG_{Va:Va:O^{2-}} \\ &+ RT(y_{Ti^{2+}} \ln y_{Ti^{2+}} + y_{Ti^{3+}} \ln y_{Ti^{3+}} + y'_{Va} \ln y'_{Va}) + RT(y_{Ti} \ln y_{Ti} + y''_{Va} \ln y''_{Va}) + {}^EG^{TiO_x}, \end{aligned} \tag{3.3}$$

where

$$\begin{aligned} {}^EG^{TiO_x} &= y_{Ti^{2+}} y_{Ti^{3+}} y_{Ti} L_{Ti^{2+},Ti^{3+}:Ti:O^{2-}} + y_{Ti^{2+}} y'_{Va} y_{Ti} L_{Ti^{2+},Va:Ti:O^{2-}} + y_{Ti^{3+}} y'_{Va} y_{Ti} L_{Ti^{3+},Va:Ti:O^{2-}} \\ &+ y_{Ti^{2+}} y_{Ti^{3+}} y''_{Va} L_{Ti^{2+},Ti^{3+}:Va:O^{2-}} + y_{Ti^{2+}} y'_{Va} y''_{Va} L_{Ti^{2+},Va:Va:O^{2-}} + y_{Ti^{3+}} y'_{Va} y''_{Va} L_{Ti^{3+},Va:Va:O^{2-}} \\ &+ y_{Ti^{2+}} y_{Ti} y''_{Va} L_{Ti^{2+}:Ti,Va:O^{2-}} + y_{Ti^{3+}} y_{Ti} y''_{Va} L_{Ti^{3+}:Ti,Va:O^{2-}} + y'_{Va} y_{Ti} y''_{Va} L_{Va:Ti,Va:O^{2-}}, \end{aligned} \tag{3.4}$$

and y'_{Va} and y''_{Va} correspond the vacancies in the first and the second sublattices, respectively.

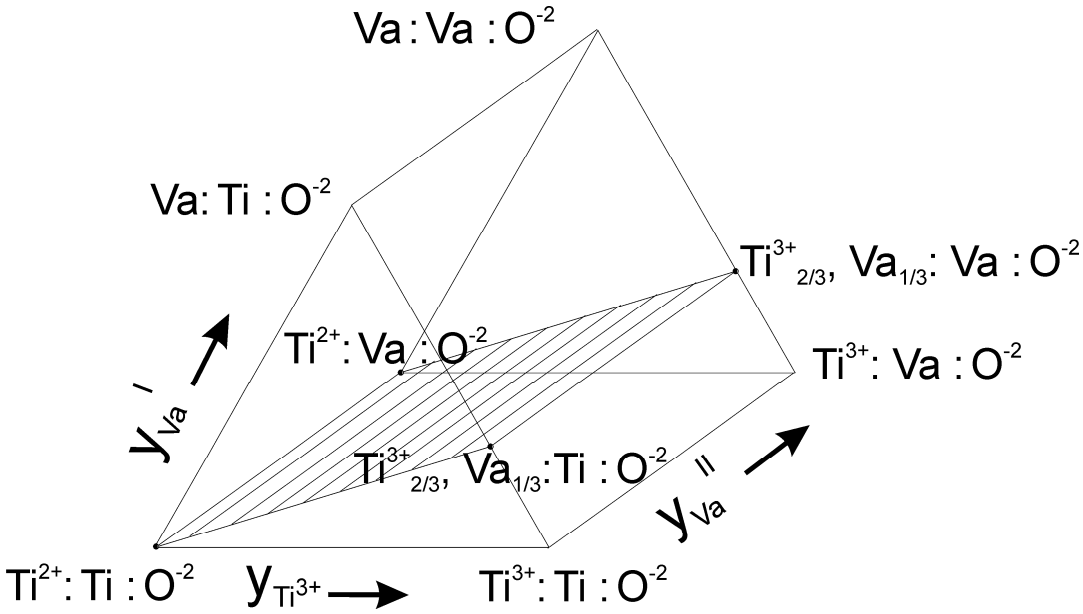

Fig. 3.2. The composition square of the TiO_x phase with the model $(Ti^{2+}, Ti^{3+}, Va)_1(Ti, Va)_1(O^{-2})_1$. The shaded plane shows the possible compositions without a net charge. y'_{Va} and y''_{Va} are the fractions of vacancies in the first and second sublattices , respectively.

The sublattice model is shown as a prism in Fig. 3.2. Most of the corners correspond to unphysical compounds with a net charge. Two corners correspond to the neutral compounds, i.e., $(Ti^{2+})_1\ (Ti)_1\ (O^{2-})_1$ and $(Ti^{2+})_1\ (Va)_1\ (O^{2-})_1$ and another two neutral end-members are obtained by combination of Ti^{3+} and vacancies on the first sublattice, *i.e.*, $(Ti^{3+}_{.667}\ Va_{.333})_1(Ti)_1(O^{2-})_1$ and $(Ti^{3+}_{.667}\ Va_{.333})_1(Va)_1(O^{2-})_1$.

3.2.9. The TiO_{2-z} (rutile) phase

The two-sublattice model $(Ti^{4+},Ti^{3+}, Zr^{+4})_1(O^{2-},Va)_2$ is adopted for the description of both oxygen non-stoichiometry in the binary Ti-O system and the solubility of zirconia in rutile in the TiO_2-ZrO_2 subsystem (Table 1, Appendix). The Gibbs energy of the rutile phase with both oxygen non-stoiciometry and solubility of zirconia is given by Eqs. 2.13-2.14.

For the modelling of the oxygen non-stoichiometry of rutile in the binary Ti-O system, the solubility of zirconium is omitted. Stoichiometric titanium dioxide in its stable modification rutile has a structure with two atomic positions in the unit cell, one for Ti^{4+} (2*a*) and one for O^{2-} (4*f*). Non-stoichiometric rutile has an O/Ti ratio less than two. The nature of the defect structure in TiO_{2-z} is not yet fully understood and there is some controversy in the literature. The experimental data suggest the existence of either doubly charged oxygen vacancies and free electrons [1983Zad, 1967Alc, 2000Jac, 1962Kof, 1964For, 1985Mar] or their combination with interstitially dissolved titanium Ti^{+3} ions [1963Blu, 1979Dir, 1975Pic]. In the present work the oxygen vacancy model is preferred. The lack of negative charges in the anion sublattice due to oxygen vacancies is effectively compensated by substitution of Ti^{3+} for Ti^{4+} in the cation sublattice, and thus, non-stoichiometry of rutile can be expressed as $(Ti^{4+},Ti^{3+})_1(O^{2-},Va)_2$. The molar Gibbs energy is then defined as

$$\begin{aligned} G^{TiO_{2-x}} &= y_{Ti^{4+}} y_{O^{2-}} {}^{\circ}G_{Ti^{4+}:O^{2-}} + y_{Ti^{3+}} y_{O^{2-}} {}^{\circ}G_{Ti^{3+}:O^{2-}} + y_{Ti^{4+}} y_{Va} {}^{\circ}G_{Ti^{4+}:Va} + y_{Ti^{3+}} y_{Va} {}^{\circ}G_{Ti^{3+}:Va} \\ &+ RT\left(y_{Ti^{4+}} \ln y_{Ti^{4+}} + y_{Ti^{3+}} \ln y_{Ti^{3+}}\right) + 2RT\left(y_{O^{2-}} \ln y_{O^{2-}} + y_{Va} \ln y_{Va}\right) + {}^{E}G^{TiO_{2-x}}. \end{aligned} \tag{3.5}$$

Due to the narrow non-stoichiometry range of rutile the excess term ${}^{E}G^{TiO_{2-x}}$ is set equal to 0 in this assessment. The °*G*-terms correspond to the Gibbs energy of different compounds formed by considering only one specie in each sublattice. The model is shown by the composition square in Fig. 3.3. The neutral end-member ${}^{\circ}G_{Ti^{4+}:O^{2-}}$ corresponds to the stoichiometric rutile, while the other three end-members, *i.e.* corners of the composition square, correspond to unphysical compounds with a net charge. The neutral compound $TiO_{1.5}$ located at the neutral line (Fig. 3.3.) is obtained by the combination of $(Ti^{3+})(O^{2-})_2$ and $(Ti^{4+})(Va)_2$ and corresponds to the hypothetical Ti_2O_3 compound with a rutile-related structure and the molar Gibbs energy

$${}^{\circ}G_{TiO_{1.5}} = \frac{1}{2}{}^{\circ}G_{R-Ti_2O_3} = \frac{3}{4}{}^{\circ}G_{Ti^{3+}:O^{2-}} + \frac{1}{4}{}^{\circ}G_{Ti^{3+}:Va} + 2RT\left(\frac{3}{4}\ln\frac{3}{4} + \frac{1}{4}\ln\frac{1}{4}\right), \tag{3.6}$$

where the last term is due to the ideal entropy of mixing at the anion sublattice.

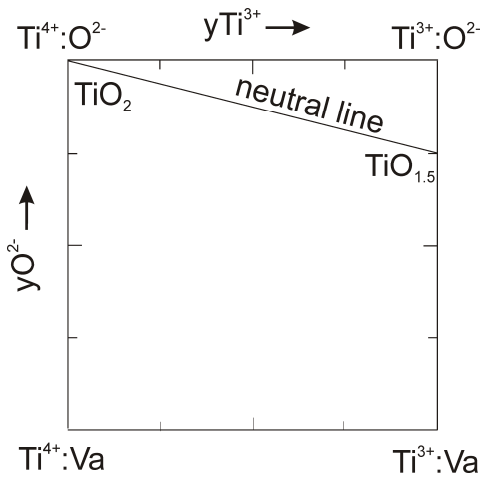

Fig. 3.3. The composition square of the TiO_{2-z} phase with the model $(Ti^{4+}, Ti^{3+})_1(O^{2-},Va)_2$. The combinations with the electroneutrality are marked as neutral line. $y_{Ti^{3+}}$ and $y_{O^{2-}}$ are the site fractions of Ti^{3+} in the first sublattice and of O^{2-} in the second one.

Additional two end-members can be defined by Eqs. 3.7 and 3.8:

$$°G_{Ti^{4+}:Va} = °G_{TiO_2} - °G_{O_2(g)} \tag{3.7}$$

$$°G_{Ti^{4+}:O^{2-}} + °G_{Ti^{3+}:Va} = °G_{Ti^{4+}:Va} + °G_{Ti^{3+}:O^{2-}} \ , \tag{3.8}$$

where the term $°G_{Ti^{4+}:Va}$ (Eq. 3.7) is chosen to be the reference and the last one, $°G_{Ti^{3+}:Va}$ is determined using the reciprocal relation given by Eq. 3.8.

Similarly to the zirconia solid solutions (Section 3.2.6.) the solubility of zirconia in rutile is only modelled in the TiO_2-ZrO_2 system. In this case, the oxygen non-stoichiometry of rutile is omitted and it can be described by $(Ti^{+4}, Zr^{+4})_1 (O^{-2})_2$ model.

3.2.10. The $(Cu,Ti)O_z$ and $CuTi_2O_z$ phases

In the present study the model for the CuTi phase, $(Cu,Ti)_1$ $(Cu,Ti)_1$ [1996Kum] was extended into the ternary system Cu-Ti-O by introducing the one more sublattice for interstitial oxygen and vacancies. The same was done for the $CuTi_2$ phase which is modelled as a stoichiometric compound in the binary system. Because the stoichiometric CuTi (*tP*4, *P*4/*nmm*) and $CuTi_2$ (*tI*6, *I*4/*nmm*) phases have the ordered *fcc* and *bcc* structure, respectively, the number of sites on the interstitial sublattices was given to the same as in the corresponding interstitial solid solution models. Therefore, the formula unit for CuTi becomes $(Cu, Ti)_{.5}$ $(Cu, Ti)_{.5}(O, Va)_1$. The Gibbs energy of the $(Cu,Ti)O_z$ phase is expressed as follows:

$$\begin{aligned} G^{(Cu,Ti)O_z} &= y'_{Cu}y''_{Cu}y_O{}^oG_{Cu:Cu:O} + y'_{Cu}y''_{Ti}y_O{}^oG_{Cu:Ti:O} + y'_{Cu}y''_{Cu}y_{Va}{}^oG_{Cu:Cu:Va} \\ &+ y'_{Cu}y''_{Ti}y_{Va}{}^oG_{Cu:Ti:Va} + y'_{Ti}y''_{Cu}y_O{}^oG_{Ti:Cu:O} + y'_{Ti}y''_{Ti}y_O{}^oG_{Ti:Ti:O} \\ &+ y'_{Ti}y''_{Cu}y_{Va}{}^oG_{Ti:Cu:Va} + y'_{Ti}y''_{Ti}y_{Va}{}^oG_{Ti:Ti:Va} \\ &+ 1/2\,RT(y'_{Cu}\ln y'_{Cu} + y'_{Ti}\ln y'_{Ti}) \\ &+ 1/2\,RT(y''_{Cu}\ln y''_{Cu} + y''_{Ti}\ln y''_{Ti}) \\ &+ RT(y_{Va}\ln y_{Va} + y_O\ln y_O) + {}^EG^{(Cu,Ti)O_z}. \end{aligned} \tag{3.9}$$

The excess Gibbs energy is

$$\begin{aligned} {}^EG^{(Cu,Ti)O_z} &= y'_{Cu}y'_{Ti}(y''_{Cu}y_{Va}L_{Cu,Ti:Cu:Va} + y''_{Ti}y_{Va}L_{Cu,Ti:Ti:Va} + y''_{Cu}y_OL_{Cu,Ti:Cu:O} \\ &+ y''_{Ti}y_OL_{Cu,Ti:Ti:O}) + y''_{Cu}y''_{Ti}(y'_{Cu}y_{Va}L_{Cu:Cu,Ti:Va} + y'_{Ti}y_{Va}L_{Ti:Cu,Ti:Va} \\ &+ y'_{Cu}y_OL_{Cu:Cu,Ti:O} + y'_{Ti}y_OL_{Ti:Cu,Ti:O}) + y_Oy_{Va}(y'_{Ti}y''_{Ti}L_{Ti:Ti:O,Va} \\ &+ y'_{Cu}y''_{Cu}L_{Cu:Cu:O,Va} + y'_{Cu}y''_{Ti}L_{Cu:Ti:O,Va} + y'_{Ti}y''_{Cu}L_{Ti:Cu:O,Va}), \end{aligned} \tag{3.10}$$

where y'_{Cu}, y'_{Ti} and y''_{Cu} , y''_{Ti} are the site fractions of the Cu and Ti on the first and second sublattices, respectively, and $y_O = 1 - y_{Va} = z$.

The model $(Cu)_{1/3}$ $(Ti)_{2/3}$ $(O, Va)_1$ was adopted for the description of the dissolution of oxygen in $CuTi_2$. The Gibbs energy is given as

$$G^{CuTi_2O_z} = y_{Va}G_{Cu:Ti:Va} + y_O G_{Cu:Ti:O} + RT(y_O \ln y_O + y_{Va} \ln y_{Va}) + y_{Cu} y_{Ti} y_{Va} y_O L_{Cu:Ti:O,Va}, \quad (3.11)$$

where $y_O = 1 - y_{Va} = z/3$.

4. BINARY SYSTEMS

The systems Cu-O, Zr-O, Cu-Pb, Cu-Ti and Cu-Zr are accepted from the literature. They are briefly presented in this Chapter. The thermodynamic description of the Ti-O system using the associate solution model for the liquid phase was evaluated in this thesis. The description of the liquid phase in the Pb-O system was revised using both, the associate and two-sublattice model. The influence of the applied models on the thermodynamic properties of the liquid phase in the ternary Cu-Pb-O, Cu-Ti-O and Cu-Zr-O systems will be shown in Chapters 5.1 - 5.3. For this purpose, the parameters of the two-sublattice ionic liquid model reported by Hallstedt and Gauckler [2003Hal] for Cu-O and Lee [1994Lee] for Ti-O systems were accepted. The equivalence between the ionic two-sublattice and associate model in a binary system, where the cation and anion show only one oxidation state was demonstrated by Hillert et al. [1985Hil1]. However, if the oxidation state of metal can vary, there is no direct translation between the models. The equivalence also breaks down in ternary and higher-order systems because there are more compositional variables in the associate model than in the two-sublattice one.

The complete miscibility between Ti and Zr in both *bcc* and *hcp* solid solutions is present in the Ti-Zr system and two invariant equilibrium points at 1813 (~ 40 at. % Zr) and 878 K (~ 50 at. % Zr)[1986Mas] correspond to the reactions liquid ↔ *bcc* and *bcc* ↔ *hcp*, respectively. Intermetallic compounds, Ti_4Pb and Pb_3Zr_5 are confirmed in the Ti-Pb and Pb-Zr systems [1986Mas], respectively, while the existence of Ti_2Pb and $PbZr_5$ is doubtful. Phase relations in the Ti-Pb and Pb-Zr systems are not well established, particularly the phase equilibria involving the liquid phase, while the experimental information for the Pb-rich part of phase diagrams is completely missing. Thermodynamic parameters of the binary Pb-Zr, Pb-Ti and Ti-Zr systems are not considered in this thesis since extrapolations into the multicomponent Cu-Pb-Zr-Ti-O system concerning metal-rich solid solutions based on Pb, Zr and Ti are not relevant in the optimization of manufacturing and sintering conditions of the PZT (PbO-ZrO_2-TiO_2) ceramics with copper. At the same time, the solubility of the Pb, Zr,Ti and O in *fcc*-Cu is

important for practical applications and it is considered in the systems Cu-O, Cu-Pb, Cu-Ti and Cu-Zr described in this Chapter.

4.1. The Ti-O system

Most of the crystallographic data concerning to the condensed phases of the Ti-O system have been reported by Murray and Wriedt [1987Mur]. The titanium metal exists in two modifications, αTi (*hcp*) and βTi (*bcc*) with extensive oxygen solubility giving the interstitial solid solutions. The Ti-O system contains TiO_x with a wide homogenity range, non-stochiometric rutile, TiO_{2-z} which is an oxygen rich phase as well as several stoichiometric compounds between the monoxide and rutile with the generalized formula Ti_nO_{2n-1} ($n \geq 2$) which are called Magneli phases, Ti_3O_2 and αTiO, a low-temperature modification of TiO_x solid solution (Table 4.1.1). TiO_{2-z} and Ti_2O_3 are well known compounds. The highest possible value of n in Ti_nO_{2n-1} is yet to be experimentally investigated. It was suggested that discrete equilibrium phases exist for $n \leq 99$ [1972Roy], while the maximum value of n is estimated to be 28 by Jacob et al. [2000Jac] based on composition of the Magneli phases in equilibrium with TiO_{2-z}. Magneli phases have the crystal structures derived from the rutile structure by crystallographic shear. In addition to rutile, TiO_2 has two metastable low-pressure modifications (anatase and brookite) and two nonequilibrium high-pressure forms.

Several modeling works of the Ti-O system were done [1964Kau, 1992Sau, 1992Paj, 1994Lee, 1997Lee, 1993Eri, 1999Wal, 2006Kan, 2006Can]. Magneli phases and the non-stoichiometry of rutile were first taken into account in the work of Eriksson and Pelton [1993Eri], for the modeling of the Ti_2O_3-TiO_2 subsystem. The most extensive evaluation of the Ti-O system was done by Waldner and Eriksson [1999Wal]. They presented complete Ti-O phase diagram from pure titanium to gaseous oxygen including Magneli phases. For the modelling of TiO_x solid solution, the two-sublattice definition based on bond energy model [1993Oat, 1996Oat] was adopted. A substitutional model used for description of the liquid phase [1964Kau, 1992Sau, 1992Paj] is clearly a very crude

approach for the system with strong interactions, such as Ti-O. The two-sublattice ionic liquid model [1994Lee, 1997Lee, 1999Wal] is physically well-sounded; however, it may

Table 4.1.1 Solid phases of the binary Ti-O system.

Phase, temp. range (K)	Pearson symbol	Space group	Prototype	Lattice parameter (pm) and angles	Comments
αTi T< 1155	*hP*2	$P6_3/mmc$	Mg	a=b=295.08; c=468.55; γ=120°	pure Ti at 298 K [1968Paw]
βTi 1155 < T < 1943	*cI*2	$Im\bar{3}m$	W	a=331.11;	pure Ti [1959Spr]
Ti_3O_2 T< 1193	*hP*5	*P*6/*mmm*	–	a=b=499.15; c=287.94; γ=120°	[1959And]
TiO_x 733 < T< 2043	*cF*8	*Fm*3*m*	rocksalt, NaCl	a=420.43;	[1997Bar]
αTiO T< 1213	*mC16*	*A*2/*m*	–	a=585.5; b=934.0; β=107.53°	[1967Wat]
Ti_2O_3 T< 2115	*hR*30	$R\bar{3}c$	corundum, α-Al_2O_3	a=542.5; α=56.73°	[1957And]
Ti_3O_5 800 < T< 2050	*mC*32	*C*2/*m*	–	a=975.7; b=380.2; c=945.2; β=93.11°	[1957And]

Ti_4O_7
T< 1940
	*aP*44	$P\bar{1}$	–	a=559.1; b=713.1;
				c=1248.7;
				α=95°; β=98.33°;
				γ=108.88°
					[1973Mer]

Ti_5O_9	*aP*28	$P\bar{1}$	–	a=556.9; b=712.0;
				c=886.5;
				α=97.55°; β=112.34°;
				γ=108.50°
					[1960And]

Ti_6O_{11}	*aC*68	$A\bar{1}$	–	a=556.6; b=714.4; c=2047; α=98.5°; β=120.8°; γ=108.50°	[1963And]
Ti_7O_{13}	*aP*40	$P\bar{1}$	–	a=554; b=713; c=1536; α=98.9°; β=125.5°; γ=108.50°	[1963And]
Ti_8O_{15}	*aC*92	$A\bar{1}$	–	a=557; b=713.3; c=3746; α=98.9°; β=125.5°; γ=108.50°	[1963And]

Ti_9O_{17}	*aI*52	$P\bar{1}$	–	a=552.72; b=714.13;
				c=2227.88;
				α=99.26°; β=130.34°;
				γ=108.50°
					[1963And]

Rutile T< 2143	*tP*6	$P4_2/mnm$	rutile, TiO_2	a = b = 459.37; c = 295.87;	[1982Gon]

result in unexpected miscibility gaps in higher-order systems at high temperatures (see Chapter 5.2). The quasichemical model for the liquid phase [1993Eri, 2006Kan] may be superior to both ionic and associate formalisms but, unfortunately it was developed for only limited composition range, *i.e.*, between Ti_2O_3 and TiO_2. The modeling work reported by author of this thesis [2006Can] is done using an associate model for the liquid, which can successfully be used for calculations in multicomponent systems containing Ti and O. In addition, the TiO_x solid solution was remodeled using a compound energy formalism, which is compatible with most of the commercial software for thermodynamic calculations.

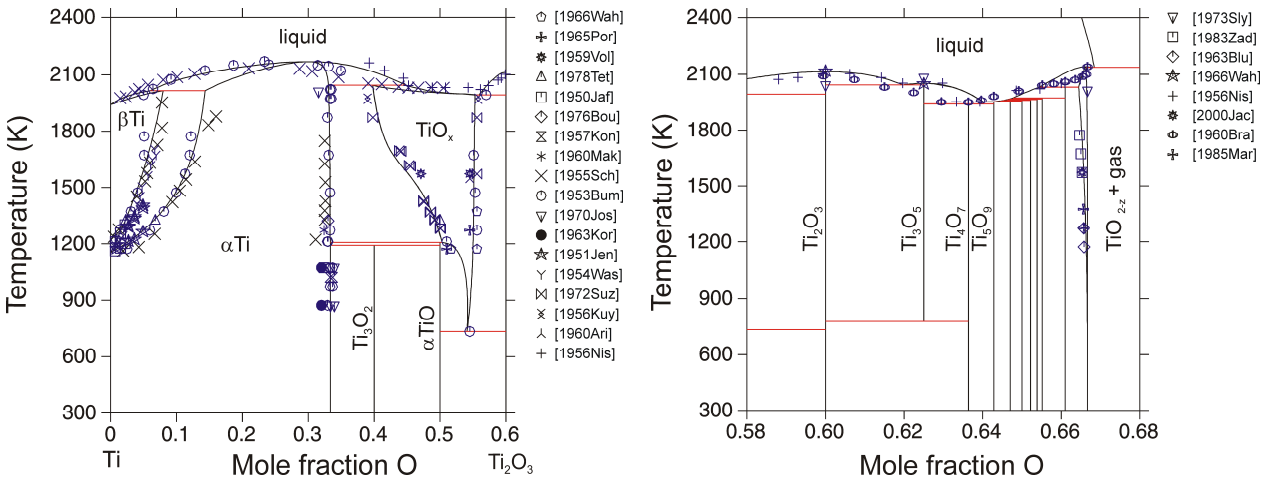

(a) (b)

Fig. 4.1.1 Calculated Ti-O phase diagram up to 60 at.% O (a) and between Ti_2O_3 and rutile in comparison with experimental data.

The optimized thermodynamic parameters are compiled in the Appendix (Table 1). Fig. 4.1.1a shows the phase diagram of Ti-O system calculated up to 60 at.% of oxygen in the temperature range 300 - 2400 K for the total pressure of 1 bar in comparison with experimental data. The phase diagram showing the equilibria in the composition range between Ti_2O_3 and rutile together with experimental data is presented in Fig. 4.1.1b. The descriptions of Magneli phases are taken from Ref. [1999Wal] and are very slightly modified for the Ti_4O_7, Ti_5O_9 and Ti_7O_{13} to better fit the phase boundaries. It is evident that the present calculation is well consistent with the most of experimental information.

In addition, it should be noted that the calculated phase diagrams in Figs. 4.1.1a and b are very similar to those already presented by Waldner and Eriksson [1999Wal]. Some minor differences originate from the different modelling of the liquid phase. Therefore, these calculated results are not discussed here in details, but intended to demonstrate the ability of the associate model to describe phase equilibria in the Ti-O system. However, the liquid + rutile + gas equilibrium is predicted to be of eutectic type [2006Can] instead of peritectic one calculated in Ref. [1999Wal]. The calculated fractions of different associates in the liquid phase at 2150 K are shown in Fig. 4.1.2. Waldner and Eriksson [1999Wal] published similar diagram for the limited composition range (Ti - TiO_2) and mentioned the strong disproportionation of Ti^{3+} onto Ti^{2+} and Ti^{4+}. Their conclusion is confirmed in the present work, since the fraction of the $TiO_{1.5}$ specie at the composition of 60 at.% O is around 0.65. Additionally, it is found that the TiO specie also disproportionates into Ti and $TiO_{1.5}$.

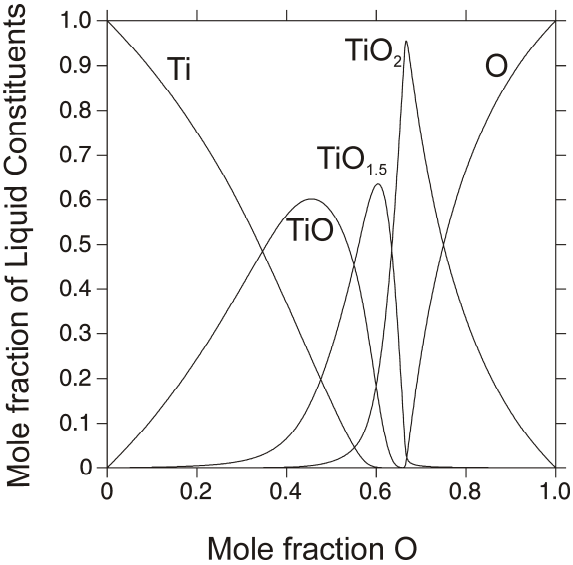

Fig. 4.1.2 Calculated species distribution in the liquid at 2150 K.

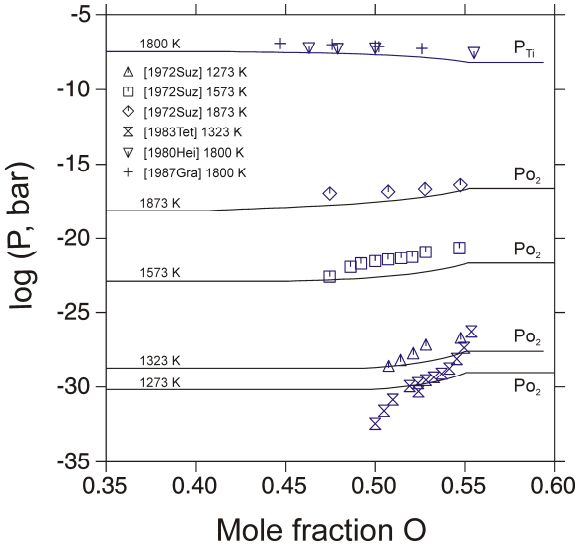

Fig. 4.1.3 Calculated partial pressures of oxygen and titanium over the TiO_x solid solution in comparison with experimental data.

Fig. 4.1.3 shows the calculated partial pressure of oxygen and titanium over the TiO_x solid solution together with experimental points. The calculated and measured values are

in good agreement. At the lowest temperature of 1273 K, the experimental data of Tetot et al. [1983Tet] show a considerable scatter, which is not surprising for the measurements of such low pressures.

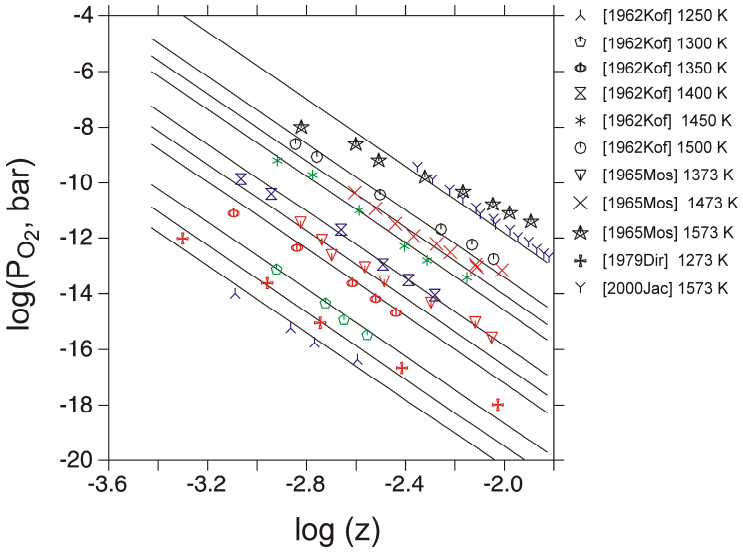

Fig. 4.1.4 Calculated partial pressures of oxygen within the homogeneity range of rutile TiO_{2-z} along with experimental points.

The compound energy model used for rutile is able to give a good correspondence between the calculated and measured partial pressure of oxygen within its homogeneity range (Fig. 4.1.4). As a result of the optimization, the enthalpy and entropy of melting of TiO_2 are 67268.7 J/mol and 31.417 J/(mol K), respectively, which can be compared to the values reported in JANAF tables [1998Cha] (calculated values): 68000 J/mol, and 31.121 J/(mol K), respectively. The optimized melting temperature of rutile is 2141.2 K. The heat capacity of liquid TiO_2 is assumed to have the same temperature dependence, as for solid phase.

4.2. The Pb-O system

In the Pb-O system, there are five compounds, PbO, Pb_3O_4, $Pb_{12}O_{17}$, $Pb_{12}O_{19}$, and PbO_2. PbO exists in two stable modifications, as a red tetragonal form αPbO (litharge) and a yellow orthorhombic form βPbO (massicot) with a transition temperature of 762 K

[1998Ris] (Table 4.2.1). βPbO melts congruently at 1159 K under an oxygen pressure of 1 bar. There are no reports about the oxygen saturation limit in solid Pb, but it is certainly extremely small and could not be detected [1988Wri]. The liquid phase exhibits a large miscibility gap. Various parts of the Pb-O system have been assessed by different authors, while a consistent set of Gibbs energy functions is reported by Risold and co-workers [1998Ris]. The description of the liquid phase in the Pb-O system has been modified in the present work based on reasonable data selection by applying additional constraint from the ternary Cu-Pb-O system. Preliminary calculations have clearly shown that the existing thermodynamic description of the Pb-O system [1998Ris] inevitably results in an overestimating of the oxygen solubility in the metallic liquid of the ternary Cu-Pb-O system (see Chapter 5.1). Indeed, according to [1998Ris] the oxygen solubility in liquid lead is as high as 7 at.%, whereas the oxygen content in Cu-Pb liquids of ternary Cu-Pb-O system, which contain more than 50 at.% Pb, does not exceed 1 at.% [1954Geb, 1984Ani] (Fig. 5.1.8, Section 5.1). Therefore, the description of the liquid phase in the Pb-O system has been modified [2005Can]. The calculations with the parameters from Ref. [1998Ris] show close agreement with the most reliable data on the stability limits of the higher oxides in the PbO-PbO_2 part. For the Pb-PbO range, the spread in the data concerning the miscibility gap in the liquid phase is large and results of the least-squares optimization depend on the selected dataset. All experimental studies are confined to temperatures below 1473 K. The choice made in Ref. [1998Ris] results in the calculated phase diagram at a pressure of 1 bar, where the miscibility gap is predicted to close just above 1800 K. The binary interaction parameters were reoptimized using the experimental data on the oxygen solubility and activity in the Pb-rich [1959Bra, 1964Alc, 1974Kux, 1976Cha, 1977Ise, 1979Tas1, 1979Ots, 1981Ots] and PbO-rich liquid [1974Kux, 1977Ise]. The parameters are listed in Appendix (Tables 1 and 2).

The calculated solubility and activity of oxygen in the metallic liquid in comparison with experimental data are shown in Figs. 4.2.1. A very good agreement between the calculations and measurements can be seen. The binary phase diagram of the Pb-O system is shown in Fig. 4.2.2. The critical point of the miscibility gap is now shifted to about 4700 K.

Table 4.2.1 Solid phases of the binary Pb-O system.

Phase, temp. range (K)	Pearson symbol	Space Group	Prototype	Lattice parameters (pm) and angles	Comments
(Pb) T < 600.5	*cF*4	$Fm\bar{3}m$	Cu	a = 495.02	pure Pb at 298 K [1986Mas]
αPbO T < 760	*tP*4	*P*4/*nmm*	PbO	$a = b$ = 397.44; c = 502.20	mineral name: litharge [1985Boh]
βPbO T > 760	*oP*8	*Pbcm*	PbO	a = 589.31; b = 549.04; c = 475.28	mineral name: massicot [1985Hil2]
βPbO_2	*tP*6	$P4_2/mnm$	TiO_2	$a = b$ = 496.12; c = 338.52	mineral name: plattnerite [1981Har, 1926Fer]
αPbO_2	*oP*12	*Pbcn*	$FeNb_2O_6$	a = 494.70; b = 595.10 c = 549.70	mineral name: scrutinyite [1952Zas]
Pb_3O_4	*tP*28	$P4_2/mbc$	Pb_3O_4	$a = b$ = 882; c = 659	mineral name: minium [1965Fay]
Pb_2O_3	*mP*20	$P2_1/a$	-	a = 781.40; b = 562.7; c = 846.5; β = 124.97°	[1970Bou]

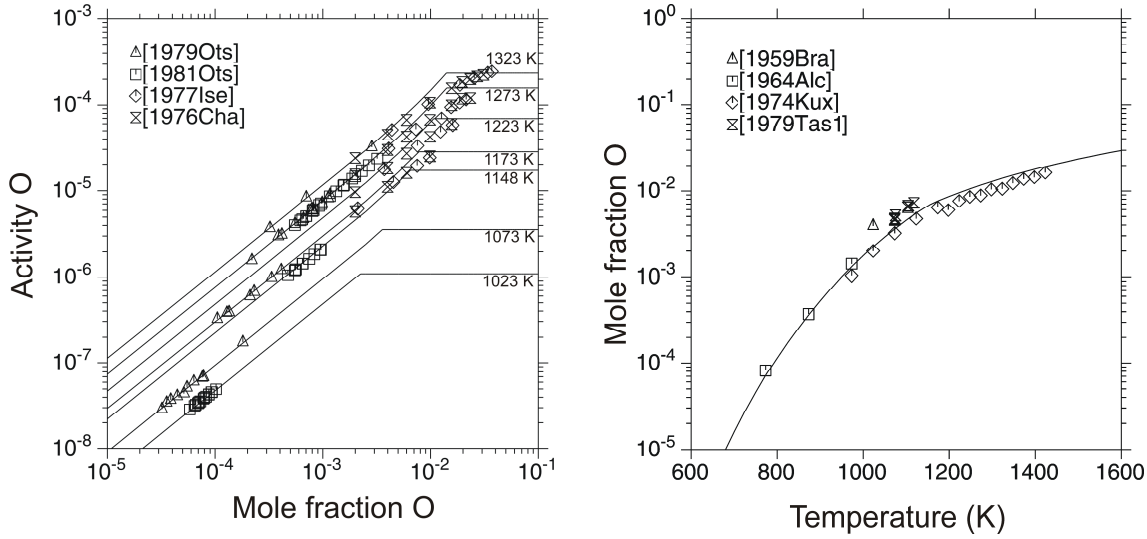

(a) (b)

Fig. 4.2.1 Calculated oxygen activity between 1023 and 1323 K (a) and solubility (b) in the Pb-rich liquid of the binary Pb-O system superimposed with experimental measurements.

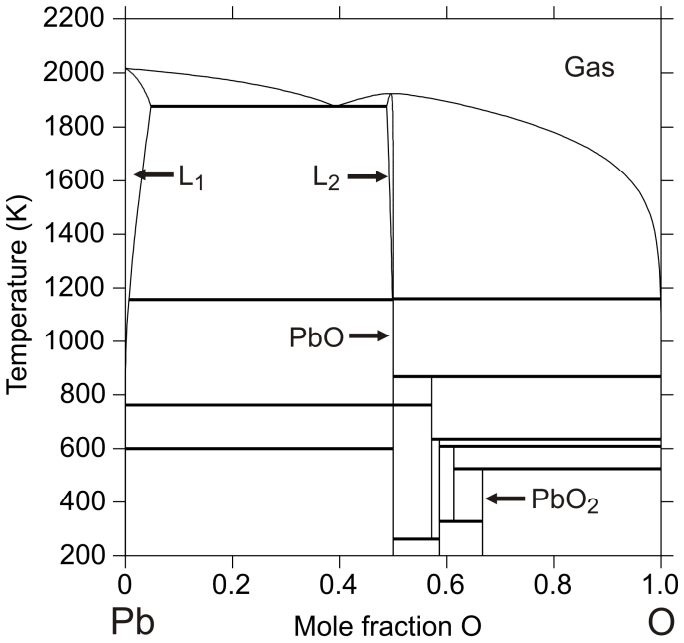

Fig. 4.2.2 The calculated Pb-O phase diagram at 1 bar total pressure.

4.3.The Cu-O system

In the Cu-O system, there are two stable oxides, Cu_2O (cuprite) and CuO (tenorite) (Table 4.3.1). In the liquid state there is a miscibility gap between Cu and Cu_2O below 1623 K. The oxygen solubility in solid Cu does not exceed 0.02 at.%. In air atmosphere, Cu_2O decomposes at 1397 K, while CuO dissociates at 1300 K. Several thermodynamic assessments of the Cu-O system have been published using the associate solution model [1983Sch, 1992Bou, 2004Cla] and the partially ionic model [1994Hal, 2003Hal] for the liquid phase. In the present work, for the thermodynamic modeling of multi-component system, the associate solution model is selected for description of liquid in Cu-O system [1992Bou]. Fig. 4.3.1 shows the calculated Cu-O phase diagram.

Table 4.3.1 Solid phases of the binary Cu-O system.

Phase, temp. range (K)	Pearson symbol	Space Group	Prototype	Lattice parameters (pm) and angles	Comments
(Cu) T < 1357.87	*cF*4	$Fm\bar{3}m$	Cu	*a* = 361.46	pure Cu at 298 K [1986Mas]
CuO	*mS*8	*C*2/*c*	CrS	*a* =469.01; *b* =342.01; *c* = 513.11; β = 99.54°	mineral name: tenorite [1998Mas]
Cu_2O	*cP*6	$Pn\bar{3}m$	Cu_2O	*a* = 426.72	mineral name: cuprite [1998Mas]

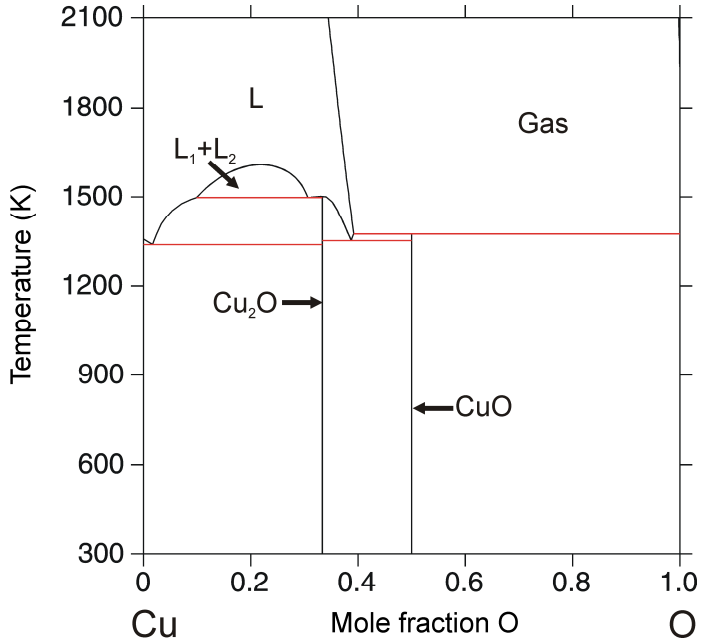

Fig. 4.3.1 The calculated Cu-O phase diagram at 1 bar total pressure [1992Bou].

4.4. The Zr-O system

The only one stable oxide ZrO_2, with the congruent melting point at about 2980 K, exists in Zr-O system presenting three structural modifications: monoclinic (α) below 1400 K, intermediate tetragonal (β) up to 1798 K, and cubic (γ) stable up to the melting point (Table 4.4.1). The cubic form has a homogeneity range towards oxygen deficiency formed by vacancies on the oxygen sublattice. The two other modifications have no

significant homogeneity range. Both solid forms of metallic zirconium, αZr (hexagonal close-packed, *hcp*) and βZr (body-centred cubic, *bcc*), show a remarkable solubility of oxygen. The *hcp* phase possesses a very large homogeneity range up to 35 at.% O and melts congruently at 2580 K (~ 25 at.% O). A detailed review of the experimental phase diagram and thermodynamic information for the Zr-O system was reported by Abriata et al. [1986Abr]. Several groups contributed to the thermodynamic modeling of the Zr-O system [1998Che, 2004Che1, 2001Lia, 2002Arr, 2004Che2, 2004Wan, 2006Wan]. The latest modeling work of Wang [2006Wan] is based on most recent and reliable experimental data for the $\alpha ZrO_2 \leftrightarrow \beta ZrO_2$ phase transformation. It was accepted in the present study. The calculated phase diagram is shown in Fig. 4.4.1.

Table 4.4.1 Solid phases of the binary Zr-O system.

Phase, temp. range (K)	**Pearson symbol**	**Space Group**	**Prototype**	**Lattice parameters (pm) and angles**	**Comments**
αZr T < 1136	*hP*2	$P6_3/mmc$	Mg	$a = b = 323.17$; $c = 514.76$; $\gamma = 120°$	[1960Lic]
βZr 1136 < T < 2128	*cI*2	$Im\bar{3}m$	W	$a = 360.90$;	[1986Mas]
αZrO_2 T < 1478	*mP*12	$P2_1/c$	-	$a = 515.104$; $b = 520.31$; $c = 531.514$; $\beta = 99.197°$	[2002Win] mineral name: baddeleyite
βZrO_2 1478 < T < 2650	*tP*6	$P4_2/nmc$	HgI_2	$a = b = 359.482$; $c = 518.247$;	[2000Bou]
γZrO_2 T > 2650	*cF*12	$Fm3m$	CaF_2	$a = 494.72$;	[2000Bou]

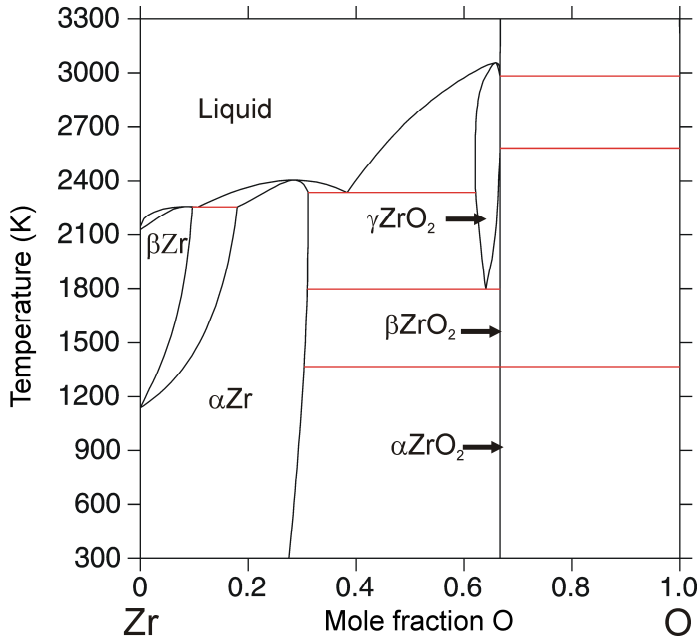

Fig. 4.4.1 The calculated Zr-O phase diagram at 1 bar total pressure [2006Wan].

4.5. The Cu-Pb system

The binary phase diagram of the Cu-Pb system shows a miscibility gap in the liquid phase, which closes above 1273 K. Since no intermediate phases exist in this system, it consists just of a monotectic reaction and an eutectic reaction. The terminal solid solutions are very limited at either end. Several thermodynamic assessments of the Cu-Pb system have been published [1986Nie, 1986Hay, 1991Tep, 2000Wan]. The thermodynamic dataset of Hayes and co-workers [1986Hay] is selected, because the calculated miscibility gap in the liquid phase agrees well with the most recent experimental report [1999Kha]. Also, a reasonable value for the solid solubility of Pb in (Cu) of 0.05 at.% at 873 K and a good fit to the experimental data on enthalpy and entropy of mixing of the liquid phase is obtained. The calculated phase diagram is shown in Fig. 4.5.1.

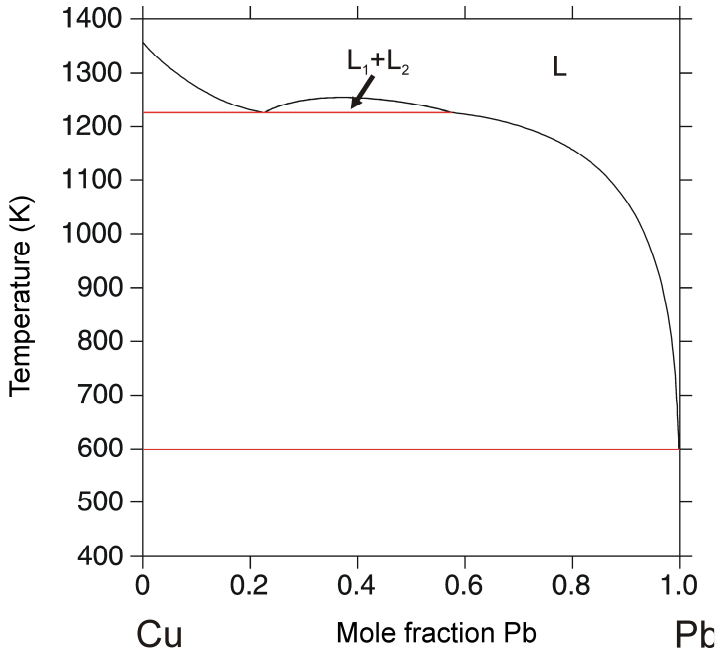

Fig. 4.5.1 The calculated Cu-Pb phase diagram [1986Hay].

4.6. The Cu-Ti system

The Cu-Ti system is characterized by a series of invariant reactions involving the liquid phase and seven intermetallic compounds (Table 4.6.1). A critical evaluation of phase diagram was done by [1958Han, 1965Ell, 1969Shu, 1973Hul, 1983Mur, 1994Mur, 1994Oka]. The compounds Cu_2Ti, Cu_3Ti_2, Cu_4Ti_3 and $CuTi_2$ are essentially stoichiometric. The compounds Cu_4Ti and CuTi show homogeneity ranges which extend on either sides of their stoichiometric composition. The enthalpy of mixing of the liquid is highly exothermic [1982Kle] and thus contributes to a large stability of the liquid phase with respect to the crystalline phases. This high stability promotes the existence of eutectic and peritectic points at much lower temperatures than the melting point of the pure components. A thermodynamic calculation of the phase diagram was performed by [1970Kau, 1978Kau, 1983Mur, 1985Sau, 1991Zen], but without considering the stable phases Cu_3Ti_2 and Cu_2Ti, while the non-stoichiometry of CuTi and Cu_4Ti was ignored. The thermodynamic modeling of the Cu-Ti system was also reported by Kumar et al. [1996Kum] as a substantial improvement of previous assessments. Most recently, Canale

and Servent [2002Can] experimentally confirmed the existence of the $CuTi_3$ phase and the description of this non-stoichiometric phase was adopted in the calculated phase diagram of the Cu-Ti system (Fig. 4.6.1).

Table 4.6.1 Solid phases of the binary Cu-Ti system.

Phase, temp. range (K)	**Pearson symbol**	**Space Group**	**Prototype**	**Lattice parameters (pm) and angles**	**Comments**
$CuTi_3$	*tP*4	*P*4/*mmm*	$CuFePt_2$	*a*=*b*=415.8; *c*=359.4;	[1951Kar]
$CuTi_2$ T < 1278	*tI*6	*I*4/*mmm*	$MoSi_2$	*a*=*b*=294.38; *c*=1078.61;	[1963Mue]
CuTi T < 1258	*tP*4	*P*4/*nmm*	γCuTi	*a* = *b* = 310.8; *c* = 588.7;	[1951Kar]
Cu_4Ti_3	*tI*14	*I*4/*mmm*	Ti_3Cu_4	*a* = *b* = 312; *c* = 1994;	[1964Sch]
Cu_3Ti_2 T < 1148	*tP*10	*P*4/*nmm*	Ti_2Cu_3	*a* = *b* = 313; *c* = 1395;	[1964Sch]
Cu_2Ti	*oC*12	*Amm*2	Au_2V	*a*=438; *b*=797; *c*=449;	[1964Sch]
Cu_4Ti T < 1158	*oP*20	*Pnma*	Au_4Zr	*a*=453; *b*=434.2; *c*=1293;	[1968Pfe]

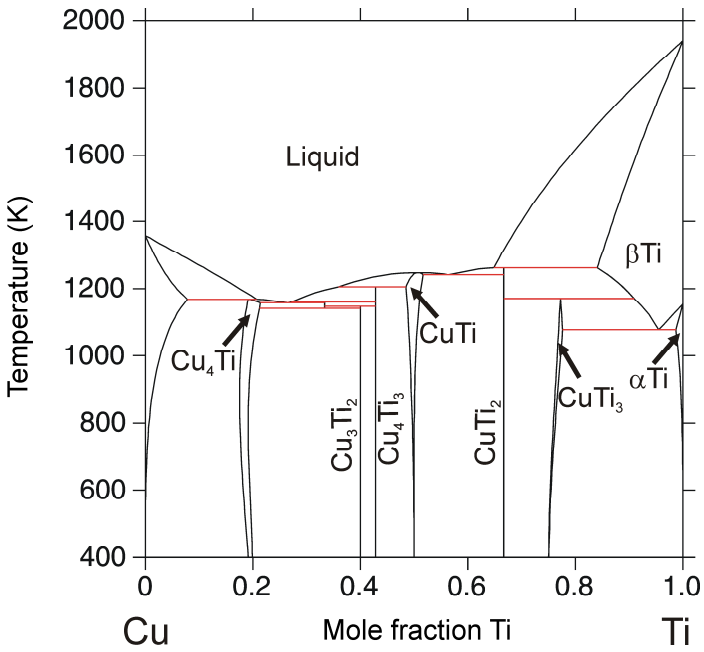

Fig. 4.6.1 The calculated Cu-Ti phase diagram [1996Kum] with the $CuTi_3$ phase included [2002Can].

4.7. The Cu-Zr system

.

The Cu-Zr system is also characterized by a series of peritectic and eutectic reactions and several intermetallic compounds (Table 4.7.1). However, there is a lot of confusion in the literature regarding the compositions of these compounds, particularly for the Cu-rich ones [1986Mas, 1986Kne, 1985Gli, 1983Sud, 1989Som, 1978Kuz]. It is generally accepted that there are six intermetallic phases in the Cu-Zr system [1985Gli, 1986Mas, 1984Lou, 1990Ari] and all of them are essentially stoichiometric. The solubility of zirconium in copper is ~ 0.1 at.% at 1250 K [1948Rau, 1960Saa], while the maximum solubility of copper in *bcc* zirconium (βZr) is about 2 at.% [1953Lun]. A few modeling studies of the Cu-Zr system were performed [1985Sau, 1988Bor, 1991Luo, 1994Zen]. In the modeling work reported by Luoma and Talja [1991Luo] all phases, except for $CuZr_2$, tend to decompose at room temperature. The latest one reported by Zeng et al. [1994Zen] included all six compounds: Cu_5Zr, $Cu_{51}Zr_{14}$, Cu_8Zr_3, $Cu_{10}Zr_7$, CuZr and $CuZr_2$ (Fig. 4.7.1).

Table 4.7.1 Compounds of the binary Cu-Zr system.

Phase, temp. range (K)	Pearson symbol	Space Group	Prototype	Lattice parameters (pm) and angles	Comments
$CuZr_2$ T < 1273	*tI*6	*I*4/*mmm*	$MoSi_2$	*a*=*b*=322.04; *c*=1118.32;	[1962Nev]
CuZr 988 < T < 1208	*cP*2	$Fm\bar{3}m$	CsCl	*a* =326.20;	[1980Car]
Cu_5Zr T < 1285	*cF*24	*Fm*4*m*	$AuBe_5$	*a* = 687;	[1980For]
Cu_8Zr_3 T < 1248	*oP*44	*Pnma*	Hf_3Cu_8	*a* = 786.93; *b* = 998.48; *c* = 815.47;	[1975Bse, 1976Bse]
$Cu_{51}Zr_{14}$ T < 1388	*hP*65	*P*6/*m*	$GdAg_{3.6}$	*a*= *b*= 1124.44; *c*=828.15; γ=120°	[1975Gab]
$Cu_{10}Zr_7$ T < 1168	*oC*68	*C*2*ca*	Zr_7Ni_{10}	*a*=1267.29; *b*=931.63; *c*=934.66;	[1975Bse, 1976Bse]

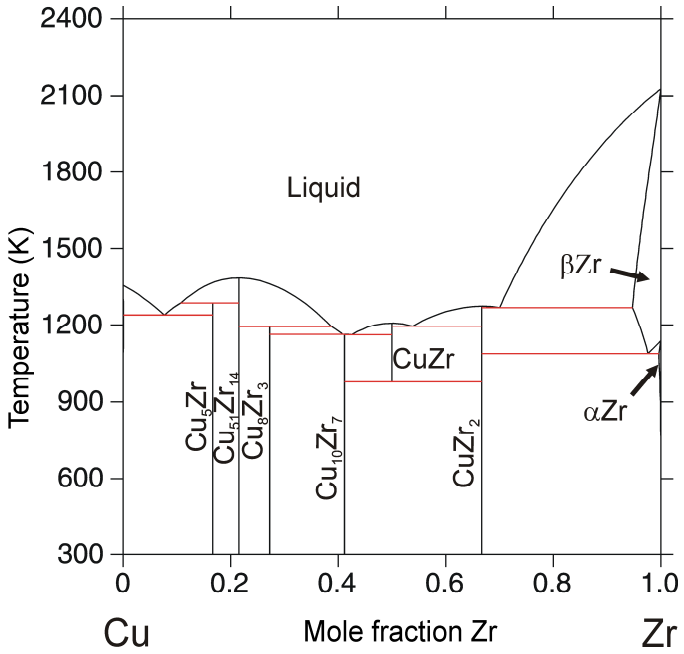

Fig. 4.7.1 The calculated Cu-Zr phase diagram [1994Zen].

5.TERNARY SYSTEMS

The ternary Cu-Pb-O, Cu-Ti-O and Cu-Zr-O systems are presented in this Chapter. The literature information on the ternary Cu-Pb-Zr and Cu-Pb-Ti systems is missing. In the modelling work of the ternary Cu-Ti-Zr system reported by Arroyave et al. [2003Arr], because of the insufficient experimental information, the Gibbs energy of Cu based solid solution was extrapolated from the lower-ordered systems without using the ternary interaction parameters. In addition, the objective of the present study is the prediction of the phase relations, in which the *fcc*-Cu is involved, while the description of the phase relations and thermodynamic properties of the other phases (*fcc*-Pb and *hcp*- and *bcc*-Ti and Zr) in the "metallic" part of the multicomponent Cu-Pb-Zr-Ti-O system is less relevant. Therefore, the ternary Cu-Pb-Zr, Cu-Pb-Ti, Cu-Ti-Zr systems are omitted in this thesis.

5.1. The Cu-Pb-O system

Although extensive experimental studies of the Cu-Pb-O system have been carried out in the past, no critical assessment has been reported so far. A review of the literature data on the Cu-Pb-O system, which includes publications before 1984 has been presented by Chang and Hsieh [1989Cha].

Two stoichiometric ternary compounds were identified, the cubic murdochite Cu_6PbO_8, space group $Fm\bar{3}m$ (lattice parameter a = 921.02 pm) [1955Chr, 1969Win, 1983Dub] and monoclinic Cu_2PbO_2, space group $C2/c$ (lattice parameters in pm: a = 822.25, b = 828.94, c = 601.48 and β = 132.62°) [1954Geb, 1994Szi]. Winchell and Wenden [1969Win] obtained murdochite under hydrothermal conditions at 543 K as a by-product of the synthesis of diaboleite $Pb_2CuCl_2(OH)_4$ from solutions of $CuCl_2{\cdot}2H_2O$ and $Pb(OH)_2$. However, attempts of Dubler and co-workers [1983Dub] to reproduce these results were not successful. Single crystals of the Cu_2PbO_2 compound were prepared by recrystallization from a molten mixture (PbO-Cu_2O) and investigated by X-ray diffraction [1994Szi].

The available experimental data on phase equilibria in the Cu-Pb-O system are given in Table 5.1.1. Isothermal sections at 1473 K [1954Geb, 1984Ani] and 1423 K [1954Hof], a quasibinary section Cu_2O-PbO [1954Geb, 1954Hof, 1979Fis] and an isobaric CuO_x-PbO section in air [1967Gad, 1990Kit] are available in the literature. The copper-rich corner of the miscibility gap has also been studied by Gerlach and co-workers [1967Ger]. Isothermal sections at 1473 K reported by two groups [1954Geb, 1984Ani] are in a good agreement. A schematic liquidus projection of the Cu-Pb-O system and Scheil reaction scheme based on the known data for three binary systems Cu-O, Pb-O and Cu-Pb and selected data for the Cu-Pb-O ternary [1954Geb, 1967Gad, 1967Ger] were given by Chang and Hsieh [1989Cha].

The study of Gebhardt and Obrowski [1954Geb] is the most extensive one, while the data of Hofmann and Kohlmeyer [1954Hof] are inconsistent with the so far accepted Cu-Pb binary system. The quasibinary section Cu_2O-PbO [1954Geb] shows no solubility between Cu_2O and PbO in the solid state, but an eutectic reaction at 953 K and ~ 76 mol% PbO. At temperatures below ~ 835 K, the formation of the ternary compound Cu_2PbO_2 from Cu_2O and PbO was observed [1954Geb]. The eutectic, Liquid $\leftrightarrow$ Cu_2O + βPbO was detected at 1017 K and the peritectoid reaction Cu_2O + βPbO $\leftrightarrow$ Cu_2PbO_2 occured at 968 K. Both temperatures are in good agreement with the DTA curves of Cu_2PbO_2 reported by Szillat and Teske [1994Szi]. Results of Gadalla [1967Gad] and Kitaguchi and co-workers [1990Kit] indicate the existence of the eutectic reaction, L $\leftrightarrow$ CuO + βPbO, which occurs at 78 mol% PbO and at a temperature of 1085 K [1967Gad] or 1062 ± 3 K [1990Kit]. Above 1300 K, the liquid and Cu_2O coexist in equilibrium with the gas phase due to the peritectic reaction L + Cu_2O $\leftrightarrow$ CuO. Both studies of the isobaric CuO_x-PbO section in air [1967Gad, 1990Kit] are consistent with each other.

The solidification behaviour of the copper-rich alloys as a function of the content of impurity (oxygen and lead) has been described in terms of microscopic observations by Clavaguera-Mora and co-workers [1999Cla]. Their results based on the investigation of primary crystallization fields of the samples with different Pb/O ratio have confirmed the invariant phase equlibria reported earlier [1954Geb].

Table 5.1.1 Selection of experimental information for the Cu-Pb-O system: phase diagram data.

Reference	Experimental Technique	Measured quantity, temperatures, compositions
[1954Geb]	Quenching, chemical and metallographic analysis	Composition of liquids along the miscibility gap at 1473 K Liquidus of the quasibinary section Cu_2O-PbO Invariant equilibria
[1984Ani]	Quenching and chemical analysis	Composition of liquids along the miscibility gap at 1473 K
[1954Hof]	Quenching, chemical and metallographic analysis	Composition of liquids along the miscibility gap at 1423 K Liquidus of the quasibinary section Cu_2O-PbO
[1979Fis]	Differential thermal analysis	Liquidus in PbO-rich part of the quasibinary section Cu_2O-PbO
[1967Gad]	Thermogravimetry and microstructural analysis	Composition of the coexisting phases on the isobaric section CuO_x-PbO in air
[1990Kit]	Quenching, X-ray diffraction, thermogravimetry, differential thermal analysis	Liquidus of the isobaric section CuO_x-PbO in air
[1967Ger]	Quenching, chemical and metallographic analysis	Composition of liquids along the miscibility gap at 1523 K
[1999Cla]	Microstructural analysis	Solidification of Cu-rich alloys by continuous casting

The activity of oxygen in the ternary Cu-Pb-O system has been measured by EMF technique with a solid electrolyte [1984Ani, 1979Tas2, 1980Tas, 1971Jac, 1974Pic, 1975Jan, 1991Par] (Table 5.1.2). Anik and Frohberg [1984Ani] reported the oxygen activity map in copper-lead melt at 1473 K. Jacob and Jeffes [1971Jac] measured the activity coefficient of oxygen in the Cu-Pb liquid alloys (non-saturated with oxygen) in the whole range of compositions at 1373 K. Other investigations are confined to either the Cu-rich or Pb-rich region of the ternary system. Several groups investigated the effect of copper on the activity coefficient of oxygen and first order interaction coefficient in liquid lead [1980Tas, 1971Jac, 1991Par]. The results obtained by two groups at 1173 K [1980Tas, 1971Jac] are in a good agreement up to 10 at.% Cu, while Parbhakar et al.

[1991Par] found the opposite composition dependence. The effect of lead on the activity coefficient of oxygen liquid copper between 1373 and 1473 K has been investigated by Taskinen and Taskinen [1979Tas2], Anik and Frohberg [1984Ani] and Pichugin and co-workers [1974Pic], at 1423 K by Janke and Fischer [1975Jan], and at 1373 K by Jacobs and Jeffes [1971Jac]. Three datasets [1984Ani, 1979Tas2, 1971Jac] are in rather good agreement, while data from other studies [1974Pic, 1975Jan] show large negative or positive deviations.

Table 5.1.2 Selection of experimental information for the Cu-Pb-O system derived from EMF measurements.

Reference	**Measured quantity, temperatures, compositions**
[1984Ani]	Activity of oxygen in Cu-Pb melt at 1473 K
[1971Jac]	Activity of oxygen in Cu-Pb melt between 1023 and 1373 K
[1979Tas2]	Effect of Pb on the activity of oxygen in liquid Cu between 1373 and 1473 K
[1974Pic]	Effect of Pb on the activity of oxygen in liquid Cu at 1473 K
[1975Jan]	Effect of Pb on the activity of oxygen in liquid Cu at 1423 K
[1980Tas]	Effect of Cu on the activity of oxygen in liquid Pb between 1001 and 1173 K
[1991Par]	Effect of Cu on the activity of oxygen in liquid Pb between 967 and 1095 K

5.1.1. Experimental results

Since thermodynamic data of Cu_2PbO_2 compound are missing, the experimental part in this section is related to the measurement of enthalpy of formation of Cu_2PbO_2. According to Ref. [1954Geb, 1994Szi] the Cu_2PbO_2 exists on the quasibinary Cu_2O-PbO section. According to the objectives of this thesis, *i.e.*, the investigation of the stability of copper with PbO and Cu_2PbO_2, it was also necessary to study the phase relations in the Cu-Cu_2O-PbO-Pb subsystem.

Figs. 5.1.1 and 5.1.2 show the results of Rietveld refinement of XRD patterns and SEM images of the specimen with the Cu_2O:PbO molar ratio of 1:1 annealed at 910 K for 260 h, respectively. In the X-ray diffraction patterns two phases were observed, the dominant Cu_2PbO_2 (99.3 wt.%) and a small amount of the βPbO phase (0.7 wt.%). Results of Rietveld refinement show good agreement between available crystallographic data of the ternary Cu_2PbO_2 compound [1994Szi] and those of the sample obtained in this work (Table 5.1.3.). The SEM analysis of the specimen reveals the presence of a third phase. Beside the light grey Cu_2PbO_2 and the white PbO a dark grey Cu_2O phase was observed (Figs. 5.1.2a and 5.1.4.2b) indicating that the reaction of the precursor mixture of Cu_2O and PbO was not completed after 260h at 910 K. Due to the lower absorption coefficient of Cu_2O in comparison with PbO, Cu_2O phase is not observed by X-ray analysis and from stoichiometric relation its amount is less than 1 wt.%. The average chemical composition of the phases obtained by EDX is shown in Table 5.1.4.

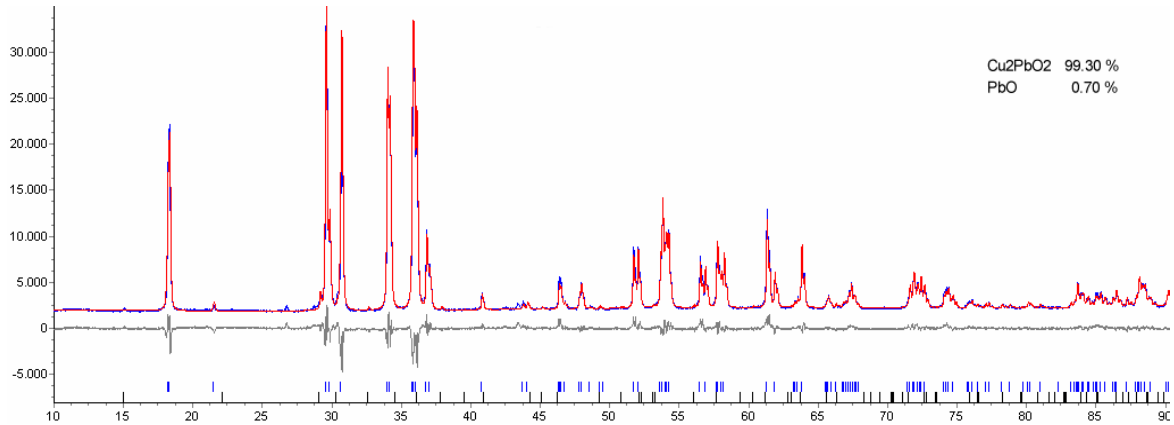

Fig. 5.1.1 Rietveld refinement of XRD pattern of the sample with the Cu_2O:PbO molar ratio of 1:1 after annealing at 910 K for 260 h. Bottom curve presents the difference between experimental and calculated patterns. The tick marks show the position of reflections originating from Cu_2PbO_2 (top) and βPbO (bottom).

Formation of the Cu_2PbO_2 compounds according to the reaction $Cu_2O + PbO = Cu_2PbO_2$ is found to be exothermic: the enthalpy of reaction is – 25.4 ± 1 $kJ \cdot mol^{-1}$ at 968 ± 5 K. The heat flow curve is well reproducible (Fig. 5.1.3) and the

Table 5.1.3 Results of Rietveld refinement of the sample with the Cu_2O:PbO molar ratio of 1:1 annealed at 910 K for 260 hours.

Phase	**Cu_2PbO_2**				**PbO**	
Amount [wt.%]	99.3				0.7	
Space group	*C*2/*c*				*Pbcm*	
Lattice parameter						
a [nm]	0.82214				0.58931	
b [nm]	0.82801				0.54904	
c [nm]	0.60103				0.47528	
β [deg]	132.62					
Site	Cu1 (4*a*)	Cu2 (4*c*)	Pb1 (4*e*)	O1 (8*f*)	Pb1 (4*d*)	O1 (4*d*)
Ion	Cu^{+1}	Cu^{+1}	Pb^{+2}	O^{-2}	Pb^{+2}	O^{-2}
Occupancy	1	1	1	1	1	1
x	0	0.25	0	0.17273	0.2297	-0.1347
y	0	0.25	0.375	0.19898	-0.0116	0.0917
z	0	0	0.25	0.21777	0.25	0.25

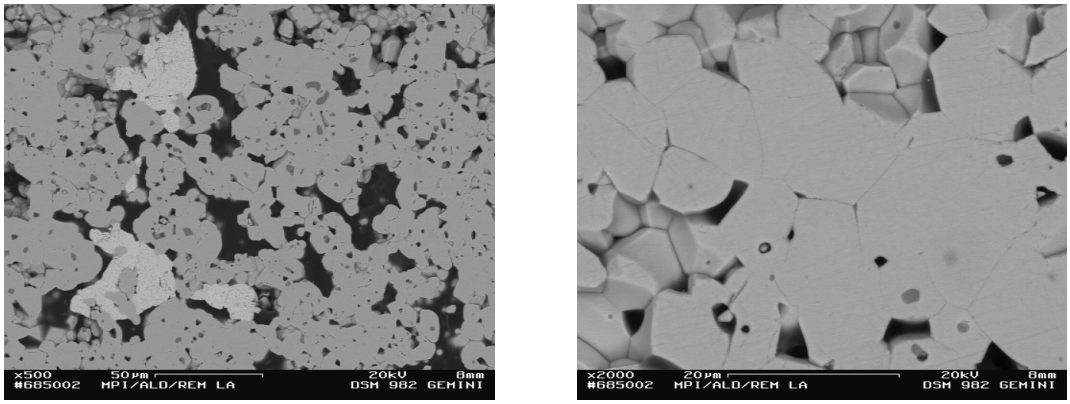

a) b)

Fig. 5.1.2 Microstructure of the specimen with the Cu_2O: PbO molar ratio of 1:1 annealed at 910 K for 260 h. Magnification ×500 (a) and ×2000 (b). (Grey matrix: Cu_2PbO_2, light areas: PbO, dark grey areas: Cu_2O, black areas: pores)

Table 5.1.4 Chemical composition of the light grey, white and dark grey phase in Fig. 5.1.2.

Phase	**Cu_2PbO_2 (light grey)**	**PbO (white)**	**Cu_2O (dark grey)**
Composition [at.%]			
Pb	19.3	50.5	0.1
Cu	42.5	1.1	68.1
O	38.2	48.4	31.8

calculated enthalpy is an average value from two runs. During the heating of the compound up to 1073 K, two overlapped endothermic effects on the heat flow curve were observed around 1020 K (Fig. 5.1.3). They have been related to the decomposition of the ternary compound Cu_2PbO_2 = Cu_2O + βPbO and to the eutectic reaction Cu_2O + βPbO → Liquid, *i.e.*, the melting of samples giving liquid and Cu_2O. During cooling, two exothermic peaks were observed. They have been related to the eutectic solidification at 1017 K and the formation of the ternary Cu_2PbO_2 compound at 968 K. The eutectic temperature of 1017 ± 5 K is in good agreement with the published data of Szillat and Teske [1994Szi]. The SEM analysis of specimens after calorimetric measurements revealed plate-like grains of the light grey Cu_2PbO_2 phase and globular grains of the dark grey Cu_2O phase (Fig. 5.1.4). The average chemical composition of the phases obtained by EDX is shown in Table 5.1.5. Little changes in the chemical composition of the light and dark grey phases (Cu_2PbO_2 and Cu_2O) after heating samples at 1073 K are observed, while the chemical composition of the white PbO phase is changed significantly during melting and solidification, so that higher lead oxides may have been formed.

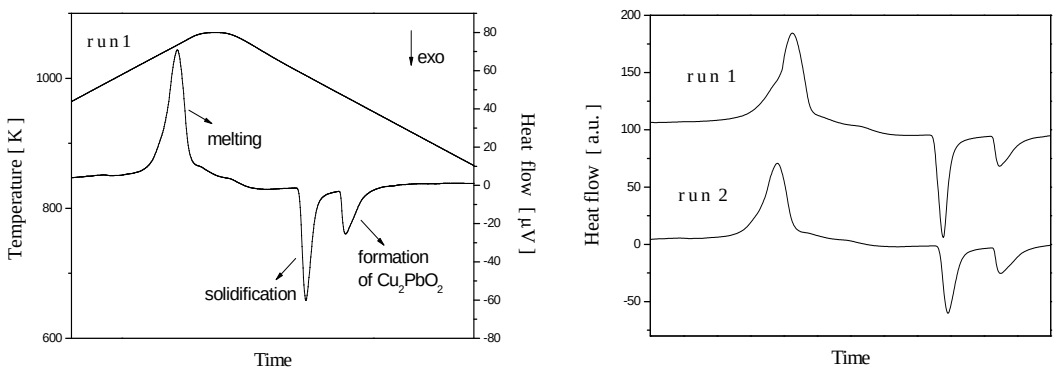

Fig. 5.1.3 Heat flow curves of the Cu_2PbO_2 compound.

At 1073 K the alloy is consisted of liquid and Cu_2O. With cooling the remaining liquid then solidifies at around 1017 K (Fig. 5.1.3) what corresponds to the eutectic reaction Liquid → Cu_2O + βPbO. The large volume shrinkage leads to the formation of pores in the interdendritic regions. Peritectoid reaction of formation of the Cu_2PbO_2 compound from Cu_2O and βPbO at 968 ± 5 K took place after solidification has finished. Using the Rietveld refinement technique the amount of the Cu_2PbO_2 phase in the samples

after calorimetric measurement was found to be 56 ± 2 wt.% (Fig. 5.1.5). The worse fit of the XRD pattern compared to Fig. 5.1.1 is probably due to the preferred orientation during solidification and growth of crystals. Enthalpy of formation of the Cu_2PbO_2 compound was determined by computation of the area under the second peak in the cooling part of the heat flow curves (Fig. 5.1.3). Since not all the sample consisted of Cu_2PbO_2 compound, calculated area is divided by factor 0.56 to evaluate the enthalpy per gram.

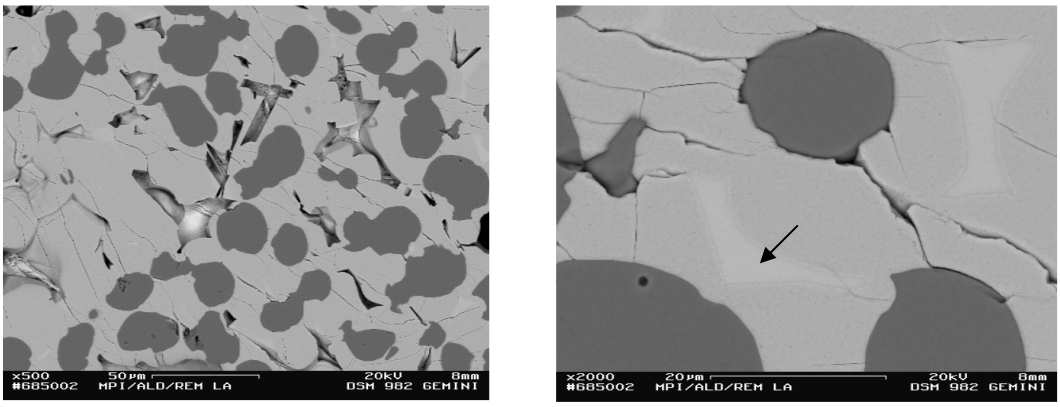

a) b)

Fig. 5.1.4 SEM images of the Cu_2PbO_2 sample after calorimetric measurement: dark grey phase is Cu_2O, light grey phase is Cu_2PbO_2 and white phase is PbO and higher lead oxides (shown by arrow). Magnification ×500 (a) and ×2000 (b).

Table 5.1.5 Results of EDX analysis of the Cu_2PbO_2 samples after calorimetric measurement.

Phase	**Light grey**	**White**	**Dark grey**
Composition [at.%]			
Pb	17.9	66.6	-
Cu	40.1	3.4	65.8
O	42.0	30.0	34.2

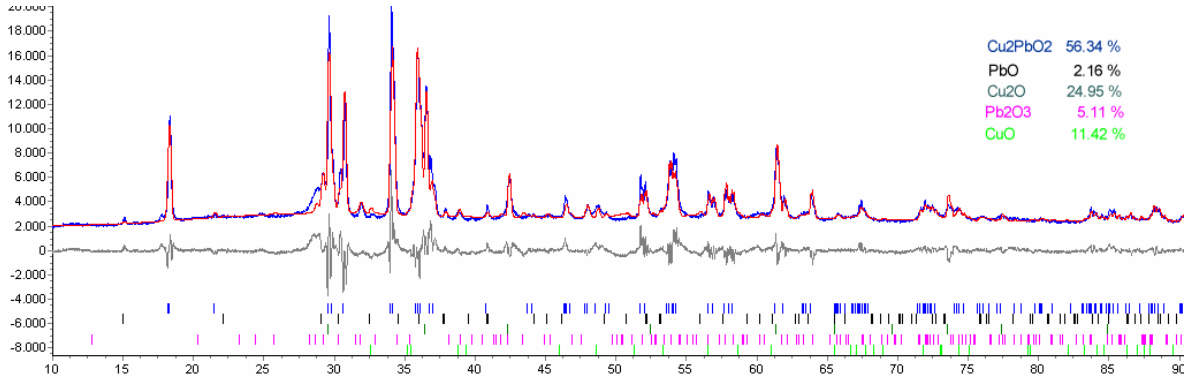

Fig. 5.1.5. Rietveld refinement of XRD pattern of the Cu_2PbO_2 sample after calorimetric measurement. (Bottom curve presents the difference between experimental and calculated patterns. The tick marks show the position of reflections originating from Cu_2PbO_2, βPbO, Cu_2O, Pb_2O_3 and CuO in the order from top to the bottom)

5.1.2. Thermodynamics

Ternary interaction parameters of the liquid phase using both two-sublattice ionic and associate models have been optimized on the base of the selected literature data [1954Geb, 1967Gad, 1979Fis, 1971Jac, 1980Tas, 1990Kit] (data of Gebhardt and Obrowski [1954Geb] have been used partially) as well as data obtained in this work. The selection is made after careful analysis of the data and several trial optimizations ensuring self-consistency of the thermodynamic dataset. Experimental data which show less reliability were not used, but they are also included in the calculated phase diagrams for comparison.

5.1.3. Discussion

The resulting parameters of the two-sublattice ionic liquid model are shown in Appendix (Table 2). Fig. 5.1.6 shows the calculated activity coefficient of oxygen in the copper-lead melt at temperatures ranging from 1001 to 1373 K in comparison with selected experimental data. The calculations are in better agreement with the measurements of Jacobs and Jeffes [1971Jac] than with those of Taskinen and Holopainen [1980Tas]. It is probably because the oxygen concentration was estimated

from the EMF data on the copper-free lead-oxygen melt and was used as a fixed value in the calculations of activity of oxygen by Taskinen and Holopainen [1980Tas], while Jacobs and Jeffers [1971Jac] calculated oxygen concentrations from a mass balance on oxygen in the alloys. The calculated and measured activities of oxygen in the copper-lead melt at 1473 K are given in Fig. 5.1.7. The agreement between calculated and measured values [1984Ani] is quite satisfactory.

The calculated isothermal section at 1473 K (Fig. 5.1.8) shows a large miscibility gap between the metallic and oxide liquids, which connect to the miscibility gaps of Cu-O and Pb-O binary subsystems along with the experimentally measured compositions. The calculated tie-lines are well consistent with experimental observations [1954Geb, 1984Ani], *i.e.*, the Pb-rich oxide liquid coexists with Cu-rich metallic liquid (Fig. 5.1.8). Such shape of the liquid miscibility gap and oxygen activities in the copper-lead melt at 1473 K (Fig. 5.1.7), were only possible to calculate with large interaction parameters for the liquid phase. By only extrapolation from binary subsystems, the oxygen solubility in the Cu-Pb melt was significantly overestimated (by factor of 10). However, the observed

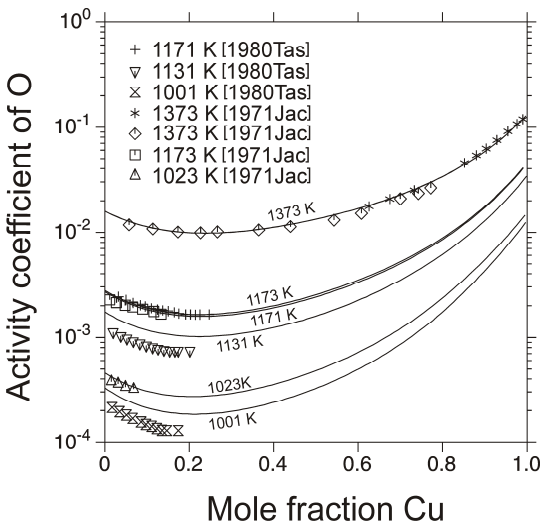

Fig. 5.1.6 Calculated activity coefficient of oxygen in copper-lead melt with the corresponding experimental points.

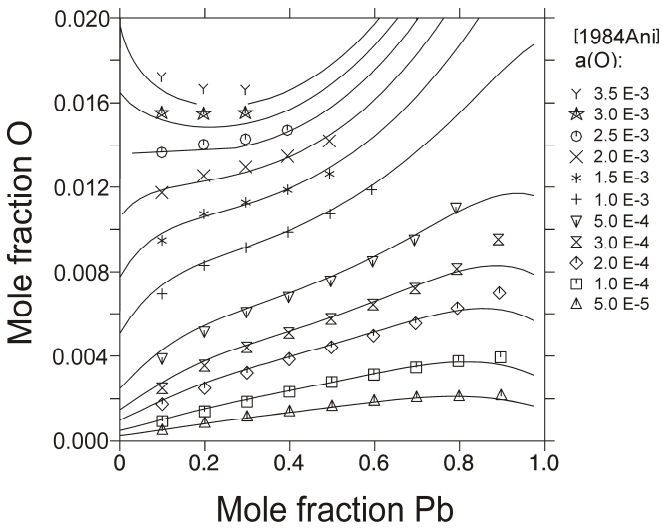

Fig. 5.1.7 Calculated activity of oxygen in copper-lead melt at 1473 K in comparison with the experimental data [1984Ani].

undulation of the oxide liquid phase boundary between 30 and 80 mol% Pb [1954Geb, 1984Ani] could not be exactly reproduced. It is believed that more interaction parameters, than can be adjusted using the available data, are necessary to account for this peculiarity. Especially, oxygen activity data of oxide liquid are missing. The calculated isothermal section at 1523 K is consistent with the results of Gerlach [1967Ger] (Fig. 5.1.9), however the data of Hofmann [1954Hof] show deviations from the calculated isothermal section at 1423 K (Fig. 5.1.10) as well as from the accepted data of other authors (in the present assessment).

The calculated projection of the monovariant liquidus lines is shown in Fig. 5.1.11. According to the present work, the solidification sequence in the Cu-Pb-O system (Fig. 5.1.12) is consistent with the Scheil reaction scheme proposed by Chang and Hsieh [1989Cha], but the temperatures of the eutectics are somewhat higher (Table 5.1.6).

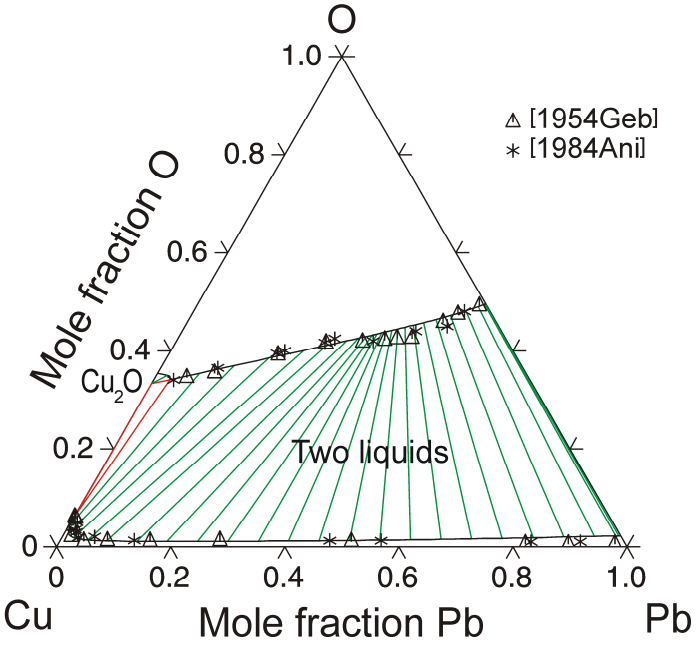

Fig. 5.1.8 Isothermal section of the Cu-Pb-O phase diagram at 1473 K superimposed with experimental measurements. Phase equilibria involving gas phase have been neglected.

The calculated quasibinary section Cu_2O-PbO and an isobaric section CuO_x-PbO in air are presented in Figs. 5.1.13 and 5.1.14, respectively. Both diagrams include

experimental results from different reports [1954Ger, 1954Hof, 1979Fis, 1976Gad, 1990Kit] as well as experimental results obtained in the preset work. The data of Fischer [1979Fis], which belong to the PbO-rich part of the Cu_2O-PbO quasibinary system are consistent with the calculated liquidus. The Cu_2O-liquidus reported by Gebhardt and Obrowski [1954Geb] is well reproduced above 1000 K. Another measurement of the liquidus in the Cu_2O-PbO system [1954Hof] shows large negative deviations. At the same time, the eutectic temperature measured in this work is about 80 K higher compared to Ref. [1954Geb], but it is in good agreement with the data of Szillat and Teske [1994Szi]. The calorimetric technique applied in this work seems to be more accurate in comparison with the DTA analysis used by Gebhardt and Obrowski [1954Geb]. In fact, the reported eutectic point at 953 K [1954Geb] is very close to the temperature of the peritectoid reaction $Cu_2O + \beta PbO \leftrightarrow Cu_2PbO_2$, at 968 K measured in our work. The calculated isobaric section CuO_x-PbO in air is well-consistent with experimental liquidus data [1990Kit] (Fig. 5.1.14). The calculated thermodynamic properties of Cu_2PbO_2 are shown in Table 5.1.7.

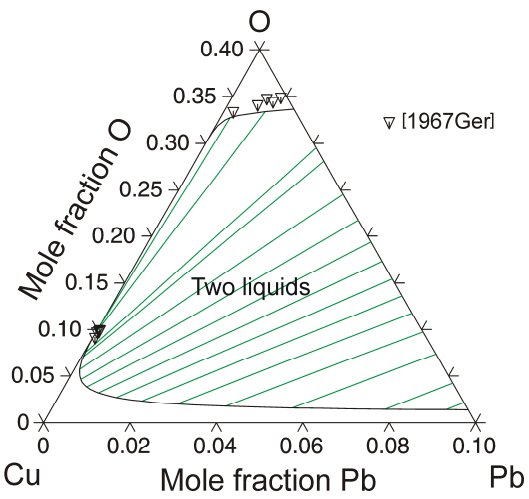

Fig. 5.1.9 Isothermal section of the Cu-Pb-O phase diagram at 1523 K compared with experimental measurements (copper rich part).

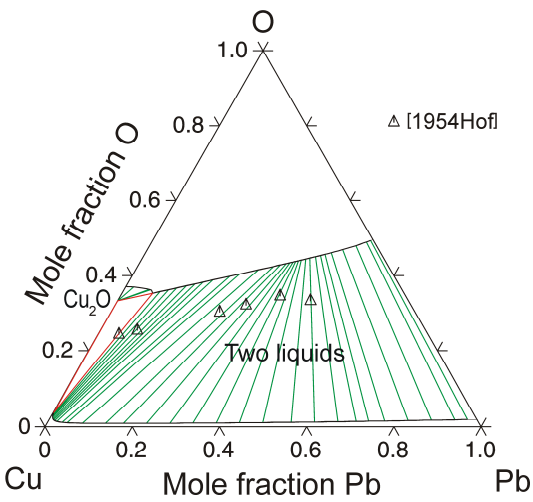

Fig. 5.1.10 Isothermal section of the Cu-Pb-O phase diagram at 1423 K superimposed with experimental measurements. Phase equilibria involving gas phase have been neglected.

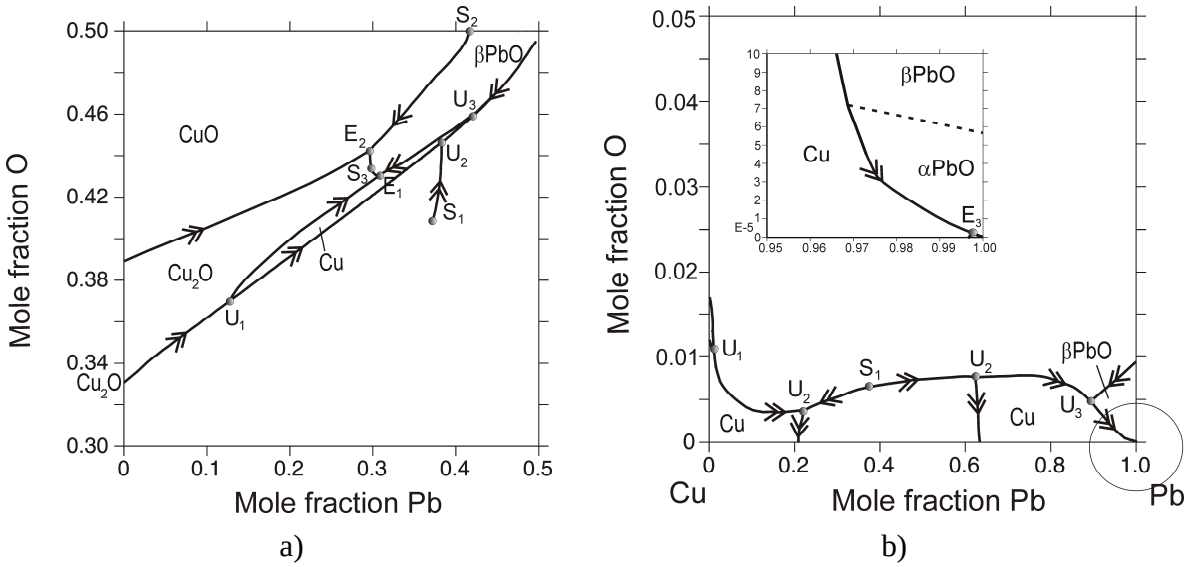

Fig. 5.1.11 Calculated projection of the monovariant liquidus lines in the ternary Cu-Pb-O system: oxygen-rich part (a) and metal-rich part (b). Fields of primary crystallization are indicated. Inset shows the magnified Cu-rich part.

Table 5.1.6 Invariant equilibria in the Cu-Pb-O system.

	Reaction	Type	T_{cal} (K)	T_{exp} (K)	Reference
U_1	$L_1 + Cu_2O \leftrightarrow (Cu) + L_3$	Transitional	1335.8	1313	[1989Cha]
U_2	$L_1 + L_3 \leftrightarrow L_2 + (Cu)$	Transitional	1229.2	1227	[1989Cha]
U_3	$L_2 + L_3 \leftrightarrow (Cu) + \beta PbO$	Transitional	1109.4	1120	[1989Cha]
E_1	$L_3 \leftrightarrow (Cu) + Cu_2O + \beta PbO$	Eutectic	976.5	950	[1989Cha]
E_2	$L_3 \leftrightarrow CuO + Cu_2O + \beta PbO$	Eutectic	1000.5	940	[1989Cha]
E_3	$L_2 \leftrightarrow (Cu) + (Pb) + \alpha PbO$	Eutectic	599.4	589	[1989Cha]
S_1	$L_1 + L_2 + L_3$	Critical point	-	1323	[1989Cha]
S_2	$L_3 \leftrightarrow CuO + \beta PbO$	Saddle point	1063.2	1085	[1967Gad]
				1062	[1990Kit]
S_3	$L_3 \leftrightarrow Cu_2O + \beta PbO$	Saddle point	1008.5	953	[1954Geb]
				1033	[1994Szi]
				1017	[This work]

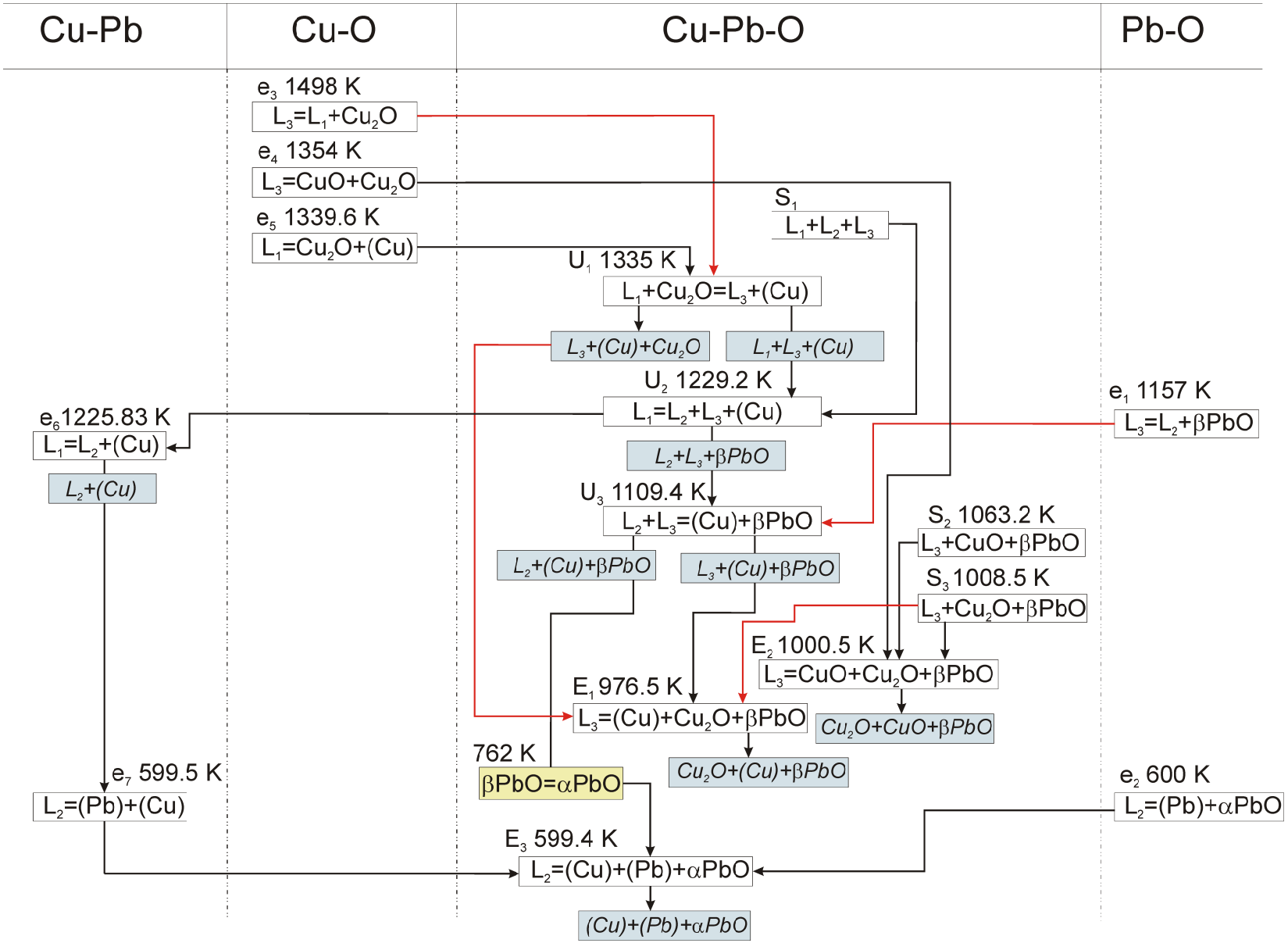

Fig. 5.1.12 Scheil reaction scheme of the Cu-Pb-O system.

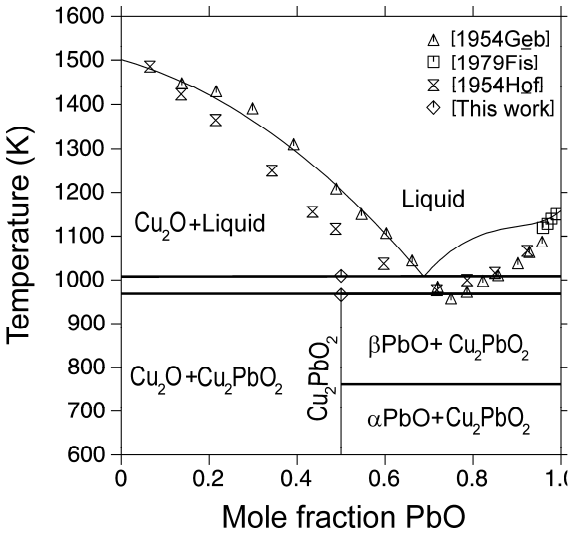

Fig. 5.1.13 Calculated quasibinary section Cu_2O-PbO as compared with experimental measurements.

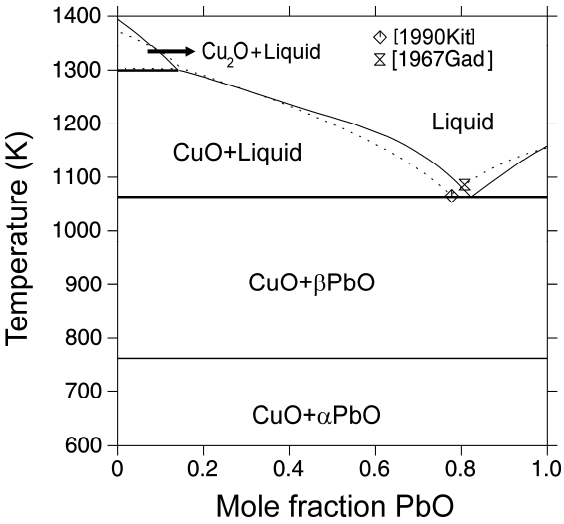

Fig. 5.1.14 Calculated isobaric section CuO_x-PbO in air as compared with experimental measurements. Dashed line presents the data of Kitaguchi *et.al.* [1990Kit].

Table 5.1.7 Calculated thermodynamics functions of Cu_2PbO_2 at 298.15 K.

$\Delta_f H°$ [kJ·mol^{-1}]	$S°$ [J·mol^{-1}·K^{-1}]	$\Delta_f G°$ [kJ·mol^{-1}]
– 413.086	135.165	– 353.165

By using the associate solution model for the description of the liquid, in general, worse agreement between calculated and experimental data was obtained in comparison with that produced by ionic liquid model, as it is shown in Fig. 5.1.15 for example. The higher calculated solubility of oxygen in the metallic liquid at 1473 K in comparison with the experimental data [1954Geb, 1984Ani] can be seen in Fig. 5.1.16. The calculated quasibinary Cu_2O-PbO section is very similar that obtained using the two-sublattice model for liquid (Fig. 5.1.13). On the other hand, the calculated liquidus below 1200 K at the isobaric section CuO_x-PbO in air (Fig. 5.1.17) shows slight discrepancy compared with the experimental data [1967Gad, 1990Kit]. The calculated temperature of reaction

S_2 is 30 K higher than the experimentally measured one [1967Gad, 1990Kit]. Such feature is related to the difficulties to handle the parameters to fit data of both, oxide and metallic liquid. Only by extrapolations from the lower-order systems three closed miscibility gaps exist near to the boundary binary systems instead of one large liquid miscibility gap. The increase of the Gibbs energy of liquid by introducing the ternary interaction parameters makes it unstable in the region of immiscibility, but it also causes the oxide liquid to be less stable. Still, all calculated phase diagrams show satisfactory agreement with the selected experimental data.

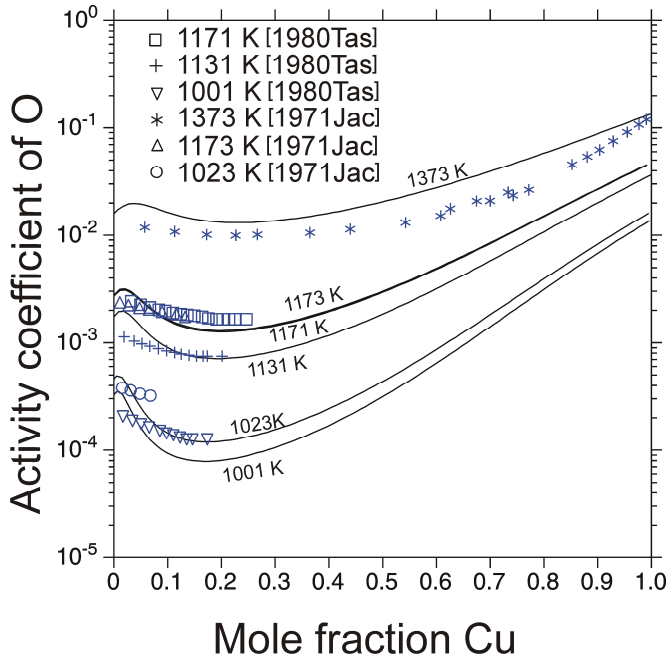

Fig. 5.1.15 Calculated activity coefficient of oxygen in copper-lead melt with the corresponding experimental points.

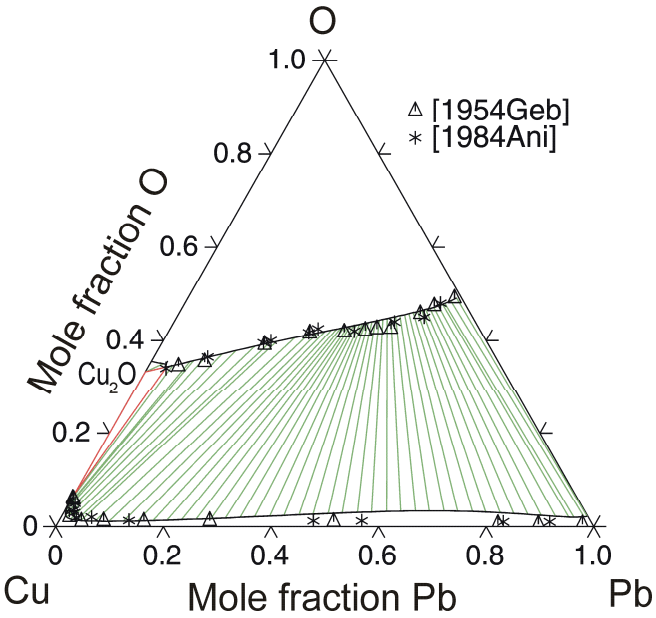

3

Fig. 5.1.16 Isothermal section of the Cu-Pb-O phase diagram at 1473 K superimposed with experimental measurements. Phase equilibria involving gas phase have been neglected.

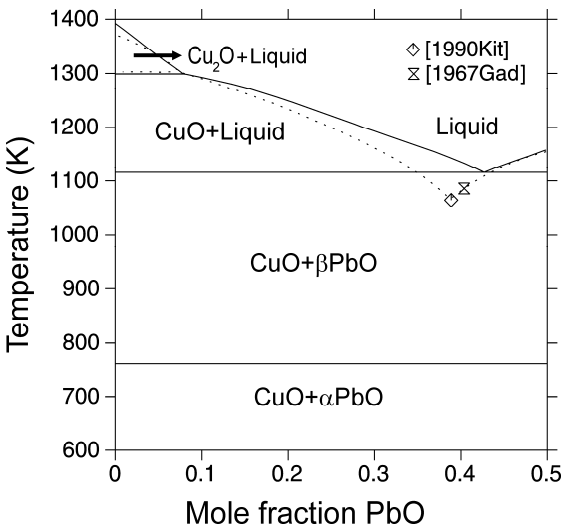

Fig. 5.1.17 Calculated isobaric section CuO_x-PbO in air as compared with experimental measurements. Dashed line presents the data of Kitaguchi *et.al.* [1990Kit].

.

5.2. The Cu-Ti-O system

Three ternary phases, Cu_3TiO_4, Cu_3Ti_3O and Cu_2Ti_4O were found to be stable in the Cu-Ti-O system (Table 5.2.1). The existence of M_6X-type compounds (Cu_3Ti_3O and Cu_2Ti_4O) in the metal-rich part of the ternary Cu-Ti-O phase diagram was reported by Kelkar et.al [1993Kel, 1994Kel]. The crystal structure of Me_2Ti_4O compounds (Me = Cu, Ni, Co, Fe and Mn) were investigated by several authors [1939Lav, 1952Ros, 1952Jou, 1963Mue]. Cu_2Ti_4O has been reported as ordered *fcc* phases with a very large unit cell by Laves and Wallbaum [1939Lav] and Rostoker [1952Ros]. The *Fd*3*m* space group for the Cu_2Ti_4O compound has been confirmed by Mueller and Knott [1963Mue] and more recently by Kelkar et. al [1993Kel]. A hexagonal Cu_3TiO_4 compound was found to exist in the oxide-rich part of Cu-Ti-O system [1974Hay, 1977Ran], which was also confirmed by Kato and Kubo [1967Kat], while the Cu_3TiO_5 compound was obtained by

Table 5.2.1 Solid phases in the Cu-Ti-O system.

Phase, temp. range (K)	Pearson symbol	Space Group	Prototype	Lattice parameters (pm) and angles	Comments
Cu_2Ti_4O	*cF*112	*Fd*3*m*	Fe_3W_3C	*a*= 1143.53	[1993Kel] [1963Mue] [1951Kar]
Cu_3Ti_3O	*cF*112	*Fd*3*m*	Fe_3W_3C	*a*=1125	[1993Kel] [1951Kar]
Cu_3TiO_4 1212 < T < 1280	*hP*8	*P*63/*mmc*	-	*a*=304.0; *b*=304.0; *c*=1146.05; *γ=120°*	[1974Hay]

rapid cooling from the melt. This compound is metastable and its presence is related with the slow kinetic of decomposition at temperatures below 1173 K. Contrary to the findings of Beals et. al [1958Bel] on the $CuTiO_3$ phase, no indication was obtained about the formation of any compound between CuO and TiO_2 by Gadalla and White [1966Gad1]. Range and Ketterl [1977Ran] reported the crystal structure of two modifications of the Cu_3TiO_4 compound to be very similar and contain Cu^+ with linear, and both Cu^{2+} and Ti^{4+} with trigonally distorted octahedral coordination.

Only a few works on the phase equilibria in the Cu-Ti-O system have been published [1993Kel, 1994Kel, 1966Gad1]. Isothermal sections in the metal-rich part of the diagram at 1198 and 1212 K were reported by Kelkar et.al [1993Kel, 1994Kel], while Gadalla and White [1966Gad1] studied the equilibrium relationships in the CuO-Cu_2O-TiO_2 system. Isobaric sections CuO_x-TiO_2 in air and oxygen [1966Gad1] indicate the absence of any ternary compound and the existence of a limited range of TiO_2 solid solution. Depending on the temperature and partial pressure of oxygen, CuO_x corresponds to either Cu_2O or CuO. At the same time, the isothermal section of the CuO-Cu_2O-TiO_2 system at 1253 K reported by Hennings [1980Hen] shows the presence of Cu_3TiO_4. The existence of Cu_3TiO_4 at temperatures below 1280 K was confirmed by Pejryd and Rosen [1982Pej], while the molten phase was found to occur above 1280 K [1980Hen, 1982Pej]. This melting temperature is in good agreement with data of the liquidus surface of the CuO-Cu_2O-TiO_2 system reported by Gadalla and White [1966Gad1]. A significant feature of ternary isothermal sections [1993Kel, 1994Kel] is the formation of two distinct M_6X-type compounds, Cu_2Ti_4O and Cu_3Ti_3O. Kelkar et al. [1993Kel, 1994Kel] restricted investigation to the region where the M_6X-type compounds are present. A region in the Cu-rich corner of the sections at 1198 and 1218 K was drawn tentatively. Samples in this region had melted and subsequently reacted with the quartz tube during annealing. The single phase field of the ternary compounds Cu_2Ti_4O and Cu_3Ti_3O is estimated. The upper limit of O solubility in both compounds is likely to be restricted to the maximum number of O atoms which can be accommodated in the structure, which is 14.29 at. %. There are no more than 16 large "interstitial" sites which oxygen can occupy within each unit cell containing 96 Ti and Cu atoms [1963Mue]. The lower limit of oxygen solubility in Cu_2Ti_4O was reported to be 13.07 at. % [1993Kel]. The available phase diagram data on the ternary Cu-Ti-O system are presented in Table 5.2.2.

Thermodynamics of the double oxide phase Cu_3TiO_4 was investigated by means of measurements of the oxygen partial pressure and EMF [1980Hen, 1982Pej] (Table 5.2.3.). The lowest temperature of the existence of Cu_3TiO_4 was found to be 1212 K

[1982Pej] and 1140 K [1980Hen], while the highest temperature is 1280 K [1980Hen, 1982Pej]. According to Hennings [1980Hen], Cu_3TiO_4 shows nonstoichiometry and its composition fluctuates between $Cu_3TiO_{4.3}$ and $Cu_3TiO_{3.9}$. Opposite to results obtained by Hennings [1980Hen], Pejryd and Rosen [1982Pej] reported that there is no variation in oxygen content of Cu_3TiO_4. EMF measurements applied by Pejryd and Rosen [1982Pej] seem to be more accurate in comparison with results reported by Hennings [1980Hen]. The phase exists only in a narrow range of temperatures (1218-1280 K) and partial pressures of oxygen ($-1.4 < log(P_{O_2}$, atm) < -0.7) [1980Hen, 1982Pej]. Cu_3TiO_4 dissociates into Cu_2O and TiO_2 with decreasing the partial pressure of oxygen, while at too high partial pressures of oxygen it decomposes into CuO and TiO_2. On the base of known thermodynamics of the binary edge systems, Kelkar et al. [1994Kel] estimated the very high negative value of the free energy of formation of the two M_6X-type compounds, Cu_2Ti_4O and Cu_3Ti_3O, suggesting that these compounds are thermodynamically stable. The dependence of the activity of oxygen on the concentration

Table 5.2.2 Selection of experimental information for the Cu-Ti-O system: phase diagram data. The column "Use" indicates whether the values were used (+) or not used (–) in the assessment.

Reference	**Experimental Technique**	**Use**	**Measured quantity, temperatures, compositions**
[1966Gad1]	Thermogravimetry and microstructural analysis	+	Composition of the coexisting phases on the isobaric sections CuO_x-PbO in air and oxygen
[1980Hen]	X-ray, SEM, EDS and thermogravimetry	+	Isothermal section of CuO-Cu_2O-TiO_2 system at 1253 K.
[1993Kel]	Quenching, X-ray, optical and electron microscopy, DTA, TGA	+	Coexisting phases on the isothermal section at 1198 K in the metal-rich region. Melting points of M_6X-type compounds
[1994Kel]	Air-quenching, electron microscopy, WDS	+	Coexisting phases on isothermal section at 1212 K in the metal-rich region.

of titanium in liquid copper at 1373-1473 K using the electromotive force method has been investigated by Batalin and Kuzmenko [1982Bat].

Table 5.2.3 Selection of experimental information for the Cu-Ti-O system: thermodynamic data. The column "Use" indicates whether the values were used (+) or not used (–) in the assessment.

Reference	**Experimental Technique**	**Use**	**Measured quantity, temperatures, compositions**
[1980Hen]	Thermogravimetry	+	Partial pressure of oxygen over Cu_3TiO_4, CuO, Cu_2O and TiO_2 phases in the temperature range 1160-1280 K.
[1982Pej]	EMF	+	Partial pressure of oxygen over Cu_3TiO_4, CuO, Cu_2O and TiO_2 phases in the temperature range 770-1355 K.
[1982Bat]	EMF	–	Effect of Ti on the activity of oxygen in liquid Cu between 1373 and 1473 K

5.2.1. Thermodynamic optimization

The data used in the optimization of the Cu-Ti-O system are indicated in Tables 5.2.2 and 5.2.3. The two sublattice ionic model $(Cu^{1+},Cu^{2+},Ti^{2+},Ti^{3+},Ti^{4+})_p(O^{2-},Va^{q-})_q$ was first applied for the description of the liquid in the ternary Cu-Ti-O system. The thermodynamic assessments of the binary edge systems Cu-O [2003Hal], Ti-O [1994Lee], and Cu-Ti [1996Kum] were accepted from literature. Although the binary systems Cu-Ti and Ti-O do not possess a liquid miscibility gap, the calculated tie-lines at 1500 K show, however, that Ti-rich oxide liquid coexists with Cu-rich metallic liquid (Fig. 5.2.1a). In addition, it was observed that the liquid miscibility gap widens with increasing temperature. Despite the corresponding experimental data are missing, the very low solubility of copper in Ti-rich oxide liquid and of titanium in Cu-rich liquid, respectively, at high temperatures is unreasonable giving an extended miscibility gap. The appearance of such a liquid miscibility gap is affected by reciprocal reactions

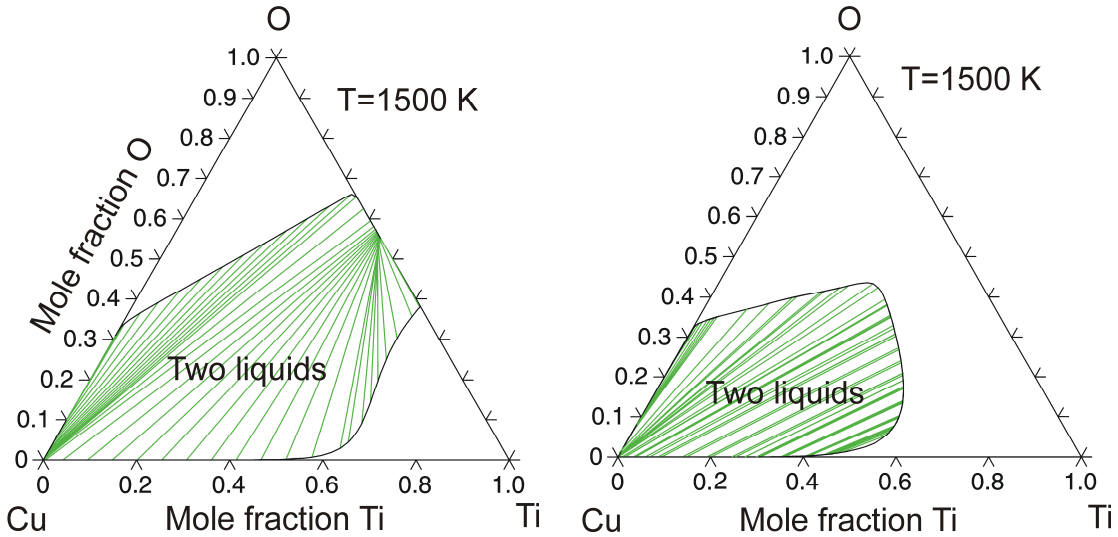

(a) (b)

Fig. 5.2.1 The calculated isothermal sections of the Cu–Ti–O system at 1500 K using the two-sublattice model for the liquid phase: extrapolated from lower order systems (a) and with incorporation of the ternary interaction parameter (b). Phase equilibria involving gas and condensed phases have been neglected.

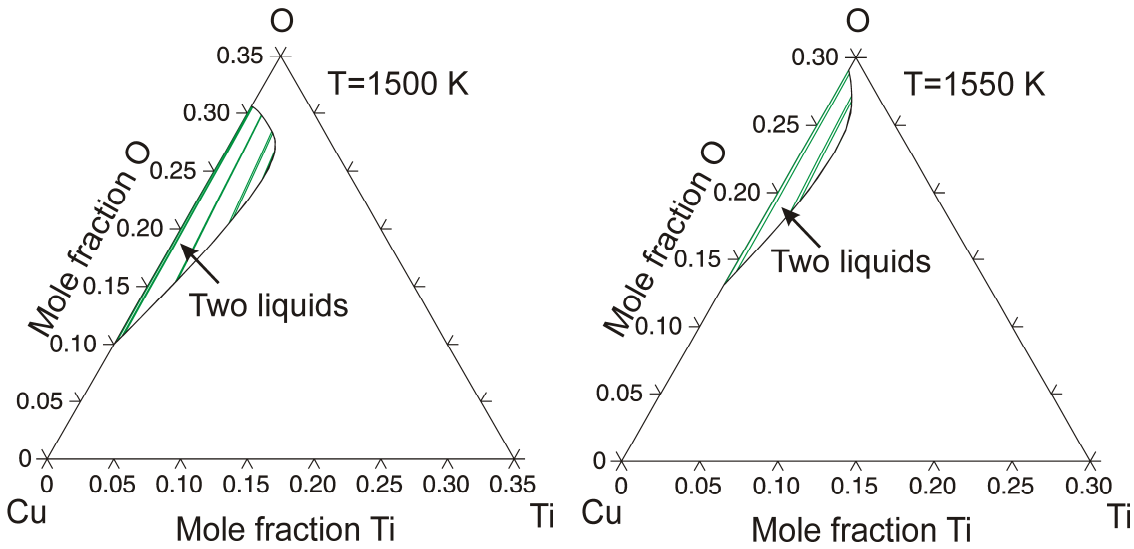

(a) (b)

Fig. 5.2.2 The calculated partial isothermal sections of the Cu–Ti–O system at 1500 (a) and 1550 K (b) using the associate solution model for the liquid phase. Phase equilibria involving gas and condensed phases have been neglected.

between species. Since the Ti-rich oxide liquid is very stable and coexist with Cu-rich metallic liquid, the influence of ternary (Cu^{1+}, Ti^{2+}: O^{2-}), (Cu^{1+}, Ti^{3+}: O^{2-}) and (Cu^{1+}, Ti^{4+}: O^{2-}) interaction parameters on the Gibbs energy of the liquid was tested. However, only the (Cu^{1+}, Ti^{2+}: O^{2-}) parameter has shown a significant tendency to decreasing the Gibbs energy of liquid phase for compositions rich in titanium-oxides and suppressing the miscibility gap towards the Cu-O edge system (Fig. 5.2.1b). Adjusting the Gibbs energies of the hypothetical end-members, (Ti^{2+}: Va) and (Cu^{1+}: O^{2-}) cannot prevent a demixing behavior. At the same time, using the associate solution model (Cu, Cu_2O, O, Ti, TiO, $TiO_{1.5}$, TiO_2), by only extrapolation from the binaries subsystems, the liquid miscibility gap is not present on the isothermal sections at temperatures above 1600 K, while the narrow miscibility gap exists on isothermal sections between 1500 and 1550 K (Fig. 5.2.2).

5.2.2. Discussion

The calculated isothermal section at 1218 K with the use of the associate solution model is in very good agreement with experimental data reported by Kelklar et al. [1993Kel, 1994Kel] (Fig.5.2.3), except for the three phase field containing the low-temperature Ti_3O_2 phase. According to the literature data [1987Mur] and the assessed Ti-O system (Chapter 4.1), Ti_3O_2 decomposes at 1197.31 K and therefore can not be present at 1218 K. The calculated maximum solubility of copper in αTi at 1218 K is 1.83 at. %, while the solubility of oxygen in $CuTi_2$ and CuTi is 2.5 and 1.6 at.%, respectively. These results are consistent with the data reported by Kelkar and Carim [1993Kel].

The calculated copper, titanium and oxygen activities in the three phase regions 3, 4 and 6 at 1218 K (Fig. 5.2.3) are shown in Table 5.2.4 together with the values estimated

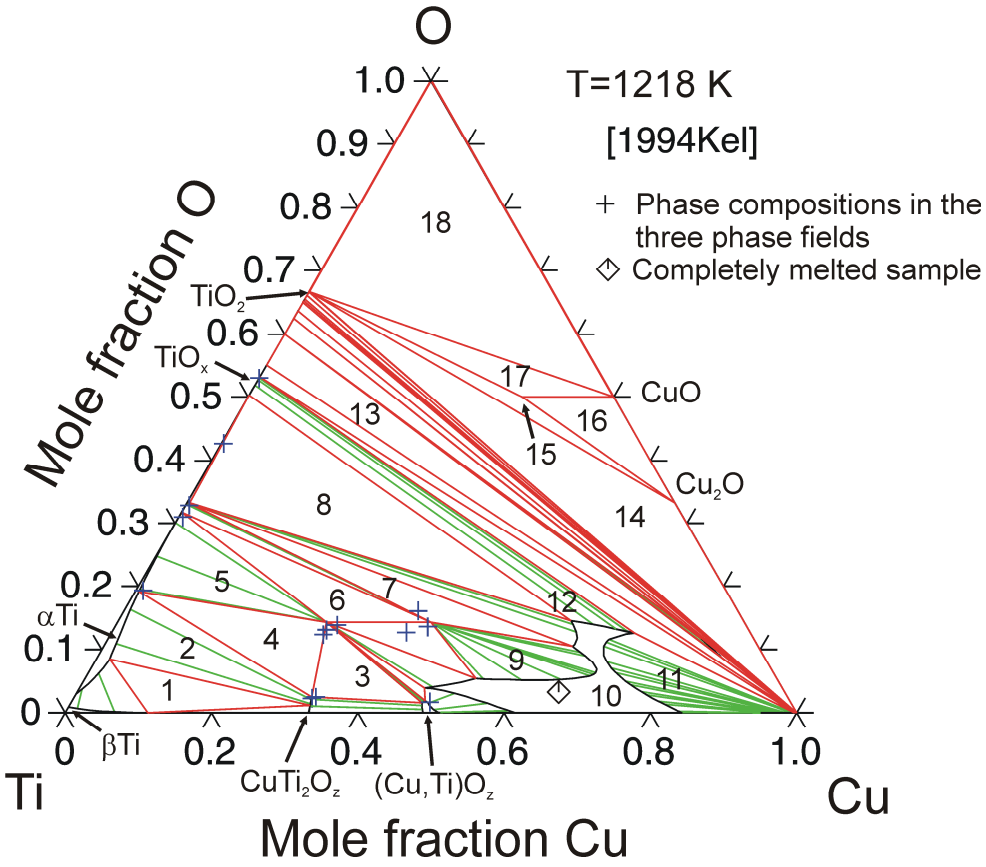

1. αTi + βTi + $CuTi_2O_z$

2. αTi + $CuTi_2O_z$

3. $CuTi_2O_z$ + Cu_2Ti_4O + $(Cu,Ti)O_z$

4. αTi + $CuTi_2O_z$ + Cu_2Ti_4O

5. αTi + Cu_2Ti_4O

6. αTi + Cu_2Ti_4O + Cu_3Ti_3O

7. αTi + Cu_3Ti_3O + Liquid

8. αTi +TiO_x + Liquid

9. Cu_3Ti_3O + Liquid

10. Liquid

11. Cu + Liquid

12. TiO_x + Liquid

13. TiO_x + Ti_2O_3 + Cu

14. Cu + Cu_2O + TiO_2

15. Cu_2O + TiO_2 + Cu_3TiO_4

16. Cu_2O + CuO + Cu_3TiO_4

17. CuO + TiO_2 + Cu_3TiO_4

18. CuO + TiO_2 + Gas

Fig. 5.2.3 Isothermal section of the Cu-Ti-O phase diagram at 1218 K and 1 bar pressure compared with experimental measurements [1994Kel].

by Kelkar et al. [1994Kel]. The calculated partial pressures of oxygen (Table 5.2.4) show good agreement with those reported by Kelkar et al [1994Kel] what indicate the stability of the ternary M_6X-type compounds at 1218 K. The reported oxygen activities in Cu-Ti

liquid alloys [1982Bat] are not taken into consideration. Originally measured EMF data are missing while the 1 wt. % solution of oxygen in copper was chosen as the standard state for the calculation of oxygen activity in Cu-Ti melt.

Table 5.2.4 The calculated activity values of Ti, Cu and O in regions 3, 4 and 6 at 1218 K (Fig. 5.2.3) together with the estimated* ones by Kelkar et al. [1994Kel].

Region	a_{Ti}	a_{Cu}	**log** P_{O_2}
3	0.608	0.365	- 39.107
4	0.718	0.262	- 39.109
	0.66*	0.14*	- 38.2*
6	0.276	0.505	- 36.927
	0.40*	0.17*	- 36.9*

The calculated melting points of Cu_2Ti_4O and Cu_3Ti_3O are 1490 and 1383 K, respectively, while the Kelkar and Carim [1993Kel] reported an almost 90 K lower melting temperature for Cu_2Ti_4O. The peritectic melting of both compounds is controlled by Gibbs energies of three phases in equilibrium, *i.e.*, Cu_2Ti_4O or Cu_3Ti_3O, αTi and the liquid phase. The Gibbs energy of the ternary M_6X-type compounds and αTi are adjusted to be consistent with the reported isothermal section at 1218 K (Fig. 5.2.3) and with the estimated Gibbs energy of the formation of ternary compounds [1994Kel]. The ternary (Cu, Ti, TiO) interaction parameter in the liquid phase was introduced to assure the solubility of oxygen in the Cu-rich liquid as well as to control the temperature of the peritectic melting of the ternary M_6X-type compounds. However, at the same time with decreasing the melting point of Cu_2Ti_4O, the melting point of Cu_3Ti_3O also decreases. The lower melting temperature measured for Cu_2Ti_4O in comparison with the calculated one is probably due to the presence of impurity phases (< 4 %) [1993Kel]. In addition, the DTA analysis was performed in argon with the unknown partial pressure of oxygen and the characterization of the melted samples was not done. According to the present assessment, all three ternary compounds melt incongruently (Table 5.2.5). Calculated thermodynamic properties of the ternary compounds (Table 5.2.6) are compared with estimated ones by Kelkar et al. [1994Kel].

The stability diagram of the CuO-Cu_2O-TiO_2 system is given in Fig. 5.2.4. The calculated partial oxygen pressure of the double oxide Cu_3TiO_4 is consistent with data reported in the literature [1980Hen, 1982Pej]. The Cu_3TiO_4 compound exists in the narrow temperature range from 1204 K up to the its melting point at 1271 K and under partial oxygen pressure of log(P_{O_2} , bar) < - 0.67, *i.e.* lower than in air.

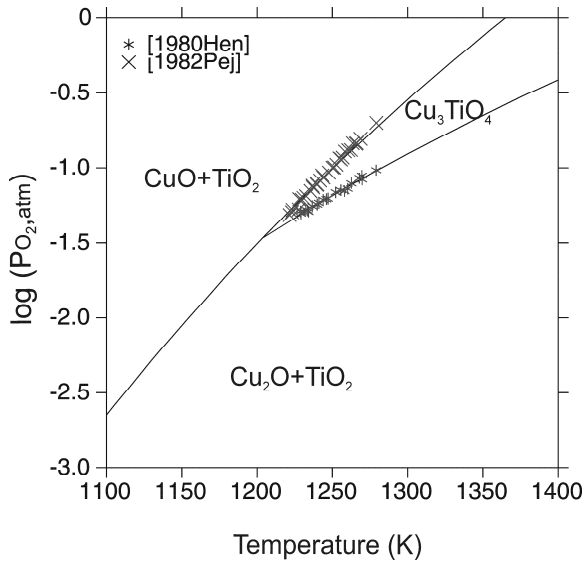

Fig. 5.2.4 The calculated and measured partial pressures of oxygen on the Cu_3TiO_4 phase superimposed with experimental measurements.

The calculated isobaric sections in air and oxygen in comparison with the experimental data [1966Gad1] are given in Figs. 5.2.5 and 5.2.6. The calculations are consistent with the results of Gadalla and White [1966Gad1].

The calculated projection of the monovariant liquidus lines is shown in Figs. 5.2.7a-e, while the Scheil reaction scheme is given in Fig. 5.2.8. The calculated isothermal sections at high temperatures (Figs. 5.2.9 - 5.2.11) show reasonable phase relations in the sense that the ternary compounds disappear and the liquid single-phase region enlarges as the temperature increases.

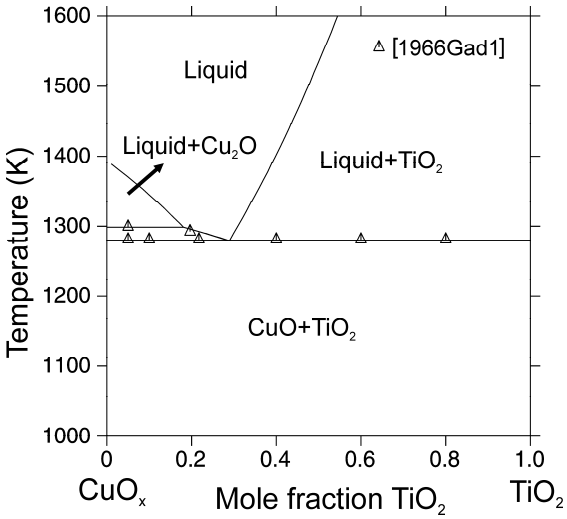

Fig. 5.2.5 The calculated isobaric section CuO_x-TiO_2 in air as compared with experimental measurements [1966Gad1].

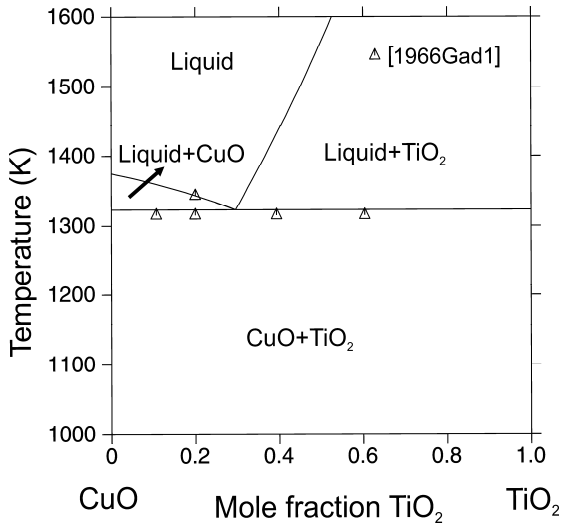

Fig. 5.2.6 The calculated isobaric section CuO-TiO_2 in oxygen as compared with experimental measurements [1966Gad1].

Table 5.2.5 Melting points of ternary compounds in Cu-Ti-O system.

Reaction	**Composition in at. %**		***T* (K)**	**Ref.**
	Cu	**O**		
$L_1 + \alpha Ti \leftrightarrow Cu_2Ti_4O$	33.38	11.91	1490.8	[This work]
			1400	[1993Kel]
$L_1 + \alpha Ti \leftrightarrow Cu_3Ti_3O$	45.37	13.20	1383	[This work]
			1383	[1993Kel]
$L_2 + TiO_2 + CuO \leftrightarrow Cu_3TiO_4$	43.64	46.06	1270.6	[This work]
			1280	[1980Hen, 1982Pej]

Table 5.2.6 The calculated thermodynamics properties of the Cu_2Ti_4O, Cu_3Ti_3O and Cu_3TiO_4 compounds at 298.15 K (values in parentheses are estimated by Kelkar et al. [1994Kel]).

Compound	**$\Delta_f H°$ [kJ·mol^{-1}]**	**$\Delta_f S°$ [J·mol^{-1}·K^{-1}]**	**$\Delta_f G°$ [kJ·mol^{-1}]**
Cu_2Ti_4O	-496.592	291.41	-583.475
			(-502.320)
Cu_3Ti_3O	-490.460	293.91	-578.089
			(-510.692)
Cu_3TiO_4	-1252.467	199.956	-1312.084

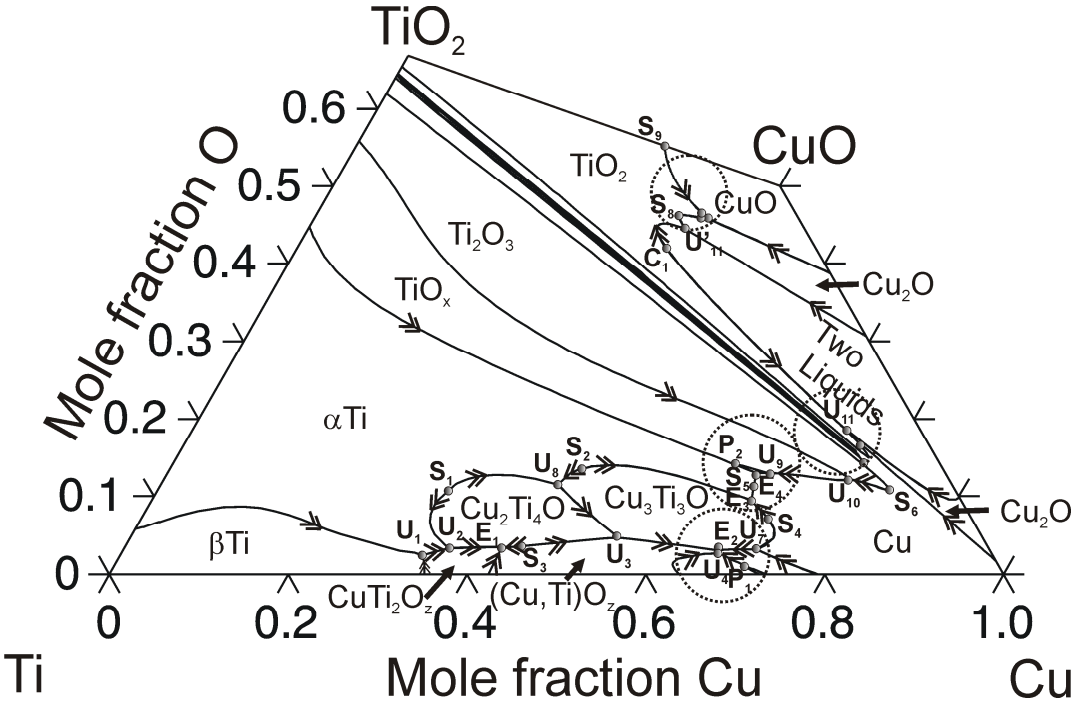
TiO2
CuO
Mole fraction O
0.6
0.5
0.4
0.3
0.2
0.1
0
TiO2
CuO
Ti2O3
TiOx
Cu2O
Two Liquids
αTi
βTi
Cu2Ti4O
Cu3Ti3O
Cu
Cu2O
CuTi2Oz
(Cu,Ti)Oz
0
0.2
0.4
0.6
0.8
1.0
Ti
Mole fraction Cu
Cu

a)

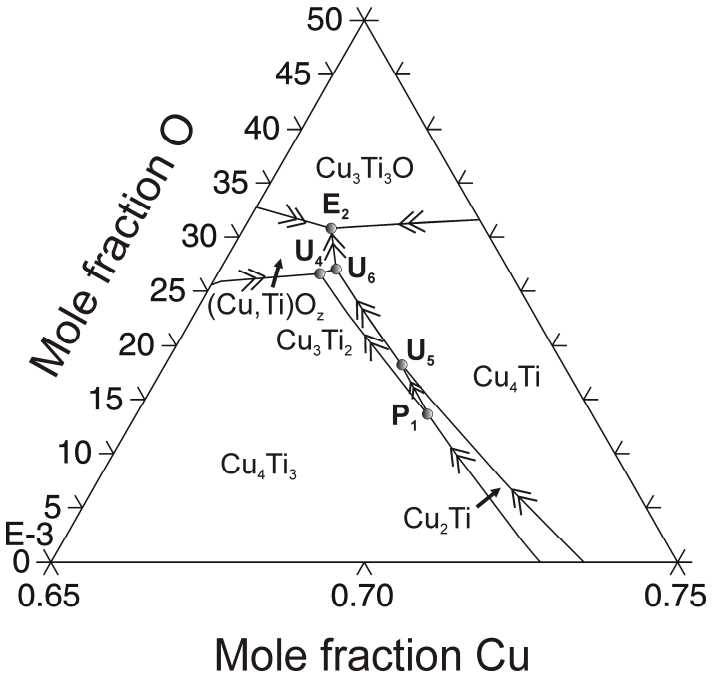
50
45
40
35
30
25
20
15
10
5
E-3
0
Mole fraction O
Cu3Ti3O
E2
U4
U6
(Cu,Ti)Oz
Cu3Ti2
U5
Cu4Ti
P1
Cu4Ti3
Cu2Ti
0.65
0.70
0.75
Mole fraction Cu

b)

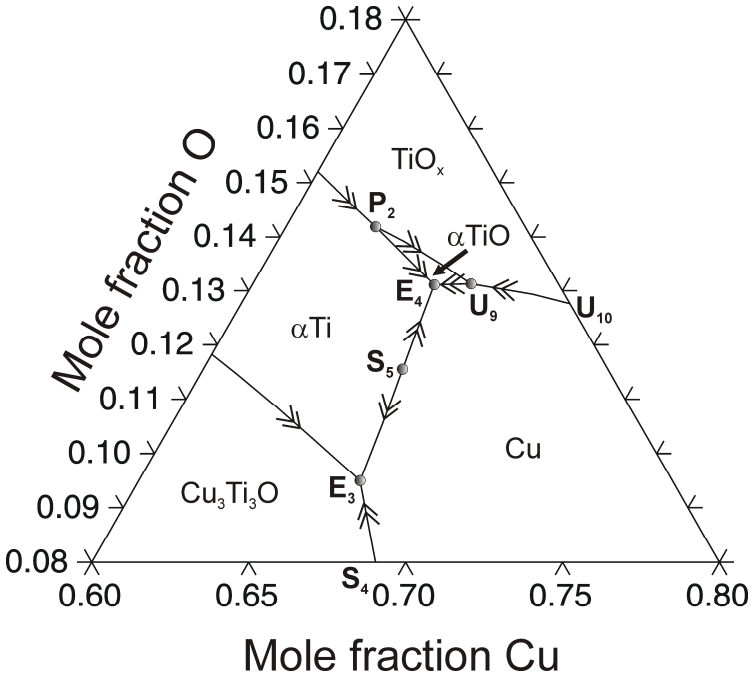
0.18
0.17
0.16
0.15
0.14
0.13
0.12
0.11
0.10
0.09
0.08
Mole fraction O
TiO$_x$
P$_2$
αTiO
E$_4$
U$_9$
U$_{10}$
αTi
S$_5$
Cu
Cu$_3$Ti$_3$O
E$_3$
S$_4$
0.60
0.65
0.70
0.75
0.80
Mole fraction Cu

c)

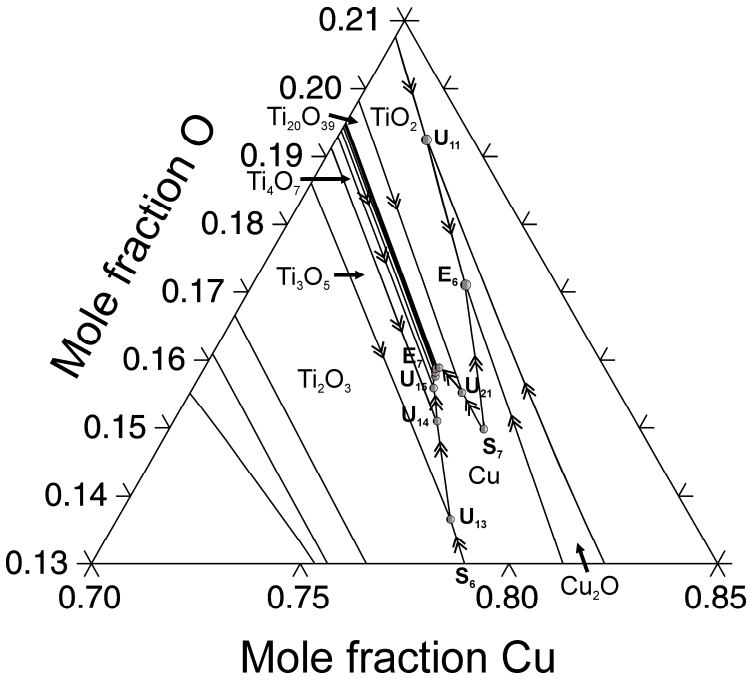
0.21
0.20
0.19
0.18
0.17
0.16
0.15
0.14
0.13
Mole fraction O
Ti$_{20}$O$_{39}$
TiO$_2$
U$_{11}$
Ti$_4$O$_7$
Ti$_3$O$_5$
E$_6$
E$_7$
U$_{15}$
U$_{21}$
U$_{14}$
Ti$_2$O$_3$
S$_7$
Cu
U$_{13}$
S$_6$
Cu$_2$O
0.70
0.75
0.80
0.85
Mole fraction Cu

d)

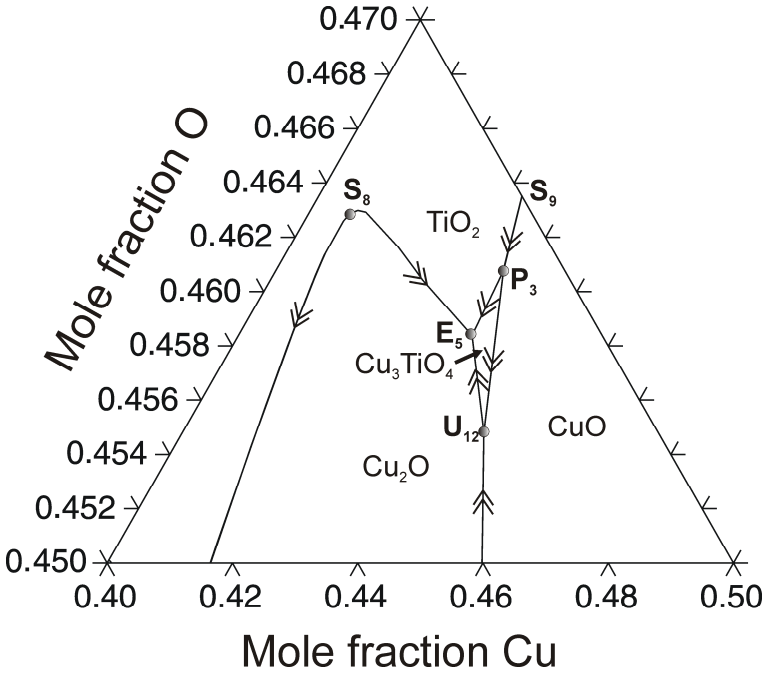

e)

Fig. 5.2.7 The calculated projection of the monovariant liquidus lines in the ternary Cu-Ti-O system (a) and magnified parts: Cu-rich part (b), O-rich part (c) and enlarged view on the invariant reactions involving Magneli phases (d). Fields of primary crystallization are indicated.

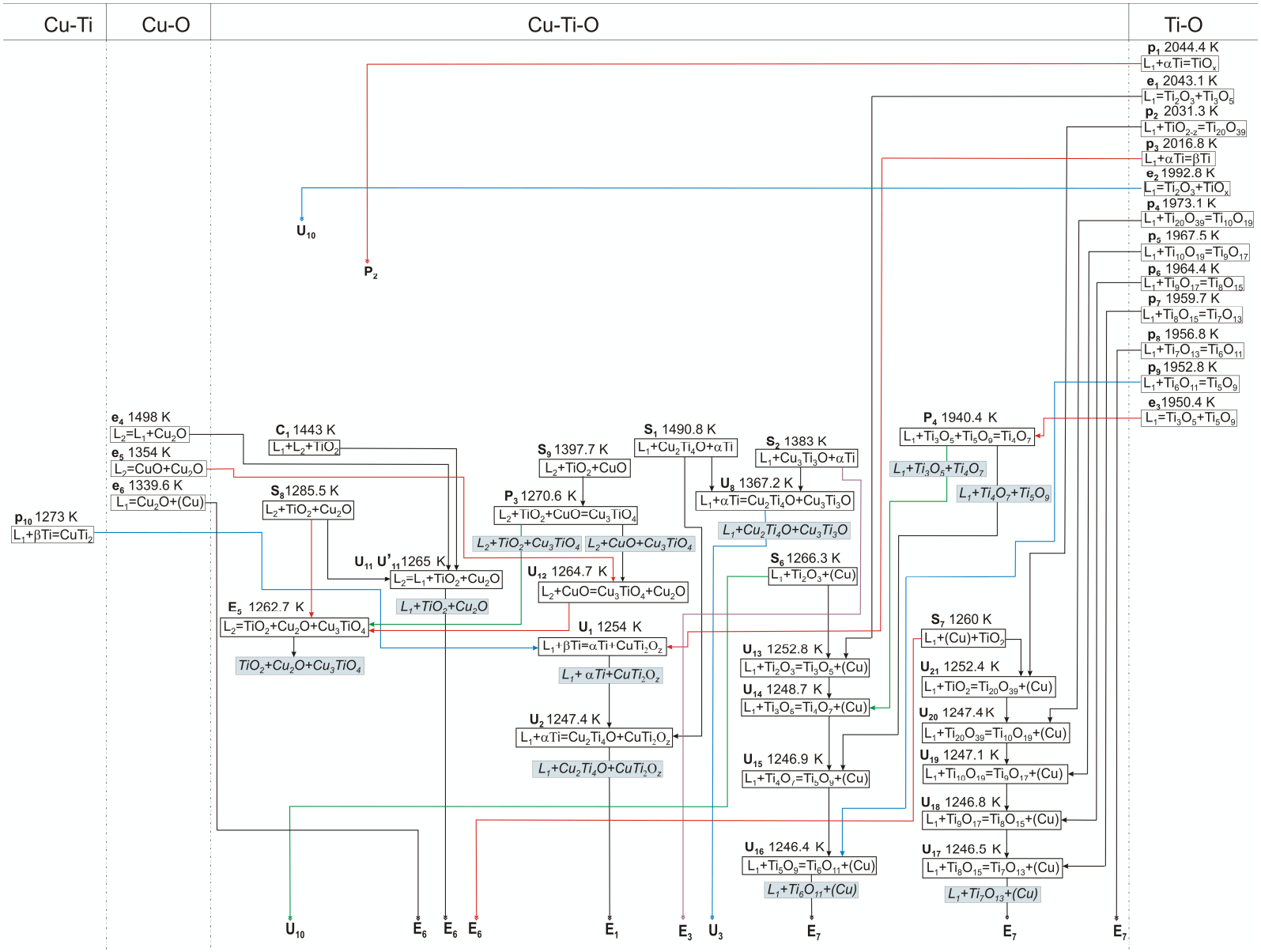
Cu-Ti
Cu-O
Cu-Ti-O
Ti-O
p1 2044.4 K
L1+αTi=TiOx
e1 2043.1 K
L1=Ti2O3+Ti3O5
p2 2031.3 K
L1+TiO2-z=Ti20O39
p3 2016.8 K
L1+αTi=βTi
e2 1992.8 K
L1=Ti2O3+TiOx
p4 1973.1 K
L1+Ti20O39=Ti10O19
p5 1967.5 K
L1+Ti10O19=Ti9O17
p6 1964.4 K
L1+Ti9O17=Ti8O15
p7 1959.7 K
L1+Ti8O15=Ti7O13
p8 1956.8 K
L1+Ti7O13=Ti6O11
p9 1952.8 K
L1+Ti6O11=Ti5O9
e3 1950.4 K
L1=Ti3O5+Ti5O9
U10
P2
e4 1498 K
L2=L1+Cu2O
e5 1354 K
L2=CuO+Cu2O
e6 1339.6 K
L1=Cu2O+(Cu)
p10 1273 K
L1+βTi=CuTi2
C1 1443 K
L1+L2+TiO2
S8 1285.5 K
L2+TiO2+Cu2O
U11 U'11 1265 K
L2=L1+TiO2+Cu2O
L1+TiO2+Cu2O
E5 1262.7 K
L2=TiO2+Cu2O+Cu3TiO4
TiO2+Cu2O+Cu3TiO4
S9 1397.7 K
L2+TiO2+CuO
P3 1270.6 K
L2+TiO2+CuO=Cu3TiO4
L2+TiO2+Cu3TiO4
L2+CuO+Cu3TiO4
U12 1264.7 K
L2+CuO=Cu3TiO4+Cu2O
S1 1490.8 K
L1+Cu2Ti4O+αTi
U8 1367.2 K
L1+αTi=Cu2Ti4O+Cu3Ti3O
L1+Cu2Ti4O+Cu3Ti3O
S2 1383 K
L1+Cu3Ti3O+αTi
S6 1266.3 K
L1+Ti2O3+(Cu)
U1 1254 K
L1+βTi=αTi+CuTi2Oz
L1+αTi+CuTi2Oz
U2 1247.4 K
L1+αTi=Cu2Ti4O+CuTi2Oz
L1+Cu2Ti4O+CuTi2Oz
U13 1252.8 K
L1+Ti2O3=Ti3O5+(Cu)
U14 1248.7 K
L1+Ti3O5=Ti4O7+(Cu)
U15 1246.9 K
L1+Ti4O7=Ti5O9+(Cu)
U16 1246.4 K
L1+Ti5O9=Ti6O11+(Cu)
L1+Ti6O11+(Cu)
P4 1940.4 K
L1+Ti3O5+Ti5O9=Ti4O7
L1+Ti3O5+Ti4O7
L1+Ti4O7+Ti5O9
S7 1260 K
L1+(Cu)+TiO2
U21 1252.4 K
L1+TiO2=Ti20O39+(Cu)
U20 1247.4 K
L1+Ti20O39=Ti10O19+(Cu)
U19 1247.1 K
L1+Ti10O19=Ti9O17+(Cu)
U18 1246.8 K
L1+Ti9O17=Ti8O15+(Cu)
U17 1246.5 K
L1+Ti8O15=Ti7O13+(Cu)
L1+Ti7O13+(Cu)
U10
E6
E6
E6
E1
E3
U3
E7
E7
E7

Continued

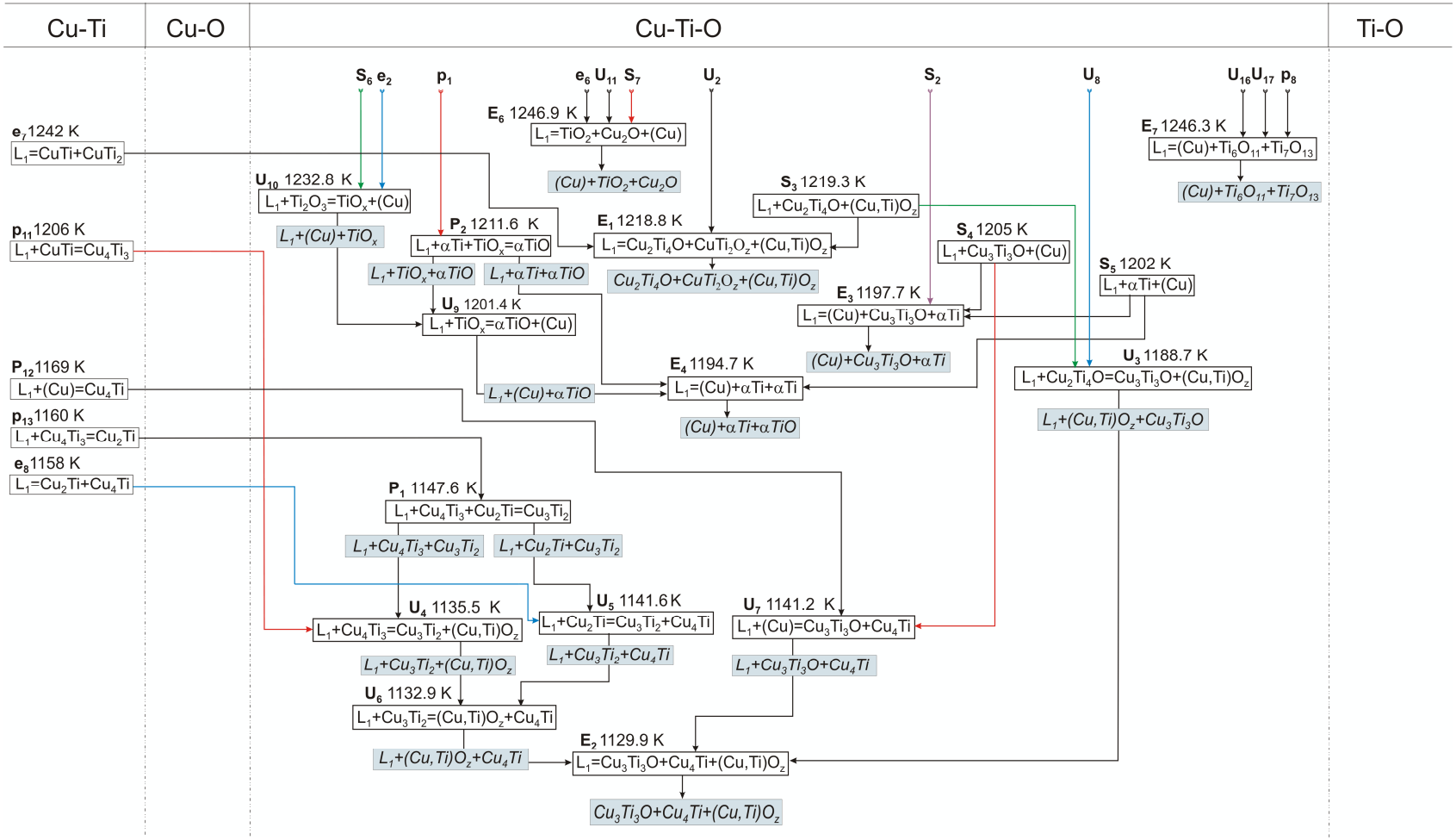

Fig. 5.2.8 Scheil reaction scheme of the Cu-Ti-O system.

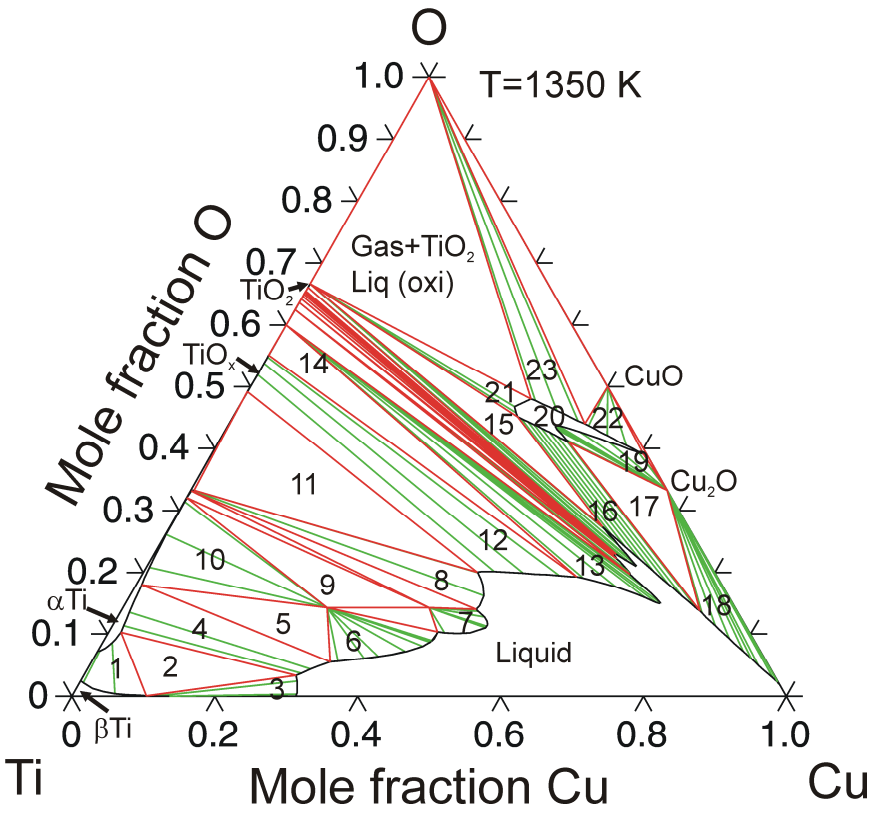

1. αTi + βTi

2. αTi + βTi + Liquid

3. βTi + Liquid

4. αTi + Liquid

5. αTi +Cu_2Ti_4O + Liquid

6. Cu_2Ti_4O + Liquid

7. Cu_3Ti_3O + Liquid

8. αTi + Liquid

9. αTi + Cu_2Ti_4O + Cu_3Ti_3O

10. αTi + Cu_2Ti_4O

11. αTi + TiO_x + Liquid

12. TiO_x + Liquid

13. Ti_2O_3 + Liquid

14. TiO_x + Ti_2O_3 + Liquid

15. TiO_2 + Two Liquids

16. Two Liquids

17. Cu_2O + Two Liquids

18. Cu_2O + Liquid

19. Cu_2O + Liquid

20. Liquid

21. TiO_2 + Liquid

22. CuO + Liquid

23. Liquid + Gas

Fig. 5.2.9 The calculated isothermal section of the Cu-Ti-O phase diagram at 1350 K and 1 bar pressure.

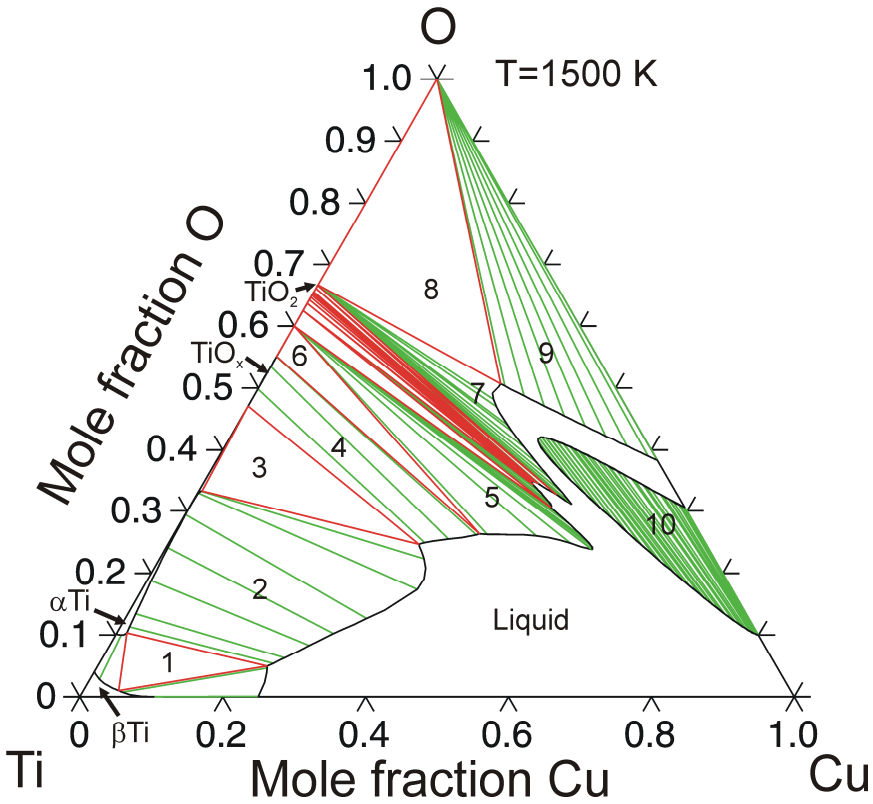

1. αTi + βTi + Liquid

2. αTi + Liquid

3. αTi + TiO_x + Liquid

4. TiO_x + Liquid

5. Ti_2O_3 + Liquid

6. TiO_x + Ti_2O_3 + Liquid

7. TiO_2 + Liquid

8. TiO_2 + Liquid + Gas

9. Liquid + Gas

10. Two Liquids

Fig. 5.2.10 The calculated isothermal section of the Cu-Ti-O phase diagram at 1500 K and 1 bar pressure.

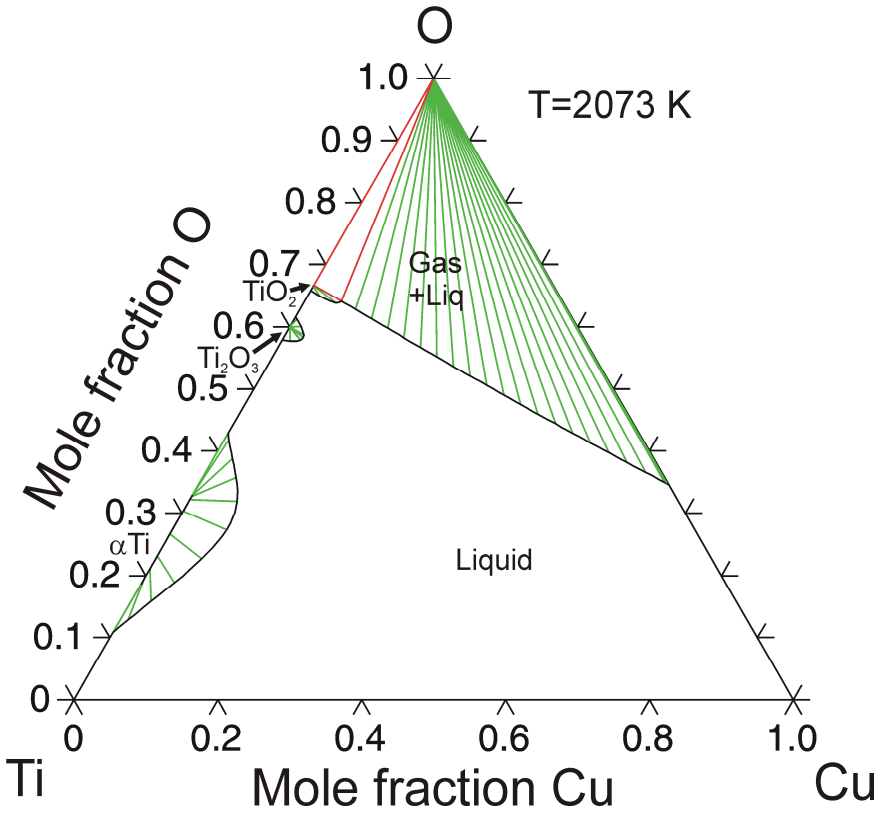

Fig. 5.2.11 The calculated isothermal section of the Cu-Ti-O phase diagram at 2073 K and 1 bar pressure.

5.3.The Cu-Zr-O system

The isobaric section CuO_x-ZrO_2 in air and oxygen were investigated and the liquidus surface in the CuO-Cu_2O-ZrO_2 system was proposed by Gadalla and White [1966Gad2]. The melting of the samples heated in oxygen and air was found to occur at 1370 K and 1403 K, respectively. However, the results obtained for the air treated samples are not consistent with the binary Cu-O system and the melting point of Cu_2O at 1393 K. The existence of ternary compounds in the oxygen rich part of diagram was not observed [1966Gad2], while data (phase equilibria and thermodynamic) for the metal rich side are completely missing.

5.3.1. Experimental results

Six powder mixtures of CuO (or Cu_2O) + ZrO_2 in the molar ratios 1:3, 1:1 and 3:1 were prepared (Chapter 3.1) for the investigation of the existence of ternary compounds in the Cu-Zr-O system. Fig. 5.3.1 shows DTA and TG curves of the samples heated in oxygen (CuO+ZrO_2 in the molar ratio 1:3) and argon (Cu_2O+ZrO_2 in the molar ratio 1:3). The XRD patterns of these samples after DTA analysis are given in Fig. 5.3.2. Almost identical DTA, TG and XRD results were obtained for different CuO (Cu_2O) : ZrO_2 molar ratios. The slight weight change observed at lower temperatures for both samples heated in argon and oxygen, is probably due to evaporation of water and ethanol used in preparation procedure. Due to reduction of Cu_2O to copper of the sample treated in argon (25 mol. % Cu_2O + 75 mol. % ZrO_2) the presence of three phases was detected in the XRD patterns (Fig. 5.3.2). It is consistent with the weight loss observed in TG experiments (Fig. 5.3.1). At the same time, no changes in weight (Figs. 5.3.1) were observed at temperatures above 600 K in the sample heated in oxygen. It should be noted that both DTA curves do not show significant heat effects. Two phases, CuO and ZrO_2, were observed in the XRD patterns of the sample after heating in oxygen (Fig. 5.3.2) indicating that there is no difference in comparison with the start mixture.

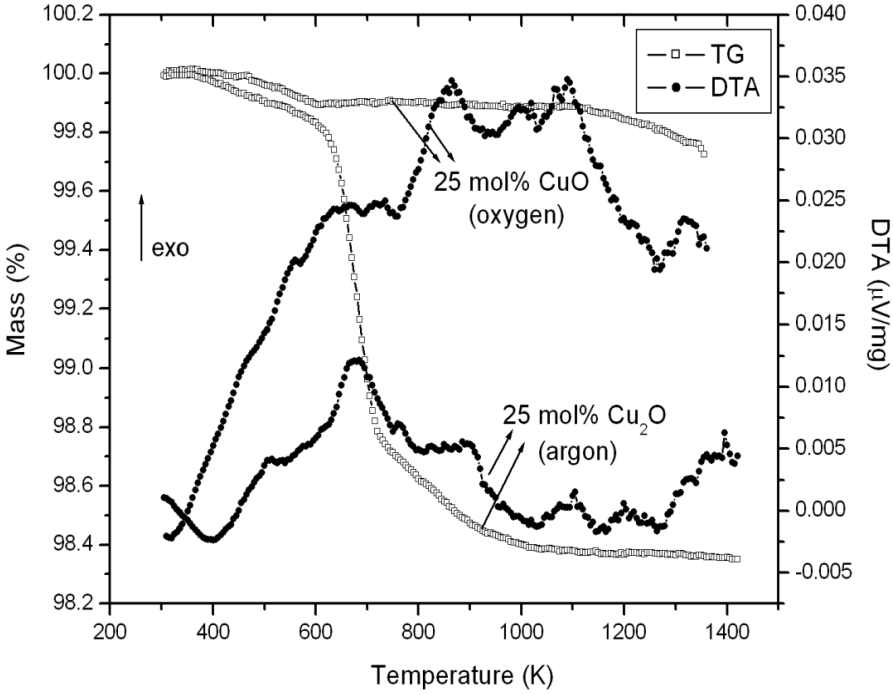

Fig. 5.3.1 DTA and TG curves of samples heated in oxygen ($CuO+ZrO_2$ in the molar ratio 1:3) and in argon (Cu_2O+ZrO_2 in the molar ratio 1:3).

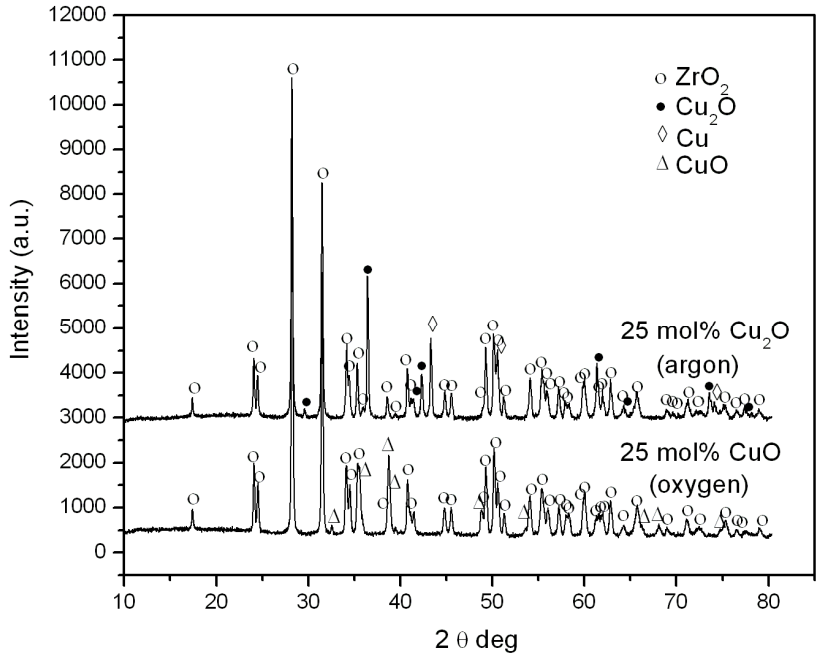

Fig. 5.3.2 XRD patterns of samples heated in oxygen ($CuO+ZrO_2$ in the molar ratio 1:3) and in argon (Cu_2O+ZrO_2 in the molar ratio 1:3).

5.3.2. Thermodynamic calculations and discussion

The extrapolated isothermal sections from lower order systems at 1500 K on the basis of the ionic two-sublattice model $(Cu^{1+},Cu^{2+},Zr^{4+})_p(O^{2-},Va^{q-})_q$ and the associate solution model (Cu, Cu_2O, O, Zr, ZrO_2) for the description of liquid phase are shown in Figs. 5.3.3a and 5.3.3.b, respectively. The extended miscibility gap in Fig. 5.3.3a is an artefact of the two-sublattice ionic model, which tails to describe a short range ordering in the liquid phase as it was already explained in the Chapter 5.2. Therefore, the associate solution model was adopted for description of the liquid phase in the ternary Cu-Zr-O system.

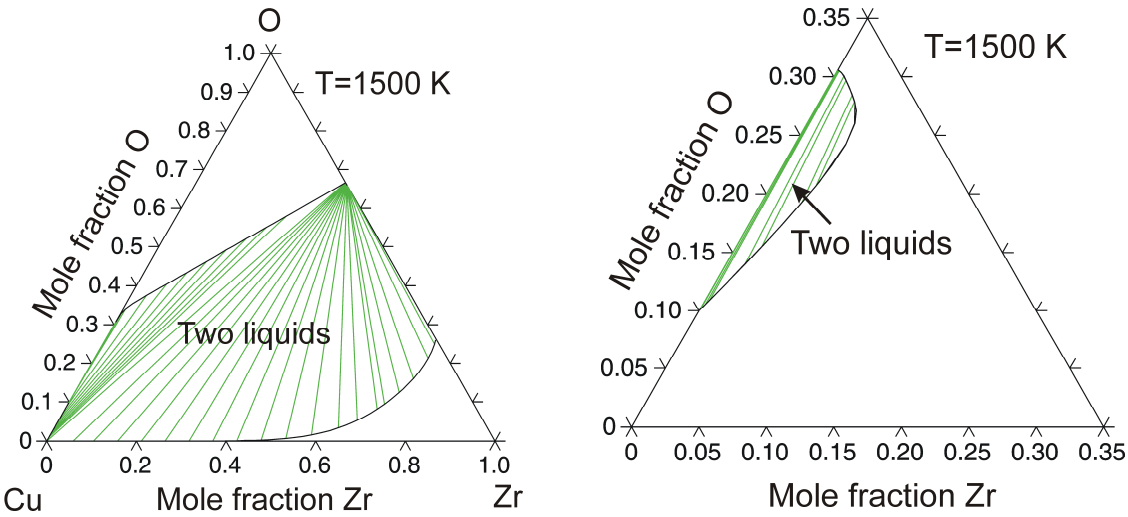

a) b)

Fig. 5.3.3. The extrapolated isothermal sections from lower order systems of the Cu-Zr-O system at 1500 K using the two-sublattice ionic (a) and associate solution model for the liquid phase (b). Phase equilibria involving gas and condensed phases have been neglected.

Due to the lack of experimental information and already existing agreement between available experimental data and calculated phase diagrams by only extrapolation from the binary subsystems Cu-O, Zr-O and Cu-Zr (Figs. 5.3.4 - 5.3.6), optimization of the Cu-Zr-O system was not performed.

The calculated temperature of the eutectic reaction L ↔ βZrO_2+ Cu_2O in air at 1392.4 K (Fig. 5.3.4) is slightly lower in comparison with the measured one at 1401 K [1966Gad2], but it is consistent with the assessed Cu-O binary system. The uncertainty of measurements was not reported in the work of Gadalla and White [1966Gad2]. The solubility of Cu_2O in the liquid is less than 0.2 mol. % at the eutectic temperature which is just below the melting of Cu_2O. The calculated isobaric section in oxygen (Fig. 5.3.4) is in good agreement with the experimental data [1966Gad2].

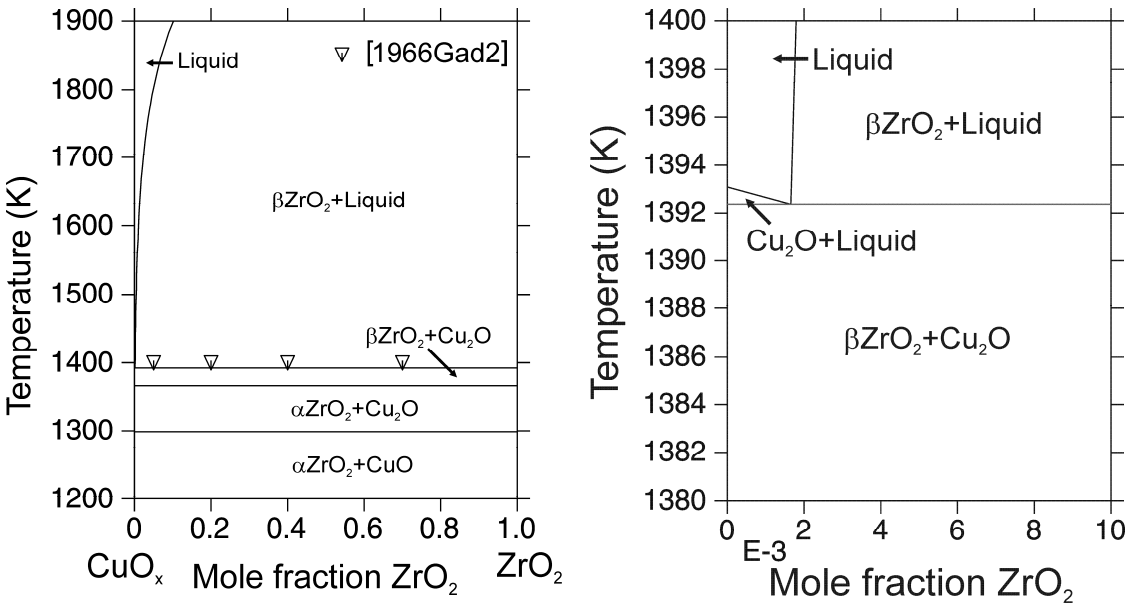

a) b)

Fig. 5.3.4 Calculated isobaric section of CuO_x-ZrO_2 in air (a) and enlarged CuO_x-rich side of the diagram (b).

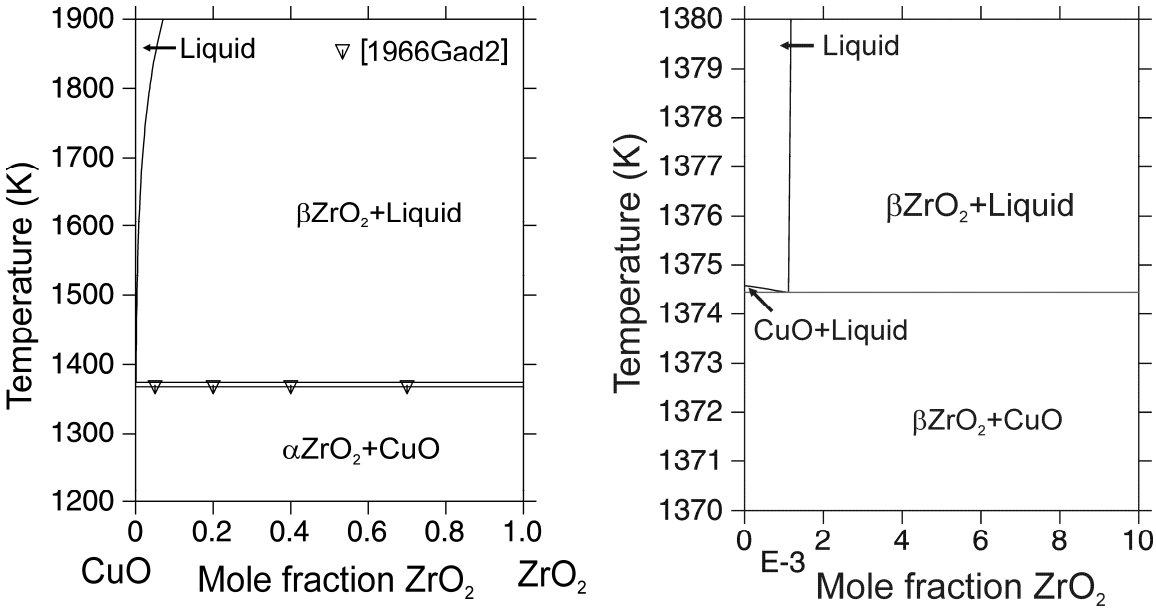

a) b)

Fig. 5.3.5 Calculated isobaric section of CuO-ZrO_2 in oxygen (a) and enlarged CuO-rich side of the diagram (b).

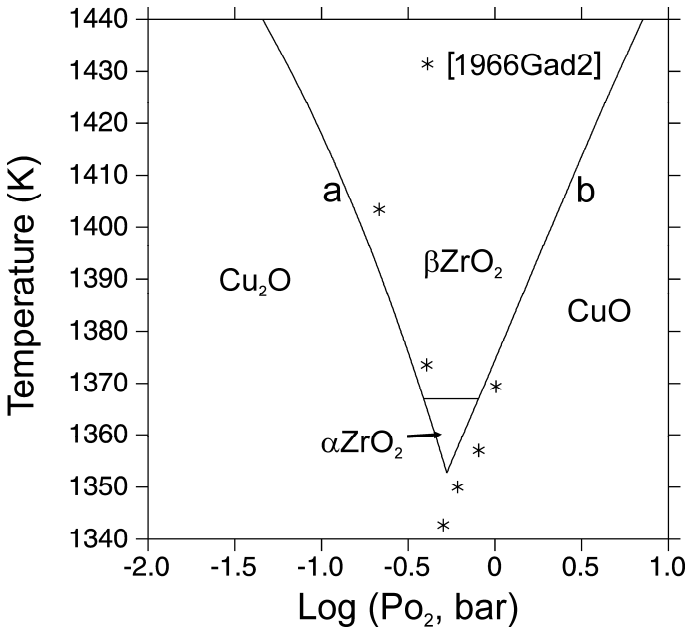

Fig. 5.3.6 Calculated effect of partial pressure of oxygen on the temperature of monovariant reactions Liquid ↔ (α/or β)ZrO_2 + Cu_2O (a) and Liquid + (α/or β)ZrO_2 ↔ CuO (b) in comparison with experimental data of Gadalla and White [1966Gad2].

Fig. 5.3.6 shows the effect of the partial pressure of oxygen on the temperature of the monovariant reactions Liquid ↔ (α/or β)ZrO_2 + Cu_2O (a) and Liquid + (α/or β)ZrO_2 ↔ CuO (b). The intersection of the lines a and b corresponds to the ternary eutectic Liquid ↔ αZrO_2 + Cu_2O + CuO. A good agreement between calculations and measured data can be seen.

The calculated isothermal sections (Fig. 5.3.7) and projection of monovariant liquidus lines (Figs. 5.3.8) show the predicted phase equlibria. A closed liquid miscibility gap is present on the isothermal section at 1540 K near to the binary Cu-O system (Fig. 5.3.7c). The homogeneity region of the liquid phase reasonably widens with increasing temperature (Fig. 5.3.7d).

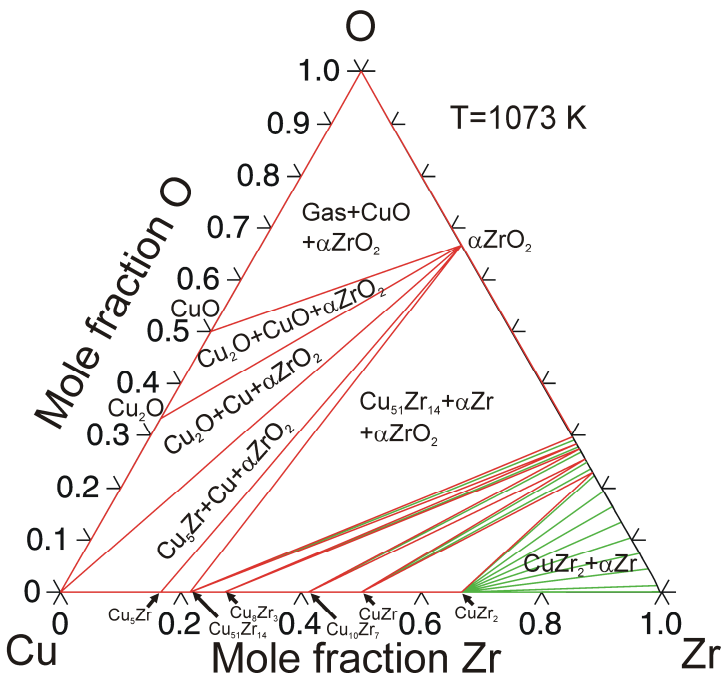

a)

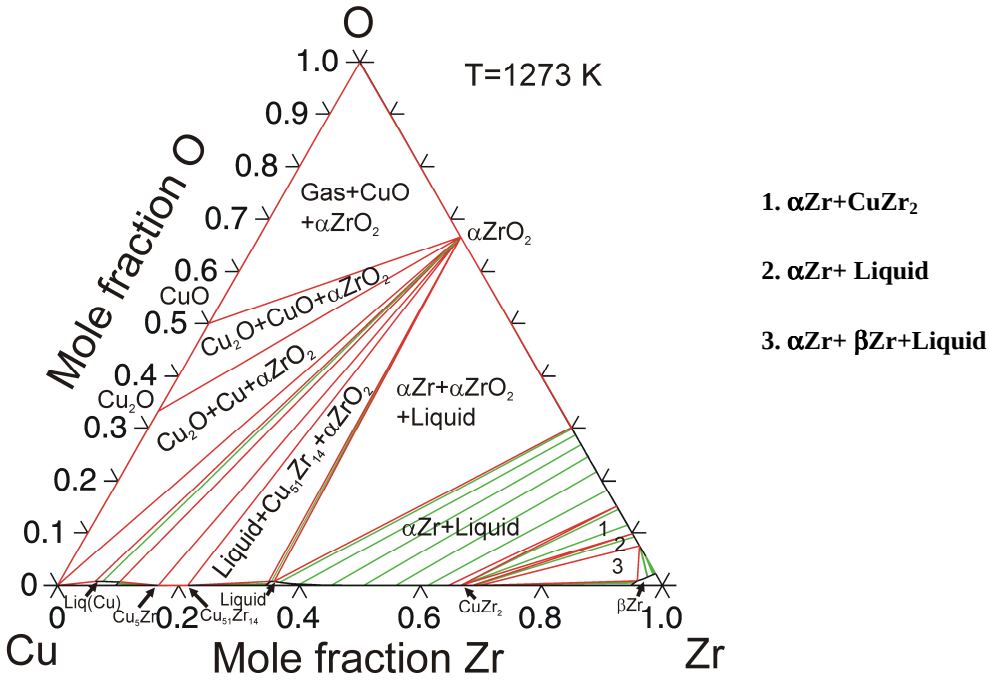
O
T=1273 K
Mole fraction O
Gas+CuO
+αZrO2
αZrO2
CuO
Cu2O+CuO+αZrO2
Cu2O
Cu2O+Cu+αZrO2
Liquid+Cu51Zr14+αZrO2
αZr+αZrO2
+Liquid
αZr+Liquid
1
2
3
Liq(Cu)
Cu5Zr
Liquid
Cu51Zr14
CuZr2
βZr
Cu
Mole fraction Zr
Zr
1. αZr+CuZr2
2. αZr+ Liquid
3. αZr+ βZr+Liquid

b)

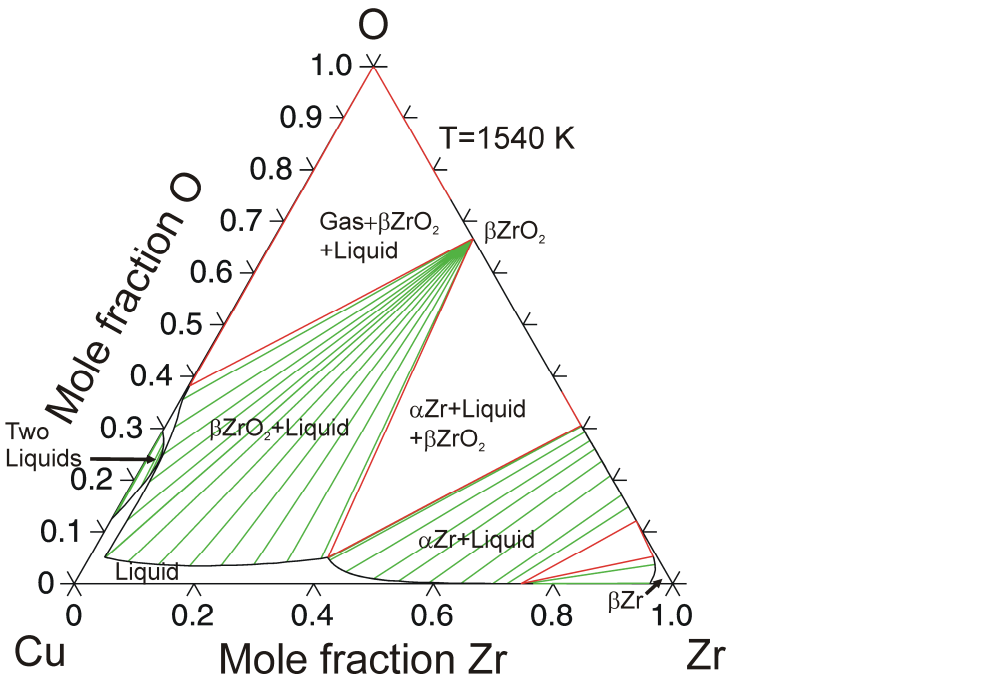
O
T=1540 K
Mole fraction O
Gas+βZrO2
+Liquid
βZrO2
Two
Liquids
βZrO2+Liquid
αZr+Liquid
+βZrO2
αZr+Liquid
Liquid
βZr
Cu
Mole fraction Zr
Zr

c)

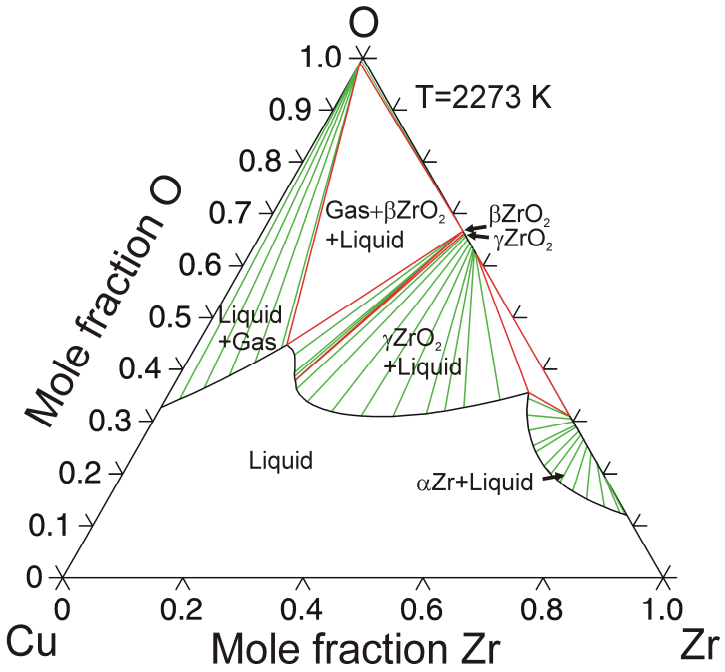

d)

Fig. 5.3.7 Calculated isothermal sections of the Cu-Zr-O system at 1073 (a), 1273 (b), 1540 (c) and 2273 K (d) and 1 bar pressure.

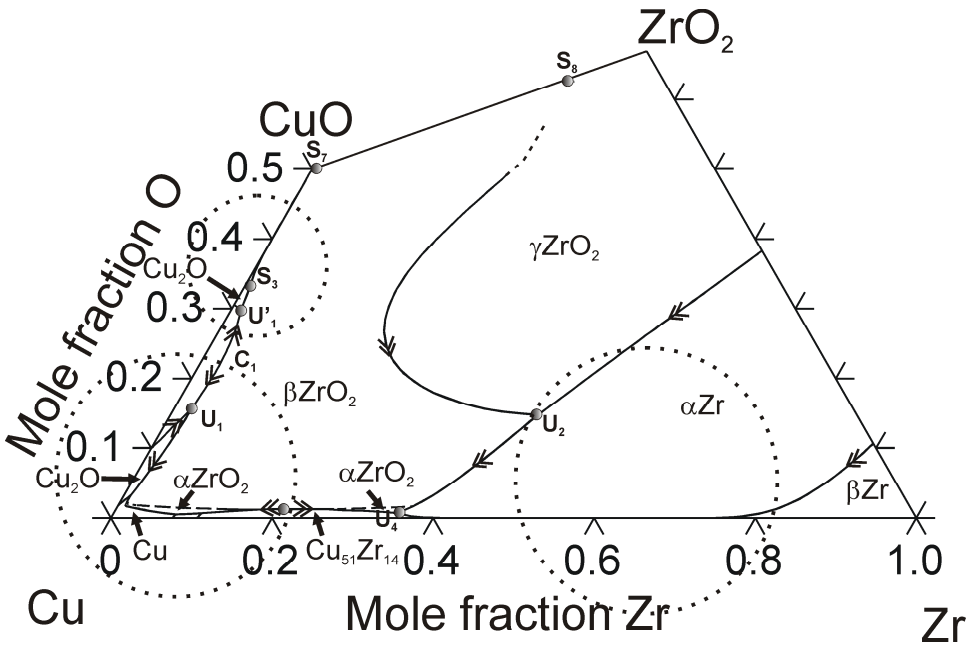

a)

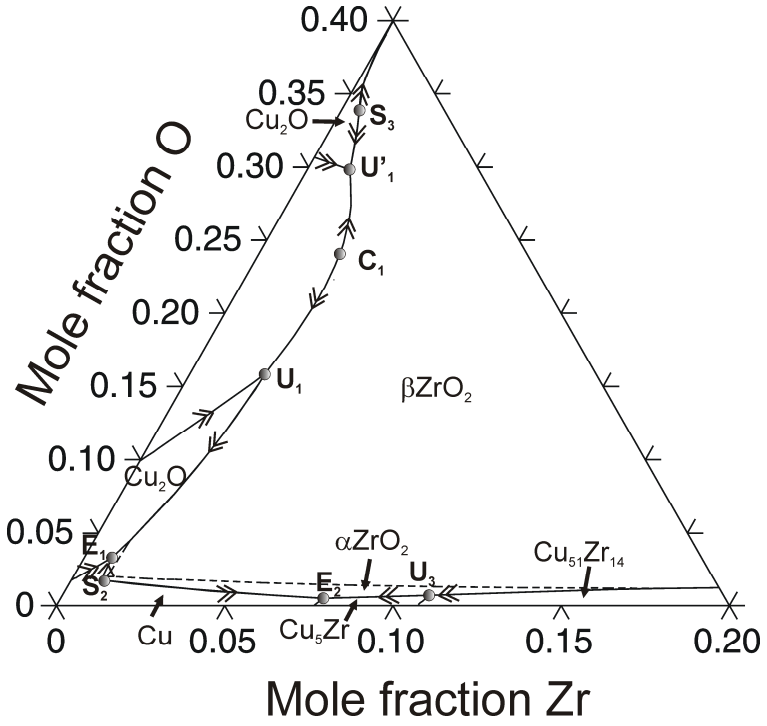
0.40
0.35
0.30
0.25
0.20
0.15
0.10
0.05
0
Mole fraction O
Cu2O
S3
U'1
C1
U1
βZrO2
Cu2O
E1
S2
αZrO2
E2
U3
Cu51Zr14
Cu
Cu5Zr
0
0.05
0.10
0.15
0.20
Mole fraction Zr

b)

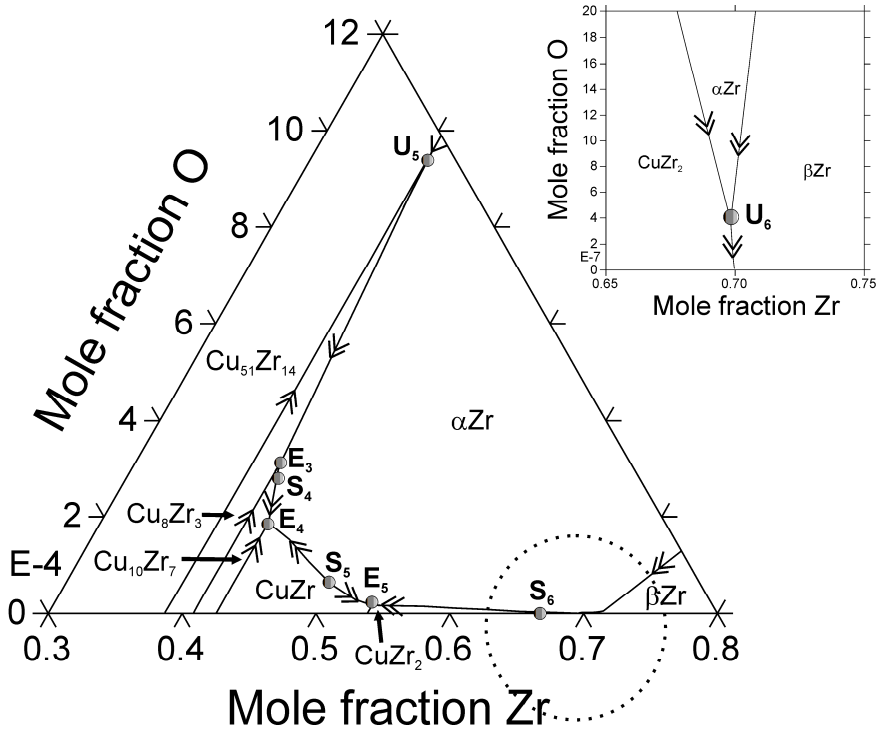
12
10
8
6
4
2
E-4
0
Mole fraction O
U5
Cu51Zr14
αZr
E3
S4
Cu8Zr3
E4
Cu10Zr7
S5
E5
CuZr
S6
βZr
CuZr2
0.3
0.4
0.5
0.6
0.7
0.8
Mole fraction Zr
Mole fraction O
αZr
CuZr2
βZr
U6
0.65
0.70
0.75
Mole fraction Zr

c)

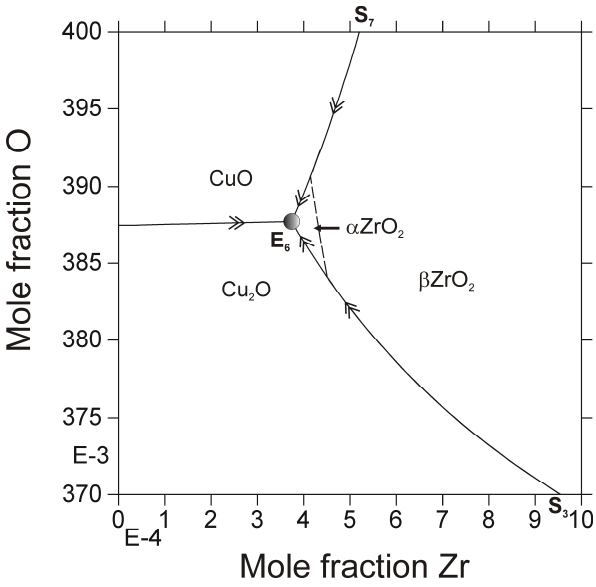

d)

Fig. 5.3.8 The calculated projection of the monovariant liquidus lines in the ternary Cu-Zr-O system (a) and magnified parts: Cu-rich part (b), Zr-rich part (c) and O-rich part (d). Fields of primary crystallization are indicated.

An upper critical point C_1 exists on the monovariant liquidus curve $U_1C_1U'_1$ (Fig. 5.3.8a) and at this point the composition of the both liquids is the same. At the critical temperature liquid is in equilibrium with βZrO_2. Peculiarity of monovariant line $U_1S_2E_2$ (Fig. 5.3.8b) is due to the extrapolated description of the liquid. By introducing ternary interaction parameters smooth curve can be obtained. However, using ternary interaction parameters without sufficient experimental information cannot be justified and can create unexpected problems upon extrapolation in to higher-order systems. Scheil reaction scheme of the Cu-Zr-O system is given in Fig. 5.3.9.

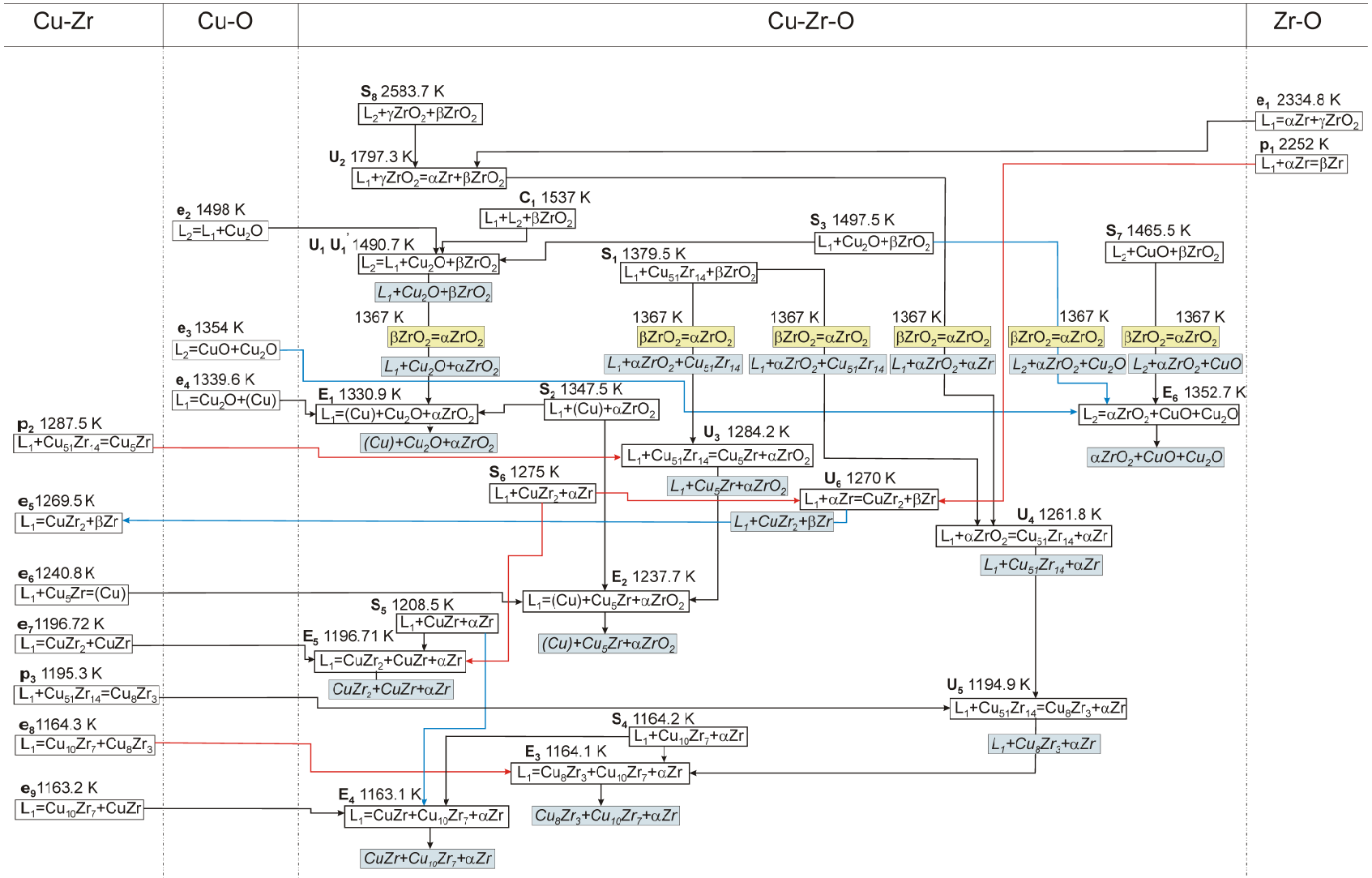

Fig. 5.3 Fig. 5.3.9 Scheil reaction scheme of the Cu-Zr-O system

6. QUASITERNARY $PbO-ZrO_2-TiO_2$ SYSTEM

Experimental studies of the three ternary O-Pb-Zr, O-Pb-Ti and O-Zr-Ti systems are confined to the investigation of lead zirconate ($PbZrO_3$), lead titanate ($PbTiO_3$) and zirconium titanates ($ZrTiO_4$, $ZrTi_2O_6$) as well as of the quasibinary systems $PbO-ZrO_2$, $PbO-TiO_2$ and ZrO_2-TiO_2.

The modelling of the quasibinary $PbO-ZrO_2$ and $PbO-TiO_2$ systems was done by Koo et al. [1999Koo] and Soh et al. [1994Soh], respectively. Thermodynamic assessments of the ZrO_2-TiO_2 system were published by several authors [1992Yok, 2000Gon, 2001Par]. However, they differ markedly from each other. The thermodynamic modelling of the quasiternary $PbO-ZrO_2-TiO_2$ system has not been done so far. In the present work the three boundary systems were reassessed using the most recent experimental information to obtain a self-consistent thermodynamic description of the $PbO-ZrO_2-TiO_2$ system based on the available data on phase equlibria and thermodynamic properties.

6.1. Survey of the literature information

6.1.1. $PbO-ZrO_2$

Literature information belong mainly to investigations of the crystallographic and dielectric properties of the lead zirconate with only a few phase diagram and thermodynamic studies. Three stable perovskite-type phases have been found at the $PbZrO_3$ composition: the orthorhombic low-temperature (α, up to 504 K) phase is antiferroelectric, the intermediate (γ, from 504 to 507 K) is ferroelectric, and the cubic high-temperature (β, up to the melting point $T_m = 1843$ K) phase is paraelectric (Table 6.1). The paraelectric → ferroelectric → antiferoelectric phase transition temperatures depend on the oxygen non-stoichiometry and on the compositional deviations caused by the sublimation of PbO [1985Ujm]. Until now, the basic structure parameters have mainly been investigated for the antiferroelectric phase. The questions

regarding the existence of polarization and the true crystal structure of lead zirconate are still open.

The quasibinary section of the PbO-ZrO_2 system was published by Fushimi and Ikeda [1967Fus]. Cubic $PbZrO_3$ decomposes to tetragonal ZrO_2 and a liquid phase containing ~ 90 mol. % PbO at 1843 K [1967Fus]. A few investigations have been performed in the PbO-rich part of the PbO-ZrO_2 system [1967Fus, 1981Jac, 1967Har] but the results are contradictory. [1967Har] reported that the X-ray analysis of the samples PbO + ZrO_2 in 1:1 molar ratio heated to 1563 K indicated the presence of β$PbZrO_3$, monoclinic ZrO_2, and αPbO. The latter had a tetragonal structure rather than the orthorhombic structure of yellow βPbO. This finding was confirmed by Jacob and Shim [1981Jac] by heating an equimolar mixture of βPbO and α ZrO_2 up to 1228 K, followed by cooling in air and X-ray analysis. The schematically proposed phase relations in the PbO-rich part of PbO-ZrO_2 phase diagram [1981Jac] and assessed phase diagram [1999Koo] mainly were based on the similarity with those reported by Rase [1971Ras] for PbO-TiO_2 system. This observation is not in accord with the phase diagram of [1967Fus] as well as with the experimental results obtained in the present work. Fushimi and Ikeda [1967Fus] preformed the DTA analysis of the PbO+ZrO_2 mixtures containing more than 95 mol. % PbO. The strong peak at 1178 ± 5 K was observed for the all investigated samples which correspond to the peritctic reaction L + β$PbZrO_3$ ↔ βPbO and the PbO content in the liquid at the peritectic temperature exceeds 99 mol. %. The experimental results obtained in this thesis show a solubility of 1.3 ± 2 mol. % ZrO_2 in orthorhombic βPbO at 1043 K (see Chapter 7). This result is consistent with reported PbO-rich part of phase diagram by Fushimi and Ikeda [1967Fus] and findings of Ikeda et al. [1962Ike] that in the solid state PbO dissolves up to 4 mol. % ZrO_2, but it is contradictory with the proposed PbO-rich part of PbO-ZrO_2 diagram [1981Jac] and stabilization of the tetragonal αPbO solid solution up to its melting, as well as with the assessed PbO-ZrO_2 system [1999Koo].

Thermodynamic properties of $PbZrO_3$ were investigated by several groups [1993Gos, 1996Ono, 1979Sch, 1969Hae, 1973Hol, 1981Jac, 1999Pop]. The experimental investigations were mainly performed on the high-temperature cubic modification,

$\beta PbZrO_3$, except the study of [1993Gos] on the low-temperature orthorhombic, $\alpha PbZrO_3$, modification. Onodera et al. [1996Ono] measured the heat capacity of single crystals of antiferroelectric $\alpha PbZrO_3$ in a wide temperature region (from room temperature to 650 K) by AC calorimetry, but have drawn the curve in arbitrary units. The heat capacity curve showed a sharp change at 504.5 K, due to transformation into the high-temperature modification $\beta PbZrO_3$. The transition entropy was reported to be ΔS = 1.65 $J \cdot mol^{-1} \cdot K^{-1}$. Gospodinov et al. [1993Gos] reported the thermodynamic functions (C_p, S, $H_T - H_{298}$) of the low-temperature orthorhombic modification (α) from room temperature to 504 K.

The low-temperature heat capacity data of $\alpha PbZrO_3$ are missing, while the results of Gospodinov [1993Gos] are not consistent with the measured thermodynamic properties [2001Ran, 1969Hae, 1973Hol, 1999Pop] and the PbO-ZrO_2 phase diagram reported by Fushimi and Ikeda [1967Fus]. The Gibbs energy of formation of lead zirconate calculated from earlier vapor pressure studies (assuming that the vapor phase consists entirely of monomeric PbO molecules) [1979Sch, 1973Hol, 1969Hae] is inconsistent with the EMF measurements reported by Jacob and Shim [1981Jac] and the calculated PbO-ZrO_2 quasibinary phase diagram, which suggests decomposition of lead zirconate to tetragonal ZrO_2 and a liquid phase containing ~ 90 mol. % PbO at 1843 K. Since the vapor phase over pure solid and liquid PbO consist of polymeric species of type Pb_nO_n ($1 \leq n \leq 6$) results based on the vapor pressure measurements differ significantly from those obtained by EMF measurements [1981Jac]. At the same time, most recent data from the vapor pressure measurement reported by Popovic et al. [1999Pop] (existence of PbO^+ and Pb_2O^{2+} ions was experimentally detected) show good agreement with results of Jacob and Shim [1981Jac]. Recently, the enthalpy of formation of $PbZrO_3$ was measured by drop solution calorimetry [2001Ran]. The heat content and entropy of $\beta PbZrO_3$ are not known, while thermodynamic data for the other phases (liquid, PbO solid solutions) are completely missing.

6.1.2. PbO-TiO_2

The experimental phase diagram of this system has been reported by several authors [1971Ras, 1980Eis]. However, there is no agreement about the existence of intermediate compounds and their homogeneity ranges. The equilibrium phases in the PbO-TiO_2 system are the PbO solid solution (tetragonal and orthorhombic), liquid, rutile and $PbTiO_3$ with a perovskite-type structure, while the existence of Pb_2TiO_4 and $Pb_2Ti_2O_8$ is doubtful. Only one intermediate compound, $PbTiO_3$, was reported in the PbO-TiO_2 quasibinary system by Rase et al. [1971Ras], while the previously reported Pb_2TiO_4 [1962Rob, 1970Bel] was not observed. $PbTiO_3$ exists in two polymorphic forms, tetragonal (α′, up to 763K) and cubic (β, 763-1558K) (Table 6.1). The ternary $PbTi_3O_7$ compound was found in the TiO_2-rich side [1968Ayk, 1980Eis] and it was included in the isobaric section PbO_x-TiO_2 in air [1980Eis]. The upper limit of stability of $PbTi_3O_7$ was supposed to be 813 K as confirmed by X-ray diffraction results.

Thermodynamic properties of $PbTiO_3$ were investigated by several groups [1973Meh, 1979Sch, 1969Hae, 1973Hol, 1982Shi, 1999Pop, 2001Ran, 2005Ros]. The enthalpy of formation of $PbTiO_3$ using the drop solution calorimetry was measured by Rane and Navrotsky [2001Ran], while the Mehrotra et al. [1973Meh] as well as Shim and Jacob [1982Shi] measured the free energy of formation. The specific heat of pure lead titanate ($PbTiO_3$) in the temperature range from 325 to 1250 K was studied by Rosetti and Maffei [2005Ros]. Vapour pressure measurements using the Knudsen technique were done by many authors [1979Sch, 1969Hae, 1973Hol, 1999Pop]. Results of Schmal et al. [1979Sch], Haerdtl and Rau [1969Hae] and Holman and Fulrath [1973Hol] are in a good agreement, while the data reported by Popovic et.al. [1999Pop] shows significant deviations.

Soh et al. [1994Soh] published the thermodynamic calculation of the PbO-TiO_2 system using a quasi-regular model to express the Gibbs energy of all solution phases. The Gibbs energy of $PbTiO_3$ compound was evaluated on the base of estimated thermodynamic properties (heat capacity) compiled by Barin [1989Bar].

6.1.3. ZrO_2-TiO_2

The solid solutions with Zr:Ti molar ratio ranging from 1:1 to 1:2 are the only stable compounds in the ZrO_2-TiO_2 system. Two structural modifications are known: high temperature disordered and low temperature ordered phase [1983Mch, 1986Mch, 2004Tro1, 2004Tro2] (Table 6.1). Two types of ordered structures with different stoichiometries were reported by Park et al. [1996Par]. $ZrTiO_4$ is known to undergo a successive ordering transition between 1400 and 1100 K [1954Cou, 1996Par]. Above 1400 K it crystallizes in an orthorhombic αPbO_2 type structure, with the random distribution of Zr and Ti over the octahedral site [1967New, 1986Bor] (Table 6.1). Slow cooling of the disordered polymorph below 1400 K results in distinct shortening of the crystallographic *b*-axis, which is due to increasing order of Zr and Ti, as evident by the formation of superstructure reflections [1996Par]. Park et al [1996Par] suggested that the ordering transition occurs in several steps from the normal phase (disordered $\beta Zr_{1-x}Ti_xO_4$, T >1400 K) via an incommensurate state (partially ordered $\alpha ZrTiO_4$, 1400 > T > 1100 K) to the commensurate phase (ordered $\alpha' ZrTiO_4$,). The fully ordered phase $\alpha' ZrTiO_4$ has a composition close to $ZrTi_2O_6$ [1986Mch] but the same structure also occurs for $Zr_5Ti_7O_{24}$ [1986Bor].

The ZrO_2-TiO_2 phase diagram has been studied intensively over many years [1951Sow, 1954Bro, 1954Cou, 1965Coc, 1965Web, 1967Nog, 1968Nog, 1972Ono, 1980She, 1986Mch, 1998Kob, 2004Tro1, 2005Tro]. However, no general agreement among the proposed phase diagrams exists. While detailed phase diagrams are available for the high-temperature regions above 1473 K [1954Cou, 1967Nog, 1980She], where reactions proceed rapidly, the low-temperature phase relations are not well established. Experimental studies disagree significantly on the location of the two-phase field tetragonal-monoclinic ZrO_2 solid solutions [1954Bro, 1965Web, 1968Nog, 1972Ono, 2005Tro] because heating and cooling experiments are characterised by a hysteresis effect. Another problem is caused by sluggish kinetics and difficulty in performing experiments at relatively low temperatures (< 1473 K). Discrepancies are mainly concerned with the existence of intermediate compounds and their homogeneity range.

Three intermediate compounds were reported by Troitzsch et al [2005Tro] and McHale et al. [1986Mch], while earlier studies indicated the absence of any compounds in the system and the presence of partial solid solutions [1937Bue, 1951Sow, 1972Ono]. Both, McHale and Roth [1986Mch] and Troitzsch et al [2004Tro1, 2005Tro] reported the existence of the disordered high-temperature $\beta Zr_{1-x}Ti_xO_4$ phase with a wide homogeneity range, while its stability range and adjacent phase field with the ordered low-temperature phases $\alpha ZrTiO_4$ and $ZrTi_2O_6$ differ significantly. The low-temperature technique of solid solution formation via coprecipitation from alkoxides solution was used as an alternative method of preparation for a wider range of compositions in the system ZrO_2-TiO_2 [1986Mch], to enable the determination of the low-temperature solid solution region and structure without the influence of prior high-temperature heat treatment. Although, there is an agreement between different authors [1986Mch, 2005Tro] about the existence of intermediate compounds and solid solution of the end-members (titania, monoclinic and tetragonal zirconia), the solubility ranges markedly differ, particularly in the ZrO_2-rich range, close to monoclinic-tetragonal transformation. In addition, experimental data on the homogeneity range of the cubic zirconia are missing and it has been drawn tentatively [1954Bro, 1968Nog, 1980She, 1998Kob]. Liquidus and solidus were studied by Shevchenko et al. [1980She], Coughanour et al. [1954Cou] and Noguchi and Mizuno [1967Nog]. Liquidus of the system has two inflections, which correspond to 35 and 60 mole % TiO_2 [1980She], and eutectic point at 73 mole % and 1993 K [1980She] or 80 mole % TiO_2 and 2033 K [1954Cou]. High temperature $\beta ZrTiO_4$ phase melts incongruently at 2093 [1954Cou] or 2103 K [1980She].

The thermodynamic data of formation and molar heat capacity from 5 to 380 K of $ZrTiO_4$ compound were measured by Hom et al. [2001Hom]. No other works concerning the thermodynamics of the phases in this system are available.

6.1.4. PbO-ZrO_2-TiO_2

The perovskite-structured ferroelectrics in the $Pb(Zr_xTi_{1-x})O_3$ (PZT) system provide an unusual example of a complete solid solution between the congruently and

incongruently melting compounds $PbTiO_3$ and $PbZrO_3$ [1965Web, 1971Ras, 1971Moo, 1973Hol, 1999Pop]. At high temperatures, $Pb(Zr_xTi_{1-x})O_3$ crystallise as disordered substitional solid solutions to a cubic perovskite prototype phase of symmetry *Pm*3*m* for all values of *x*. Intermediate solid solutions compositions with different Zr/Ti ratio adopt orthorhombic, tetragonal and rhombohedral symmetries at temperatures between 273 and 763 K due to a variety of cation shifts, octahedral tilts and deformations [1971Jaf] (Table 6.1). Recent literature data indicate also the existence of monoclinic modification at low temperatures [2000Noh, 2000Sou, 2001Sou, 2001Fra]. At room temperature these include the lower-symmetry antiferroelectric, orthorhombic structure ($\alpha PbZr_xTi_{1-x}O_3$ phase) of $PbZrO_3$ [1997Cor]. All its solid solutions with more than 10 mol % of $PbTiO_3$ are ferroelectric. With increasing Ti content, two ferroelectric rhombohedral phases are observed up to around x ≈ 0.5 where there is transition into a ferroelectric tetragonal phase ($\alpha' PbZr_xTi_{1-x}O_3$) continuing to the end-member $PbTiO_3$ [1978Gla]. At room temperature, the rhombohedral low-temperature phase ($\gamma' PbZr_xTi_{1-x}O_3$) has the space group $R\bar{3}c$ and exhibits both cation shifts and octahedral tilting [1998Cor]. As temperature increases the octahedral tilts are known to disappear [1978Gla] leading to the phase transformation to the high-temperature rhombohedral phase ($\delta PbZr_xTi_{1-x}O_3$) and space group $R\bar{3}m$. A further increase in temperature diminishes the cation shifts until the final phase transition into the cubic perovskite structure ($\beta PbZr_xTi_{1-x}O_3$ phase) occurs. The monoclinic-tetragonal phase transition was observed at low temperatures in $PbZr_xTi_{1-x}O_3$ solid solutions in the vicinity of the morphotropic phase boundary (MPB) (x = 0.5–0.55) [2000Noh, 2001Noh, 2000Sou, 2001Fra, 2002Ara, 2005Bou].

The experimental phase diagram of the PZT system at higher temperatures was investigated by few groups [1965Web, 1967Fus, 1971Moo] (Table 6.2), while there were many studies concerning the low-temperature phase relations [1953Saw, 1971Jaf, 1982Leo, 1986Fes, 1989Ere, 1995Vie, 1997Mis, 2001Noh, 2002Ara, 2005Bou]. Webster et al. [1965Web] published the isothermal section at 1373 K for the titania and zirconia rich part of $PbO-ZrO_2-TiO_2$ system ($ZrO_2-TiO_2-PbTiO_3-PbZrO_3$), while the isothermal sections at 1373, 1473 and 1573 K of the PbO-rich part of the system were studied by

Fushimi and Ikeda [1967Fus]. The pseudobinary section $PbZrO_3$-$PbTiO_3$ was reported by Fushimi and Ikeda [1967Fus] and Moon et al. [1971Moo]. The temperature of the peritectic reaction, L + βZrO_2 (tetragonal) → $\beta PbZr_xTi_{1-x}O_3$ (x ~ 0.4), was found to be 1613 [1967Fus] or 1633 K [1971Moo], while somewhat lower solidus and liquidus temperatures were measured in [1971Moo]. Results of these studies are in satisfactory agreement and differences are within the uncertainty of measurements. Work of Holman

Table 6.1 Solid phases.

Phase, temp. range (K)	**Pearson symbol/ Space Group/ Prototype**	**Lattice parameters (pm) and angles**	**Comments**
$\beta PbZr_xTi_{1-x}O_3$ 507 < T < 1843	*cF** *Fm-3m* –	*a* = 415 *a* = 414.49	pure $PbZrO_3$[1951Saw] $PbZr_{.9}Ti_{.1}O_3$ [1978Gla]
$\gamma PbZrO_3$ 504 < T < 507	*cF** *F2mm* –	–	[1982Tan]
$\alpha PbZr_xTi_{1-x}O_3$ T< 504 x > 0.9	*oP*40 *Pbam* –	*a* = 588.194; *b* =1178.206; *c* = 822.946	pure $PbZrO_3$ at 298 [1998Tes]
$\alpha' PbZr_xTi_{1-x}O_3$ *T< 763 x < ~ 0.5	*tP*5 *P4mm* –	**a* =**b* = 390.231 * *c* = 403.292 ***a* =* **b* = 395.251 ** *c* = 414.84	* pure $PbTiO_3$ at 298 [2002San] * *$PbZr_{.2}Ti_{.8}O_3$ [2000Fra]
$\gamma' PbZr_xTi_{1-x}O_3$ ~ 0.6 < x < ~ 0.95 T < ~ 423	*hR*10 $R\bar{3}c$ –	*a* = *b* = 585.64 *c* = 1439.51 β =120°	$PbZr_{.9}Ti_{.1}O_3$ [1978Gla]
$\delta PbZr_xTi_{1-x}O_3$ x > 0.5 T < ~ 660	*hR*5 $R\bar{3}m$ –	*a* = *b* = *c* = 410.01 α = β = γ =89.73°	$PbZr_{.75}Ti_{.25}O_3$ [1988Jir]
$\varepsilon PbZr_xTi_{1-x}O_3$ 0.50 < x < 0.52	*mS*10 C_1m_1 –	*a* = 570.82; *b* = 570.78; *c* = 414.14; β = 90.199°	$PbZr_{.52}Ti_{.48}O_3$ [2001Fra]
$PbTi_3O_7$ T < 813	*mP*22 $P12_1/m_1$ –	*a* = 1071.85; *b* = 381.21; *c* = 657.77; β = 98.277°	at 298 K [1974Kat]
$\beta Zr_xTi_{1-x}O_4$ 1443 < T < 2103 0.41 < x <0.59	*oP*12 *Pbcn* αPbO_2	*a* = 480.422; *b* = 548.253; *c* = 503.132	[1986Bor] mineral name: Srilankite
$\alpha ZrTiO_4$ 1343 < T < 1443	– *Pbcn* –	*a* = 960; *b* = 530; *c* = 500	[1992Chr, 2006Don]
$\alpha' ZrTiO_4$ ($ZrTi_2O_6$, $Zr_5Ti_7O_{24}$) T < 1343	*oP*36 *Pbcn* –	*a* = 1435.74; *b* = 532.47; *c* = 502.00	[1986Bor]

Table 6.2 Selection of experimental information for the $PbO-ZrO_2-TiO_2$ system: phase diagram data.

Reference	Experimental Technique	Measured quantity, temperatures, compositions
[1954Bro]	X-ray diffraction	Subsolidus phase relations in the ZrO_2-TiO_2 quasibinary at 1253 and 1643 K.
[1954Cou]	X-ray diffraction, Optical pyrometry	Liqudus and solidus of the quasibinary ZrO_2-TiO_2 section.
[1965Web]	X-ray diffraction, Differential thermal analysis, Optical microscopy, Chemical analysis	Subsolidus phase relations in the system $PbO-ZrO_2-TiO_2$ at 1373 K; Zirconia rich part of ZrO_2-TiO_2 quasibinary system: Solvus of monoclinic-tetragonal transformation and solubility of titania in zirconia solid solution in temperature range 873-1373 K.
[1967Nog]	Brightness pyrometry in the solar furnace (cooling curves)	Liquidus of the quasibinary ZrO_2-TiO_2 system.
[1967Fus]	X-ray diffraction, Quenching	Liquidus and subsolidus of the quasibinary $PbO-ZrO_2$ section. Phase relations in the $PbO-ZrO_2-TiO_2$ system: isothermal, isobaric section at 1373, 1473 and 1573 K in air; liquidus and solidus of $PbZrO_3-PbTiO_3$ section.
[1968Nog]	Brightness pyrometry in the heliostat-type solar furnace Quenching, X-ray diffraction	Liquidus of the quasibinary ZrO_2-TiO_2 system; Solid solution boundaries at lower temperature: phase boundary of the monoclinic and tetragonal zirconia solid solutions.
[1971Ras]		Liquidus and subsolidus of the quasibinary $PbO-TiO_2$ system;
[1972Ono]	High temp. X-ray diffraction, Differential thermal analysis	Zirconia rich part of ZrO_2-TiO_2 quasibinary system: Solvus of monoclinic-tetragonal transformation of zirconia solid solutions
[1971Moo]	X-ray diffraction, Quenching	Liquidus and solidus of $PbZrO_3-PbTiO_3$ section.
[1980She]	X-ray diffraction, Differential thermal analysis	Liquidus and solidus of the quasibinary ZrO_2-TiO2 system.
[1980Eis]	X-ray diffraction, Differential thermal analysis and themogravimetry, Thermobalance (by molar ratio O/Pb)	Air isobar of the PbO_x-TiO_2 and ternary TiO_2-PbO_2-Pb system. Subsolidus phase relations and stability range of phases based on the dissociation curves using the thermobalance to follow equilibrium loss in O/Pb weight. Stability range of intermediate phases ($PbTiO_3$ and $PbTi_3O_7$) below 973 K.
[1986Mch]	X-ray diffraction, Neutron powder diffraction	Subsolidus of of the quasy binary ZrO_2-TiO_2 section. Phase relations between 1273 and 1773 K. Stability range of $ZrTiO_4$ and $ZrTi_2O_6$ phases.
[1998Kob]	X-ray diffraction, Differential thermal analysis	Subsolidus of of the quasy binary ZrO_2-TiO_2 section. Metastable phase relationships.Homogenity range of $ZrTiO_4$ phase.
[2004Tro1]	X-ray diffraction, Rietveld analysis	Subsolidus of the quasibinary ZrO_2-TiO_2 section: Stability and homogeneity range of the ordered and disordered $ZrTiO_4$ phases; phase boundaries of titania and zirconia solid solutions and intermediate ($ZrTiO_4$) phases.
[2005Tro]	X-ray diffraction, Rietveld analysis	Subsolidus of the quasibinary ZrO_2-TiO_2 section: Solvus of monoclinic-tetragonal transformation of the zirconia solid solutions; stability and homogeneity range of the ordered and disordered intermediate phases; phase boundaries of titania and zirconia solid solutions and intermediate ($ZrTiO_4$) phases.

Table 6.3 Selection of experimental information for the $PbO-ZrO_2-TiO_2$ system: thermodynamic data.

Reference	Experimental Tecnique	Measured quantity, temperatures, compositions
[1969Hae]	Knudsen effusion	PbO potential above the lead titanate, lead zirconate and $Pb(Ti_{1-x}Zr_x)O_3$ solid solutions in the temperature range 1073 – 1350 K.
[1973Meh]	EMF	Gibbs energy of formation of $PbTiO_3$ compound in the temperature range 1073 – 1273 K.
[1973Hol]	Knudsen effusion	PbO potential above the lead titanate, lead zirconate and $Pb(Ti_{1-x}Zr_x)O_3$ for x=0.5 in temperature range 1073 – 1350 K; Non-stoichiometry of lead zirconate-lead titanate: Lead oxide, titania and zirconia activities as functions of composition in the lead-titanate and lead-zirconate single phase region; Activity coefficient of PbO as a function of $Pb(Ti_{1-x}Zr_x)O_3$ composition at 1373 and 1473 K.
[1979Sch]	EMF Knudsen effusion	Gibbs energy of formation of $PbTiO_3$ and $PbZrO_3$ compounds in the temperature range 673 – 946 K. PbO potential above the lead titanate, lead zirconate and $Pb(Ti_{1-x}Zr_x)O_3$ solid solutions in the temperature range 673 – 1300 K.
[1982Shi]	EMF	Gibbs energy of formation of $PbTiO_3$ compound in the temperature range 1075 – 1350 K.
[1981Jac]	EMF	Gibbs energy of formation of $PbZrO_3$ compound between 1073 – 1673 K
[1993Gos]	DSC	Specific heat of the $PbZrO_3$ compound in the temperature range 400 – 480 K.
[1999Pop]	Knudsen effusion	Lead oxide activity above the lead titanate, lead zirconate and $Pb(Ti_{1-x}Zr_x)O_3$ solid solutions in the temperature range 1000 – 1350 K.
[2001Hom]	Adiabatic calorimetry Solution calorimetry	Specific heat of the $ZrTiO_4$ compound in the temperature range 13 – 400 K; Enthalpy of formation at 973 and 1073 K.
[2001Ran]	Solution calorimetry Drop solution calorimetry	Enthalpy of formation of the lead titanate, lead zirconate and $Pb(Ti_{1-x}Zr_x)O_3$ solid solutions and heat of mixing at 973 K.
[2005Ros]	High-temp. DSC	Specific heat of the $PbTiO_3$ compound in the temperature range 323 – 1273 K, enthalpy and entropy of tetragonal – cubic phase transition.

et al. [1973Hol] was mainly concerned with the width of the homogeneity range of $\beta Pb_{1-y}\square_y(Zr_xTi_{1-x})O_{3-y}$ solid solution at 1373 K.

Thermodynamic properties of the $\beta PbZr_xTi_{1-x}O_3$ solid solutions are mainly derived from the PbO-vapor pressure measurements using the Kundsen technique [1969Hae, 1973Hol, 1979Sch, 1999Pop]. Rane et al. [2001Ran] reported the standard enthalpies and heat of mixing in the cubic lead zirconate titanate solid solutions using drop solution calorimetry (Table 6.3).

6.2. Thermodynamic optimization

Phase equilibria in the PbO-TiO_2 system are accepted from the work of Rase et.al. [1971Ras], except for the PbO-rich side. The Gibbs energy of the tetragonal and cubic lead titanate is based on most recent experimental information [2005Ros]. Simillary to the previous work [1999Koo] only the high-temperature $PbZrO_3$ phase is included in the assessment of the PbO-ZrO_2 system. The phase relations in the PbO-rich part of the PbO-ZrO_2 system are based on the results of Fushimi and Ikeda [1967Fus] and those obtained in the present work (see Chapter 7). The present assessment of ZrO_2-TiO_2 system is mainly based on the most recent and extensively investigated phase diagram published by Troitzsch et al [2005Tro]. The thermodynamic data for the $ZrTiO_4$ compound [2001Hom] are used together with the determined phase boundaries of the two phase regions zirconium titanate + zirconia solid solution and zirconium titanate + titania solid solution. Both, low- and high-temperature $ZrTiO_4$ phases are included in the assessment and in view of insufficient experimental information they are modelled as separate phases. In addition, the solubility of titania in the monoclinic zirconia is based on the carefully selected experimental data [1971Ono], while the homogeneity range of the cubic zirconia is estimated. Optimisation in PbO-ZrO_2-TiO_2 system was done using the phase equilibria data reported by Fushimi and Ikeda [1967Fus] coupled with measured partial pressure of lead oxide over the PZT solid solutions [1969Hae, 1973Hol, 1979Sch, 1999Pop].

6.3. Discussion

The resulting set of parameters is shown in Appendix (Table 1). By expanding the interaction parameters of the liquid to higher order terms a better fit of experimental data might be obtained. However, the experimental data themselves are not conclusive enough and, therefore, the introduction of higher order terms (particularly for the liquid phase, ${}^{1}L$ and ${}^{2}L$) was not considered.

The calculated phase diagrams of the binary PbO-TiO_2, PbO-ZrO_2 and ZrO_2-TiO_2 systems are presented on the Figs. 6.1, 6.2 (a and b) and 6.3 (a, b and c), respectively.

The Gibbs energy of both, tetragonal $\alpha PbTiO_3$ and cubic $\beta PbTiO_3$ modifications are evaluated in the present work (Table 6.4). The thermodynamic properties of lead titanate differ significantly from those reported in the modelling work of Soh et al [1994Soh] based on the estimated values of heat capacity. Fig. 6.4 shows the comparison of the calculated and experimentally measured heat capacity of lead titanate reported by Rossetti et al. [2005Ros]. The peak observed at 760 K corresponds to phase transformation $\alpha PbTiO_3 \rightarrow \beta PbTiO_3$. Due to insufficient number of experimental data points at temperatures below the phase transformation $\alpha PbTiO_3 \rightarrow \beta PbTiO_3$, the heat capacities of both phases are taken to be equal. Calculated and experimentally measured thermodynamic properties of lead zirconate are also shown in Table 6.4. Since the heat content of $\beta PbZrO_3$ is not known, it is described using the Neumann-Kopp rule, while a good agreement between calculated and measured enthalpy of formation [2001Ran] was obtained. The enthalpy of formation and entropy of $\beta Zr_xTi_{1-x}O_4$ (x = 0.5) at 298 K are in good agreement with data reported by Hom et al [2001Hom]. Heat capacity was measured up to 400 K, while the data above this temperature up to 1800 K were extrapolated [2001Hom]. Since extrapolated data are not considered in this work and there are only few measured points above 298 K, the heat capacity of $\beta Zr_xTi_{1-x}O_4$ (x = 0.5) is described

Table 6.4 Calculated and experimentally measured thermodynamics functions of $\alpha' PbTiO_3$, $\beta PbZrO_3$ and $\beta Zr_xTi_{1-x}O_4$ compounds at 298.15 K.

Compound	**$\Delta_f H°$ [kJ·mol^{-1}]**	**$\Delta S°$ [J·mol^{-1}·K^{-1}]**	**$\Delta_f G°$ [kJ·mol^{-1}]**	**Reference**
$\alpha' PbTiO_3$	-1199.02	112.47	-1232.55	This work
	-1199.74 ± 2.88			[2001Ran]
$\beta PbZrO_3$	-1318.00	129.19	-1356.51	This work
	-1319.18 ± 4.66			[2001Ran]
$\beta Zr_xTi_{1-x}O_4$ (x = 0.5)	-2024.01	116.22	-2058.66	This work
	-2024.1± 4.5	116.71 ± 0.31		[2001Hom]

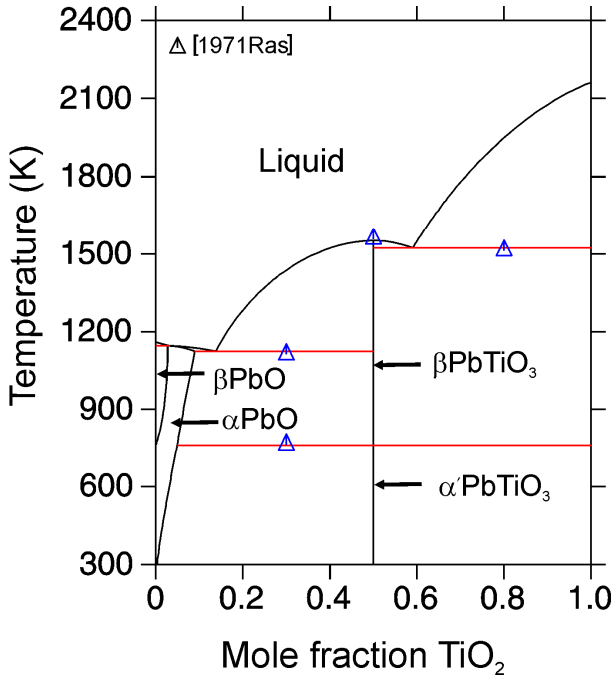

Fig. 6.1 The calculated PbO-TiO_2 phase diagram in comparison with the experimental data [1971Ras].

Table 6.5 Invariant equilibria in the PbO-TiO_2 system.

Reaction, mol. % TiO_2					Type	*T* (K)	Reference
L	↔	βPbTiO$_3$	+	TiO_2	Eutectic		
59.03					e_2	1522.97	This work
59.00±0.1						1513	[1971Ras]
L	↔	βPbTiO$_3$			Congruent		
						1551.61	This work
						1558	[1971Ras]
L	↔	βPbTiO$_3$	+	αPbO	Eutectic		
13.77				8.95	e_3	1124.19	This work
13.80±0.1				–		1111	[1971Ras]
L	+	βPbO	↔	αPbO	Peritectic		
3.10				2.75	p_3	1145.06	This work
αPbTiO$_3$	↔	βPbTiO$_3$			Solid-state		
					transform.	760.81	This work
						760±2	[2005Ros]

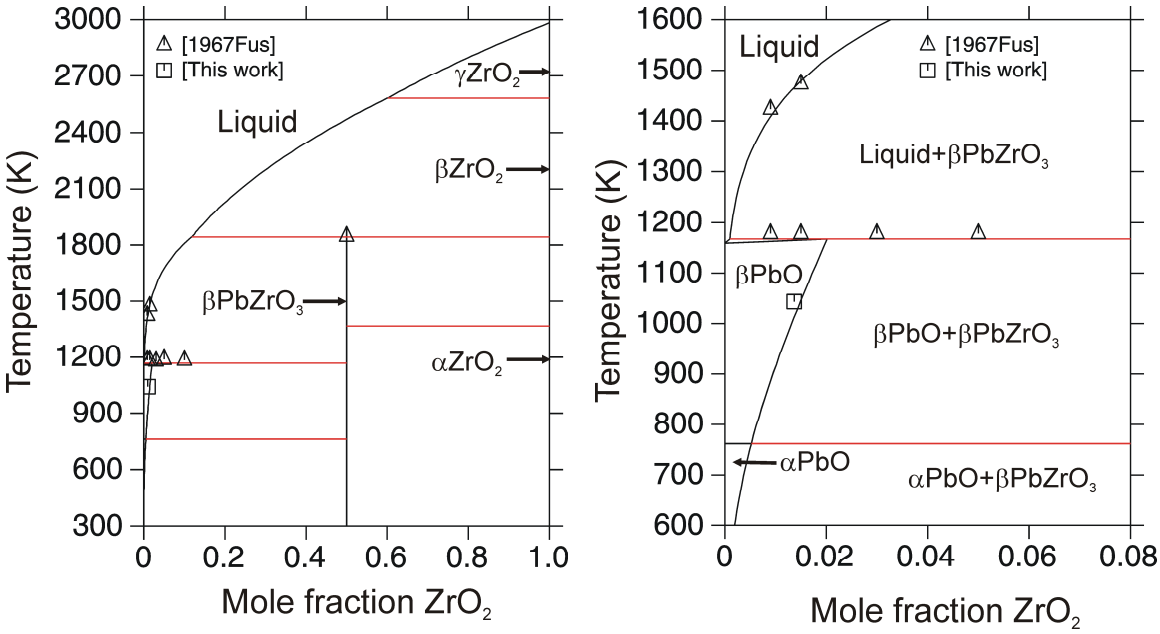

a) b)

Fig. 6.2 The calculated PbO-ZrO_2 phase diagram (a) and magnified PbO-rich part (b) compared with experimental measurements.

by the Neumann-Kopp rule which shows good fit with the measured data up to 400 K (Fig. 6.5). Calculated partial pressure of lead oxide over $\beta PbTiO_3$ is in good agreement with data reported by Schmahl et al. [1979Sch], Haerdtl and Rau [1969Hae] and Holman and Fulrath [1973Hol] (Fig. 6.6), while the data of Popovic et al. [1999Pop] are inconsistent with the selected experimental informations in PbO-TiO_2 system. The calculated partial pressure of lead oxide over $\beta PbZrO_3$ fits well the data reported by Popovic et al. [1999Pop] and Jacob and Shim [1971Jac], while the results of other authors [1969Hae, 1973Hol, 1979Sch] are inconsistent with the phase diagram reported by Fushimi and Ikeda [1967Fus]. The agreement between calculated and measured values for the $\beta PbZr_xTi_{1-x}O_3$ solid solutions [1969Hae, 1973Hol, 1979Sch, 1999Pop] is quite satisfactory. The data obtained by Knudsen technique [1969Hae, 1973Hol, 1979Sch, 1999Pop] have been partially used in optimization (the partial pressure reported by Popovic et al. [1999Pop] was measured over the nonequilibrated phases for the most of investigated compositions).

Table 6.6 Invariant equilibria in the PbO-ZrO_2 system.

Reaction, mol. % ZrO_2					Type	*T* (K)	Reference
L	+	γZrO_2	↔	βZrO_2	Peritectic		
60.18					p_4	2584.00	This work
L	+	βZrO_2	↔	$\beta PbZrO_3$	Peritectic		
11.86					p_5	1842.54	This work
–						1843	[1967Fus]
L	+	$\beta PbZrO_3$	↔	βPbO	Peritectic		
0.1				2.02	p_6	1167.31	This work
< 1.00				–		1178±5	[1967Fus]
–				<4.00		–	[1962Ike]

The calculated invariant equilibria in the PbO-TiO_2 system compared with the experimental ones are presented in Table 6.5. The peritectic reaction Liquid + βPbO → αPbO occurs at 1145 K and 2.75 mol. % TiO_2 dissolved in tetragonal αPbO solid solution (Table 6.5). Matsuo and Sasaki [1963Mat] reported that orthorhombic βPbO dissolves some TiO_2 and converted itself to tetragonal αPbO. This finding is in accordance with the tentatively drawn solubility of TiO_2 (less than 2 mol. %) in βPbO by Rase et.al.[1971Ras]. Since, the solubility of TiO_2 in βPbO phase is probably very small, it is not taken in account in the present work. In addition, the thermodynamic and phase boundary data for αPbO and βPbO are missing.

$\beta PbZrO_3$ compound melts incongruently at 1842.54 K and 88.14 mol. % PbO in the liquid (Table 6.6). The calculated maximal solubility of zirconia in tetragonal, βPbO, solid solution is 2.02 mol. % at temperature 1167.31 K of the peritectic reaction, Liquid + $\beta PbZrO_3$ → βPbO. The reported solubility of ZrO_2 in PbO solid solution at 1125 K is less than 4 mol. % ZrO_2 [1962Ike], while the measured one in present work at 1043 K is 1.3 ± 2 mol. %.

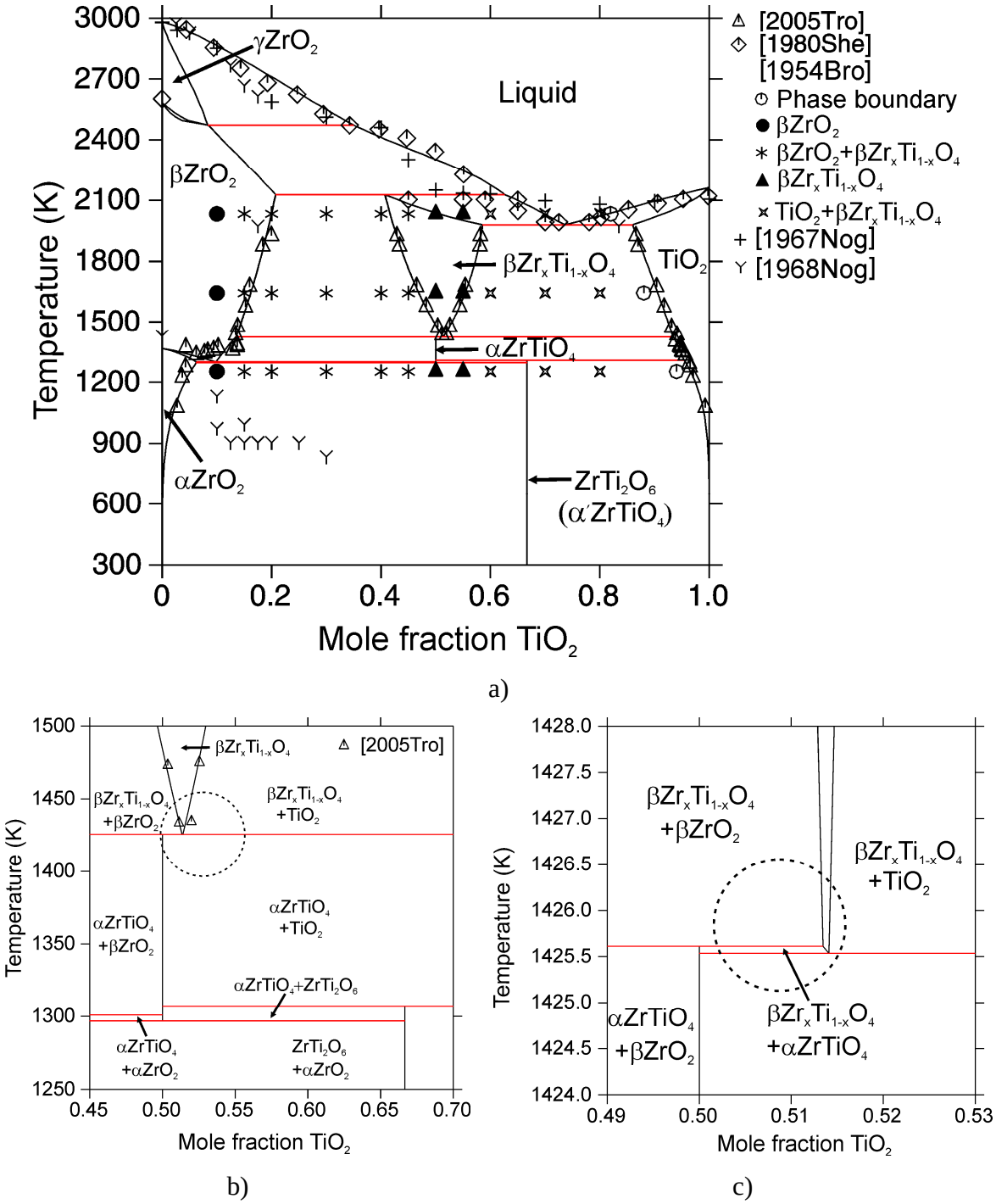

Fig. 6.3 The calculated ZrO_2-TiO_2 phase diagram with the corresponding experimental points (a) and enlarged view of the central part of diagram (b, c).

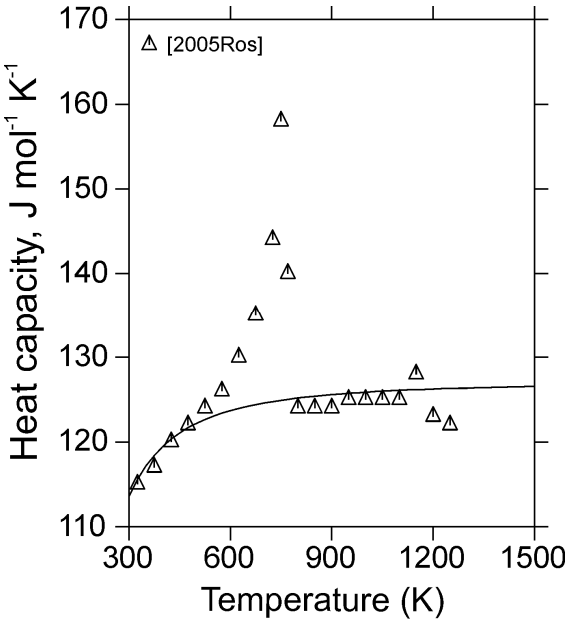

Fig. 6.4 Comparison of the calculated and measured heat capacity of $PbTiO_3$.

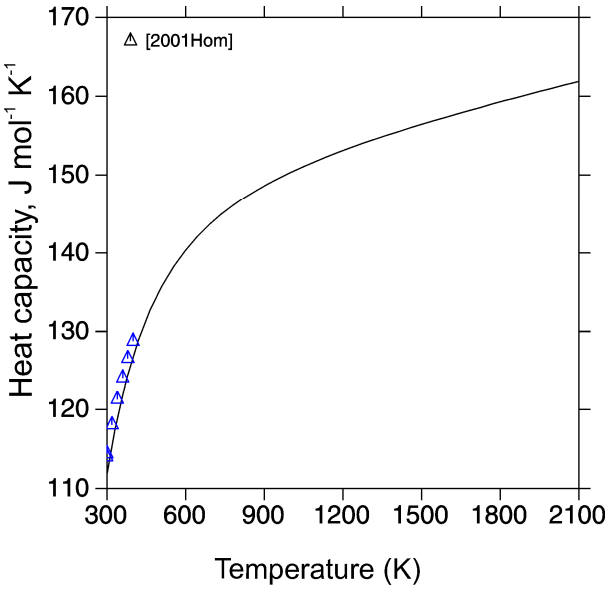

Fig. 6.5 Comparison of the calculated and measured heat capacity of $\beta Zr_xTi_{1-x}O_4$ (x = 0.5).

The calculated invariant equlibria in the ZrO_2-TiO_2 system are compared with the experimental ones in Table 6.7. Agreement between calculated and experimental data is very good, except in the ZrO_2-rich side near to eutectoid reaction $\beta ZrO_2 \rightarrow \alpha ZrO_2$ +

$\alpha ZrTiO_4$ which occurs at somewhat lower temperature than suggested in [2005Tro] and [1972Ono]. On the other hand, Webster et al. [1965Web] as well as Noguchi and Mizuno [1968Nog] found significantly lower reaction temperature (923 K), what is probably due to the shorter annealing time in their experiments. Consequently, at low temperatures the kinetic is very sluggish and equilibrium is not reached. Measured solubility of titania in βZrO_2 up to 1900 K [1986Ban, 2005Tro] supports the calculated value of 20.75 mol. % at the temperature of 2128.70 K for the peritectic reaction Liquid + $\beta ZrO_2 \rightarrow \beta Zr_xTi_{1-x}O_4$ obtained in the present work (Table 6.7). The calculated solubility of titania in αZrO_2 is 6.3 mol. % at the eutectoid temperature, what is close to the results reported by Ono [1972Ono] (Table 6.7).

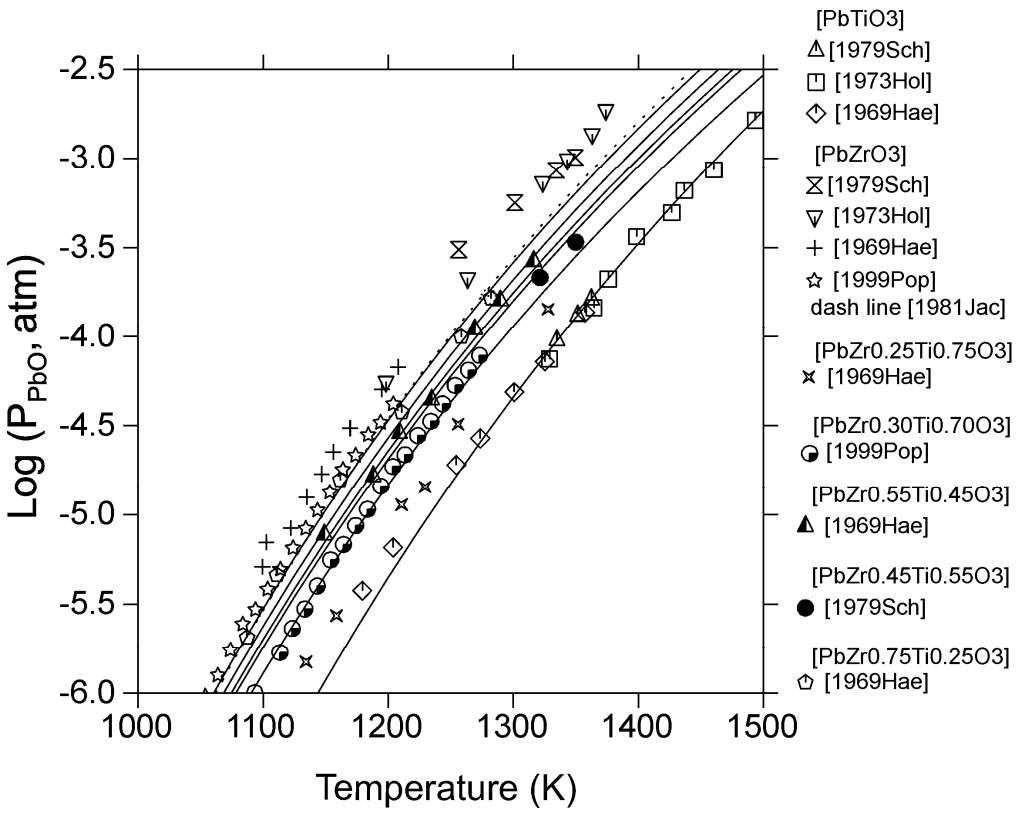

Fig. 6.6 The calculated and measured partial pressure of lead oxide over the end members, $\beta PbZrO_3$, $\beta PbTiO_3$ and $\beta PbZr_xTi_{1-x}O_3$ solid solutions superimposed with experimental measurements.

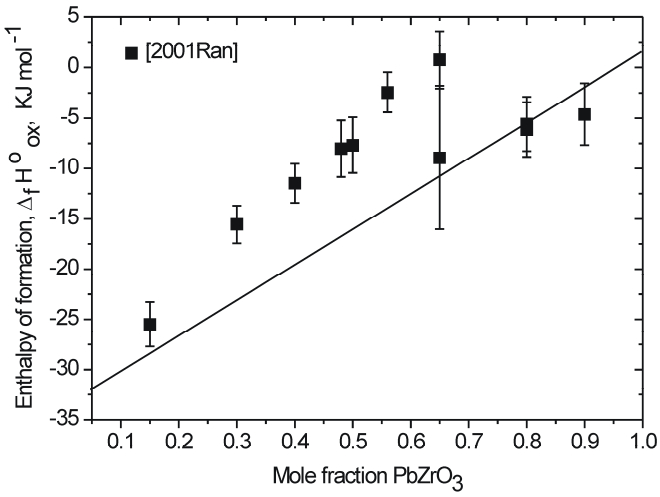

Fig. 6.7 The calculated enthalpy of formation of the $\beta PbZr_xTi_{1-x}O_3$ solid solutions from oxides at 298 K in comparison with experimental measurements [2001Ran].

The ZrO_2-rich part of the phase diagram above 2500 K, except the liquidus, is estimated in the present work. Due to the difficulties in conducting experiments at such high temperatures no reliable information in this region could be taken into account. Experimentally registered anomalies on the liquidus curve [1967Nog, 1980She] are well consistent with calculations. These anomalies correspond to the peritectic reactions, p_2 and p_1 shown in Table 6.7. The calculated liquidus is consistent with the data of Shevchenko et al. [1980She], while the other measurement of the liquidus in the ZrO_2-TiO_2 system [1967Nog] shows large negative deviations.

Fig. 6.7 shows the calculated enthalpy of formation of the $\beta PbZr_xTi_{1-x}O_3$ solid solutions from oxides at 298 K as compared with experimental data of Rane and Navrotsky [2001Ran]. The measured enthalpies show the regular mixing behavior with the uncertainty of measurements which is sometime higher than the measured values. However, when extrapolating these data to high temperatures the phase relations become inconsistent with the selected experimental information in the present work and the behavior of the ideal mixing is accepted. Nevertheless, the agreement between calculation and experiment is quite good. The calculated section $PbTiO_3$-$PbZrO_3$ is shown in Fig. 6.8. The $PbTiO_3$-$PbZrO_3$ system cannot be rigorously treated as a quasibinary one and this phase diagram is an interesting example, in which a congruently

Table 6.7 Invariant equilibria in the ZrO_2-TiO_2 system.

		Reaction, mol. % TiO_2			**Type**	***T* (K)**	**Reference**
L	↔	$\beta Zr_xTi_{1-x}O_4$	+	TiO_2	Eutectic		
73.70		58.60		85.98	e_1	1978.32	This work
75.30		–		–		1973	[1968Nog]
73.00		–		~ 82		1993±20	[1980She]
80.00		~ 60		~ 85		2033	[1954Cou]
L	+	βZrO_2	↔	$\beta Zr_xTi_{1-x}O_4$	Peritectic		
62.62		20.75		40.71	p_1	2128.70	This work
52.00		–		–		2093	[1968Nog]
60.00		–		–		2143	[1980She]
55.00		–		50.00		2093	[1954Cou]
L	+	γZrO_2	↔	βZrO_2	Peritectic		
34.99		8.32		8.45	p_2	2473.41	This work
16.70		–		–		2616	[1968Nog]
35.00		–		–		2473	[1980She]
βZrO_2	↔	αZrO_2	+	$\alpha ZrTiO_4$	Eutectoid		
9.89		6.30		50.00		1300.94	This work
–		12		($ZrTi_2O_6$?)		923	[1968Nog]
–		5		(TiO_2)		1354	[1972Ono]
~ 12		~ 9		~ 49		1357	[2005Tro]
$ZrTi_2O_6$	↔	$\alpha ZrTiO_4$	+	TiO_2	Peritectoid		
66.67		50.00		95.42		1307.2	This work
~ 67		(β $ZrTiO_4$)		–		~ 1473	[1986Mch]
~ 61		50.00		94.84		~ 1340	[2005Tro]
$\beta Zr_xTi_{1-x}O_4$	↔	$\alpha ZrTiO_4$	+	TiO_2	Eutectoid		
51.41		50.00		93.41		1425.41	This work
51.35		49.45		93.48		~ 1420	[2005Tro]

melting and an incongruently melting compound form a solid solution over the entire range of composition. The diagram includes experimental results from different reports [1967Fus, 1971Moo]. Deviation between calculations and experimental data is within the uncertainty of measurements. The calculated isothermal section at 1373 K (Fig. 6.9) is consistent with those reported in literature [1962Ike, 1965Web]. The non-stoichiometry of the lead titanate-lead zirconate solid solution [1962Ike, 1973Hol], *i.e.*, the deviation from the ratio $\frac{PbO}{ZrO_2 + TiO_2} = 1$ is not taken in account in the present work. In the region,

where the PbO content is more than 50 mol. %, the calculated isothermal sections at 1373, 1473 and 1573 K and the tie-lines (Figs. 6.10a, 6.10b and 6.10c) are compared with the experimentally determined ones [1967Fus]. At lower temperatures, the solubility of the ZrO_2 in the liquid phase increases with increasing $PbZrO_3$ content (Figs. 6.10a and 6.10b), while it is almost constant at 1573 K (Fig. 6.10c). Such a trend is consistent with the results of Fushimi and Ikeda [1967Fus].

The calculated projection of the monovariant liquidus lines is shown in Figs. 6.11a and 6.11b. According to the present work, the solidification sequence in the PbO- TiO_2-ZrO_2 system is in agreement with the schematically proposed polythermal projection by Fushimi and Ikeda [1967Fus], where the solubility surface for zirconia dominates in the system. The calculated invariant reactions (Table 6.8) are consistent with those estimated in literature [1967Fus]. The Sheil reaction scheme of the PbO-TiO_2-ZrO_2 system is given in Fig. 6.12.

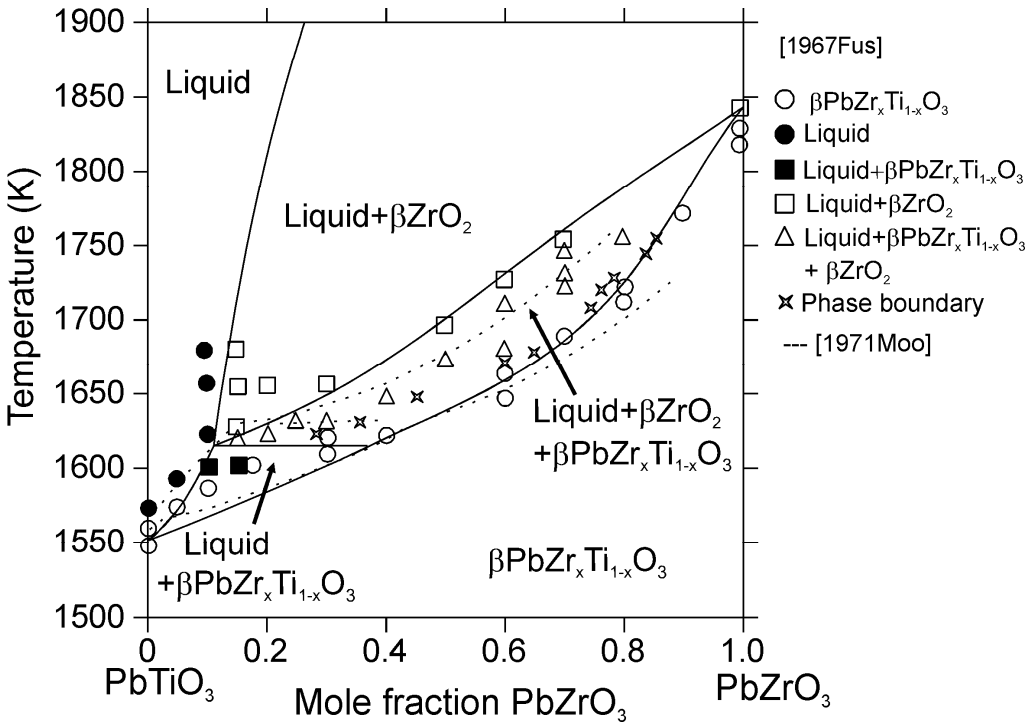

Fig. 6.8 The calculated $PbTiO_3$-$PbZrO_3$ section as compared with experimental measurements.

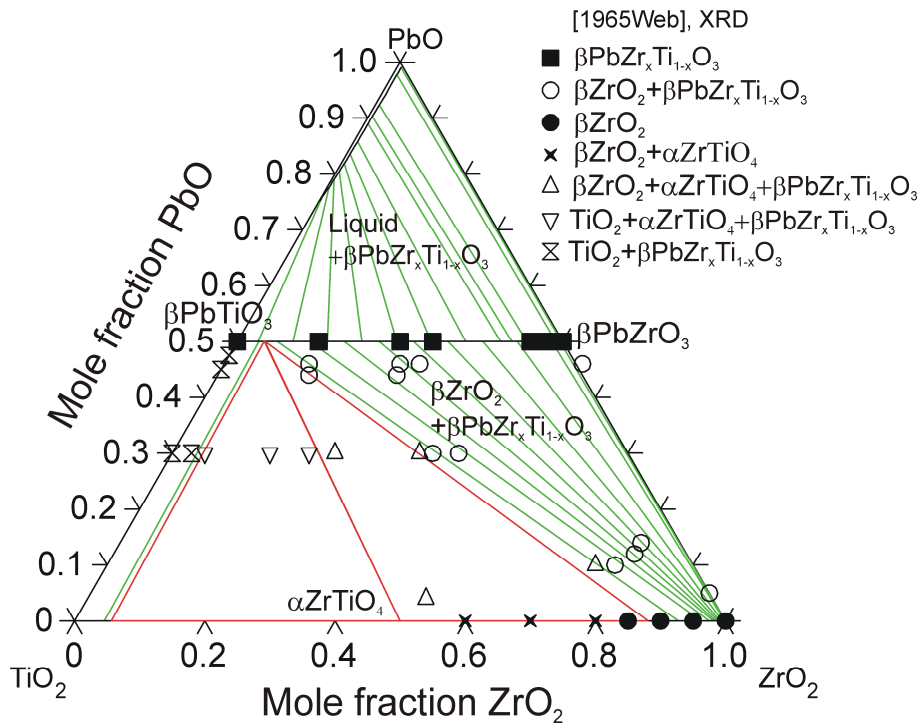

Fig. 6.9 Isothermal section of the PbO-ZrO_2-TiO_2 phase diagram at 1373 K compared with experimental measurements.

Table 6.8 Invariant equilibria in the ternary PbO-ZrO_2-TiO_2 system (temperatures in parentheses are estimated by Fushimi and Ikeda [1967Fus]).

		Reaction, mol. % ZrO_2 mol. % PbO					**Type**	***T* (K)**
L	+	βZrO_2	↔	$\beta Zr_xTi_{1-x}O_4$	+	$\beta PbZr_xTi_{1-x}O_3$	Transition	
6.11		85.13		51.00		6.36	U	1531.66
37.41		0		0		50.00		(1573)
L	↔	TiO_2	+	$\beta Zr_xTi_{1-x}O_4$	+	$\beta PbZr_xTi_{1-x}O_3$	Eutectic	
5.81		7.82		46.61		5.32	E	1521.62
36.60		0		0		50.00		(1503)
L	+	$\beta PbZr_xTi_{1-x}O_3$	+	βPbO	↔	αPbO	Peritectic	
0.08		46.31		1.82		1.49	P	1151.23
96.54		50.00		98.18		95.76		

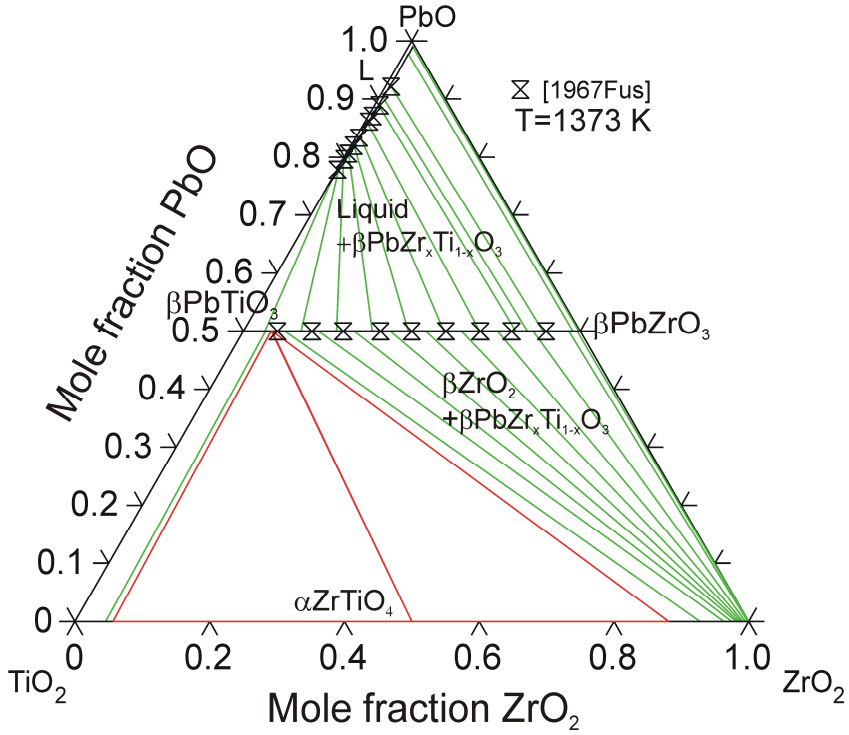
PbO
1.0
L
0.9
0.8
0.7
0.6
0.5
0.4
0.3
0.2
0.1
0
[1967Fus]
T=1373 K
Liquid
+βPbZr$_x$Ti$_{1-x}$O$_3$
βPbTiO$_3$
βPbZrO$_3$
βZrO$_2$
+βPbZr$_x$Ti$_{1-x}$O$_3$
αZrTiO$_4$
Mole fraction PbO
0
0.2
0.4
0.6
0.8
1.0
TiO$_2$
ZrO$_2$
Mole fraction ZrO$_2$

a)

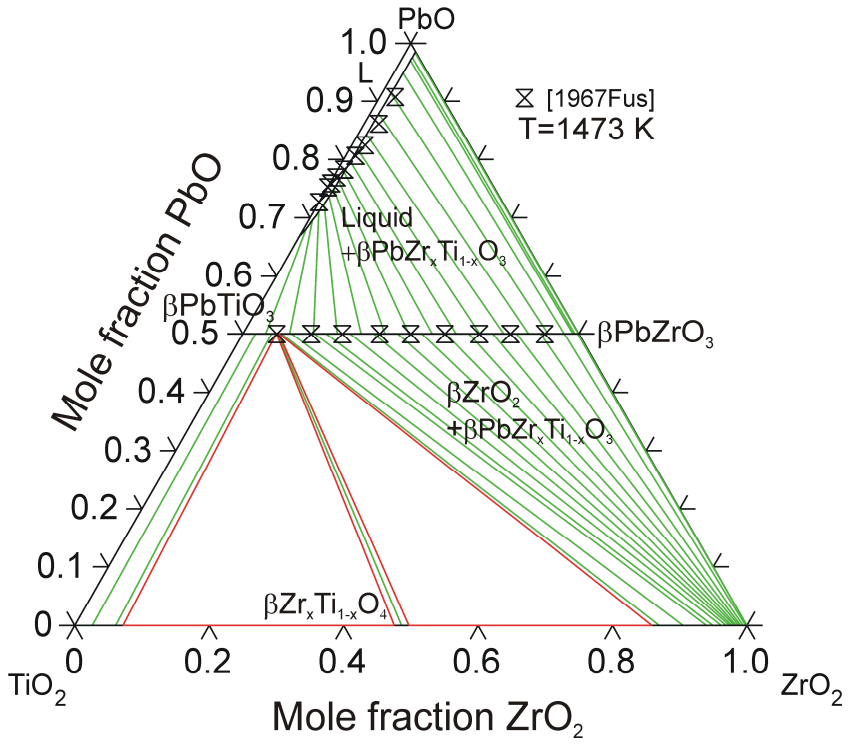
PbO
1.0
L
0.9
0.8
0.7
0.6
0.5
0.4
0.3
0.2
0.1
0
[1967Fus]
T=1473 K
Liquid
+βPbZr$_x$Ti$_{1-x}$O$_3$
βPbTiO$_3$
βPbZrO$_3$
βZrO$_2$
+βPbZr$_x$Ti$_{1-x}$O$_3$
βZr$_x$Ti$_{1-x}$O$_4$
Mole fraction PbO
0
0.2
0.4
0.6
0.8
1.0
TiO$_2$
ZrO$_2$
Mole fraction ZrO$_2$

b)

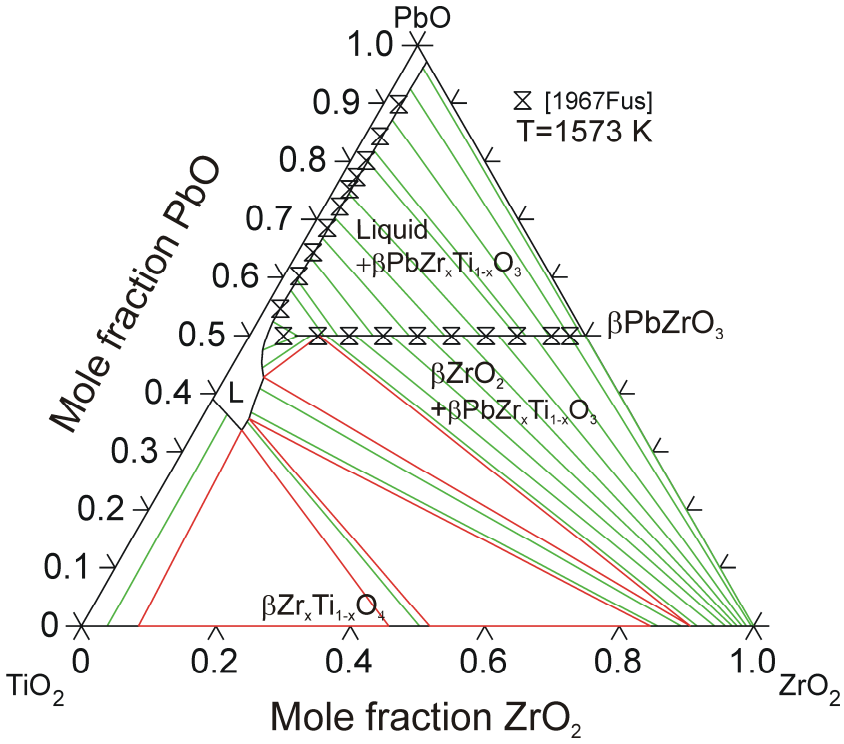

c)

Fig. 6.10 Isothermal sections of the PbO-ZrO_2-TiO_2 phase diagram and the tie lines at 1373 (a), 1473 (b) and 1573 (c) in comparison with the experimental data.

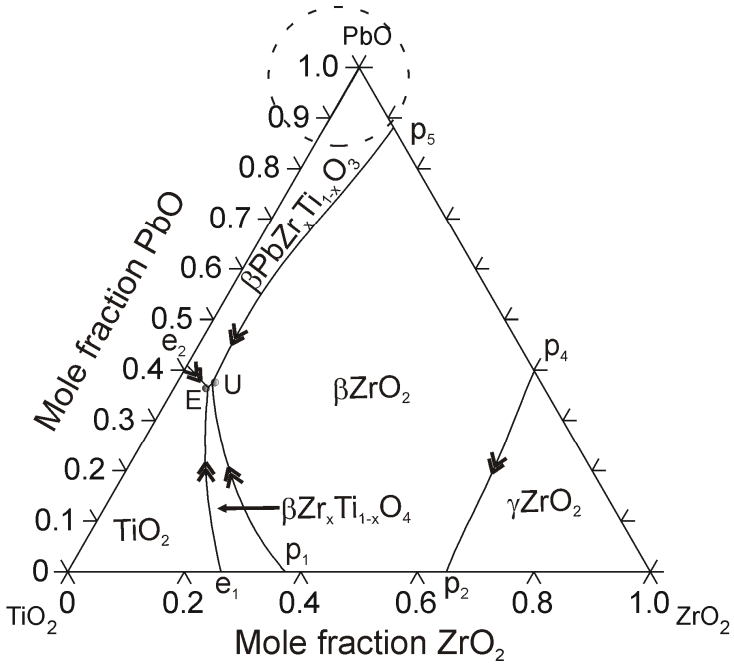

a)

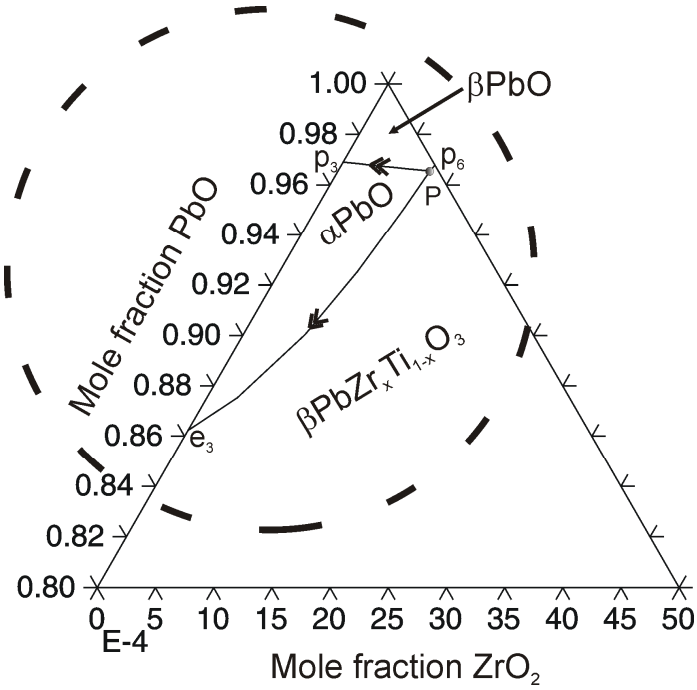

b)

Fig. 6.11 The calculated projection of the monovariant liquidus lines in the ternary PbO-ZrO_2-TiO_2 system (a) and magnified PbO-rich part (b). Fields of primary crystallization are indicated.

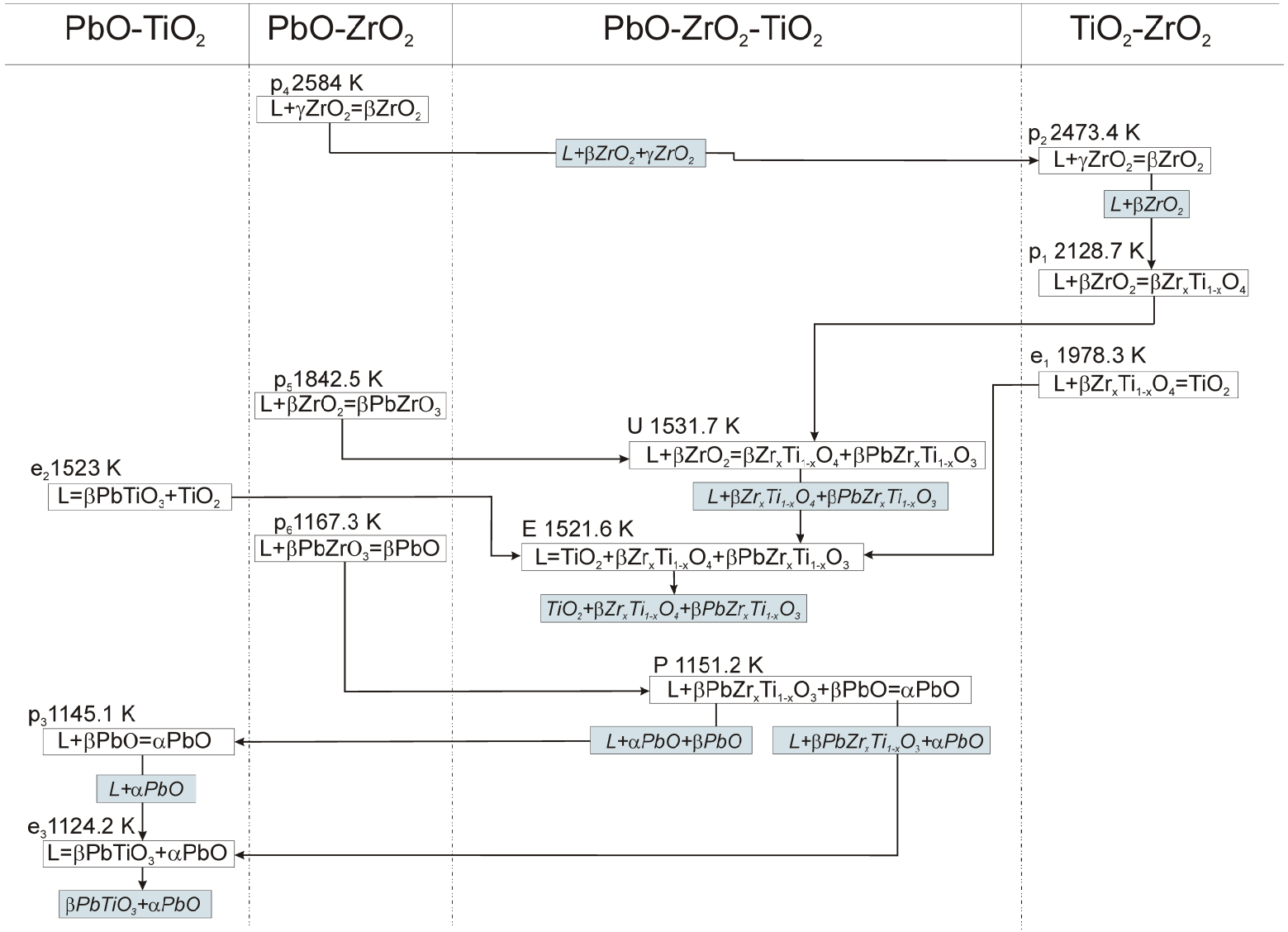

Fig. 6.12 Sheil reaction scheme of the ternary $PbO-ZrO_2-TiO_2$ system.

7. EXTRAPOLATION INTO MULTICOMPONENT Cu-Pb-Zr-Ti-O SYSTEM

The evaluated database in this thesis is reliable for extrapolating calculations in the oxygen-rich part of the multicomponent Cu-Pb-Zr-Ti-O system, *i.e.*, in the PbO-ZrO_2-TiO_2, CuO_x-PbO-ZrO_2, CuO_x-PbO-TiO_2 and CuO_x-ZrO_2-TiO_2 systems. In addition, the database can be used in prediction of phase relations among the metals and oxides, *i.e.* between copper and PZT ceramics (Cu-PbO-ZrO_2-TiO_2 system), for which purpose it is developed. Although the metallic parts of the multicomponent Cu-Pb-Zr-Ti-O system are partially included in database (See Chapters 4 and 5), it cannot be used for calculations in the Cu-Pb-Zr-Ti system and corresponding subsystems.

7.1. Evaluation of phase relations in the CuO-Cu_2O-PbO-ZrO_2 and CuO-Cu_2O-PbO-TiO_2 systems

7.1.1. Extrapolating calculations

Investigation of the phase relations in the CuO-Cu_2O-PbO-ZrO_2 and CuO-Cu_2O-PbO-TiO_2 systems and of the reactivity between copper oxides and PZT ceramics is based on the extrapolation from lower-order systems. The calculated isothermal-isobaric sections of the CuO_x-PbO-ZrO_2 and CuO_x-PbO-TiO_2 systems in air at 1043 and 1173 K are given on Figs. 7.1 and 7.2. Depending on the temperature and partial pressure of oxygen, CuO_x corresponds to either Cu_2O or CuO. The calculated tie-triangles show that CuO and lead titanate / lead zirconate can coexist with titania / or zirconia, as well as with the PbO solid solution. With increasing temperature the formation of a PbO-rich liquid occurs and it coexists with lead titanate / lead zirconate (Fig. 7.1b and 7.2b). Figs. 7.3 and 7.4 show the calculated projections of the monovariant liquidus lines in CuO_x-PbO-TiO_2 and CuO_x-PbO-ZrO_2 systems, while the invariant reactions are listed in Tables 7.1 and 7.2.

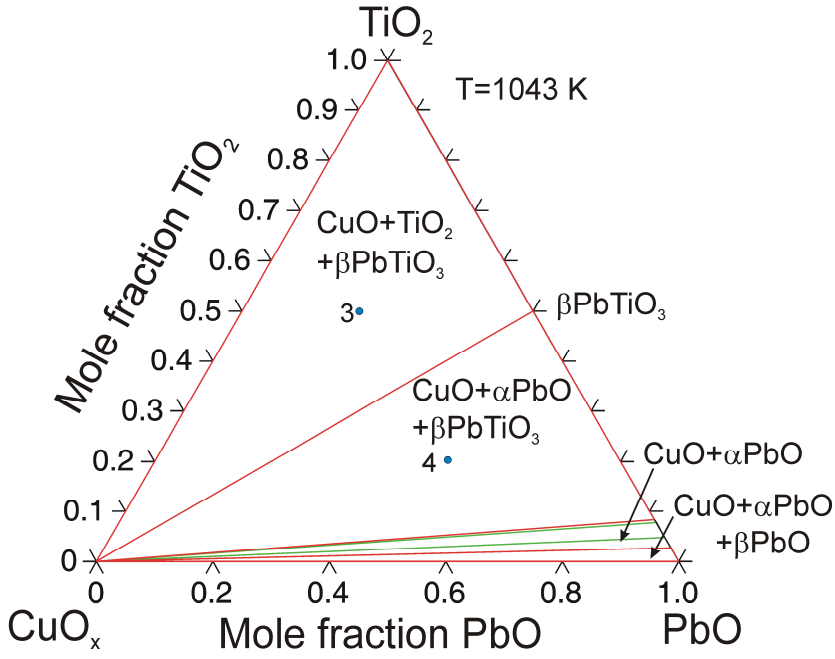

a)

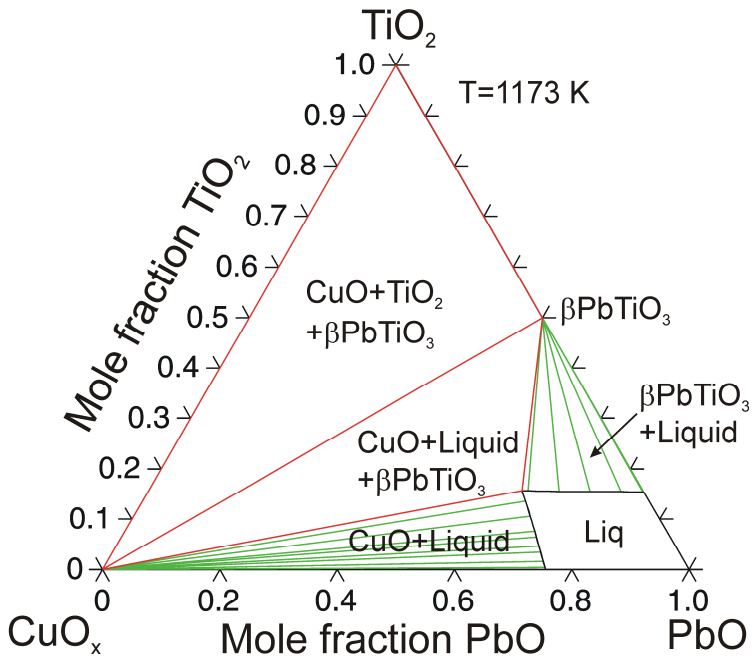

b)

Fig. 7.1 The calculated isothermal-isobaric sections of the CuO_x-PbO-TiO_2 system at $P_{O_2} = 0.21$ bar and 1043 K (a) and 1173 K (b).

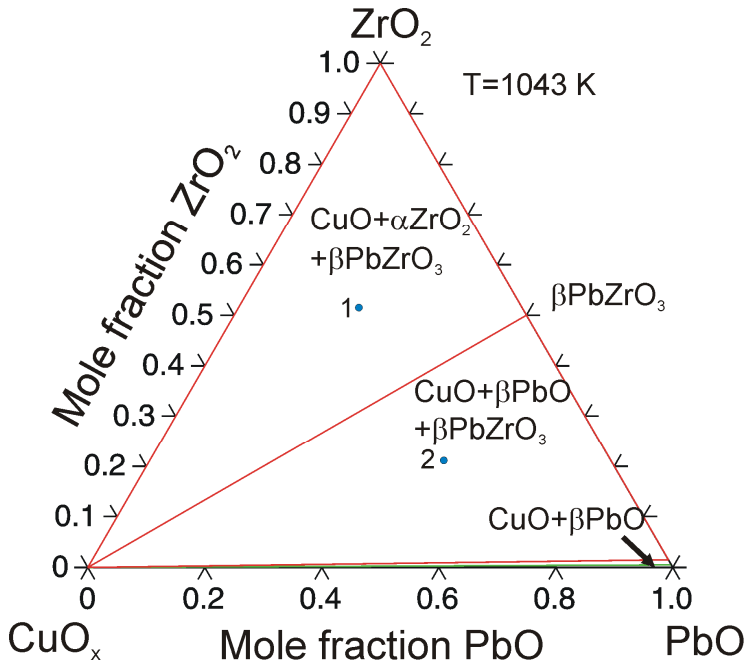

a)

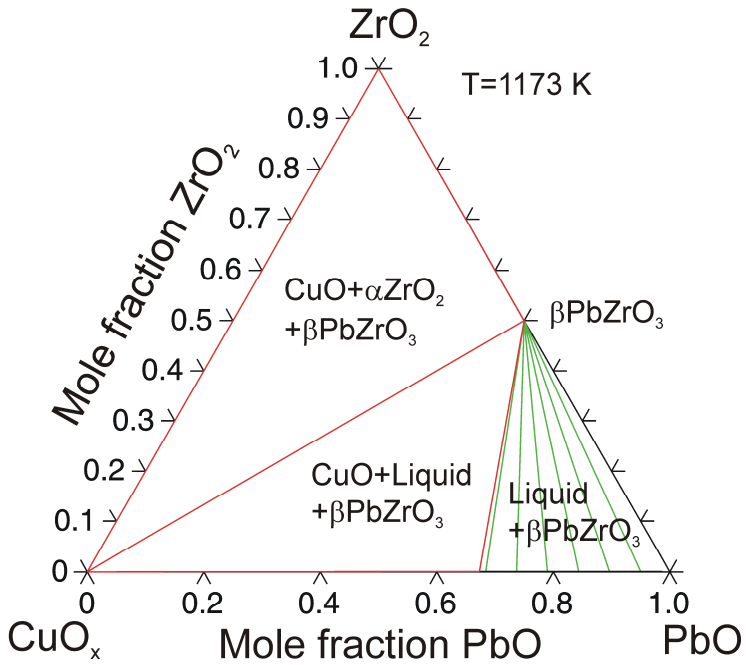

b)

Fig. 7.2 The calculated isothermal-isobaric sections of the CuO_x-PbO-ZrO_2 system at $P_{O_2} = 0.21$ bar and 1043 K (a) and 1173 K (b).

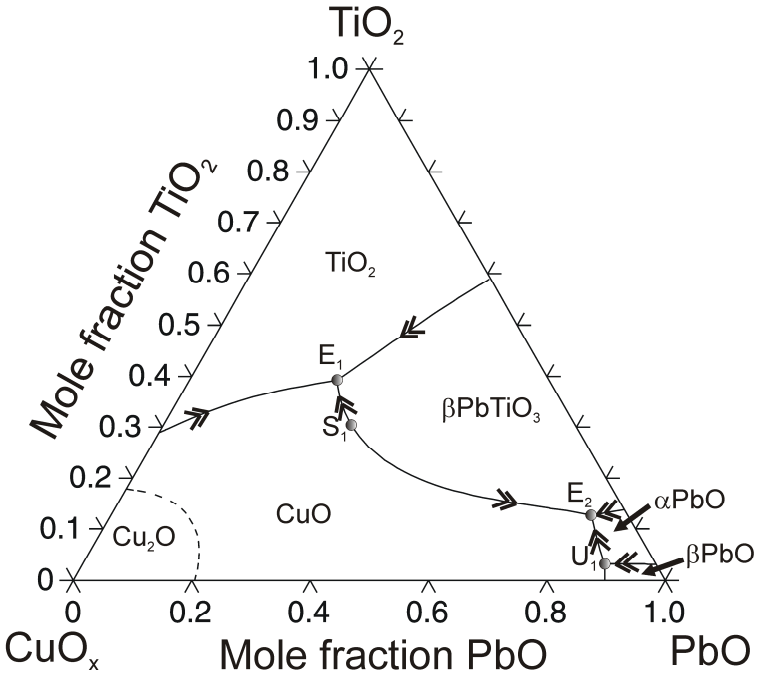

Fig. 7.3 Calculated projection of the monovariant liquidus lines in the CuO_x-PbO-TiO_2 system at $P_{O_2} = 0.21$ bar. Fields of primary crystallization are indicated.

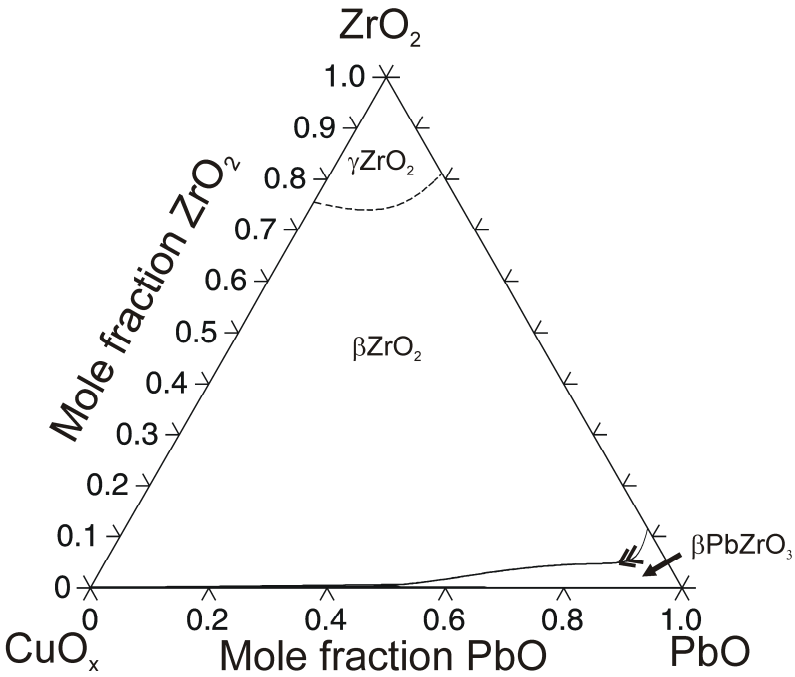

a)

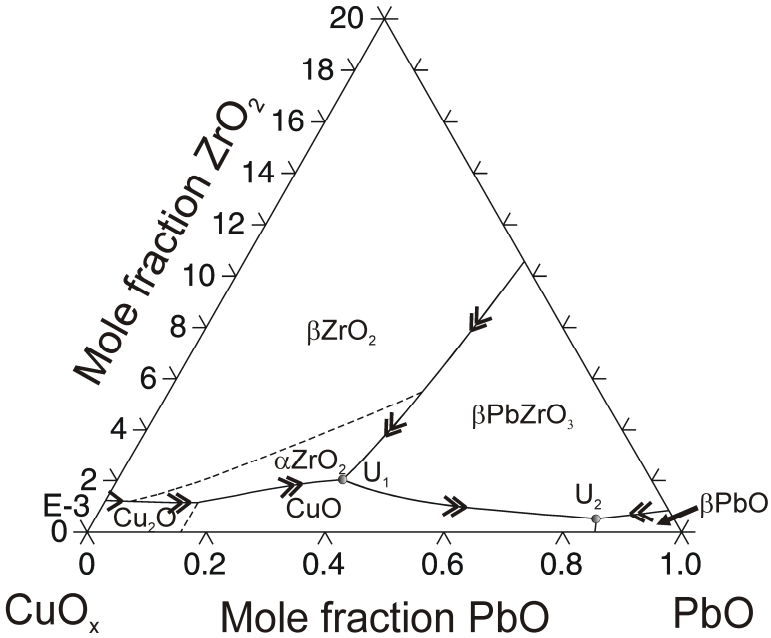

b)

Fig. 7.4 Calculated projection of the monovariant liquidus lines in the CuO_x-PbO-ZrO_2 system (a) and enlarged view of the ZrO_2-poor part (b) at $P_{O_2} = 0.21$ bar. Fields of primary crystallization are indicated.

Table 7.1 The calculated invariant equilibria in the CuO_x-PbO-TiO_2 system.

	Reaction	Type	T_{cal} (K)	T_{exp} (K)
E_1	$L \leftrightarrow CuO + PbTiO_3 + TiO_2$	Eutectic	1233.12	1235 ± 10
E_2	$L \leftrightarrow CuO + PbTiO_3 + \alpha PbO$	Eutectic	1093.27	1065 ± 10
U_1	$L + \beta PbO \leftrightarrow \alpha PbO + CuO$	Transition	1106.87	-
S_1	$L \leftrightarrow CuO + PbTiO_3$	Saddle	1211.56	-

Table 7.2 The calculated invariant equilibria in the CuO_x-PbO-ZrO_2 system.

	Reaction	Type	T_{cal} (K)	T_{exp} (K)
U_1	$L + \alpha ZrO_2 \leftrightarrow \beta PbZrO_3 + CuO$	Transition	1254.27	1235 ± 10
U_2	$L + \beta PbZrO_3 \leftrightarrow CuO + \beta PbO$	Transition	1119.49	1070 ± 10

7.1.2. Experimental results and discussion

The four prepared compositions correspond to the numerated points in Figs. 7.1a (3 and 4) and 7.2a (1 and 2). The sample treatments are described in the Chapter 3.1. The XRD, SEM, EDX and DTA analysis were performed.

The XRD patterns of the samples (Fig. 7.5) and the SEM back scattered electron images (Fig. 7.6) recovered the presence of three phases for the all investigated compositions. The average chemical composition of the phases obtained by EDX is shown in Table 7.3. The presence of the low-temperature stable modifications of $\alpha PbTiO_3$ and $\alpha PbZrO_3$ is observed (Fig. 7.5). Although, the rapid cooling was performed the phase transitions $\beta PbTiO_3 \leftrightarrow \alpha PbTiO_3$ and $\beta PbZrO_3 \leftrightarrow \alpha PbZrO_3$ took place. The XRD patterns of the sample 4 (Fig. 7.5d) show the existence of tetragonal PbO solid solution with 5.1 ± 1 at.% Ti at 1043 K (Table 7.3), while the orthorhombic high-temperature modification of PbO present in sample 2 (Fig. 7.5b) shows that the solubility of zirconium is less than 1 at.% (equivalent to 1.3 ± 2 mol. % ZrO_2), *i.e.*, within the uncertainty limits of the measurements (Table 7.3). The solubility of copper in lead titanate and lead zirconate is negligible. The measured solubility of 9.6 ± 2 mol. % TiO_2 in the tetragonal PbO at 1043 K (sample 4) is consistent with the calculated value of 7.98 mol. % TiO_2 at the same temperature (Fig. 7.1), which corresponds to the homogeneity range of PbO solid solution in the quasibinary PbO-TiO_2 diagram (Fig. 6.1, Chapter 6). From the chemical point of view, a similar trend could be expected in the case of zirconia. However, the stabilization of the low-temperature tetragonal PbO with dissolution of zirconia schematically proposed by Jacob and Shim [1982Jac] and assessed by Koo et al. [1999Koo] is not in agreement with the results obtained in the present work. All results obtained in this thesis using the applied characterization methods indicate that the solubility of zirconia in PbO is < 2 mol. %. It is possible that the equilibrium state is not reached due to a sluggish kinetic of dissolution of ZrO_2 in PbO. The slow reaction rates and difficulties with equilibrium experiments in the ZrO_2-TiO_2 system at temperatures below 1473 K are well known [1986Mch, 2004Tro1, 2005Tro]. However,

the evaporation of PbO occurs rather than formation of PbO solid solution (see Chapter 7.2) and it creates additional problems with the prolonged heat treatments.

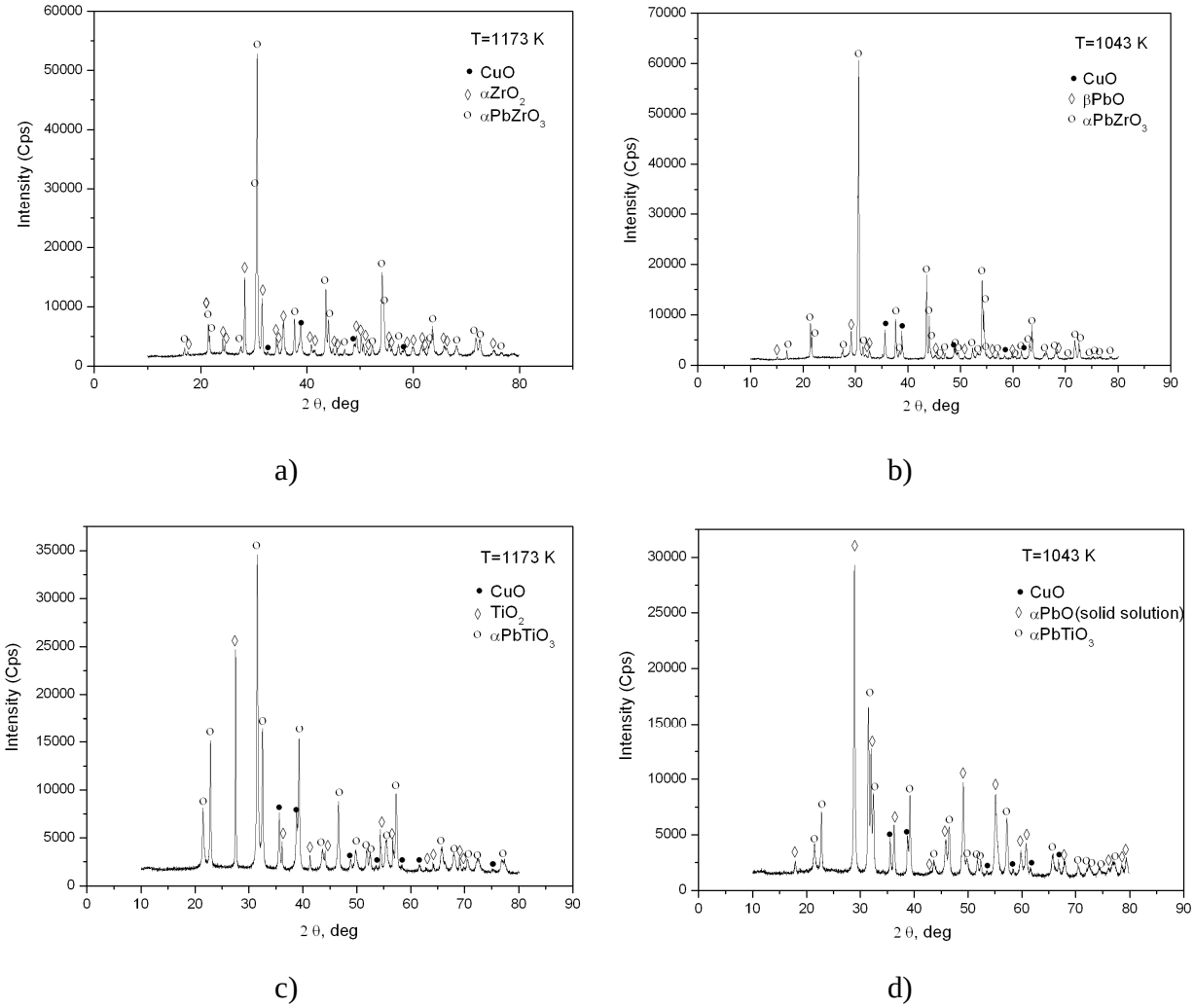

Fig. 7.5 The XRD patterns the samples 1 (a), 2 (b), 3 (c) and 4 (d) after heat treatment at 1043 K (b, d) and 1173 K (a, c) for 100 h.

Fig. 7.7 shows DTA curves of sample 1 to 4 previously heated in air at 1043 K (2, 4) and 1173 K (1, 3) for 100 h. The weak endothermic peaks observed at 504 K (samples 1, 2) and 760 K (samples 3, 4) correspond to the $\alpha PbZrO_3 \rightarrow \beta PbZrO_3$ and $\alpha PbTiO_3 \rightarrow \beta PbTiO_3$ transformation, respectively. The endothermic effects at 1235 K (Fig. 7.6a) have been related to the melting of the ZrO_2-rich (sample 1) and TiO_2-rich (sample 3) compositions. The measured melting temperature of those compositions (sample 1 and 3)

is consistent with the temperature of the predicted invariant reactions U_1 (Table 7.2) and E_1 (Table 7.1). At the same time, measured melting temperature of PbO-rich compositions (samples 2 and 4) show negative deviations in comparison with the calculated results for the invariant reactions U_2 (Table 7.2) and E_2 (Table 7.1). Such calculated results are probably an implication of using the associate solution model for the description of liquid in the Cu-Pb-O system. Indeed, the calculated temperature of the saddle point S_2 (L ↔ CuO + PbO) of the CuO_x-PbO section in air (Fig. 5.1.17, Chapter 5.1) shows positive deviation (> 30 K) compared to Refs. [1967Gad1, 1990Kit].

In general, experimental results confirm the calculations in the CuO_x-PbO-ZrO_2 and CuO_x-PbO-TiO_2 systems (Figs. 7.1 and 7.2).

Table 7.3 The average chemical composition of phases observed by EDS analysis. The uncertainty of measurements is 1 at. % (2 mol. %).

Sample	**Phase**	**Composition, at. % (mol. %)**			
		Cu (CuO)	**Pb (PbO)**	**Zr (ZrO_2)**	**O**
1	dark phase (CuO)	57.7 (99.4)	0	0	42.2
	grey phase (ZrO_2)	0.3 (0.9)	0	38.9 (99.0)	60.7
	light grey phase ($PbZrO_3$)	0.7 (1.5)	22.9 (48.4)	23.6 (50.1)	52.9
2	dark phase (CuO)	56.3 (99.6)	0	0	43.5
	grey phase ($PbZrO_3$)	0.5 (1.2)	21.9 (48.9)	22.3 (50.0)	55.3
	light phase (PbO)	1 (1.8)	55.0 (96.9)	0.8 (1.3)	43.3
		Cu (CuO)	**Pb (PbO)**	**Ti (TiO_2)**	**O**
3	dark phase (TiO_2)	0.4 (0.9)	0	38.9 (99.0)	60.8
	grey phase (CuO)	56.18 (98.48)	0	0.9 (1.4)	43.0
	light phase ($PbTiO_3$)	0.7 (1.4)	22.8 (48.4)	23.6 (50.2)	53.0
4	dark phase (CuO)	58.0 (99.8)	0	0	41.9
	grey phase ($PbTiO_3$)	0.9 (1.9)	21.9 (48.6)	22.3 (49.4)	54.9
	light phase (PbO)	1 (1.9)	47.1 (88.6)	5.1 (9.6)	46.8

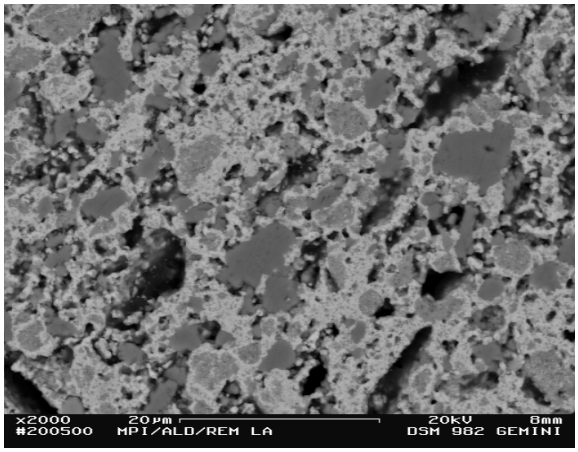

a)

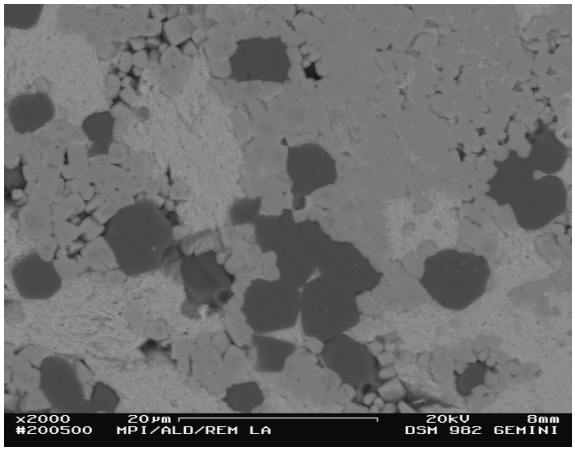

b)

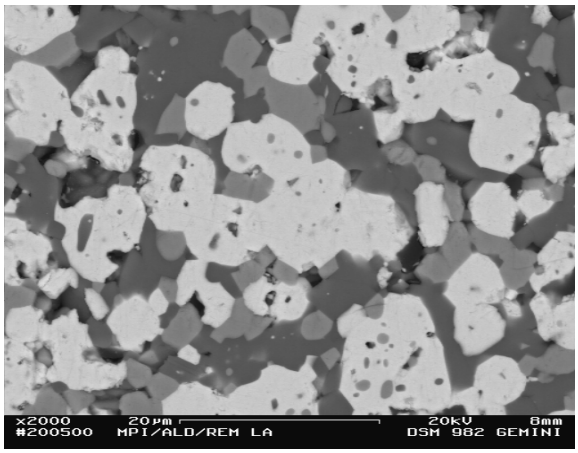

c)

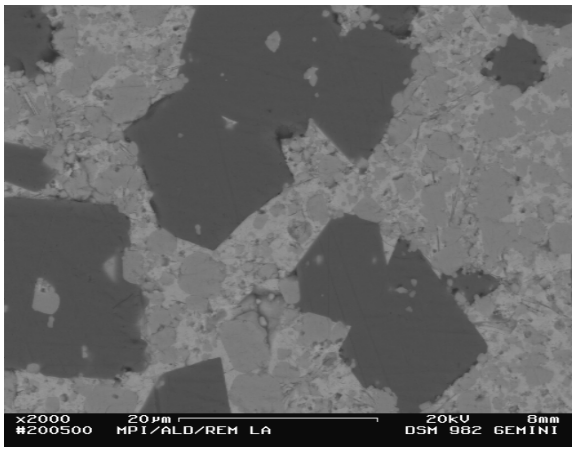

d)

Fig. 7.6 The SEM back scattered electron images of the samples 1 (a), 2 (b), 3 (c) and 4 (d) after heat treatment in air at 1043 K (b, d) and 1173 K (a, c) for 100 h. (Phase compositions are given in Table 7.3)

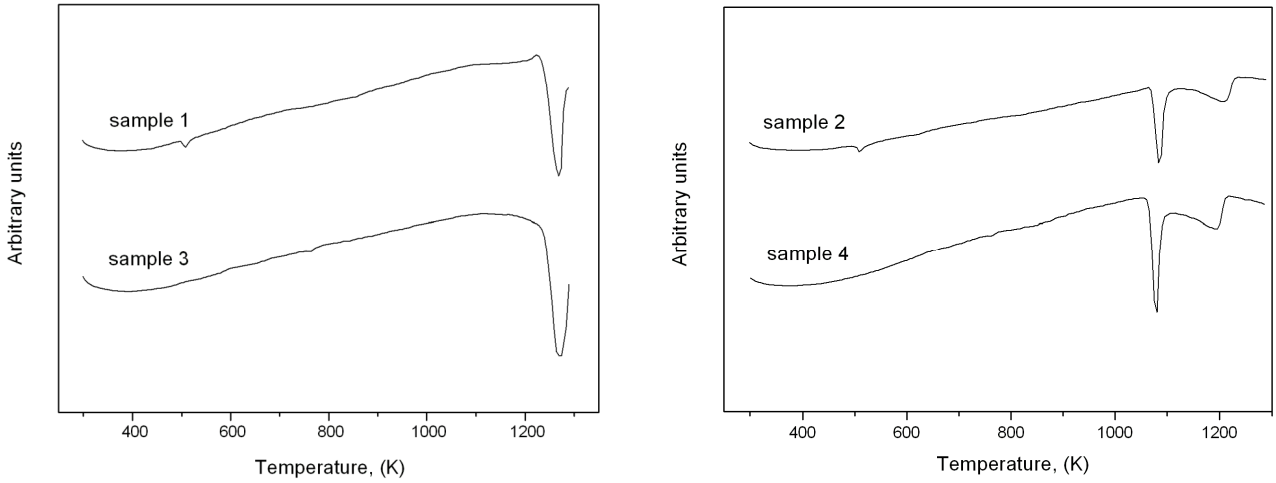

a) b)

Fig. 7.7 DTA curves in air of sample 1 to 4.

7.2. Evaluation of phase relations in the Cu-PbO-ZrO_2-TiO_2 system

7.2.1. Extrapolating calculations

The calculated chemical potential diagrams of the multi-component Cu-PbO-ZrO_2-TiO_2 system are shown in Figs. 7.8 - 7.17. The utilization of chemical potential diagrams is crucial for the prediction of the chemical compatibility of dissimilar materials, *i.e.*, copper and PZT ceramics (see Section 2.2.3). The selected values of the chemical potential of oxygen, log(P_{O_2} ,bar) and temperature in the calculated diagrams (Figs. 7.8-7.15) are chosen to be consistent with the conditions of experiments performed in this thesis. Fig. 7.8 shows the existence of copper in contact with β$PbTiO_3$ at 1073 K under partial pressure of oxygen of log(P_{O_2} ,bar)= -14. However, at 1173 K and log(P_{O_2} ,bar)= -12 there is no direct contact line between Cu and β$PbTiO_3$ (Fig. 7.9), whereas the stability areas of TiO_2 and Pb-rich liquid are adjacent and they intervene between copper and β$PbTiO_3$. It means that in the corresponding phase diagram there is no tie-line between Cu and β$PbTiO_3$, *i.e.*, they cannot exist in equilibrium under given conditions

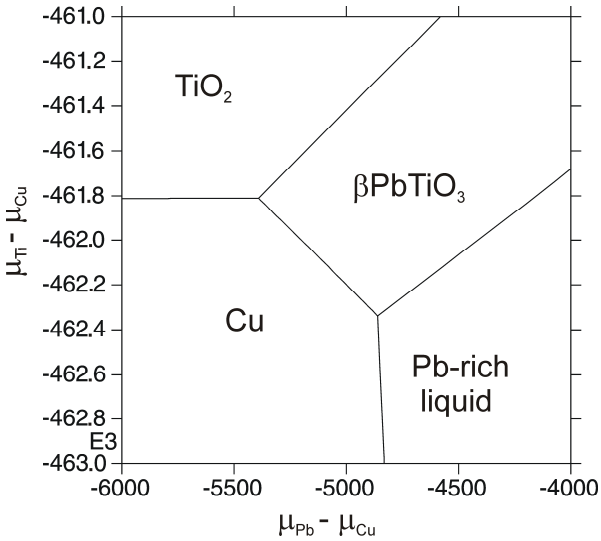

Fig. 7.8 Chemical potential diagram for the Cu-PbO-TiO_2 system at 1073 K and log(P_{O_2} ,bar)= -14.

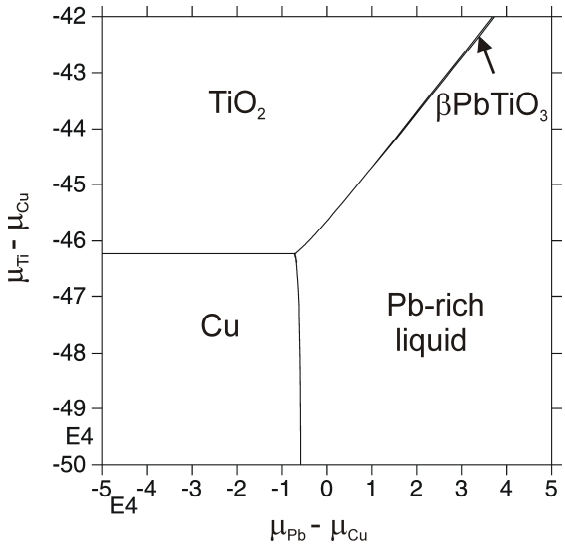

Fig. 7.9 Chemical potential diagram for Cu-PbO-TiO_2 system at 1173 K and log(P_{O_2} ,bar)= -12.

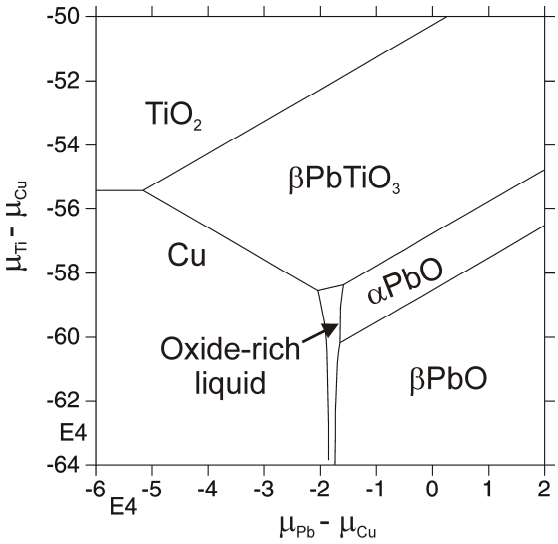

Fig. 7.10 Chemical potential diagram for the Cu-PbO-TiO_2 system at 1073 K and log(P_{O_2} ,bar)= -9.5

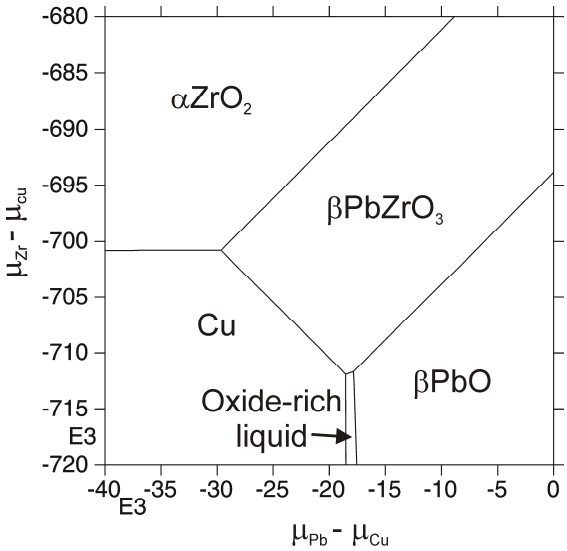

Fig. 7.11 Chemical potential diagram for Cu-PbO-ZrO_2 system at 1073 K and log(P_{O_2} ,bar)= -9.5

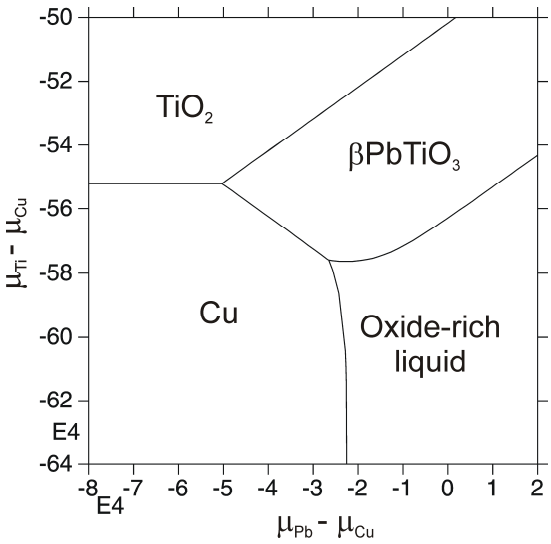

Fig. 7.12 Chemical potential diagram for the Cu-PbO-TiO_2 system at 1173 K and log(P_{O_2} ,bar)= -8.

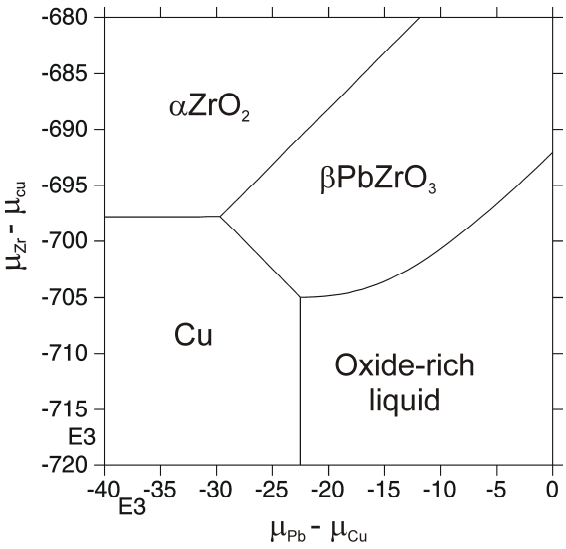

Fig. 7.13 Chemical potential diagram for the Cu-PbO-ZrO_2 system at 1173 K and log(P_{O_2} ,bar)= -8.

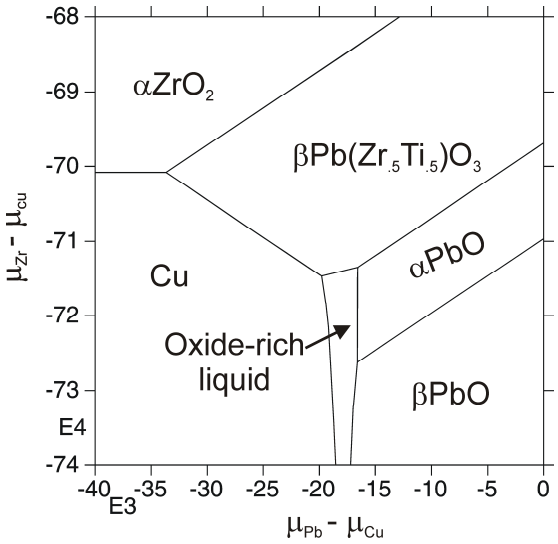

Fig. 7.14 Chemical potential diagram for the Cu-PbO-ZrO_2-TiO_2 system at 1073 K and log(P_{O_2} ,bar)= -9.5.

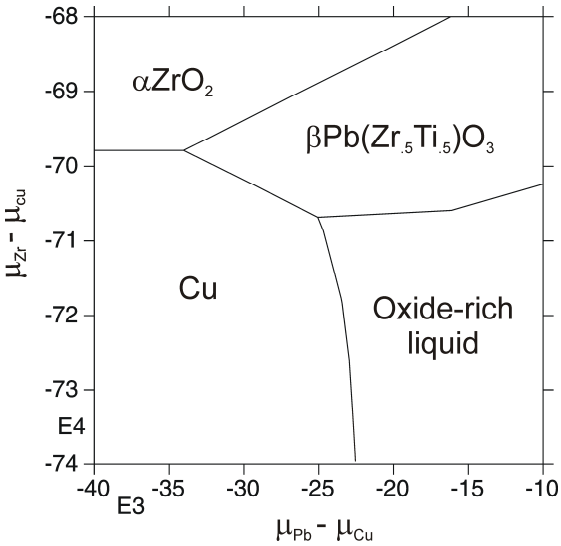

Fig. 7.15 Chemical potential diagram for the Cu-PbO-ZrO_2-TiO_2 system at 1173 K and log(P_{O_2} ,bar)= -8.

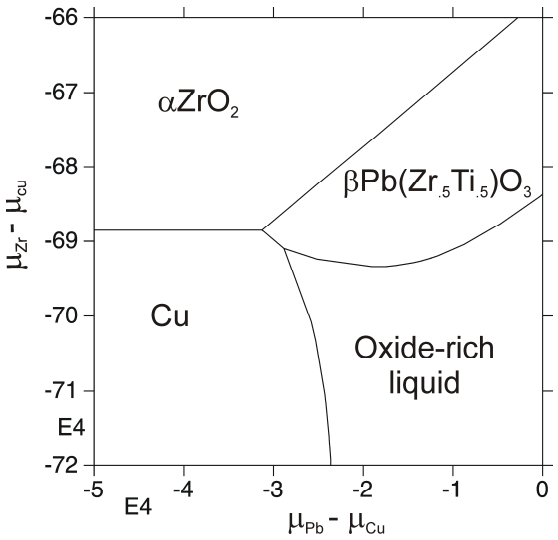

Fig. 7.16 Chemical potential diagram for the Cu-PbO-ZrO_2-TiO_2 system at 1273 K and log(P_{O_2} ,bar) = -7.

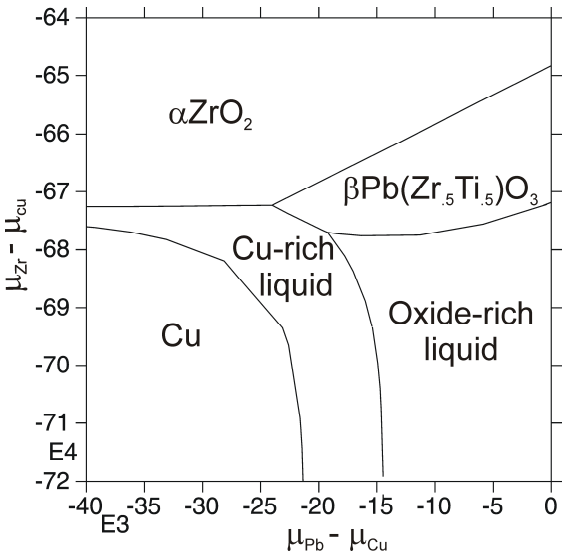

Fig. 7.17 Chemical potential diagram for the Cu-PbO-ZrO_2-TiO_2 system at 1323 K and log(P_{O_2} ,bar)= -7.

of temperature and partial pressure of oxygen. In Figs. 7.10-7.16 direct contact line between Cu and $\beta PbTiO_3$, $\beta PbZrO_3$ or $\beta PbZr_{.5}Ti_{.5}O_3$ could be seen, while the formation of oxide-rich liquid will take place for the compositions rich in PbO. With increasing temperature and partial pressure of oxygen the stability area of the oxide liquid widens (Figs. 7.10-7.16). At the same time, the length of the contact line between Cu and $\beta PbTiO_3$ (Figs. 7.10 and 7.12), $\beta PbZrO_3$ (Figs. 7.11 and 7.13) and $\beta PbZr_{.5}Ti_{.5}O_3$ (Figs. 7.14-7.16) is shorted, *i.e.* the window in terms of temperature and partial pressure of oxygen where copper coexist with $\beta PbTiO_3$, $\beta PbZrO_3$ and $\beta PbZr_{.5}Ti_{.5}O_3$ narrows. With further increasing temperature and increasing partial pressure of oxygen the Cu-rich liquid occurs as intervene phase between Cu and PZT (Fig. 7.17) and these solid phases are unstable against the formation of the Cu-rich liquid.

7.2.2. Experimental results and discussion

Five compositions were prepared and treated as described in Chapter 3.1.1 - (e). The XRD, SEM and EDX analysis were performed.

7.2.2.1. PbO-free samples

The XRD patterns of the initial mixture of sample 1 (Cu + $PbTiO_3$) and after heating in a controlled oxygen atmosphere using the Ni/NiO buffer at 1073 K (log (Po_2, bar) = -14) and 1173 K (log (Po_2, bar) = -12) for 50 h are given in Fig. 7.18. No changes in XRD patterns were observed after a heat-treatment at 1073 K in comparison with the initial mixture. At the same time, the strong peaks of the third phase, TiO_2, which are present on the XRD patterns after heat-treatment at 1173 K indicate the decomposition of lead titanate by the reaction $PbTiO_3 \leftrightarrow TiO_2 + Pb_{Liq} + 1/2\,O_2$. Due to the relatively low temperature the SEM back-scattered electron images (Figs. 7.19a and 7.19b) revealed the presence of very porous microstructure consisting of Cu (grey phase) and $PbTiO_3$ (light). Beside the grey and light areas, a dark TiO_2 phase was observed in sample 1 after heating at 1173 K (Figs. 7.19c and 7.19d). In addition, the morphology of sample 1 after heating

at 1173 K indicates that the decomposition of lead titanate with the formation of a liquid phase took place. The average chemical composition of phases obtained by EDX is shown in Table 7.4. The experimental results are consistent with the calculated diagrams (Figs. 7.8 and 7.9).

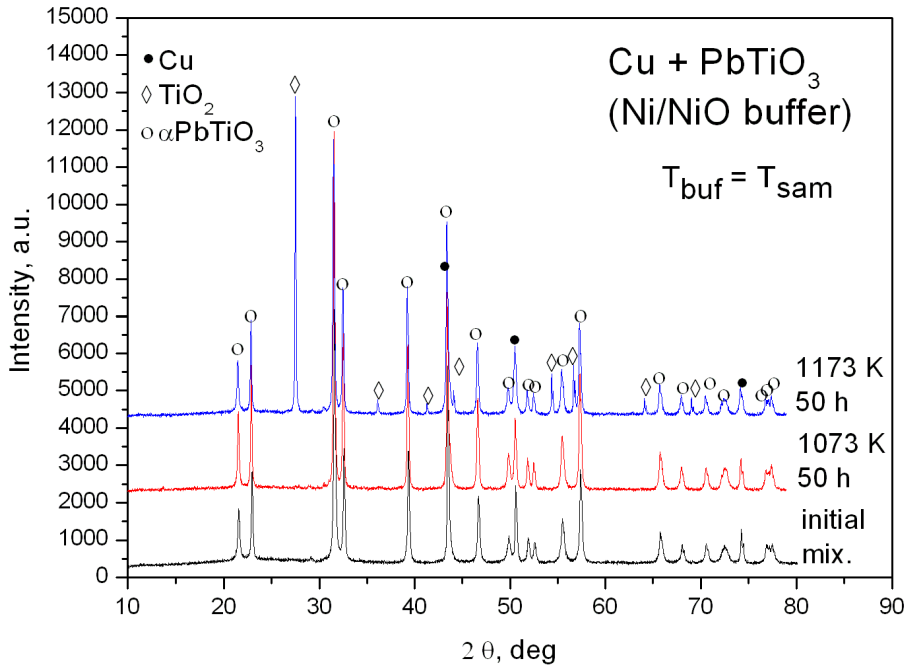

Fig. 7.18 XRD of sample 1 after heating at 1073 (log (Po_2, bar) = -14) and 1173 K (log (Po_2, bar) = -12) for 50 h using Ni/NiO buffer.

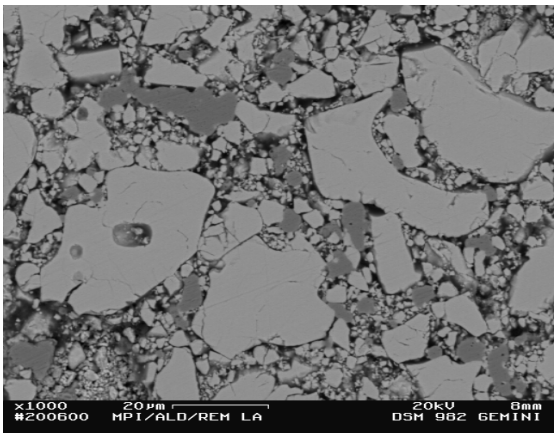

a)

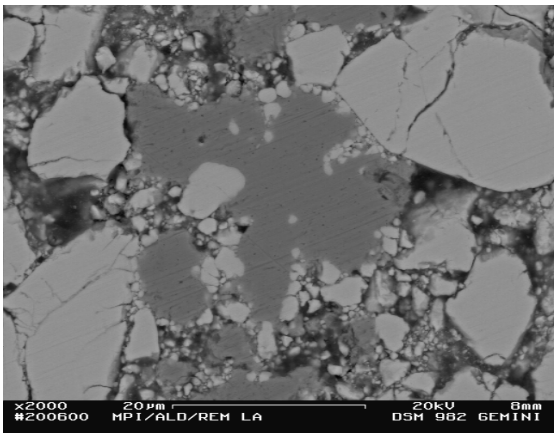

b)

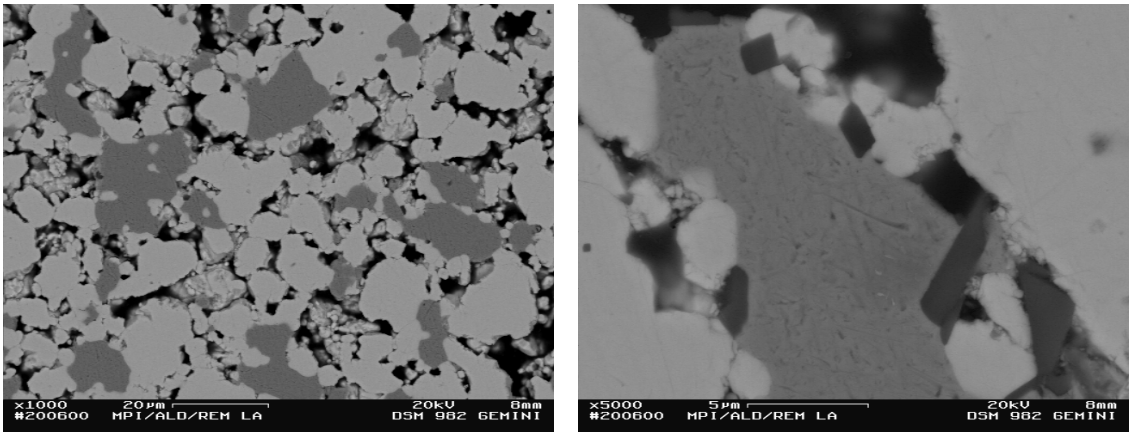

c) d)

Fig. 7.19 The SEM images of the sample 1 (Cu + $PbTiO_3$) after heating at 1073 K (log (Po_2, bar) = -14) (a and b) and 1173 K (log (Po_2, bar) = -12) (c and d) for 50 h.

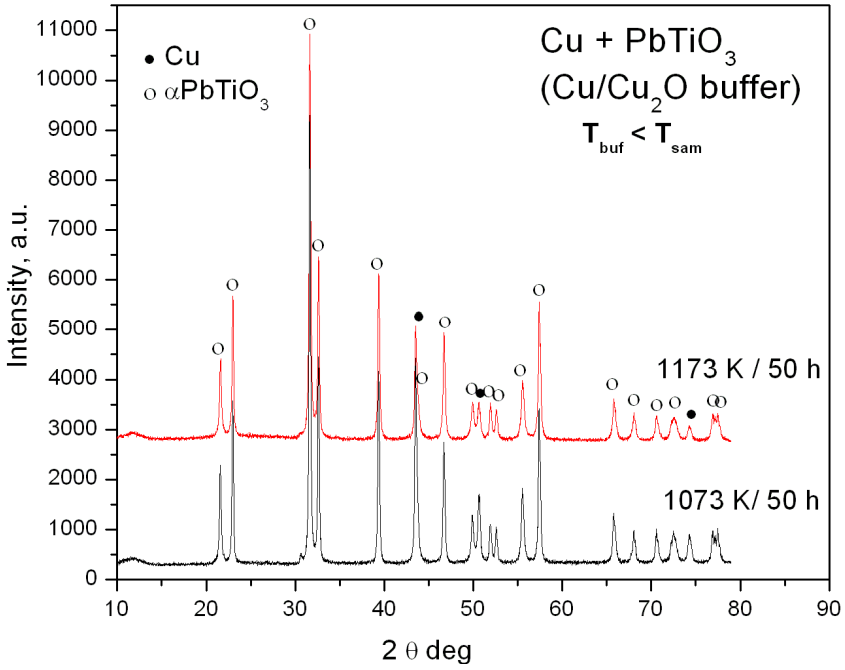

Fig. 7.20 XRD of sample 1 after heating at 1073 (log (Po_2, bar) = - 9.5) and 1173 K (log (Po_2, bar) = -8) for 50 h using Cu/Cu_2O buffer.

Table 7.4 The average chemical composition of phases observed by EDX analysis. (The uncertainty of measurements is 1 at. %)

Mixture/ Buffer/ Conditions	**Phase**	**Composition, at. %**			
		Cu	**Pb**	**Ti**	**O**
1 / Ni/NiO / 1073 K, 50 h log (Po_2, bar) = -14	grey (Cu)	98.3	0.4	0.9	0.4
	light ($PbTiO_3$) *(Figs. 7.19a,b)*	0.8	22.1	24.2	52.9
1 / Cu/Cu_2O / 1173 K, 50 h log (Po_2, bar) = -8	grey (Cu)	98.7	0	0	1.2
	light ($PbTiO_3$) *(Fig. 7.21)*	0.4	23.3	25.1	51.1
1 / Ni/NiO / 1173 K, 50 h log (Po_2, bar) = -12	dark (TiO_2)	0.4	0	35.6	64.0
	grey (Cu)	99.0	0	0	0.9
	light ($PbTiO_3$) *(Figs. 7.19c,d)*	0.7	23.2	25.2	50.9
3/ Cu/Cu_2O / 1073 K, 50 h log (Po_2, bar) = -9.5	grey (Cu)	99.1	0	0.2	0.6
	light grey ($PbTiO_3$)	0.2	23.6	25.0	51.1
	light (PbO) *(Fig. 7.25)*	0.3	51.1	5.9	42.7
		Cu	**Pb**	**Zr**	**O**
2 / Cu/Cu_2O / 1073 K, 50 h log (Po_2, bar) = -9.5	grey (Cu)	99.4	0.1	0.2	0.4
	light ($PbZrO_3$) *(Figs. 7.23a,b)*	0.9	23.2	23.5	52.4
2 / Cu/Cu_2O / 1173 K, 50 h log (Po_2, bar) = -8	dark (ZrO_2)	0.1	1.3	36.6	62.0
	grey (Cu)	99.1	0	0	0.9
	light ($PbZrO_3$) *(Figs. 7.23c-f)*	1	22.5	22.9	53.6
4 / Cu/Cu_2O / 1073 K, 50 h log (Po_2, bar) = -9.5	grey (Cu)	99.7	0	0.3	0
	light grey ($PbZrO_3$)	0.7	23.6	24.4	51.4
	light (PbO) *(Fig. 7.27)*	0.2	55.8	1.1	42.9
		Cu	**Pb**	**Ti**	**Zr**	**O**
5 / Cu/Cu_2O / 1173 K, 50 h log (Po_2, bar) = -8	grey (Cu)	99.8	0	0	0	0.7
	light ($PbZr_{.5}Ti_{.5}O_3$) *(Fig. 7.29)*	0.4	23.6	11.9	11.5	52.6

Fig. 7.20 shows the XRD patterns of the sample 1 (Cu + $PbTiO_3$) after heating in a controlled oxygen atmosphere using the Cu/Cu_2O buffer at 1073 K (log (Po_2, bar) = - 9.5) and 1173 K (log (Po_2, bar) = -8) for 50 h. The buffer was loaded in the furnace at the lower temperature then the samples as it was described in the Chapter 3.1. The change of the XRD pattern was not observed after heat-treatments. The SEM images show the presence of only two phases (Fig. 7.21), the grey one corresponds to Cu and the light one to $PbTiO_3$ without measurable solubility between them (Table 7.4). TiO_2 phase was not

observed indicating the stability of lead titanate under investigated conditions as it was predicted by the calculations (Figs. 7.10 and 7.12).

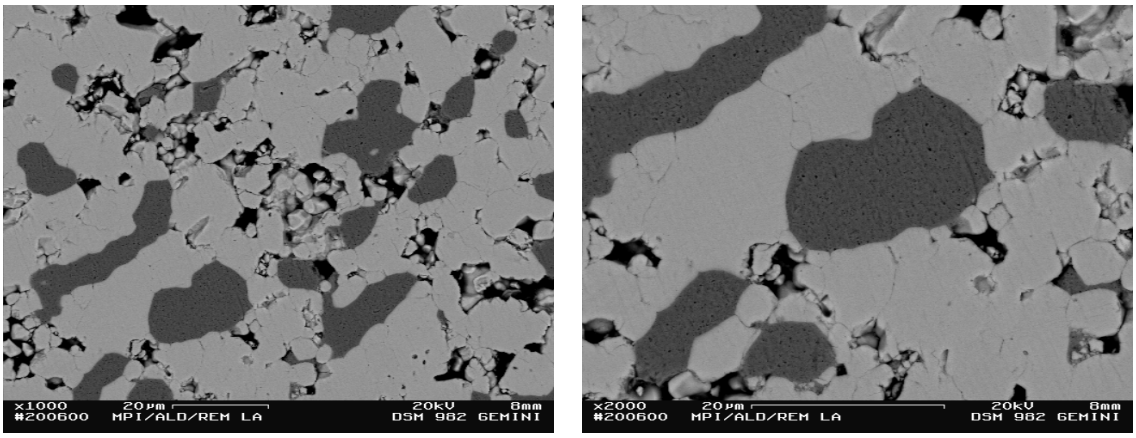

a) b)

Fig. 7.21 The SEM images (a - x1000 and b - x2000) of the sample 1 (Cu + $PbTiO_3$) after heating at 1173 K (log ($Po_{2,}$ bar) = -8) for 50 h.

Similarly, no change was observed in the XRD patterns of sample 2 (Cu + $PbZrO_3$) after heating at 1073 K (log ($Po_{2,}$ bar) = - 9.5) in comparison with the initial mixture (Fig. 7.22). Two phases, the grey Cu and light $PbZrO_3$, were observed using the electron microscopy (Fig. 7.23). The solubility of copper in $PbZrO_3$ is negligible (Table 7.4). However, the weak peak of ZrO_2 appears on the XRD patterns of the sample heat-treated at 1173 K (Fig. 7.22), which seems to be due to evaporation of PbO from $PbZrO_3$. Beside the Cu and $PbZrO_3$ phases the small grains (< 1µm) of zirconia were found only on the surface of the sample (Fig. 7.23d-f). The kinetically controlled evaporation of PbO becomes significant as the temperature increases. According to the calculated results for the closed system saturated with PbO vapor (Fig. 6.6, Chapter 6) $PbTiO_3$ shows a two order of magnitude lower partial pressure of PbO in comparison with $PbZrO_3$ at the same temperature. Therefore, the evaporation of PbO with the precipitation of TiO_2 from sample 1 treated at the same conditions (Cu/Cu_2O, 1173 K, log ($Po_{2,}$ bar) = -8) was not observed (Figs. 7.20 and 7.21). In this work, the experiments were done in an open system with continuous gas flow in order to obtain a controlled partial pressure of oxygen

over the samples. The PbO vapor was continuously transported away by the carrier gas and the equilibrium PbO vapor pressure over the samples could not be reached. The evaporation of PbO from lead titanate and lead zirconate leads to the decomposition of ceramics but this kinetically controlled process is not taken into account in the calculations of this work. In addition, it does not mean that $PbZrO_3$ is unstably with respect to PbO + ZrO_2, *i.e.* that the Gibbs energy of lead zirconate under investigating conditions (1173 K, log (Po_2, bar) = -8) is higher than for PbO + ZrO_2. The experimental observations are in agreement with the calculated diagrams in Figs. 7.11 and 7.13.

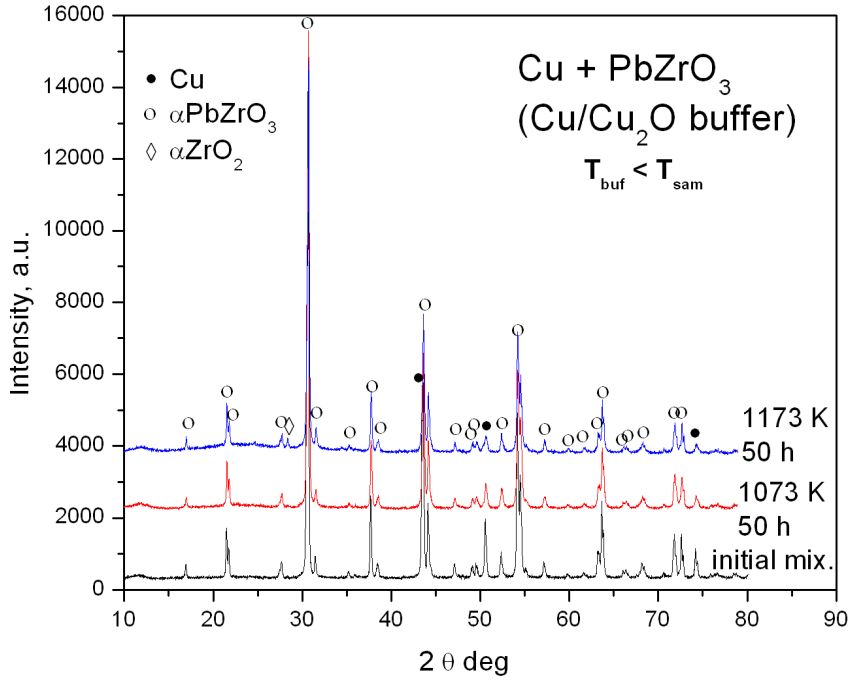

Fig. 7.22 XRD of sample 2 after heating at 1073 (log (Po_2, bar) = - 9.5) and 1173 K (log (Po_2, bar) = -8) for 50 h using Cu/Cu_2O buffer.

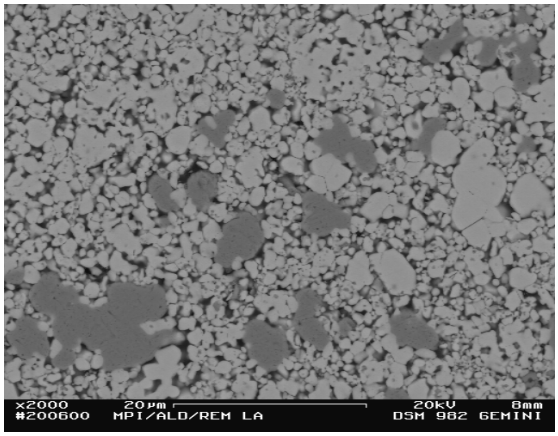

a)

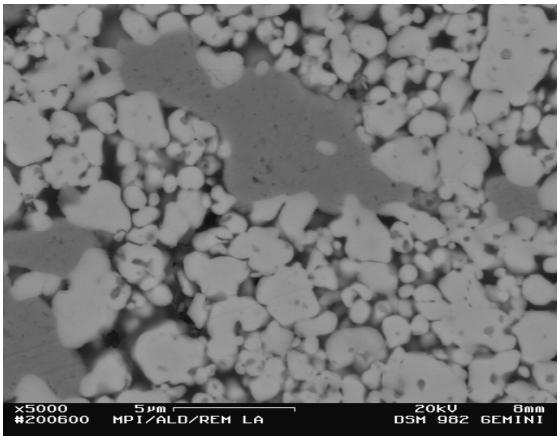

b)

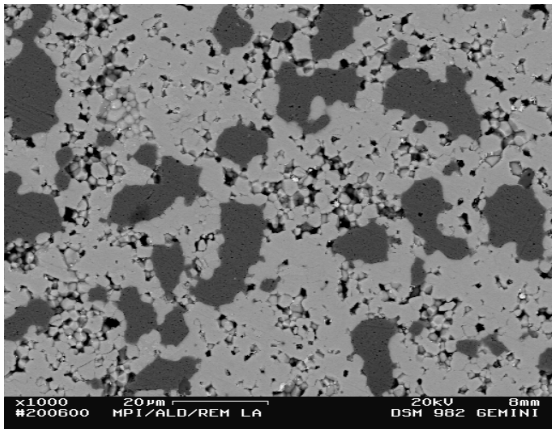

c)

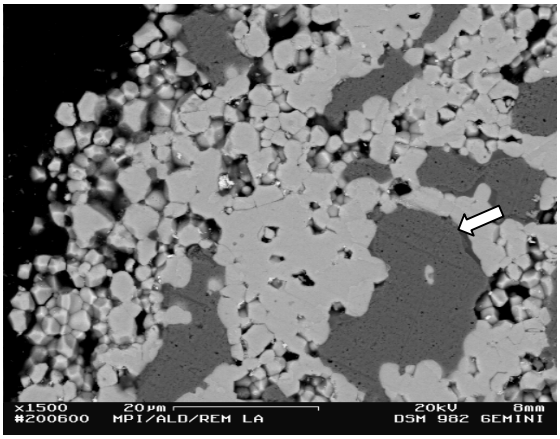

d)

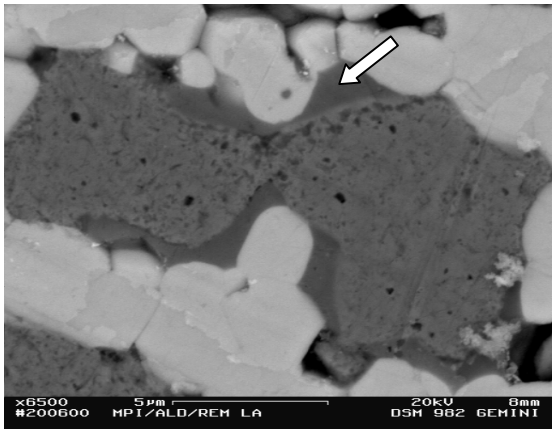

e)

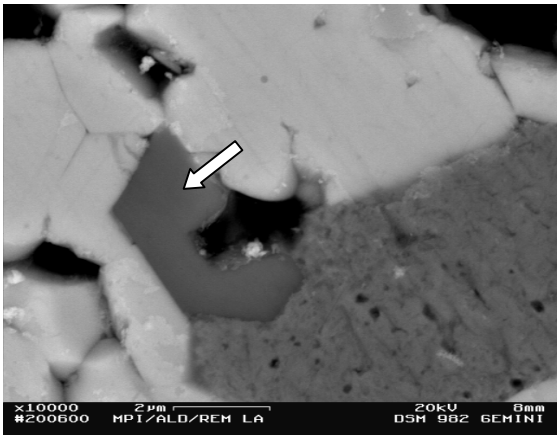

f)

Fig. 7.23 The SEM images of the sample 2 (Cu + $PbZrO_3$) after heating at 1073 K (log ($Po_{2,}$ bar) = -9.5) (a, b) and 1173 K(log ($Po_{2,}$ bar) = -8) (c, d, e, f) for 50 h. (ZrO_2 phase is shown by arrow)

7.2.2.2. PbO – bearing samples

Three phases, tetragonal αPbO solid solution, $\alpha PbTiO_3$ and Cu were observed on the XRD pattern of mixture 3 (Cu + PbO + $PbTiO_3$) after heating at 1073 K (log (Po_2, bar) = - 9.5) for 50 h using the Cu/Cu_2O buffer (Fig. 7.24). The partial melting of this sample was visually confirmed. The tetragonal αPbO solid solution (light phase), $\alpha PbTiO_3$ (light grey) and Cu (grey) can also be seen on the SEM images given in Fig. 7.25, while the average chemical composition of the phases is shown in Table 7.4. These findings are in accord with the predicted phase stabilities in Fig. 7.10. The solubility between Cu and $PbTiO_3$ was not observed. The measured solubility of titanium in αPbO is consistent with the previously reported experimental results for the CuO_x-PbO-TiO_2 system (Table 7.3) as well as with the assessed PbO-TiO_2 phase diagram (Fig. 6.1, Chapter 6).

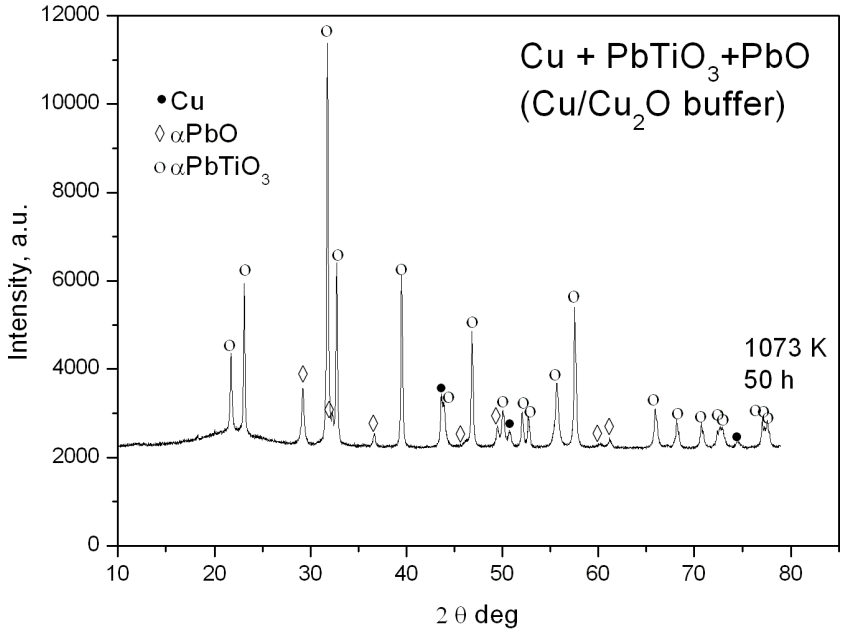

Fig. 7.24 XRD of sample 3 after heating at 1073 (log (Po_2, bar) = - 9.5) for 50 h with using the Cu/Cu_2O buffer.

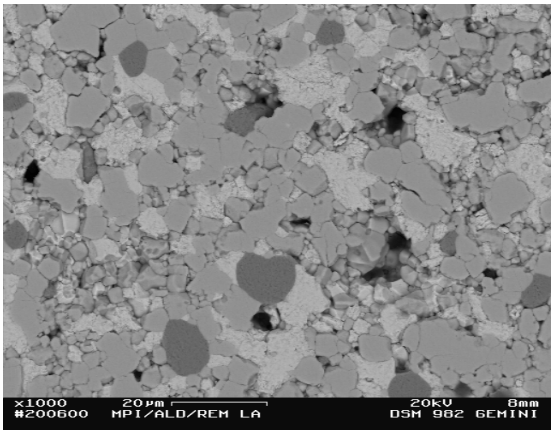

a)

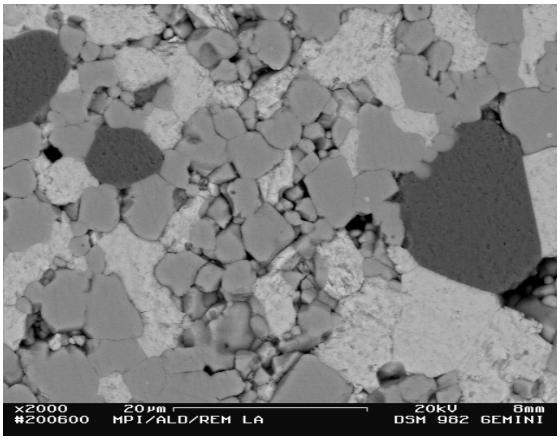

b)

Fig. 7.25 The SEM images (a - x1000 and b - x2000) of the sample 3 (Cu + PbO + $PbTiO_3$) after heating at 1073 K (log ($Po_{2,}$ bar) = -9.5) for 50 h using Cu/Cu_2O buffer.

Similarly, three phases, αPbO (light), $PbZrO_3$ (light grey) and Cu (grey) are found in sample 4 (Cu + PbO + $PbZrO_3$) (Figs. 7.26 and 7.27). Due to the evaporation of PbO the amount of this phase in the microstructure is low (Fig. 7.27). The solubility of zirconia in PbO is less than 2 mol. % at 1073 K, while the solubility between Cu and $PbZrO_3$ was again not observed (Table 7.4). It is doubtful if the melting of sample 4 took place. However, the lower fraction of the PbO solid solution observed in sample 4 (Fig. 7.26) in comparison with sample 3 (Fig. 7.24) is reasonable. The dissolution of titania and zirconia leads to the stabilization of the PbO solid solution and the decreasing of the activity of lead oxide in the PbO solid solution, *i.e.*, the partial pressure of PbO above the solid solution ($a_{PbO} = P_{PbO} / P^{o}_{PbO}$, where the a_{PbO} is the activity of PbO, P_{PbO} is partial pressure of the PbO above the αPbO solid solution and P^{o}_{PbO} is the partial pressure over the pure PbO). The solubility of zirconia in both, the liquid and PbO solid solution is less than those measured in the case of titania that suppresses the evaporation of PbO from sample 3 in comparison with sample 4.

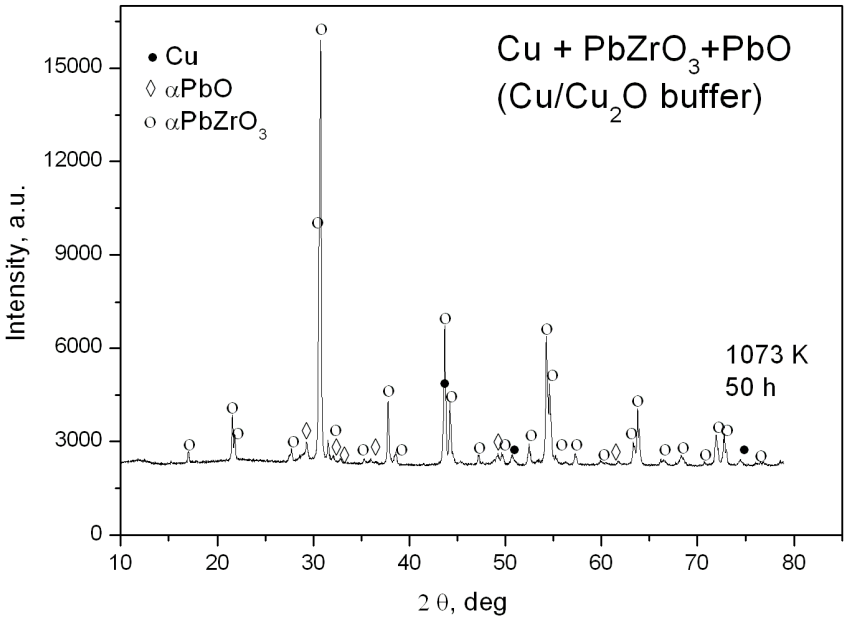

Fig. 7.26 The XRD of sample 4 after heating at 1073 (log (Po_2, bar) = - 9.5) for 50 h using Cu/Cu_2O buffer.

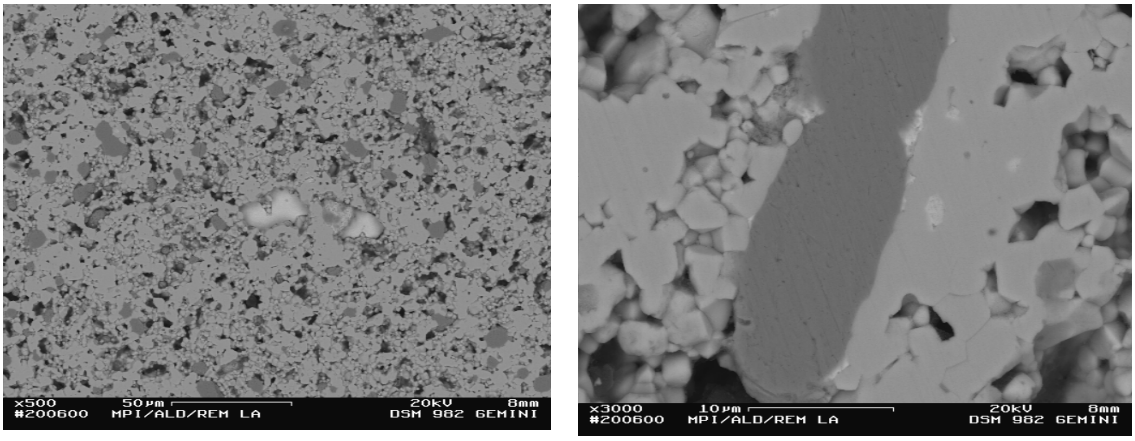

a) b)

Fig. 7.27 The SEM images (a – x500 and b – x3000) of the sample 4 (Cu + PbO + $PbZrO_3$) after heating at 1073 K (log (Po_2, bar) = -9.5) for 50 h using Cu/Cu_2O buffer.

The XRD and SEM of mixture 5 (Cu + PZT) after heating at 1073 K (log (Po_2, bar) = -9.5) and 1173 K (log (Po_2, bar) = -8) show the presence of two phases, PZT (light) and Cu (grey) (Figs. 7.28 and 7.29). The reactivity between Cu and ceramics was not

observed (Table 7.4). The obtained experimental results are well consistent with the phase relation predicted by calculations (Fig. 7.14 and 7.15).

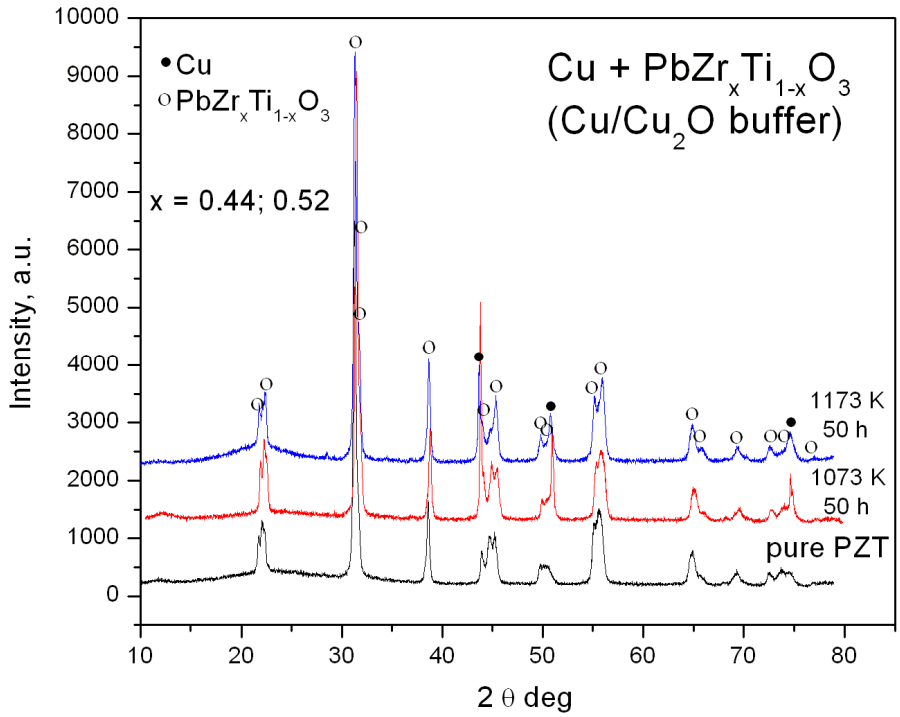

Fig. 7.28 XRD of sample 5 after heating at 1073 K (log (Po_2, bar) = - 9.5) and 1173 K (log (Po_2, bar) = - 8) for 50 h using Cu/Cu_2O buffer.

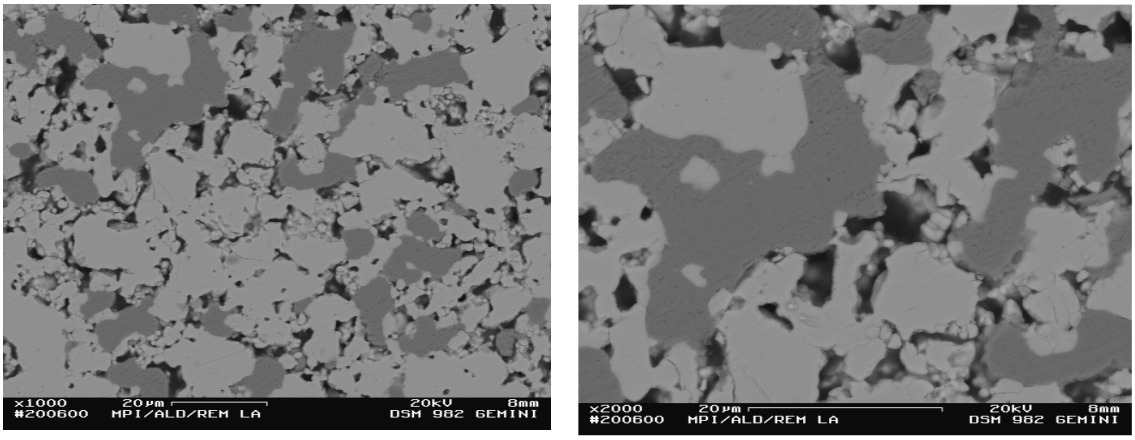

a) b)

Fig. 7.29 The SEM images (a - x1000 and b - x2000) of the sample 5 (Cu + PZT) after heating at 1173 K (log (Po_2, bar) = -8) for 50 h using Cu/Cu_2O buffer.

8. CONCLUSIONS AND OUTLOOK

The thermodynamic assessment of the multi-component Cu-Pb-Zr-Ti-O system was carried out by the CALPHAD method. Thermodynamic properties were described using the compound energy formalism (CEF) as well as the substitutional solution model for various solid phases and an associate solution model for the liquid phase. An internally consistent set of optimized Gibbs energy parameters has been derived, which provides a good description of phase equilibria at 1 bar total pressure.

The associate solution model adopted for the description of the liquid phase in the multi-component Cu-Pb-Ti-Zr-O system was found to be superior for calculating the relevant phase equilibria in comparison with the two-sublattice ionic model. Although both models can be applied with some success in the binary systems (Zr-O, Ti-O, Cu-O, Pb-O), extension to the higher-order systems (*e.g.* Cu-Ti-O) is not always equivalent as there are more compositional variables in the associate model than for the two-sublattice case. The calculated isothermal sections of Cu-Ti-O system at 1500 K using two-sublattice ionic model for liquid (Fig. 5.2.1, Chapter 5.2) show the existence of an unexpected miscibility gap at high temperatures. Such features arise from a complex Gibbs energy dependence on composition and, although the Gibbs energy of mixing can be negative over the whole composition range, inflections points give rise to the decomposition into two liquids. The essential difference between the models is in the expression of the excess Gibbs energy. Using the associate solution model the problem of extended miscibility gap in the Cu-Ti-O system is solved (Fig. 5.2.2, Chapter 5.2). The model has also been successfully employed to represent the thermodynamic properties of liquid in the Ti-O, Pb-O, Cu-Ti-O, Cu-Pb-O and Cu-Zr-O systems. A derived self-consistent set of optimized Gibbs energy parameters allows safe extrapolations into the multi-component Cu-Pb-Ti-Zr-O system.

The binary Ti-O system has been completely reassessed in the present work, while the Pb-O was adopted from the literature with some modifications in the liquid phase region. The ternary Cu-Pb-O, Cu-Ti-O and Cu-Zr-O systems have been assessed for the

first time. The ternary compounds Cu_2PbO_2, Cu_2Ti_4O, Cu_3Ti_3O and Cu_3TiO_4 are modeled as stoichiometric phases. The absence of any ternary compound in Cu-Zr-O system was proved experimentally.

The quasi-binary PbO-ZrO_2, PbO-TiO_2 and ZrO_2-TiO_2 systems, the edges of the quasi-ternary PbO-ZrO_2-TiO_2 (PZT) system, were reassessed on the basis of most recent literature data and experimental data obtained in this work. Due to the lack of experimental information, lead titanate (tetragonal, $\alpha PbTiO_3$ and cubic, $\beta PbTiO_3$) and lead zirconate (cubic form, $\beta PbZrO_3$) were considered as stoichiometric compounds, while the tetragonal and orthorhombic PbO solid solutions as well as perovskites of the series $\beta PbZr_xTi_{1-x}O_3$ were described by the substitutional solution model.

The obtained experimental results confirm the predicted phase relations in the CuO_x-PbO-ZrO and CuO_x-PbO-TiO_2 systems (Fig. 7.1a and 7.2a, Chapter 7.1). The experimentally measured solubilities of 1.3 ± 2 mol. % ZrO_2 and 9.6 ± 2 mol. % TiO_2 in PbO solid solution at 1043 K are consistent with the calculated values of 1.4 mol. % ZrO_2 and 8 mol. % TiO_2. No solubility between CuO and $\beta PbTiO_3$ / $\beta PbZrO_3$ was observed, *i.e.*, the experimentally obtained values are zero within the uncertainty of the measurements, while the calculated temperatures of invariant reactions in the CuO_x-PbO-ZrO_2 and CuO_x-PbO-TiO_2 show satisfactory agreement with the experimentally measured ones (Tables 7.1 and 7.2, Chapter 7.1).

The calculated chemical potential diagrams of the multi-component Cu-Pb-Zr-Ti-O system based on the extrapolation from the lower-order systems show a coexistence of Cu with $\beta PbTiO_3$, $\beta PbZrO_3$ and $\beta PbZr_{.5}Ti_{.5}O_3$ within a window in terms of temperature and partial pressure of oxygen (Figs. 7.8 - 7.15, Chapter 7.2). The predicted chemical stability of Cu with $\beta PbTiO_3$, $\beta PbZrO_3$ and $\beta PbZr_{.5}Ti_{.5}O_3$ is verified by experiments. The reactivity between copper and lead-titanate, lead-zirconate and PZT solid solution (x = 0.44, 0.5) was not observed using the characterization methods (XRD, SEM and EDX) applied in this work.

The results obtained in this study clearly show the chemical stability of copper and PZT ceramics at temperatures below 1273 K in reducing atmosphere (Fig. 7.14 - 7.17, Chapter 7.2). Detailed investigations of the feasibility of using copper in the piezoelectric actuators based on PZT solid solutions requires the application of additional characterization methods such as measurements of electrical and polarization properties. During the experiments performed in an open system, evaporation of PbO from lead-titanate, lead-zirconate and PZT solid solution occurs, resulting in a significant PbO loss. However, the use of excess PbO leads to the formation of a liquid phase already at 1073 K (Fig. 7.14, Chapter 7.2). Detailed investigations of the kinetics of PbO evaporation seems to be of the fundamental importance in optimization of the processing conditions (temperature and time) for PZT-based ceramics. In addition, some doping elements, such is Cd^{+2} may contribute to decreasing of PbO activity and suppression of the evaporation of PbO [1998Chu]. From this point of view, the database developed in this work is a starting point for the incorporation of new elements. In addition, the samples prepared by solid state reaction show a poor densification property. For the fabrication of multilayer actuators devices, it is necessary to develop PZT powder which has a low sintering temperature (below 1273 K) to allow co-firing with Cu.

Appendix

Table 1 Summary of the thermodynamic parameters describing the condensed phases in the Cu-Pb-Ti-Zr-O system referred to stable element reference H^{SER}. The Gibbs energy of species of the gas phase is taken from SGTE substance database [1997SGTE].

Parameter	Reference
Liquid (Cu, Cu_2O, O, Pb, PbO, Zr, ZrO_2, Ti , TiO, $TiO_{1.5}$, TiO_2)	
${}^oG^{liq}_{Cu} = +12964.736 - 9.511904T + {}^oG^{fcc}_{Cu:Va} - 5.849\text{x}10^{-21}\,T^7$ (298.15-1357.8 K)	[2001SGTE]
$= +13495.481 - 9.922344T + {}^oG^{fcc}_{Cu:Va} - 3.642\text{x}10^{29}\,T^{-9}$ (1357.77-3200 K)	
${}^oG^{liq}_{O} = {}^oG_{O} - 2648.9 + 31.44T$ (298.15-3000 K)	[2001SGTE]
${}^oG^{liq}_{Pb} = +4672.124 - 7.750583T + {}^oG^{fcc}_{Pb:Va} - 6.019\text{x}10^{-19}\,T^7$ (298.15-600.61 K)	[2001SGTE]
$= +4853.137 - 8.067135T + {}^oG^{fcc}_{Pb:Va} - 8.05448\text{x}10^{25}\,T^{-9}$ (600.61-2100 K)	
${}^oG^{liq}_{Zr} = +18147.703 - 9.080762T + {}^oG^{hcp}_{Zr:Va} + 1.6275\text{x}10^{-22}\,T^7$ (298.15-2128 K)	[2001SGTE]
$= +17804.649 - 8.91153T + {}^oG^{hcp}_{Zr:Va} + 1.343\text{x}10^{31}\,T^{-9}$ (2128-6000 K)	
${}^oG^{liq}_{Ti} = +4134.494 + 126.63427T - 23.9933TlnT - 4.777975\text{x}10^{-3}T^2$	[2001SGTE]
$- 0.106716\text{x}10^{-6}T^3 + 72636T^{-1}$ (298.15-900 K)	
$= +4382.601 + 126.00713T - 23.9887TlnT - 4.2033\text{x}10^{-3}T^2$	
$- 0.090876\text{x}10^{-6}T^3 + 42680T^{-1}$ (900-1155 K)	
$= +13103.253 + 59.9956T - 14.9466TlnT - 8.1465\text{x}10^{-3}T^2$	
$+ 0.202715\text{x}10^{-6}T^3 - 1477660T^{-1}$ (1155-1300 K)	
$= + 369519.198 - 2554.0225T + 342.059267TlnT$	
$- 163.409355\text{x}10^{-3}T^2 + 12.457117\text{x}10^{-6}T^3 - 67034516T^{-1}$	
(1300-1941 K)	
$= - 19887.066 + 298.7367T - 46.29TlnT$	
(1941-4000 K)	
${}^oG^{liq}_{Cu_2O} = - 116420.57 + 295.041T - 64.6847TlnT - 0.00483252T^2$	[1992Bou]
$+ 180748.8\,T^{-1}$ (298.15-6000 K)	
${}^oG^{liq}_{PbO} = - 219210 + 360T - 65TlnT$ (298.15-3000 K)	[1998Ris]
${}^oG^{liq}_{ZrO_2} = + 87027 - 29.17432T + {}^oG^{\gamma ZrO_2}_{Zr^{4+}:O^{2-}}$ (298.15-6000 K)	[2006Wan]
${}^oG^{liq}_{TiO} = + 77871.822 - 30.6738T + G_{Ti_1O_1}$	This work
${}^oG^{liq}_{TiO_{1.5}} = +57073.715 - 22.808T + .5G_{Ti_2O_3}$	This work
${}^oG^{liq}_{TiO_2} = +61022.452 - 28.223T + G_{TiO_2}$	This work
${}^0L^{liq}_{Cu,Cu_2O} = +19503.765 + 6.1386T$	[1992Bou]
${}^1L^{liq}_{Cu,Cu_2O} = +19099.920 - 11.2764T$	[1992Bou]
${}^2L^{liq}_{Cu,Cu_2O} = +13273.435 - 5.6023T$	[1992Bou]
${}^0L^{liq}_{Cu_2O,O} = - 86915.94 + 26.6215T$	[1992Bou]

${}^{1}L^{liq}_{Cu_2O,O} = -72521.735 + 60.10565T$	[1992Bou]
${}^{2}L^{liq}_{Cu_2O,O} = -29501.255 - 16.2635T$	[1992Bou]
${}^{0}L^{liq}_{Cu,Cu_2O,O} = -82639.99 + 10.8941T$	[1992Bou]
${}^{0}L^{liq}_{Pb,PbO} = +120315 - 19.653T$	This work
${}^{1}L^{liq}_{Pb,PbO} = -1103.25$	This work
${}^{2}L^{liq}_{Pb,PbO} = -51012$	This work
${}^{o}L^{liq}_{PbO,O} = +50000$	This work
${}^{0}L^{liq}_{Cu,Pb} = +27190.2 - 4.21329T$	[1986Hay]
${}^{1}L^{liq}_{Cu,Pb} = +2229.2 - 0.53584T$	[1986Hay]
${}^{2}L^{liq}_{Cu,Pb} = -7029.2 + 6.48832T$	[1986Hay]
${}^{3}L^{liq}_{Cu,Pb} = -7397.6 + 5.07992T$	[1986Hay]
${}^{0}L^{liq}_{Zr,ZrO_2} = +68315.312 - 40T$	[2006Wan]
${}^{1}L^{liq}_{Zr,ZrO_2} = -177515.86 + 50T$	[2006Wan]
${}^{0}L^{liq}_{ZrO_2,O} = +50000$	[2006Wan]
${}^{0}L^{liq}_{Ti,TiO} = +121427.1 - 73.4128T$	This work
${}^{1}L^{liq}_{Ti,TiO} = -77733.909 + 41.897T$	This work
${}^{o}L^{liq}_{TiO_{1.5},TiO_2} = -19200.78 + 0.236T$	This work
${}^{1}L^{liq}_{TiO_{1.5},TiO_2} = +100402.44 - 48.649T$	This work
${}^{0}L^{liq}_{PbO,Cu} = +276056.539 - 127.794T$	This work
${}^{1}L^{liq}_{PbO,Cu} = +106857.91$	This work
${}^{0}L^{liq}_{Pb,Cu_2O} = +2905.11 + 3.289T$	This work
${}^{1}L^{liq}_{Pb,Cu_2O} = +10987.73$	This work
${}^{0}L^{liq}_{PbO,Cu_2O} = -15224.26 - 10.71T$	This work
${}^{1}L^{liq}_{PbO,Cu_2O} = 9548.83 - 18.412T$	This work
${}^{0}L^{liq}_{TiO_2,Cu_2O} = -40321.9$	This work
${}^{0}L^{liq}_{Cu,Ti,TiO} = -120000 - 120T$	This work
${}^{0}L^{liq}_{PbO,ZrO_2} = -4600$	This work
${}^{0}L^{liq}_{PbO,TiO_2} = 124200 + 52.2\,T$	This work
${}^{1}L^{liq}_{PbO,TiO_2} = 16900$	This work
${}^{0}L^{liq}_{ZrO_2,TiO_2} = -170653.79 + 67.49\,T$	This work
${}^{1}L^{liq}_{ZrO_2,TiO_2} = +23686.45$	This work
${}^{2}L^{liq}_{ZrO_2,TiO_2} = -25941.76$	This work

$^{0}L^{liq}_{PbO,ZrO_2,TiO_2}$ = 60582.55 This work

fcc (Cu, Pb, Ti, Zr)$_1$ (O,Va)$_1$

$^{o}G^{fcc}_{Cu:Va}$ = – 7770.458 + 130.485235T – 24.112392$T\ln T$ – 0.00265684T^2 [2001SGTE]
+ 1.29223x10$^{-7}T^3$ +52478T^{-1} (298.15-1357.77 K)
= – 13542.026 + 183.803828T – 31.38$T\ln T$ + 3.642x10$^{29}T^{-9}$
(1357.77-3200 K)

$^{o}G^{fcc}_{Ti:Va}$ = + 6000 – 0.1T + $^{o}G^{hcp}_{Ti:Va}$ [2001SGTE]

$^{o}G^{fcc}_{Zr:Va}$ = + 7600 – 0.9T + $^{o}G^{hcp}_{Zr:Va}$ [2001SGTE]

$^{o}G^{fcc}_{Pb:Va}$ = – 7650.085 + 101.700244T – 24.5242231$T\ln T$ – 0.00365895T^2 [2001SGTE]
– 2.4395x10$^{-7}T^3$ (298.15-600.61 K)
= – 10531.095 + 154.243182T – 32.4913959$T\ln T$ + 0.00154613T^2
+ 8.05448x10$^{25}T^{-9}$ (600.61-1200 K)
= + 4157.616 + 53.139072T – 18.9640637$T\ln T$ – 0.002882943T^2
+ 9.8144x10$^{-8}T^3$ – 2696755T^{-1} + 8.05448x10$^{25}T^{-9}$ (1200-2100 K)

$^{\circ}G^{fcc}_{Ti:O}$ = + 6605.382 + 7.7366 T + $^{\circ}G_{Ti_1O_1}$ This work

$^{o}G^{fcc}_{Cu:O}$ = – 19400 + 31T + $^{o}G^{fcc}_{Cu:Va}$ + ½$^{\circ}G_{O_2(g)}$ [1992Bou]

$^{o}G^{fcc}_{Pb:O}$ = $^{o}G^{fcc}_{Pb:Va}$ +½$^{o}G_{O_2(g)}$ + 30000 This work

$^{o}G^{fcc}_{Zr:O}$ = $^{o}G^{hcp}_{Zr:Va}$ + ½$^{\circ}G_{O_2(g)}$ + 30000 This work

$^{0}L^{fcc}_{Ti:O,Va}$ = + 817.911 This work

$^{0}L^{fcc}_{Cu,Pb:Va}$ = +74090.0 – 24.69707T [1986Hay]

$^{0}L^{fcc}_{Cu,Ti:Va}$ = – 9882 [1996Kum]

$^{1}L^{fcc}_{Cu,Ti:Va}$ = + 15777 [1996Kum]

$^{0}L^{fcc}_{Cu,Zr:Va}$ = + 2233 [1994Zen]

bcc (Cu, Pb, Ti, Zr)$_1$ (O,Va)$_1$

$^{o}G^{bcc}_{Zr:Va}$ = – 525.539 + 124.9457T – 25.607406$T\ln T$ – 3.40084x10$^{-4}T^2$ [2001SGTE]
– 9.729x10$^{-9}T^3$ + 25233T^{-1} – 7.6143x10$^{-11}T^4$ (298.15-2128 K)
= – 30705.955 + 264.284163T – 42.144$T\ln T$ + 1.276058x10$^{32}T^{-9}$
(2128-6000 K)

$^{o}G^{bcc}_{Ti:Va}$ = – 1272.064 + 134.71418T – 25.5768$T\ln T$ – 0.663845x10$^{-3}T^2$ [2001SGTE]
– 0.278803x10$^{-6}T^3$ + 7208T^{-1} (298.15-1155 K)
= + 6667.385 + 105.366379T – 22.3771$T\ln T$ + 1.21707x10$^{-3}T^2$
– 0.84534x10$^{-6}T^3$ – 2002750T^{-1} (1155-1941 K)
= + 26483.26 – 182.426471T + 19.0900905$T\ln T$ – 22.00832x10$^{-3}T^2$
+ 1.228863x10$^{-6}T^3$ + 1400501T^{-1} (1941-4000 K)

$^{o}G^{bcc}_{Cu:Va}$ = + 4017 – 1.255T + $^{o}G^{fcc}_{Cu:Va}$ [2001SGTE]

$^{o}G^{bcc}_{Pb:Va}$ = + 2400 – 1.1T + $^{o}G^{fcc}_{Pb:Va}$ [2001SGTE]

$^{o}G^{bcc}_{Ti:O}$ = – 511601.02 + 83.178T + $^{o}G^{hcp}_{Ti:Va}$ + ½$^{\circ}G_{O_2(g)}$ This work

$^{o}G^{bcc}_{Cu:O}$ = – 19400 + 31T + $^{o}G^{fcc}_{Cu:Va}$ + ½$^{\circ}G_{O_2(g)}$ This work

$^{o}G^{bcc}_{Zr:O} = -515575.87 + 105T + {}^{o}G^{hcp}_{Zr:Va} + ½°G_{O_2(g)}$ [2006Wan]

$^{o}G^{bcc}_{Pb:O} = {}^{o}G^{fcc}_{Pb:Va} + ½{}^{o}G_{O_2(g)} + 30000$ This work

$^{0}L^{bcc}_{Ti:O,Va} = -25777.47 + 0.59T$ This work

$^{1}L^{bcc}_{Zr:O,Va} = -87697.561$ [2006Wan]

$^{0}L^{bcc}_{Cu,Ti:Va} = +3389$ [1996Kum]

$^{0}L^{bcc}_{Cu,Zr:Va} = -7381.13$ [1994Zen]

hcp (Cu, Pb, Ti, Zr)$_1$ (O,Va)$_{.5}$

$^{o}G^{hcp}_{Zr:Va} = -7827.595 + 125.64905T - 24.1618TlnT - 0.00437791T^2$ [2001SGTE]
$+ 34971T^{-1}$ (298.15-2128 K)
$= -26085.921 + 262.724183T - 42.144TlnT - 1.342895\text{x}10^{31}T^{-9}$
(2128-6000 K)

$^{o}G^{hcp}_{Ti:Va} = -8059.921 + 133.687208T - 23.9933TlnT - 0.004777975T^2$ [2001SGTE]
$+ 1.06716\text{x}10^{-7}T^3 + 72636T^{-1}$ (298.15-900 K)
$= -7811.815 + 133.060068T - 23.9887TlnT - 0.0042033T^2$
$- 9.0876\text{x}10^{-8}T^3 + 42680T^{-1}$ (900-1155 K)
$= +908.837 + 67.048538T - 14.9466TlnT - 0.0081465T^2$
$+ 2.02715\text{x}10^{-7}T^3 - 1477660T^{-1}$ (1155-1941 K)
$= -124526.786 + 638.878871T - 87.2182461TlnT + 0.008204849T^2$
$- 3.04747\text{x}10^{-7}T^3 + 36699805T^{-1}$ (1941-4000 K)

$^{o}G^{hcp}_{Cu:Va} = +600 + 0.2T + {}^{o}G^{fcc}_{Cu:Va}$ [2001SGTE]

$^{o}G^{hcp}_{Pb:Va} = +300 + 1T + {}^{o}G^{fcc}_{Pb:Va}$ [2001SGTE]

$°G^{hcp}_{Ti:O} = -277514.02 + 40.6543T + °G^{hcp}_{Ti:Va} + ¼°G_{O_2(g)}$ This work

$^{o}G^{hcp}_{Cu:O} = -19400 + 31T + °G^{fcc}_{Cu:Va} + ¼°G_{O_2(g)}$ This work

$^{o}G^{hcp}_{Pb:O} = {}^{o}G^{fcc}_{Pb:Va} + ½{}^{o}G_{O_2(g)} + 30000$ This work

$^{0}L^{hcp}_{Cu:O,Va} = -50000$ This work

$^{o}G^{hcp}_{Zr:O} = -286427.91 + 43.223T + °G^{hcp}_{Zr:Va} + ¼°G_{O_2(g)}$ [2006Wan]

$^{0}L^{hcp}_{Ti:O,Va} = +817.911$ This work

$^{0}L^{hcp}_{Zr:O,Va} = -37876.655 + 17.292T$ [2006Wan]

$^{1}L^{hcp}_{Zr:O,Va} = -4471.386$ [2006Wan]

$^{0}L^{hcp}_{Cu,Ti:Va} = +16334$ [1996Kum]

$^{0}L^{hcp}_{Cu,Zr:Va} = +11336.85$ [1994Zen]

$^{0}L^{hcp}_{Cu,Ti:O} = -155000$ This work

TiO$_x$ (Ti^{3+},Ti^{2+}, Va)$_1$(Ti,Va)$_1$(O^{2-})$_1$

$°G^{TiO_x}_{Ti^{2+}:Ti:O^{2-}} = -554987.484 + 84.614T + 2\,°G^{hcp}_{Ti:Va} + ½°G_{O_2(g)}$ This work

$°G^{TiO_x}_{Ti^{3+}:Ti:O^{2-}} = -560666.36 + 84.614T + 2\,°G^{hcp}_{Ti:Va} + ½°G_{O_2(g)}$ This work

$°G^{TiO_x}_{Va:Ti:O^{2-}} = °G_{Ti_1O_1} + 200000$ This work

$^{\circ}G^{TiO_x}_{Ti^{2+}:Va:O^{2-}} = {}^{\circ}G_{Ti_1O_1} + 6605.382 + 7.7366T$ This work

$^{\circ}G^{TiO_x}_{Ti^{3+}:Va:O^{2-}} = \frac{1}{2}{}^{\circ}G_{Ti_2O_3} + 5494.871 + 10.2103T$ This work

$^{\circ}G^{TiO_x}_{Ti^{3+}:Va:O^{2-}} = 0$ This work

$^{\circ}G^{TiO_x}_{Ti^{2+}:Ti,Va:O^{2-}} = 17092.532 - 3.8448T$ This work

rutile $(Ti^{3+},Ti^{4+},Zr^{4+})_1\ (O^{2-},Va)_2$

$^{\circ}G^{rut}_{Ti^{4+}:Va} = {}^{\circ}G_{TiO_2} - {}^{\circ}G_{O_2(g)}$ This work

$^{\circ}G^{rut}_{Zr^{4+}:Va} = {}^{\circ}G^{\beta ZrO_2}_{ZrO_2} - {}^{\circ}G_{O_2(g)}$ This work

$^{\circ}G^{rut}_{Ti^{4+}:O^{2-}} = {}^{\circ}G_{TiO_2}$ [1999Wal]

$^{\circ}G^{rut}_{Zr^{4+}:O^{2-}} = {}^{\circ}G^{\beta ZrO_2}_{ZrO_2} + 35000$ This work

$^{\circ}G^{rut}_{Ti^{3+}:Va} = \frac{1}{2}{}^{\circ}G_{Ti_2O_3} - \frac{3}{4}{}^{\circ}G_{O_2(g)} + 9.35T + 55781.493 - 4.0852T$ This work

$^{\circ}G^{rut}_{Ti^{3+}:O^{2-}} = \frac{1}{2}{}^{\circ}G_{Ti_2O_3} + \frac{1}{4}{}^{\circ}G_{O_2(g)} + 9.35T + 55781.493 - 4.0852T$ This work

$^{\circ}L^{rut}_{Ti^{4+},Zr^{4+}:O^{2-}} = + 3400 - 11.945T$ This work

$^{1}L^{rut}_{Ti^{4+},Zr^{4+}:O^{2-}} = + 3402.9 + 6.2T$ This work

Ti_3O_2

$^{\circ}G_{Ti_3O_2} = 3\,{}^{\circ}G^{hcp}_{Ti:Va} + {}^{\circ}G_{O_2(g)} - 1108030.7 + 195.8524T$ This work

αTiO

$^{\circ}G_{\alpha TiO} = {}^{\circ}G_{Ti_1O_1} + 7867.689 + 0.9302\,T$ This work

$^{\circ}G_{Ti_1O_1} = -551056.766 + 327015.164T^{-1} + 252.169378T - 41.994808T\ln T$ [1994Lee]
$- 0.00889792452T^2 + 1.0970448\text{x}10^{-8}T^3$ (298.15-2500 K)

Ti_2O_3

$^{\circ}G_{Ti_2O_3} = -1543640 + 185.96227T - 30.3934128T\ln T - 0.099958898T^2$ [1999Wal]
$- 5.93279345\text{x}10^{-6}T^3 - 117799.056T^{-1}$ (298.15-470 K)
$= -1585377.8 + 937.087T - 147.673862T\ln T - 0.00173711312T^2$
$- 1.53383348\text{x}10^{-10}T^3 + 2395423.68T^{-1}$ (470-2115 K)

Ti_3O_5

$^{\circ}G_{Ti_3O_5} = -2492980 - 73.26557T + 23.9073342T\ln T - 0.420155188T^2$ [1999Wal]
$+ 1.34740141\text{x}10^{-4}T^3$ (298.15-450 K)
$= -2508055.23 + 925.801T - 158.99208T\ln T - 0.0251T^2$
(450-5000 K)

Ti_4O_7

$^{\circ}G_{Ti_4O_7} = -3461530 + 2504.7933\,T - 364.36711\,T\ln T - 8443.569\,T^{0.5}$ This work
$+ 1259760\,T^{-1} + 24091400\,T^{-2}$

Ti_5O_9

$^{\circ}G_{Ti_5O_9} = -4438624 + 2987.3392T - 442.20473T\ln T - 8443.569T^{0.5}$ This work
$+ 2943680T^{-1} - 43065400T^{-2}$

Ti_6O_{11}

$^{\circ}G_{Ti_6O_{11}} = -5415950 + 3470.7726T - 520.04235T\ln T - 8443.569T^{0.5}$ [1999Wal]

$+ 4627600T^{-1} - 110222000T^{-2}$

Ti_7O_{13}

$^{\circ}G_{Ti_7O_{13}} = -6393201 + 3954.5637T - 597.87990TlnT - 8443.569T^{0.5}$ This work

$+ 6311520T^{-1} - 177379000T^{-2}$

Ti_8O_{15}

$^{\circ}G_{Ti_8O_{15}} = -7370430 + 4438.5046T - 675.71759TlnT - 8443.569T^{0.5}$ [1999Wal]

$+ 7995440T^{-1} - 244536000T^{-2}$

Ti_9O_{17}

$^{\circ}G_{Ti_9O_{17}} = -8347430 + 4922.5101T - 753.55521TlnT - 8443.569T^{0.5}$

$+ 9679360T^{-1} - 311693000T^{-2}$ [1999Wal]

$Ti_{10}O_{19}$

$^{\circ}G_{Ti_{10}O_{19}} = -9324330 + 5406.5603T - 831.39283TlnT - 8443.569T^{0.5}$ [1999Wal]

$+ 11363300T^{-1} - 378849000T^{-2}$

$Ti_{20}O_{39}$

$^{\circ}G_{Ti_{20}O_{39}} = -19093800 + 10248.699T - 1609.769TlnT - 8443.569T^{0.5}$ [1999Wal]

$+ 28202500T^{-1} - 1050420000T^{-2}$

$CuTi_2O_z$ $(Cu)_{.333}$ $(Ti)_{.667}$ $(O,Va)_1$

$^{\circ}G^{CuTi_2}_{Cu:Ti:Va} = \frac{1}{3}{}^{o}G^{fcc}_{Cu:Va} + \frac{2}{3}{}^{o}G^{hcp}_{Ti:Va} - 12131 + 4.69T$ This work

$^{\circ}G^{CuTi_2}_{Cu:Ti:O} = \frac{1}{3}{}^{o}G_{CuO} + \frac{2}{3}G^{fcc}_{Ti:O} - 15000$ This work

$^{\circ}L^{CuTi_2}_{Cu:Ti:O,Va} = -130000$ This work

CuO

$^{\circ}G_{CuO} = -171606.97 + 291.50268T - 49.0796TlnT - 0.00344816T^2$ [2003Hal]

$+ 393163.35T^{-1}$ (298.15-6000 K)

Cu_2O

$^{\circ}G_{Cu_2O} = -194216.99 + 344.07921T - 63.5877TlnT - 0.00942505T^2$ [2003Hal]

$+ 289373.5T^{-1}$ (298.15-6000 K)

$(Cu,Ti)O_z$ $(Cu,Ti)_{.5}$ $(Cu,Ti)_{.5}$ $(O,Va)_1$

$^{\circ}G^{CuTi}_{Cu:Cu:Va} = {}^{o}G^{fcc}_{Cu:Va} + 5000$ This work

$^{\circ}G^{CuTi}_{Cu:Cu:O} = {}^{o}G^{fcc}_{Cu:Va} + \frac{1}{2}{}^{\circ}G_{O_2(g)} - 19400 + 31T$ This work

$^{\circ}G^{CuTi}_{Ti:Ti:Va} = {}^{\circ}G^{hcp}_{Ti:Va} + 6000 - .1T$ This work

$^{\circ}G^{CuTi}_{Ti:Ti:O} = \frac{1}{2}G^{fcc}_{Ti:O}$ This work

$^{\circ}G^{CuTi}_{Cu:Ti:Va} = \frac{1}{2}{}^{o}G^{fcc}_{Cu:Va} + \frac{1}{2}{}^{o}G^{hcp}_{Ti:Va} - 11206 + 3.272T$ This work

$^{\circ}G^{CuTi}_{Cu:Ti:O} = \frac{1}{2}{}^{o}G^{fcc}_{Cu:Va} + \frac{1}{4}{}^{o}G_{O_2} + \frac{1}{2}G^{fcc}_{Ti:O} + 15.5T - 9700 + 3.272T$ This work

$^{\circ}G^{CuTi}_{Ti:Cu:Va} = \frac{1}{2}{}^{o}G^{fcc}_{Cu:Va} + \frac{1}{2}{}^{o}G^{hcp}_{Ti:Va} + 11206 - 3.272T + 10000$ This work

$^{\circ}G^{CuTi}_{Ti:Cu:O} = \frac{1}{2}{}^{o}G^{fcc}_{Cu:Va} + \frac{1}{4}{}^{o}G_{O_2} + \frac{1}{2}G^{fcc}_{Ti:O} + 15.5T - 9700 - 3.272T$ This work

$^{\circ}L^{CuTi}_{Cu,Ti:Cu:Va} = +7709.5$ This work

$^{\circ}L^{CuTi}_{Cu,Ti:Ti:Va} = +7709.5$ This work

$^{\circ}L^{CuTi}_{Cu:Cu,Ti:Va} = +7789$ This work

$^{\circ}L^{CuTi}_{Ti:Cu,Ti:Va} = +7789$	This work
$^{\circ}L^{CuTi}_{Cu,Ti:Cu:O} = +7709.5$	This work
$^{\circ}L^{CuTi}_{Cu,Ti:Ti:O} = +7709.5$	This work
$^{\circ}L^{CuTi}_{Cu:Cu,Ti:O} = +7789$	This work
$^{\circ}L^{CuTi}_{Ti:Cu,Ti:O} = +7789$	This work
$^{\circ}L^{CuTi}_{Ti:Cu:O,Va} = -240000$	This work
$^{\circ}L^{CuTi}_{Cu:Ti:O,Va} = -240000$	This work
Cu_2Ti	
$^{\circ}G_{Cu_2Ti} = +2\,^{o}G^{fcc}_{Cu:Va} + {}^{\circ}G^{hcp}_{Ti:Va} - 17628$	[1996Kum]
Cu_3Ti_2	
$^{\circ}G_{Cu_3Ti_2} = +3\,^{o}G^{fcc}_{Cu:Va} + 2\,{}^{\circ}G^{hcp}_{Ti:Va} - 46245 + 10.86T$	[1996Kum]
Cu_4Ti_3	
$^{\circ}G_{Cu_4Ti_3} = +4\,^{o}G^{fcc}_{Cu:Va} + 3\,{}^{\circ}G^{hcp}_{Ti:Va} - 68236 + 15.946T$	[1996Kum]
$CuTi_3$ $(Cu,Ti)_1$ $(Ti)_3$	
$^{\circ}G_{Cu:Ti} = +\,^{o}G^{fcc}_{Cu:Va} + 3\,{}^{\circ}G^{hcp}_{Ti:Va} - 37300 + 14.8T$	[2002Can]
$^{\circ}G_{Ti:Ti} = +4\,{}^{\circ}G^{hcp}_{Ti:Va} + 20000$	[2002Can]
$^{\circ}G_{Cu,Ti:Ti} = -250$	[2002Can]
Cu_4Ti $(Cu,Ti)_4$ $(Cu,Ti)_1$	
$^{\circ}G_{Cu:Cu} = +5\,^{o}G^{fcc}_{Cu:Va} + 25000$	[1996Kum]
$^{\circ}G_{Cu:Ti} = +4\,^{o}G^{fcc}_{Cu:Va} + {}^{\circ}G^{hcp}_{Ti:Va} - 30055 + 11.695T$	[1996Kum]
$^{\circ}G_{Ti:Cu} = +4\,{}^{\circ}G^{hcp}_{Ti:Va} + {}^{o}G^{fcc}_{Cu:Va} + 30055 - 11.695T + 50000$	[1996Kum]
$^{\circ}G_{Ti:Ti} = +5\,{}^{\circ}G^{hcp}_{Ti:Va} + 25000$	[1996Kum]
$^{0}L_{Cu,Ti:Cu} = +17089$	[1996Kum]
$^{0}L_{Cu,Ti:Ti} = +17089$	[1996Kum]
$^{0}L_{Cu:Cu,Ti} = -15767$	[1996Kum]
$^{0}L_{Ti:Cu,Ti} = -15767$	[1996Kum]
$CuZr_2$	
$^{\circ}G_{CuZr_2} = +\,^{o}G^{fcc}_{Cu:Va} + 2\,{}^{\circ}G^{hcp}_{Zr:Va} - 43904.01 + 5.19051T$	[1994Zen]
$CuZr$	
$^{\circ}G_{CuZr} = +\,^{o}G^{fcc}_{Cu:Va} + {}^{\circ}G^{hcp}_{Zr:Va} - 20104.24 - 7.63196T$	[1994Zen]
Cu_8Zr_3	
$^{\circ}G_{Cu_8Zr_3} = +8\,^{o}G^{fcc}_{Cu:Va} + 3\,{}^{\circ}G^{hcp}_{Zr:Va} - 148063.1$	[1994Zen]
Cu_5Zr	
$^{\circ}G_{Cu_5Zr} = +5\,^{o}G^{fcc}_{Cu:Va} + {}^{\circ}G^{hcp}_{Zr:Va} - 61794$	[1994Zen]
$Cu_{51}Zr_{14}$	

$^{\circ}G_{Cu_{51}Zr_{14}} = +51\,^{o}G^{fcc}_{Cu:Va} + 14\,^{\circ}G^{hcp}_{Zr:Va} - 843412.7$ [1994Zen]

$Cu_{10}Zr_7$

$^{\circ}G_{Cu_{10}Zr_7} = +10\,^{o}G^{fcc}_{Cu:Va} + 7\,^{\circ}G^{hcp}_{Zr:Va} - 241750$ [1994Zen]

αPbO (PbO,TiO_2,ZrO_2)

$^{o}G^{\alpha PbO}_{PbO} = -235043 + 250.4T - 46.2TlnT - 0.008T^2 + 225000T^{-1}$ [1998Ris]

(298.5-3000 K)

$^{o}G^{\alpha PbO}_{TiO_2} = {}^{o}G_{TiO_2} + 40000$ This work

$^{o}G^{\alpha PbO}_{ZrO_2} = {}^{o}G^{\alpha ZrO_2}_{ZrO_2} + 40000$ This work

$^{0}L^{\alpha PbO}_{PbO,ZrO_2} = -15000$ This work

$^{0}L^{\alpha PbO}_{PbO,TiO_2} = -60000$ This work

βPbO (PbO, ZrO_2)

$^{o}G^{\beta PbO}_{PbO} = -232910 + 244.7T - 45.9TlnT - 0.0067T^2 + 178000T^{-1}$ [1998Ris]

(298.5-3000 K)

$^{o}G^{\beta PbO}_{ZrO_2} = {}^{o}G^{\alpha ZrO_2}_{ZrO_2} + 40000$ This work

$^{o}L^{\beta PbO}_{PbO,ZrO_2} = -15000$ This work

αZrO_2 (ZrO_2, TiO_2)

$^{o}G^{\alpha ZrO_2}_{ZrO_2} = -1126163.54 + 424.890806T - 69.3875137TlnT$ [2006Wan]

$- 3.75880141\text{x}10^{-3}T^2 + 6.83\text{x}10^{5}T^{-1}$ (298.5-6000 K)

$^{o}G^{\alpha ZrO_2}_{TiO_2} = {}^{o}G_{TiO_2} + 7330$ This work

$^{0}L^{\alpha ZrO_2}_{ZrO_2,TiO_2} = 30245 - 4.1\,T$ This work

βZrO_2 (ZrO_2, TiO_2)

$^{o}G^{\beta ZrO_2}_{ZrO_2} = +5468 - 4T + {}^{o}G^{\alpha ZrO_2}_{ZrO_2}$ [2006Wan]

$^{o}G^{\beta ZrO_2}_{TiO_2} = {}^{o}G_{TiO_2} + 35000$ This work

$^{0}L^{\beta ZrO_2}_{ZrO_2,TiO_2} = -16868.73 - 6.26\,T$ This work

$^{1}L^{\beta ZrO_2}_{ZrO_2,TiO_2} = -4439.5 - 11.75\,T$ This work

γZrO_2 (Zr^{2+}, Zr^{4+}, Ti^{4+})$_1$(O^{2-},Va)$_2$

$^{o}G^{\gamma ZrO_2}_{Zr^{4+}:O^{2-}} = +10336 - 4T + {}^{o}G^{\beta ZrO_2}_{ZrO_2}$ [2006Wan]

$^{o}G^{\gamma ZrO_2}_{Zr^{4+}:Va} = {}^{\circ}G^{\gamma ZrO_2}_{ZrO_2} - {}^{\circ}G_{O_2(g)}$ [2006Wan]

$^{o}G^{\gamma ZrO_2}_{Zr^{2+}:O^{2-}} = {}^{o}G_{Zr(hcp)} + {}^{o}G_{O_2} + 11.526T - 381101.15 + 41.945T$ [2006Wan]

$^{o}G^{\gamma ZrO_2}_{Zr^{2+}:Va} = {}^{o}G_{Zr(hcp)} + 11.526T - 381101.15 + 41.945T$ [2006Wan]

$^{o}G^{\gamma ZrO_2}_{Ti^{4+}:O^{2-}} = {}^{o}G_{TiO_2} + 35000$ This work

$^{o}G^{\gamma ZrO_2}_{Zr^{4+}:O^{2-}} = {}^{\circ}G^{\gamma ZrO_2}_{ZrO_2} - {}^{\circ}G_{O_2(g)}$ This work

${}^{o}L^{\gamma ZrO_2}_{Zr^{2+},Zr^{4+}:*} = -226569.67 + 72.5T$	[2006Wan]
${}^{1}L^{\gamma ZrO_2}_{Zr^{2+},Zr^{4+}:*} = -120617.314 + 20T$	[2006Wan]
${}^{0}L^{\gamma ZrO_2}_{Zr^{4+},Ti^{4+}:O^{2-}} = 5740 - 6.26\,T$	This work
βZrTiO$_4$ (TiO$_2$, ZrO$_2$)	
${}^{o}G^{\beta TiZrO_4}_{TiO_2} = {}^{o}G_{TiO_2} + 6000$	This work
${}^{o}G^{\beta TiZrO_4}_{ZrO_2} = {}^{o}G^{\beta ZrO_2}_{ZrO_2} + 6000$	This work
${}^{0}L^{\beta TiZrO_4}_{TiO_2,ZrO_2} = 7707.8 - 1.95\,T$	This work
βPbZr$_x$Ti$_{1-x}$O$_3$ (PbTiO$_3$, PbZrO$_3$)	
${}^{o}G^{\beta PbZr_xTi_{1-x}O_3}_{PbTiO_3} = -1239466.5 + 743.544T - 127.086T\ln T + 609829.18T^{-1}$ (298.15-3000 K)	This work
${}^{o}G^{\beta PbZr_xTi_{1-x}O_3}_{PbZrO_3} = {}^{o}G^{\beta ZrO_2}_{ZrO_2} + {}^{o}G^{\beta PbO}_{PbO} - 10.71\,T$	This work
${}^{o}L^{\beta PbZr_xTi_{1-x}O_3}_{PbTiO_3,PbZrO_3} = 8.037\,T$	This work
Cu$_2$PbO$_2$	
$G_{Cu_2PbO_2} = {}^{o}G_{Cu_2O} + {}^{o}G_{\beta PbO} - 25400 + 26.24\,T$	This work
Cu$_2$Ti$_4$O	
${}^{o}G_{Cu_2Ti_4O} = 2{}^{o}G_{Cu(fcc)} + 4{}^{o}G_{Ti(hcp)} + \frac{1}{2}{}^{o}G_{O_2} - 496592$	This work
Cu$_3$Ti$_3$O	
${}^{o}G_{Cu_3Ti_3O} = 3{}^{o}G_{Cu(fcc)} + 3{}^{o}G_{Ti(hcp)} + \frac{1}{2}{}^{o}G_{O_2} - 490460$	This work
Cu$_3$TiO$_4$	
${}^{o}G_{Cu_3TiO_4} = {}^{o}G_{CuO} + {}^{o}G_{TiO_2} + {}^{o}G_{Cu_2O} + 18814.75 - 15.63T$	This work
α′PbTiO$_3$	
${}^{o}G^{\alpha' PbTiO_3}_{PbTiO_3} = -1241000 + 745.856T - 127.086T\ln T + 609829.18T^{-1}$ (298.15-3000 K)	This work
αZrTiO$_4$	
${}^{o}G^{\alpha ZrTiO_4}_{ZrO_2:TiO_2} = {}^{o}G_{TiO_2} + {}^{o}G^{\beta ZrO_2}_{ZrO_2} + 3200 - 3.63\,T$	This work
ZrTi$_2$O$_6$	
${}^{o}G^{TiZr_2O_6}_{ZrO_2:TiO_2} = 2\,{}^{o}G_{TiO_2} + {}^{o}G^{\alpha ZrO_2}_{ZrO_2} - 12100 + 7.9T$	This work

Table 2. Summary of the thermodynamic parameters describing the Cu–Pb–O system referred to stable element reference H^{SER} (two-sublattice model is adopted for the liquid).

Parameter	**Reference**
Liquid $(Cu^{1+},Cu^{2+},Pb^{2+})_p(O^{2-},Va^{q-})_q$	
${}^oG^{liq}_{Cu1}$, ${}^oG^{liq}_{Pb}$	[2001SGTE]
${}^oG^{liq}_{Cu2}$, ${}^oG^{liq}_{Cu_2O}$, ${}^oG^{liq}_{CuO}$	[2003Hal]
${}^oG^{liq}_{PbO}$	[1998Ris]
${}^0L^{liq}_{Cu^{1+}:O^{2-},Va^{q-}}$, ${}^1L^{liq}_{Cu^{1+}:O^{2-},Va^{q-}}$, ${}^2L^{liq}_{Cu^{1+}:O^{2-},Va^{q-}}$, ${}^0L^{liq}_{Cu^{1+},Cu^{2+}:O^{2-}}$	[2003Hal]
${}^0L^{liq}_{Cu^{1+},Pb^{2+}:Va^{q-}}$, ${}^1L^{liq}_{Cu^{1+},Pb^{2+}:Va^{q-}}$, ${}^2L^{liq}_{Cu^{1+},Pb^{2+}:Va^{q-}}$, ${}^3L^{liq}_{Cu^{1+},Pb^{2+}:Va^{q-}}$	[1986Hay]
${}^0L^{liq}_{Pb^{2+}:O^{2-},Va^{q-}} = +\,240630 - 39.306\,T$	This work
${}^1L^{liq}_{Pb^{2+}:O^{2-},Va^{q-}} = +\,2206.5$	This work
${}^2L^{liq}_{Pb^{2+}:O^{2-},Va^{q-}} = -\,102024$	This work
${}^0L^{liq}_{Cu^{1+},Pb^{2+}:O^{2-}} = -\,79213 + 73.8047\,T$	This work
${}^1L^{liq}_{Cu^{1+},Pb^{2+}:O^{2-}} = -\,10793 - 8.8059\,T$	This work
${}^0L^{liq}_{Cu^{2+},Pb^{2+}:O^{2-}} = -\,45240$	This work
${}^0L^{liq}_{Cu^{1+},Pb^{2+}:O^{2-},Va^{q-}} = +\,862504 - 84.8794\,T$	This work
${}^1L^{liq}_{Cu^{1+},Pb^{2+}:O^{2-},Va^{q-}} = -\,349389$	This work
${}^2L^{liq}_{Cu^{1+},Pb^{2+}:O^{2-},Va^{q-}} = +\,46115$	This work
${}^3L^{liq}_{Cu^{1+},Pb^{2+}:O^{2-},Va^{q-}} = -\,1102751$	This work
${}^4L^{liq}_{Cu^{1+},Pb^{2+}:O^{2-},Va^{q-}} = -\,26660$	This work

REFERENCES

[1926Fer] Ferrari, A., *Gazzetta Chimica Italiana*, 56 (1926) 630.

[1930Wag] Wagner, C., Schottky, W., *Z. Phys. Chem*., B11 (1930) 163.

[1937Bue] Buessem, W., Schusterius, C., Ungewiss, A., *Ber. Dtsch. Keram. Ges*., 18(10) (1937) 433.

[1939Lav] Laves, F., Wallbaum, J., *Naturwiss*., 27 (1939) 64.

[1945Tem] Temkin, M., *Acta Physicochimica USSR*, 20 (1945) 411.

[1948Red] Redlich, O., Kister, A.T., *Ind. Eng. Chem*. 40(2) (1948) 345.

[1948Rau] Raub, E., Engel, M., *Z. Metallkd.*, 39 (1948) 172.

[1950Jaf] Jaffee, R.I., Ogden, H.R., Maykuth D.J., *Trans. Metall. AIME*, 188 (1950) 1261.

[1951Jen] Jenkins, A.E., Worner, H.W., *J. Ins. Met*., 80 (1951) 157.

[1951Kar] Karlsson, N., *J. Inst. Metals*, 79 (1951) 391.

[1951Sow] Sowan, H.G., Andrews, A.I., *J. Amer. Ceram. Soc.*, 34(10) (1951) 298.

[1951Saw] Sawaguchi, E.; Maniwa, H.; Hoshino, S., *Phys. Rev.*, 83 (1951)1078.

[1952Zas] Zaslavskii, A.I., Tolkachev, S.S., *Zhurnal Fizicheskoi Khimii* 26 (1952) 743.

[1952Ros] Rostoker, W., *Trans. AIME*, 194 (1952) 209.

[1952Jou] Joukainen, A., Grant, N.J., Floe, C.F., *Trans. AIME*, 194 (1952) 766.

[1953Bum] Bumps, E.S., Kessler, H.D. and Hansen, M., *Trans. ASM*, 45 (1953) 1008.

[1953Lun] Lundin, C.E., McPherson, D.J., Hansen, M., *Trans. AIME*, 197(1953) 273.

[1953Saw] Sawagushi, E., *J. Phys. Soc. Jpn.*, 8 (1953) 615.

[1954Was] Wasilewski, R.J., Kehl, G.L., *J. Inst. Met*., 83 (1954) 94.

[1954Geb] Gebhardt, E., Obrowski W., *Z. Metallkd*. 45 (1954) 332.

[1954Hof] Hofmann, W., Kohlmeyer, J., *Z. Metallkd*. 45 (1954) 339.

[1954Bro] Brown, F.H., Duwez, P., *J. Amer. Ceram. Soc.*, 37(3)(1954) 129.

[1954Cou] Coughanour, L. W., Roth, R.S., DeProsse, V.A., *J. Res. Natl. Bur. Stand.*, 52(1) (1954) 2470.

[1955Sch] Schofield, T. H., Bacon, A.E., *J. Inst. Met*., 84 (1955) 47.

[1955Chr] Christ, C.L., Clark, J.R., *Amer. Mineral*., 40 (1955) 907.

[1956Kuy] Kuylenstierna, U., Magneli, A., *Acta Chem. Scand.*, 10(7) (1956) 1195.

[1956Nis] Nishimura, H., Kimura, H., *J. Jpn. Inst. Met*., 20 (1956) 524.

[1957And] Andersson, S., Collen, B., Kruse, G., Kuylenstierna, U., Magneli, A., *Acta Chem. Scand*., 11 (1957) 1653.

[1957Kon] Koncz, I., Koncz-Deri, M., *Period. Polytech.*, 1 (1957) 67.

[1958Han] Hansen, M., Anderko, K., Constitution of Binary Alloys, McGraw-Hill, NY, (1958) 642.

[1958Bel] Beals, M.D., Lair, R.B., Lindenthal, J.W., Titan G.m.b.H., German Patent 1,031,081 May 29, 1958; Chem. Abstr. 55, 3030a, 1961.

[1959Vol] Volf, E., Tolkachev, S.S. and Kozhina, I.I., Vestn. Leningrad Univ., 10, Ser.Fiz. Khem., 2 (1959) 87.

[1959And] Anderson, S., *Acta Chem. Scand.*, 13 (1959) 415.

[1959Spr] Spreadborough, J., Christian, J.W., *Proceed. Phys. Soc.*, London 74 (1959) 609.

[1959Bra] Bradhurst, D.H., Buchana, A.S., *Austral. J. Chem.*, 12 (1959) 523.

[1960Bra] Brauer, G., Littke, W., *J. Inorg. Nucl. Chem.*, 16 (1960) 67.

[1960Mak] Makarov, E.S., Kuzneov, L.M., *Zh. Strukt.. Khem.*, 1(2) (1960) 170.

[1960Ari] Ariya, S.M., Bogdanova, N.I., *Soviet Physics-Solid State*, 1 (7) (1960) 936.

[1960And] Anderson, S., *Acta Chem. Scand.*, 14 (1960) 1161.

[1960Saa] Saarivirta, M.J., *Trans. Metall. Soc. AIME*, 218 (1960) 431.

[1960Lic] Lichter, B.D., *Trans. Met.Soc. AIME*, 218 (1960) 1015.

[1962Kof] Kofstad, P., *J. Phys. Chem. Solids*, 23 (1962) 1579.

[1962Nev] Nevitt, M., *Trans. Metall. Soc. AIME*, 224 (1962) 195.

[1962Rob] Robinson, A.E., Joyce, T.A., *Trans. J. Brit. Ceram. Soc.*, 61(2)(1962) 85.

[1962Ike] Ikeda, T., Oakno, T., Watanabe, M., *Jpn. J. Appl. Phys.*, 1 (1962) 218.

[1963Kor] Kornilov, I.I., Glazova, V.V., *Dokl. Akad. Nauk SSSR*, 150(2) (1963) 313.

[1963Blu] Blumenthal, R.N., Whitmore, D.H., *J. Electrochem. Soc.*, 110(1) (1963) 92.

[1963And] Anderson, S., Jahnberg, L., *Arkiv. Kem.*, 21 (1963) 413-426.

[1963Mue] Mueller, M.H., Knott, H.W., *Trans. Metall. Soc. AIME*, 227 (1963) 674.

[1963Mat] Matsko, Y., Sasaki, H., *J. Amer. Ceram. Soc.*, 46(8) (1963) 409.

[1964Kau] Kaufman, L., Clougherty, E.V., AIME Metall. Soc. Conf., Metallurgy at High Pressures and High Temperatures, Vol. 22, Gordon and Breach Science Publishers Inc., New York, 1964, 322.

[1964For] Forland, K.S., *Acta Chem. Scand.*, 18 (1964) 1267.

[1964Alc] Alcock, C.B., Belford, T.N., *Trans. Faraday Soc.*, 60 (1964) 822.

[1964Sch] Schubert, K., Meissner, H.G., Rossteutscher, W., *Naturwissensch.*, 51 (1964) 507.

[1965Mos] Moser, J.B., Blumenthal, R.N., Whitmore, D.H., *J. Am. Ceram. Soc.*, 48 (1965) 384.

[1965Por] Porter, V.R., Ph. D. Thesis, Pennsylvania State University, (1965).

[1965Fay] Fayek, M.K., Leciejewich, J., *Z. Anorg. Allgem. Chem*., 336 (1965) 104.

[1965Ell] Elliot, R.P., Constitution of Binary Alloys, First Supplement, McGraw-Hill, NY, (1965) 387.

[1965Coc] Cocco, A., Torriano, G., *Ann. Chim.*, 55(3) (1965) 153.

[1965Web] Webster, A.H., McDonald, R.C., Browman, W.S., *J. Can. Ceram. Soc.*, 34 (1965) 97.

[1966Wah] Wahlback, P.G., Gilles, P.W., *J. Am. Ceram. Soc*., 49(4) (1966) 180.

[1966Gad1] Gadalla, A.M.M., White, *J., Trans., Brit. Ceram. Soc*., 65(3) (1966) 157.

[1966Gad2] Gadalla, A.M.M., White, *J., Trans., Brit. Ceram. Soc*., 65(7) (1966) 383.

[1967Alc] Alcock, C.B., Zador, S., Steele, B.C.H., *Proc. Br. Ceram. Soc*., 8 (1967) 231.

[1967Wat] Watanabe, D., Castles, J.R., *Acta Crystallogr*., 23 (1967) 307.

[1967Gad] Gadalla, A.M.M., *Sci. Ceram*. 3 (1967) 179.

[1967Ger] Gerlach, J., Kleibeler, H.J., Pawlek, F., *Metallwiss. Techn.*, 11 (1967) 1115.

[1967Kat] Kato, M., Kubo, T., *Kogyo Kagaku Zasshi*, 70 (1967) 844.

[1967Nog] Nogushi, T., Mizuno, M., *Sol. Energ.*, 11(1) (1967) 56.

[1967Fus] Fushimi, S., Ikeda, T., *J. Amer. Ceram. Soc.*, 50(3) (1967) 129.

[1967Har] Harris, N.H., Ph. D. Thesis, University of Illinois, 1967; cited in Jacob, K.T., Shim, W.W., *J. Am. Ceram. Soc.*, 64(1981) 573.

[1967New] Newnham, R.E., *J. Amer. Ceram. Soc.*, 50(1967) 216.

[1968Paw] Pawar, R.R., Deshpande, V.T., *Acta Cryst. A*, 24 (1968) 316.

[1968Pfe] Pfeifer, H.U., Bhan, , S., Schubert, K., J. *Less-Common Met*., 14 (1968) 291.

[1968Nog] Nogushi, T., Mizuno, M., *Bull. Chem. Soc. Jpn.*, 41(12)(1968) 2895.

[1968Ayk] Ayakan, J., *J. Amer. Ceram. Soc.*, 51(10) (1968) 577.

[1969Shu] Shunk, F.A., Constitution of Binary Alloys, Second Supplement, McGraw-Hill, NY, (1969) 297.

[1969Win] Winchell, E.R., Wenden, E.H., *Miner. Mag*., 36 (1969) 933.

[1969Hae] Haerdtl, K.H., Rau, H., *Mater. Res. Bull*., 3 (1968) 41.

[1970Jos] Jostsons A., McDougall P., Proc. Int. Conf. Sci. Technol. Appl. Titanium, Jeffe R.I. and Promisel N.E., Ed., London (1968), 745.

[1970Hil] Hillert, M., Staffansson, L.-I., *Act Chem. Scand*., 24 (1970) 3618.

[1970Kau] Kaufman, L., Bernstein, H., Computer Calculation of Phase Diagram, Academic Press, NY, (1970).

[1970Bou] Bouvaist, J., Weigel, D., *Acta Cryst. A*, 26 (1970) 501.

[1970Bel] Belyaev, I.N., *Russ. J. Inorg. Chem*., 15(1) (1970) 148.

[1971Jac] Jacob, T., Jeffes, J.H.E., *Trans. Inst. Mining Met*., C80 (1971) 32.

[1971Moo] Moon, R.L., Fulrath, R.M., *J. Amer. Ceram. Soc*., 54(2) (1971) 124.

[1971Ras] Rase, D.E., cited in Jaffe, B., Cook, W.R., Jaffe, H., Piezoelectric Ceramics, Academic Press, London-New-York, (1971) 117.

[1971Jaf] Jaffe, B., Cook, W.R., Jaffe, H.,Piezoelectric Ceramics, Academic Press, London-New-York, (1971) 135.

[1972Suz] Suzuki, K. , Sambogi, K., *Tetsu to Hagane*, 58 (1972) 1579.

[1972Roy] Roy, R., White, W.B., *J. Cryst. Growth*, 13/14 (1972) 78.

[1972Ono] Ono, A., *Mineral J.*, 6(6) (1972) 433.

[1973Mer] Merritt, R.R., Hyde, B.G., Bursill, L.A., Philp, D.K., *Phil. Trans. R. Soc.* A, 274 (1973) 628.

[1973Sly] Slyusar, N.P., Krivorotenko, A.D., Fomichev, E.N., Kalashnik, A.A., Bondarenko, V.P., *High Temp*., 11(1) (1973) 190.

[1973Hul] Hultgren, R., Desai, P.D., Hawkins, D.T., Gleiser, M., Kelly, K.K., Selected Values of the Thermodynamic Properties of Binary Alloys, ASM, Metal Park, OH, (1973) 117.

[1973Hol] Holman, R., Fulrath, R.M., *J. Appl. Phys.*, 44 (1973) 5227.

[1973Meh] Mehrota, M.G., Frohberg, M.G., Mathew, P.M., Kapoor M.L., *Scripta Metall.*, **7** (1973) 1047.

[1974Pre] Predel, B. and Oehme, G., *Z. Metallkde*., 65(8) (1974) 525.

[1974Pic] Pichugin, B.A., Linchevskiy, B.V., Chursin, V.M., *Izv. Akad. Nauk SSSR*, Metall. 3 (1974) 87.

[1974Hay] Hayashi, K., Mizutani, N., Kato, M., *Nippon Kagaku Kaishi*, 1 (1974) 6.

[1974Kux] Kuxmann, U., Fischer, P., *Erzmetall*., 27 (1974) 181.

[1974Kat] Kato, K., Kawada, I., Muramatsu, K., *Acta Cryst. B*, 30 (1974) 1634.

[1975Mug] Muggiano, Y.M., Gambino, M., Bros, J.P., *J. Chim. Phys*., 72(1) (1975) 83.

[1975Pic] Picard, C., Gardanian, P., *J. Solid State Chem*., 14 (1975) 66.

[1975Jan] Janke, D., Fischer, W.A., *Metall.*,29 (1975) 1189.

[1975Bse] Bsenko, L., *J. Less-Common Mater*., 40 (1975) 365.

[1975Gab] Gabathuler, P., White, P., Parthe, E., *Acta Crystallogr. B*, 31 (1975) 608.

[1976Bse] Bsenko, L., *Acta Cryst. B*, 32 (1976) 2220.

[1976Bou] Boureau, G., Gerdanian, P., *Acta Metall*., 24 (1976) 717.

[1976Cha] Charle, H., Osterwald, J., *Z. Phys. Chem. Neue Folge*, 99 (1976) 199.

[1977Mcl] McLellan, R.B., *Acta metall*., 25(11) (1977) 1241.

[1977Ise] Isecke, B., PhD Thesis, Berlin University of Technology (1977).

[1977Ran] Range, K.-J., Ketterl, F., *Z. Naturforsch.-Teil B*, 32 (1977) 1356.

[1978Gla] Glazer, A.M., Mabud, S.A., *Acta Cryst. B*, 34 (1978) 1065.

[1978Tet] Tetot, R., Picard, C., Boureau, G., Gerdanian, P., *J. Chem. Phys*., 69(1) (1978) 326.

[1978Kau] Kaufman, L., *Calphad*, 2 (1978) 117.

[1978Kuz] Kuznetsov, G.M., Fedorov, V.N., Rodnyanskaya, A.L., Nikonova, *Sov. Non-Ferrous Met. Res.*, 6 (1978) 91.

[1979Sha] Sharma R.C. and Chang Y.A., *Met. Trans. B*, (10B) (1979) 103.

[1979Dir] Dirstine, R.T., Rosa, C.J., *Z. Metallkde*, 70 (1979) 322.

[1979Tas1] Taskinen, A., *J. Chem. Thermodyn*. 8 (1979) 185.

[1979Tas2] Taskinen, A., Taskinen, P., *Z. Metallkd*. 70 (1979) 594.

[1979Fis] Fischer K., *Cryst. Res. Technol*., 14 (1979) 835.

[1979Sch] Schmahl, N.G., Schwitzgebel, G. Kling, H., Speck, E., *Mat. Res. Bull.*, 14 (1979) 1213.

[1979Ots] Otsuka, S., Kozuka, Z., *Metall. Trans.*, 10B (1979) 565, Corrections in *Metall. Trans*., 11B (1980) 319.

[1980Hei] Heideman, S.A., Reed, T.B., Gilles, P.W., *High Temp. Sci*., 13 (1980) 79.

[1980Tas] Taskinen, A., Holopainen, H., *Z. Metallkd*., 71 (1980) 729.

[1980Hen] Hennings, D., *J. Solid State Chem*., 31 (1980) 275.

[1980Car] Carvalho, E.M., Harris, I.R., *J. Master. Sci*., 15 (1980) 1224.

[1980For] Forey, P., Glimois, J.-L., Feron, J.L., Develoey, G., Becle, C., Comptes Rendus Hebdomadaires des Seances de I'Academie des Sciences, Serie C, Sciences Chimiques, 291 (1980) 177.

[1980She] Shevchenko, A.V., Lopato, L.M., Maister, I.M., Gorbunov, O.S., *Zh. Neorg. Khim.*, 25(9)(1980) 2496-2499; *Russ. J. Inorg. Chem*., 25(9) (1980) 1379.

[1980Eis] Eisa, M.A., Abadir, M.F., Gaddala, A.M, *Tran. J. Brit. Ceram. Soc*., 79 (1980) 100.

[1981Sun] Sundman, B., Agren, J., *J. Phys. Chem. Solids*, 42 (1981) 297.

[1981Har] Harada, H., Sasa, Y., Uda, M., *J. Appl. Crystall*., 14 (1981) 141.

[1981Ots] Otsuka, S., Kozuka, Z., *Metall. Trans*., 12B (1981) 616.

[1981Jac] Jacob, K.T., Shim, W.W., *J. Am. Ceram. Soc.*, 64 (1981) 573.

[1982Som] Sommer F., *Z. Metallkde*., 73(2) (1982) 72.

[1982Pej] Pejrid, L., Rosen, E., *High Temp.-High Press.*, 14 (1982) 599.

[1982Bat] Batalin, G.I., Kuzmenko, N.I., *Russ. J. Phys. Chem*., 56(10) (1982) 1586.

[1982Kle] Kleppa, O., Watanabe, S., *Met. Trans. B,* 13B (1982) 391.

[1982Shi] Shim, W.W., Jacob, K.T., *Can. Metall. Quarterly*., 21(2) (1982) 171.

[1982Leo] Leontev, N.G., Smotrakpv, V.G., Fesenko, E.G., *Izv. Akad. Nauk SSSR, Neorg. Mater*., 18(3) (1982) 449-453; *Inorg. Mater.(Engl. Transl.),* 18(3)(1982) 347.

[1982Gon] Gonschorek, W., *Z.f. Kristall.*, 160 (1982) 187.

[1982Tan] Tanaka, M., Saito, R., Tsuzuki, K., *J. Phys. Soc. Jpn.*, 51 (1982) 2635.

[1983Sch] Schmid, R., *Metall. Trans*., B 14 (1983) 475.

[1983Zad] Zador, S., Alcock, C.B., *High Temp. Sci*., 16 (1983) 187.

[1983Tet] Tetot, R., Picard, C., Gerdanian, P., *J. Phys. Chem. Solids*, 44(11) (1983) 1059.

[1983Mur] Murray, J.L., *Bull. Alloy Phase Diagrams*, 4 (1983) 81.

[1983Sud] Sudavtsova, S.V., Batalin, G.I., Kolnykov, A.V., Kuznetsov, F., *Sov. Non-Ferrous Met. Res.*, 11 (1983) 492.

[1983Dub] Dubler, E., Vedani, A., Oswald, H.R., *Acta Cryst*., C39 (1983) 1143.

[1983Mch] McHale, A.E., Roth, R.S., *J. Amer. Ceram. Soc.*, 66(2) (1983) C18.

[1984Lel] Lele S., Sastry G.V.S. and Ramanchandrarao P., *Z. Metallkde*., 75(6) (1984) 446.

[1984Ani] Anik, S., Frohberg, M.G., *Z. Metallkd*., 75 (1984) 586.

[1985Bjo] Bjorkman, B., *Calphad*, 9 (1985) 271.

[1984Lou] Lou, M.Y.-W., Grant, N.J., *Metall. Trans. A*, 15 (1984) 1491.

[1985Sau] Saunders, N., *Calphad*, 9 (1985) 297.

[1985Mar] Marucco, J.F., Poumellec B., Gautron, J., Lemasson, P., *J. Phys. Chem. Solids*, 46 (1985) 709.

[1985Gli] Glimois, J.L., Forey, P., Feron, J.L., *J. Less-Common Met*., 113 (1985) 213.

[1985Boh] Boher, P., Garnier, P., Gavarri, J.R., Hewat, A.W., *J. Solid State Chem*., 57 (1985) 343.

[1985Hil1] Hillert, M., Jansson, B., Sundman, B., Agren, J., *Met. Trans. A*, 16A, (1985) 261.

[1985Hil2] Hill, R.J., *Acta Cryst. C*, 41 (1985) 1281.

[1985Ujm] Ujma, Z.; Handerek, J.; Pisarski, M., *Ferroelectrics*, 64 (1985) 237.

[1986Dur] Duran, P., Moure, C., Mater. Chem. Phys., 15 (1986) 193.

[1986Abr] Abriata, J.P., Garces, J., Versaci, R., *Bull. Alloy Phase Diagrams*, 7 (1986) 116.

[1986Nie] Niemela, J., Calphad, 10 (1986) 77.

[1986Hay] Hayes, H., Lukas, H.L., Effenberg, G., Petzow, G., *Z. Metallkd*., 77 (1986) 749.

[1986Mas] Massalski, T., Murray, J.L., Bennett, L.H., Baker, H., Binary Alloys Phase Diagrams, vol. 1, American Society for Metals, Metals Park OH, 982 (1986).

[1986Kne] Kneller, E., Khan, Y., Gorres, U., *Z. Metallkd*., 77 (1986) 43.

[1986Mch] McHale, A.E., Roth, R.S., *J. Amer. Ceram. Soc.*, 69(11) (1986) 827.

[1986Fes] Fesenko, E.G., Eremkin, V.V., Smotrakov, V.G., *Fiz. Tverd. Tela*, 28(1) (1986) 324; *Sov. Phys.-Solid State (Engl.Transl.)*, 28(1) (1986) 181.

[1986Bor] Bordet, P., McHale, A., Santoro, A., Roth, R.S., *J. Solid. State Chem.*, 64 (1986) 30.

[1986Ban] Bannister, M.J., *J. Amer. Ceram. Soc.*, 69(11) (1986) C269.

[1987Mur] Murray J.L. and Wriedt H.A., *Bull. Alloy Phase Diag*., 8(2) (1987) 148.

[1987Gra] Granier, B., Chatillon, C., Allibert, M., *High Temp. Sci*., 23 (1987) 115.

[1988Bor] Bormann, R., Gartner, F., Haider, F., *Mar. Sci. Eng*., 97 (1988) 79.

[1988Wri] Wriedt, H.A., *Bull Alloy Phase Diagrams*, 9 (1988) 106.

[1988Jir] Jirak, Z., Kala, T., *Ferroelectrics*, 82 (1988) 79.

[1989Yok] Yokokawa, H., Kawada, T., Dokiya, M., *J. Am. Ceram. Soc*., 72(11) (1989) 2104.

[1989Som] Sommer, F., Choi, D.K., *Z. Metallkd*., 80 (1989) 263.

[1989Cha] Chang, A.Y., Hsieh, K.C., Phase Diagram of Ternary Copper-Oxygen-Metal Systems, ASM International, Metals Park, Ohio, (1989).

[1989Bar] Barin, I., Thermochemical Data of Pure Substances, VCH, Weinheim (1989).

[1989Ere] Eremkin, V.V., Smotrakov, V.G., Fesenko, E.G., *Fiz. Tverd. Tela*, 31(6) (1989) 156; *Sov. Phys.-Solid State (Engl.Transl.)*, 31(6) (1989) 1002.

[1990Zhi] Zhilum, G., Longtu, L., Hongqung, L., Xiaowen, Z., *Ferroelectrics*, 101 (1990) 93.

[1990Som] Sommer F., *J. Non-Crys. Solids*., 117 (1990) 505.

[1990Ari] Arias, D., Abriata, J.P., *Bull. Alloy Phase Diagrams*, 11 (5) (1990) 452.

[1990Kit] Kitaguchi, H., Takada, J., Oda, K., Miura, Y., *J. Mater. Res.*, 5 (1990) 1397.

[1991Zen] Zeng, K., Jin, Z., Huang, P., (Editor: B. Wu), C-MRS Int. Symp. Proc., Elsevier, Amsterdam, 5 (1991) 851.

[1991Tep] Teppo, O., Niemela, J., Taskinen, P., *Thermochim. Acta*, 185 (1991) 155.

[1991Luo] Luoma, R., Talja, J., Report TKK-V-B61, Helsinki University of Technology, Helsinki, Finland (1991).

[1991Par] Parbhakar, S.R., Aggarwal, D.R., Mathur, N.S.V., Kapoor, L.M., *Mat. Trans. JIM*, 32 (1991) 352.

[1992Gui] Gui, Z., Hu, H., Li, L., Zhang, X., *Solid State Phenom*., 25/26 (1992) 309.

[1992Sau] Saunders, N. and Chandrasekaran, L., J. Phase Equlibria, 13(6) (1992) 612.

[1992Paj] Pajunen, M., Kivilahti, J., *Z. Metallkd*., 83(1) (1992) 17.

[1992Bou] Boudene, A., Hack, K., Mohammad, A., Neuschütz, D., Zimmermann, E., *Z. Metallkd*. 83 (1992) 663.

[1992Yok] Yokokawa, H., Sakai, N., Kawada, T., Dokiya, M., Int.Conf. Sci. Technol. Zirconia V, Melbourne, Australia, August 16-21, 1992, 59-68. Edited by Badwal S.P.S., Bannister, M., Hannink, R.H.J., Technomic Publishing, Lancaster, Pennsylvania, 1993

[1992Chr] Christofferson, R., Davies, P.K., *J. Amer. Ceram. Soc*., 75 (3) (1992) 563.

[1993Moo] Moon, J.H., Jang, H.M., *J. Am. Ceram. Soc*., 76 (1993) 549.

[1993Eri] Eriksson G. and Pelton A.D., *Metall. Trans. B*, 24B (1993) 795.

[1993Oat] Oates, W.A., Wenzl, H., *Calphad*, 17(1) (1993) 35.

[1993Kel] Kelkar, G.P., Carim, A.H., *J. Am. Ceram. Soc*., 76(7) (1993) 1815.

[1993Gos] Gospodinov G.G.; Marchev V.M., *Thermochim. Acta*, 222 (1993) 137.

[1994Lee] Lee, B.J., *J. Korean Inst. Met. Mater*., 32(7) (1994) 869.

[1994Hal] Hallstedt, B., Risold, D., Gauckler, L., *J. Phase Equil.*, 15 (1994) 483.

[1994Kel] Kelkar, G.P., Spear, K.E., Carim, A.H., *J. Mater. Res*., 9(9) (1994) 2244.

[1994Oka] Okamoto, H., *J. Phase Equili.*, 15 (1994) 566.

[1994Mur] Murray, J.L., (Editors: Subramanian, P.R., Chakrabarti, D.J., Laughlin, D.E.), Phase Diagrams of Binary Copper Alloys, ASM, Metal Park, OH, (1994), 447.

[1994Zen] Zeng, K.-J., Hamalainen, M., Lukas, H.L., *J. Phase Equil.*, 15 (6) (1994) 577.

[1994Szi] Szillat, H, Teske, C.L., *Z. Anorg. Allgem. Chem.*, 620 (1994) 1307.

[1994Soh] Soh, J.R., Lee H.M., Kwon H.S., *Calphad*, 18(3) (1999) 2005.

[1995Vie] Viehland, D., *Phys.Rev. B-Condens. Matter*, 52(2) (1995) 778.

[1996Oat] Oates, W.A., Wenzl, H., Mohri, T., *Calphad*, 20(1) (1996) 37.

[1996Kum] Hari Kumar, K.C., Ansara, I., Wollants, P., Delaey, L., *Z. Metallkd.*, 87 (1996) 666.

[1996Par] Park, Y., Kim, Y., *Mat. Res. Bullet.*, 31(1) (1996) 7.

[1996Ono] Onodera, A., Kawamura, Y., Tamaki, N., Fujishita H., Roleder, K., Dec, J.,

Molak, A., *J. Korean Phys. Soc.* (Proc. Suppl.), 29 (1996) S691.

[1997Bar] Bartkowski, S., Neumann, M., Kurmaev, E.Z., Fedorenko, V.V., Shamin, S.N., Cherkashenko, V.M., Nemnonov, S.N., Winiarski, A., Rubie, D.C., *Phys. Rev. B - Condensed Matter*, 56 (1997) 10656.

[1997Lee] Lee, B.J., Saunders, N., *Z. Metallkd*., 88(2) (1997) 152.

[1997Mis] Mishra, S.K., Pandey, D., *Phylos. Mad.*, 76(2) (1997) 227.

[1997Cor] Corker, D.L., Glazer, A.M., Dec, J., Roleder, K., Whatmore, W., *Acta Cryst., Sect. B: Struct. Crystallogr. Crys. Chem.*, B53 (1997) 135.

[1997SGTE] The SGTE substance database, version 1997, SGTE (Scientific Group Thermodata Europe), Grenoble, France, 1997.

[1998Cha] Chase, M.W.Jr., J. Phys. Chem. Ref. Data, Monograph No. 9, (1998).

[1998Mas] Massarotti, V., Capsoni, D., Bini, M., Altomare, A., Moliterni, A.G.G., *Z. Kristall.* 213 (1998) 259.

[1998Che] Chevalier, P.Y., Fischer, E., *J. Nucl. Mat.*, 257 (1998) 213.

[1998Cor] Corker, D.L. Glazer, A.M., Whatmore, R.W., Stallard, A., Fauth, F., *J. Phys.: Condens. Matter*, 10 (1998) 6251.

[1998Kob] Kobayashi, K., Kato, K., Terabe, K., Yamaguchi, S., Iguchi, Y., *J. Ceram. Soc. Jpn.*, 106(8) (1998) 782.

[1998Ris] Risold, D., Nagata, I.J., Suzuki, O.R.,: *J. Phase Equil.* 19 (1998) 213.

[1998Tes] Teslic, S.; Egami, T., *Acta Cryst., Sect. B: Struct. Crystallogr. Crys. Chem.*, B54 (1998) 750.

[1999Yok] Yokakowa, H., *J.Phase Equilibria*, 20(3) (1999) 258.

[1999Wal] Waldner P. and Eriksson G., Caphad, 23 (2) (1999) 189.

[1999Cla] Clavaguera-Mora, M.T., Comas, C., Touron, L.J., *J. Mater. Sci*., 34 (1999) 4347.

[1999Koo] Koo, B.K., Liang, P., Seifert, H. J., Aldinger, F., *Korean J. Ceram.*, 5 (1999) 2005.

[1999Pop] Popovic, A., Malic, B., Benceze, L., *Rapid Commun. Mass Spectrom.*, 13 (1999) 1129.

[1999Kha] Khairulin, A.R., Stankus V.S., *J. Phase Equil*., 20 (1999) 148.

[2000Jac] Jacob, K.T., Hoque, S.M. and Waseda, Y., *Material Trans.*, JIM, 41(6) (2000) 681.

[2000Wan] Wang, P., Liu, X.J., Ohnuma, I., Kainuma, R., Ishida, K., *Calphad*, 24 (2000) 149.

[2000Gon] Gong, W., Jin, Z., Du, Y., *J. Min. Met.*, 36B:3-4 (2000) 123.

[2000Bou] Bouvier, P., Djurado, E., Lucazeau, G., Le Bihan, T., *Physical Review, Serie 3. B - Condensed Matter*, 62 (2000) 8731.

[2000Sou] Souza Filho., Lima, K.C.V., Ayala, A.P., Guedes, I., Freire, P.T.C., Mendes Filho, J., Araujo, E.B., Eiras, J.A., *Phys.Rev. B*, 61, (2000) 14283.

[2000Fra] Frantti, J., Lappalainen, J., Eriksson, S., Lantto, V., Nishio, S., Kakihana, M., Ivanov, S., Rundlof, H., *Jpn. J.Appl. Phys., Part 1*, 39 (2000) 5697.

[2000Noh] Noheda, B., Gonzalo, J.A., Cross, L.E., Guo, R., Park, S.E., Cox, D.E., Shirane, G., *Phys.Rev. B-Condens. Matter*, 61(13) (2000) 8687.

[2001Kau] Kaufman, L., *Calphad*, 25 (2001) 141.

[2001Spe] Spencer, P.J., *Calphad*, 25 (2001) 163.

[2001SGTE] The SGTE unary database, version 4.4, SGTE (Scientific Group Thermodata Europe), Grenoble, France, 2001.

[2001Hil] Hillert, M., *J. Alloys Compd*., 320 (2) (2001) 161.

[2001Lia] Liang, P., Dupin, N., Fries, S.G., Seifert, H.J., Ansara, I., Lukas, H.L., Aldinger, F., *Z. Metallkd*, 92 (2001) 747.

[2001Noh] Noheda, B., Cox, D.E., Shirane, G., Guo, Jones, B., R., Cross, L.E., *Phys.Rev. B*, 63 (2001) 014103.

[2001Hom] Hom, B.K., Stevens, R., Woodfield, B.F., Baerio-Goates, J., Putnam, R.L., Helean, K.B., Navrotsky, A., *J. Chem. Thermodynamics*, 33 (2001). 165.

[2001Fra] Frantti, J., Lappalainen, J., Eriksson, S., Ivanov, S., Lantto, V., Nishio, S., Kakihana, M., Rundloef, H., *Ferroelectrics*, 261 (2001) 193.

[2001Sou] Souza Filho, A.G., Lima, K.C.V., Ayala, A.P., Guedes, I., Freire, P.T.C., Mendes Filho, J., Araujo, E.B., Eiras, J.A., *Phys.Rev. B*, 63, (2001) 176103.

[2001Par] Park, J.H., Liang, P., Seifert H.J., Aldinger, F., Koo, B.K., *Korean J. Ceram.*, 7(1) (2001) 11.

[2001Ran] Rane M.V., Navrotsky A., *J. Solid State Chem.*, 161 (2001) 402.

[2002And] Andersson, J.O., Helander, T., Höglund, L., Shi, P., Sundman, B., *Calphad*, 26 (2002) 273.

[2002Arr] Arroyave, R., Kaufman, L., Eagar, T.W., *Calphad*, 26 (2002) 95.

[2002Can] Canale, P., Servent, C., *Z. Metallkd.*, 93 (2002) 273.

[2002Win] Winterer, M., Delaplane, R., McGreevy, R, *J. Appl. Crystall.*, 35 (2002) 434.

[2002Ara] Araujo, E.B., Yukimitu, K., Moraes, J.C.S., Pelaio, L.H.Z., Eiras, *J.Phys. : Condens. Matter*., 14 (2002) 5195.

[2002San] Sani, A., Hanfland, M., Levy, D., *J. Solid State Chem.*, 167 (2002) 446.

[2003Hal] Hallstedt, B., Gauckler, L., *Calphad* 27 (2003) 177.

[2003Arr] Arroyave, L., Eagar, T.W., R., Kaufman, *J. Alloys Compd.*, 351 (2003) 158.

[2004Che1] Chevalier, P.Y., Fischer, E., Cheynet, B., *Calphad*, 28 (2004) 15.

[2004Che2] Chen, M., Hallstedt, B., Gauckler, L.J., *Solid State Ion.*, 170 (2004) 255.

[2004Wan] Wang, C., Zinkevich, M., Aldinger, F., *Calphad*, 28 (2004) 281.

[2004Tro1] Troitzsch, U., Christy, A.G., Ellis D.J., *J. Amer. Ceram. Soc.*, 87(11) (2004) 2058.

[2004Cla] Clavaguera-Mora, M.T., Touron, J.L., Rodriguez-Viejo, J., Clavaguera, N., *J. Alloys Compd*., 377 (2004) 8.

[2004Tro2] Troitzsch, U., Ellis D.J., Christy, A.G., Europ. *J. Mineral.*, 16 (2004) 577.

[2005Yok] Yokakowa, H., Yamaji, K., Horita, T., Sakai, N., Brito, E., *Materials Sci. Forum*, 502 (2005) 111.

[2005Can] M. Čančarević, M. Zinkevich, F. Aldinger, *Z.Metallknd.*, 96(8) (2005) 879.

[2005Tro] Troitzsch, U., Ellis D.J., *J. Mat. Sci.*, 40(17) (2005) 4571.

[2005Ros] Rossetti G.A., Maffei N., *J.Phys. : Condens. Matter.*, 17 (2005) 3953.

[2005Bou] Bouzid, A., Bourim, E.M., Gabbay, M., Fantozzi, G., *J. Europ. Ceram. Soc.*, 25 (2005) 3213.

[2006Zin] Zinkevich, M., Djurovic, D., Aldinger, F., *Solid State Ionics*, 177 (2006) 989.

[2006Wan] Wang, C., Ph.D. Thesis, University of Stuttgart, 2006.

[2006Kan] Kang, Y.-B., Jung, I.-H., Lee, H.-G., *Calphad*, 30 (2006) in press.

[2006Can] M. Čančarević, M. Zinkevich, F. Aldinger, Thermodynamic description of the Ti-O System Using Associate Model for the Liquid Phase, submitted to *Calphad.*

[2006Don] Dondi, M., Matteucci, F., Cruciani, G., *J. Solid State Chemi*., 179 (2006) 233.

CURRICULUM VITAE

Personal:

Name: Marija Čančarević born Backović
Date of birth: 8. September 1970.
Place of birth: Sabac, Serbia
Nationality: Serbian
Material status: Married, one child

Education:

1977-1985 Primary School , Gornji Milanovac, Serbia

1985-1989 High School (Gymnasium), Gornji Milanovac, Serbia

1989-1995 Graduate stady at the Department of Metallurgical Engineering, Faculty of Technology and Metallurgy, University of Belgrade, Serbia
Dipl. Ing. in Metallurgy
Diploma work: The Development of Forging Technology for “Ball Housing"

1996 – 2002 Postgraduate stady at the Department for Metal Forming, Faculty of Technology and Metallurgy, University of Belgrade, Serbia
M.Sc. Degree in Metallurgy
Master thesis: Investigation of the Microstructure, Mechanical and Deformation Properties of the Copper Alloy with 5mass. % Nickel and 2.5mass. % Titanium

2003-2007 Ph. D. work at the Max Planck Institute for Metal Research and University of Stuttgart, Department Prof. Dr. Aldinger, Stuttgart, Germany
Ph. D. Degree in Material Science
Ph.D. Thesis: Thermodynamic optimization of the PbO-ZrO_2-TiO_2 (PZT) system and its application to the processing of composites of PZT ceramics and copper

Employments and Positions:

1995-1996 Engineer for Quality Control of the Forging Technology,
Car Factory " FAD", G. Milanovac, Serbia

1996-present Researcher
Department of Material Sciences, Institute of Nuclear Science "Vinca", University of Belgrade

2003-2007 Scholarship of the Max-Planck Institute for Metal Research, Department Prof. Dr. Aldinger, Stuttgart, Germany